Synthesis of Novel Staurosporine Analogues as Potential Kinase Inhibitors

by

Alet van der Westhuyzen

Thesis presented in partial fulfilment of the requirements for the degree of Master of Science in the Faculty of Science at Stellenbosch University

Supervisor: Prof. Willem A. L. van Otterlo

Co-supervisor: Dr. Stephen C. Pelly

Faculty of Natural Science

Department of Chemistry and Polymer Science

March 2015

DECLARATION

By submitting this thesis electronically, I declare that the entirety of the work contained therein is my own, original work, that I am the sole author thereof (save to the extent explicitly otherwise stated), that reproduction and publication thereof by Stellenbosch University will not infringe any third party rights and that I have not previously in its entirety or in part submitted it for obtaining any qualification.

December 2014

ABSTRACT

Protein kinases are enzymes that promote phosphorylation – transferring a phosphate group from ATP to a substrate protein. Due to the central involvement of kinases in growth factor signaling, cell cycle control, apoptosis and angiogenesis, they have been linked to cancer development and are attractive drug targets for cancer therapeutics. Staurosporine is a natural, potent kinase inhibitor, initially isolated from the bacterium *Streptomyces staurosporeus*. It does not serve as a viable therapeutic drug since it exhibits poor selectivity. However, this natural product has been widely used in research and serves as a "structural muse" for the design of protein kinase inhibitors with improved specificity and selectivity.

This project involved the synthesis of potential reversible and irreversible kinase inhibitors inspired by the natural product staurosporine. A primary objective was to develop compounds with improved selectivity, while maintaining the potency of staurosporine. The design strategy incorporated a driving portion, resembling the structural features of staurosporine, carrying a specific warhead to form a reversible or irreversible interaction within the kinase domain. This project comprises of two main parts – the design of pyrrolocarbazole structures and the generation of structures based on the "open" form of the indolocarbazoles. The development of the pyrrolocarbazole compounds was motivated by the encouraging results exhibited by 6-(3-hydroxypropyl)pyrrolo[3,4-*c*]carbazole-1,3(2*H*,6*H*)-dione (**29**), previously synthesized in our group.

The major steps involved in the synthesis were the reduction, oxidation, Wittig, Diels-Alder and aromatization reactions. Introducing different warheads, allowed for the generation of unaromatized and aromatized pyrrolocarbazole target compounds having an *N*-tether hydroxyl, propargyl and nitrile functionality. The synthesis of the "open" form structures utilized click chemistry. The synthetic methodology towards the bisaryl maleimide structures involved a "double click" approach, which presented various challenges. In addition, the synthesis of indolyl maleimide click products also proved to be difficult. Finally, a promising route towards bisamino maleimide compounds led to the development of two target compounds containing the acryloyl and propargyl warhead functionality respectively.

Biochemical screening by German collaborators against the wild type, and two mutant forms of the EGFR kinase, was undertaken with the target compounds, utilizing the HTRF KinEASE-TK assay. Overall, only the aromatized pyrrolocarbazole *N*-two carbon linker hydroxyl target compound exhibited inhibitory activity in the μM range. Finally, a number of optimization measures are described to potentially improve the inhibitory activity of both the pyrrolocarbazole compounds and bisamino maleimides.

UITTREKSEL

Proteïn kinase is ensieme wat fosforilasie bevorder – deur ń fosfaat groep van ATP na ń substraat proteïn oor te plaas. As gevolg van die sentrale betrokkenheid van kinase in groei-faktor seine, beheer oor sel siklus, apoptosis asook angiogenesis, is hulle gekoppel aan kanker sel toename en is ń aantreklike middel vir kanker-terapie. Staurosporine is ń natuurlike, sterk kinase onderdrukker, aanvanglik geïsoleer van die bakterium *Streptomyces staurosporeus*. Ongelukkig dien dit nie as ń bruikbare geneesmiddel nie as gevolg van die tekort aan selektiwiteit – vele kinases word geteiken. Nietemin, word die natuurlike produk algemeen gebruik in navorsing en dien as ń "strukturele muse" vir die ontwerp van proteïn kinase onderdrukkers met verbeterde selektiwiteit en meer spesifiek.

Die projek behels die sintese van potensiële omkeerbare en onomkeerbare kinase onderdrukkers wat geïnspireer is deur die natuurlike produk staurosporine. ń Primêre doel was om verbindings te ontwikkel met beter selektiwiteit, wat die effektiwiteit van staurosprine behou. Die ontwerp strategie inkorporeer ń dryfdeel wat ooreenstem met die struktuur van staurosporine en ń spesifieke aanvalpunt wat hopelik ń omkeerbare of onomkeerbare interaksie binne die kinase-omgewing sal vorm. Die projek bestaan hoofsaaklik uit twee dele nl. die ontwerp van pyrrolokarbasoolstrukture, asook strukture wat die "oop" vorm van die indolokarbasole namaak.

Die ontwikkeling van die pyrrolokarbasool samestellings was gemotiveer deur die bemoedigende resultate vertoon deur 6-(3-hydroxypropyl)pyrrolo[3,4-*c*]carbazole-1,3(2*H*,6*H*)-dione (**29**) wat voorheen in ons navorsings-groep gesintiseer was. Die hoofsaaklike stappe betrokke gedurende die sintese was reduksie, oksidasie, Wittig, Diels-Alder en aromatisering reaksies. Die bekendstelling van verskeie aanvalpunte, maak die ongearomatiseerde en aromatiseerde pyrrolokarbasool teikenprodukte met ń *N*-koolstof binding met hidroksiel, propargiel en nitriel funksionele groepe moontlik. Die sintese van die "oop" vorm strukture gebruik "click" chemie. Die metode om die sintese van die bisariel-malimied strukture na te streef behels ń "dubbele click" wyse, wat baie uitdagings gehad het. Verder het die sintese van die indolyl-malimied "click" produkte ook verskeie problem opgelewer. Uiteindelik het ń baie belowende roete na bisamino-malimied verbindings gelei, en die ontwikkeling van twee teiken produkte, met ń akryloyl en propargiel aanvalpunt funktionele groepe, was bereik.

Biochemiese keuring deur Duitse medewerkers teen die wilde tipe, asook twee mutant vorms van die EGFR kinase, was onderneem teen die teiken verbindings, met gebruik van die HTRF KinEASE-TK toets. Oor die algeheel, was die aromatiese pyrrolokarbasool met die *N*-koolstof verbinding met die

hidroksiel groep, die enigste verbinding wat onderdrukkende aktiviteit in die µM grens getoon het. Verskeie optimisering strategieë was bespreek om die potentiële onderdrukkings aktiwiteit van die pyrrolokarbasool en bisamino-malimied verbindings te verbeter.

ACKNOWLEDGEMENTS

Personal acknowledgements

Firstly, I would like to thank my supervisor, Prof Willem A. L. van Otterlo, for his utmost guidance, support, time and positivity. I will forever be grateful to you for the opportunities you've given me. To my co-supervisor, Dr Stephen C. Pelly, for always being willing to help, offer advice and make me laugh. Also to Dr Gareth Arnott, for always having a free minute to answer any of my mechanistic questions. It's been a great privilege to have been part of the group of medicinal and organic chemistry (GOMOC). Not only has it been an enjoyable work environment, but I have found a friend in each of you.

My four pillars of strength: To my parents, words can't describe the love, respect and appreciation I have for you. For all the sacrifices you have made to offer me the best possible education, encouraging me to invest in myself, and strive to be great. To my bodyguards - thanks for knowing me, loving me, teasing me and making me tough − I am truly blessed to have you two as my brothers. I would also like to acknowledge my grandparents who have played a vital role in my upbringing and education.

To my best friend and companion, you have been by my side through the highs and lows. You've motivated me when I felt hopeless, and took me dancing when I got tired. Luke, thanks for dreaming with me and always making me laugh.

"…those who hope in the Lord will renew their strength. They will soar on wings like eagles; they will run and not grow weary, they will walk and not be faint." –Isaiah 40:31. Above all, I praise and thank our Heavenly Father.

Additional acknowledgements

To Dr Jaco Brand and Ms Elsa Malherbe, for your friendliness and assistance whenever I needed help with my NMR spectra. I would also like to acknowledge Dr Marietjie Stander and CAF for the MS data. A special thanks to Prof. Daniel Rauh and Julian Engel at the Technische Universität Dortmund for their work on the biological screening assays.

Without funding, this MSc would not have been possible. Therefore I would like to acknowledge the National Research Foundation (NRF) for their contribution in the form of a bursary. In addition, I would like to extend my appreciation to Stellenbosch University and the Helpmekaar Studiefonds.

CONTENTS

LIST OF ABBREVIATIONS

Abl – Abelson murine leukemia viral oncogene homolog 1

AcOH – Acetic acid

AK – Atypical kinases

ALK – Activin receptor-like kinase

ALL – Acute lymphoblastic leukemia

Ar – Aromatic

BCR – Breakpoint cluster region

BEI – Binding efficiencies

bFGF – basic Fibroblast growth factor

BIOS – Biology-orientated synthesis

BMPs – Bone morphogenic proteins

Boc_2O – Di-*tert*-butyl dicarbonate

Brsm – Before recovery of starting material

CAMK – Calcium/calmodulin-dependent protein kinase

cAMP –Cyclic adenosine monophosphate

CAMs – Cell-cell adhesion molecules

Car – Carbazole

CK – Casein kinase

CML – Chronic myelogenous (or myeloid) leukemia

CuAAC – Copper(I)-catalyzed azide alkyne cycloaddition

Cys – Cysteine

DBU – 1,8-Diazabicyclo[5.4.0]undec-7-ene

DDQ – 2,3-Dichloro-5,6-dicyano-1,4-benzoquinone

DIPEA – *N*,*N*-Diisopropylethylamine

DMAP – 4-Dimethylaminopyridine

DMF – *N*,*N*-Dimethylformamide

DMSO – Dimethyl sulfoxide

DNA – Deoxyribonucleic acid

DOS – Diversity-orientated synthesis

EGF – Epidermal growth factor

EGFR – Epidermal growth factor receptor

EST – Expressed sequence tag

EtOAc – Ethyl acetate

FDA – Food and Drug Administration

FGFR – Fibroblast growth factor receptor

FRET – Förster resonance energy transfer

GDFs – Growth and differentiation factors

GS – Growth signals

GSK – Glycogen synthase kinase

HEK – Human embryonic kidney

HER2 – Human epidermal growth factor receptor 2

HGF – Hepatocyte growth factor

HTRF – Homogeneous time-resolved fluorescence

HRMS – High resolution mass spectrometry

IARC – International Agency for Research on Cancer

Ile – Isoleucine

IR – Infrared

KFEF – Kinase focused evolved fragment

L858R – Leucine 858 mutation

Leu – Leucine

LSP – Local space pattern

MeCN – Acetonitrile

MeOH – Methanol

Met – Methionine

Mp – Melting point

MS – Mass spectrometry

NCI – National Cancer Institute

NMR – Nuclear magnetic resonance

NSCLC – Non-small-cell lung carcinoma

OED – Oxford English Dictionary

PDB – Protein data bank

PDGFR – Platelet-derived growth factor receptor

PDK – Phosphoinositide –dependent protein kinase

PDK1 – Phosphoinositide dependent kinase 1

PDK1 – Phosphoinositide-dependent kinase-1

Phe – Phenylalanine

PKA – Protein kinase A

PKC – Protein kinase C

PSSC – Protein structure similarity cluster

RT – Room temperature

RTKs – Receptor tyrosine kinases

RuAAC – Ruthenium-catalyzed azide alkyne cycloaddition

SCONP – Structural classification of natural products

Ser – Serine

SF – Scatter factor

Src – Sarcoma

T790M – Threonine790 mutation

TBAF – Tetrabutylammonium fluoride

TBAHS – Tetrabutylammonium hydrogen sulfate

TBB – Tetrabenzotriazole

TEA – Triethylamine

TFA – Trifluoroacetic acid

THF – Tetrahydrofuran

Thr – Threonine

TK – Tyrosine kinase

TKL – Tyrosine kinase-like

TLC – Thin layer chromatography

TMP – 2,2,6,6-Tetramethylpiperidine

TMSA – Trimethylsilylacetylene

Tyr – Tyrosine

Val – Valine

VEGFR – Vascular endothelial growth factor receptor

WHO – World Health Organization

PREFACE

A note to the reader regarding the interpretation of NMR spectra

An unconventional labeling system was used for the interpretation of the ^{1}H and ^{13}C NMR spectra. The indole moiety was labeled first in an alphabetical order and an anti-clockwise manner. Hence, once an atom received a label, the label remained constant for the subsequent intermediates, with only the transforming functional groups changing. This assignment was applied to ease the analysis of spectra and improve the ease of reading when referring to the same atom in different substrates.

CHAPTER 1 – CANCER

1.1 Cancer

1.1.1 Definition and statistics

In 1889 the word 'cancer' was defined by the Oxford English Dictionary (OED) as "a malignant growth or tumor in different parts of the body that tends to spread indefinitely and to reproduce itself and also to return after removal; it eats away or corrodes the part in which it is situated and generally ends in death."[1] This term has embedded itself in our thought patterns, notorious for its uncontrollable, lethal and devastating process.[2] Metaphors of decay, destruction and hideous consumption have been associated with the word 'cancer'. These implications account for its use not only when referring to the pathological condition, but when talking about insidious, uncontrollable and frightening things.[2] According to the definition, the outcome of cancer is mortality. Extensive research and progress in the field of cancer has led to the definition being changed for the first time in 111 years. The OED now defines cancer as "what happens when a group of cells grow in a disorderly and uncontrollable way and invade neighboring tissues. They may or may not later spread into distant parts of the body. The cancer process is shared by over 200 diseases."[1]

Despite the rapid developments and enormous amount of research over the past 20 years, cancer continues to be a leading cause of death and a worldwide killer.[3] Globally, one in five men and one in six women will develop cancer before the age of 75. Furthermore, one in eight men and one in twelve women will die from this disease.[4] According to the World Health Organization (WHO) a global 'tidal wave' of cancer is on the horizon, warning that by 2035 approximately 24 million people will have the disease (figure 1).[5] The International Agency for Research on Cancer (IARC) reported that in 2012 there were 14.1 million new cases, 8.2 million cancer deaths and 32.6 million people living with cancer (within 5 years of diagnosis) worldwide. The number of cancer cases is expected to rise to 22 million annually within the next two decades, while deaths are predicted to rise to 13 million per year.[6] Previously thought of as a first world disease, statistics show an alarming increase of cancer cases and mortality in developing countries. More than 60% of global cancer cases occur in Africa, Asia and Central and South America, accounting for 70% of the world's cancer deaths.[4]

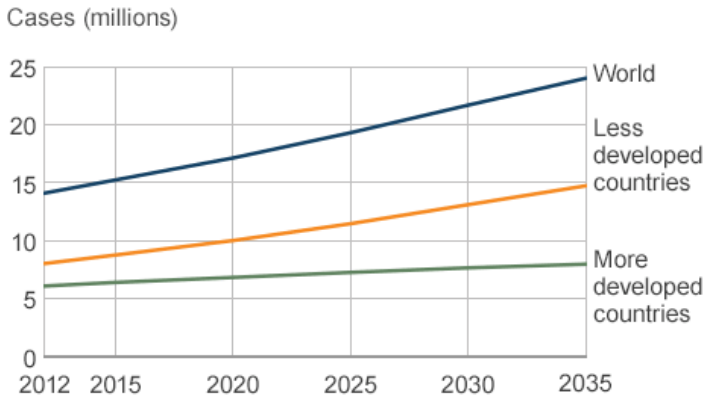

Figure 1
Graph illustrating the predicted cancer cases worldwide. Image reproduced from following reference.[5]

This global cancer burden is attributed mainly to population growth and increasing lifespan, placing further strain on developing countries due to the lack of early detection and access to treatment.[6] In addition, the costs spent on treatment, together with the economic and social inactivity from premature death and disability has damaging effects on economies worldwide.[4] WHO reported an approximate total annual economic cost of cancer reaching US $ 1.16 trillion in 2010.[6] According to the IARC, primary prevention is essential to address the alarming rise of the cancer burden.[5] Efficient strategies towards prevention and early detection are crucial to complement the crucial research carried out over the last few decades to develop improved cancer treatments.[6]

Over the past two centuries, significant discoveries in the cancer field have established a rich and complex body of knowledge of this remarkably diverse neoplastic disease. New observations and findings lead to more questions, adding further layers of complexity to understanding cancer. In 1971, President Nixon signed the National Cancer Act, declaring "war" on cancer and providing funds for the support of cancer research and application of research results – fuel for the revolution in molecular biology.[7] Although cancer remains an extremely complicated pathologic condition and challenging questions persist, many scientists foresee cancer research developing into a logical science where the intrinsic complexity of the disease will become understandable.[8]

1.1.2 Hallmarks of cancer

In cancer research, a logical framework of organizing principles, known as hallmarks, have been proposed, in order to have a better understanding of the biology of this disease.[9] Before discussing these hallmarks, a simple explanation of tumorigenesis is given. As mentioned in the introductory paragraph, cancer is a term given to a group of diseases that can develop in virtually any of the body's tissues. Each form of cancer has its unique features, but the basic processes that generate cancer are similar.[10]

A representation of the progression of cancerous cells is illustrated in figure 2. All cancers start in the body's fundamental unit of life - when cells' genetic material become damaged or changed, producing mutations. These mutations affect the orderly manner of cell proliferation, transcription, growth, migration, differentiation and death.[11] Cells generated from the abnormal ancestral cell and its offspring also display uncontrollable activity. These abnormal cells form a mass of tissue known as a tumor which may be cancerous or benign. An *in situ* tumor is formed when the tumor remains in the tissue of origin, while malignant tumors invade nearby tissue generating new tumors (metastases) in the body.[10] Tumor formation and progression however, is not dependent on cancer cells alone, but consists of an intricate network of distinct cell types that participate in heterotypic interactions and influence growth through a "tumor microenvironment."[9]

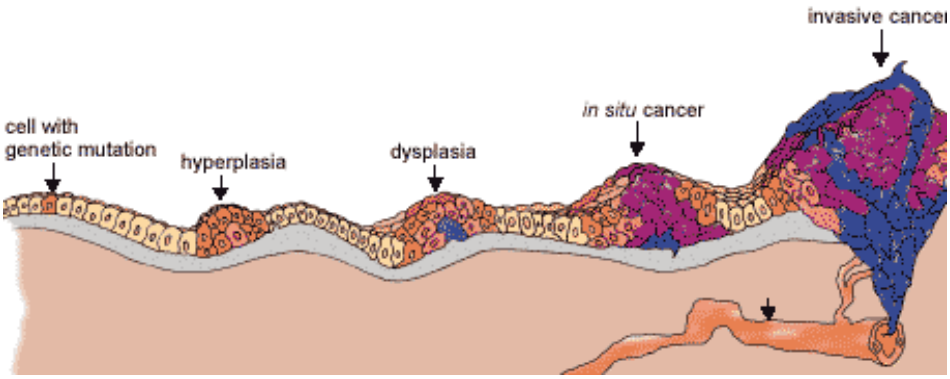

Figure 2
Representation of the progression of cancerous cells. Image reproduced from following reference.[10]

The transformation of normal human cells into malignant derivatives is a multistep process that develops over time, reflecting a long and complex succession of genetic changes.[10] Hanahan and Weinberg enumerated six biological capabilities acquired during this multistep development, known as the hallmarks of cancer. They include sustaining proliferative signaling, evading growth suppressors, resisting cell death, enabling replicative immortality, inducing angiogenesis, and activating invasion and metastasis (Figure 3). These six hallmarks are used to explain and rationalize the ability of cancer cells to overcome the anticancer defense mechanism hardwired into cells and tissues.[8-9] Here follows a brief explanation of each acquired capability:

A) Sustaining proliferative signaling

There are two main classes of genes which play a critical role in controlling the cell cycle, namely: proto-oncogenes (encourage cell division) and tumor-suppressor genes (inhibit cell division). Proto-oncogenes code for proteins that receive and process growth-stimulating signals from other cells.[10]

The signaling starts with the production of mitogenic growth signals (GS) which are transmitted into the cell by specific transmembrane receptors. These GS convey a stimulatory signal to different proteins thereby activating genes to promote growth.[8] When proto-oncogenes become mutated they are called oncogenes. Oncogenes cause the proteins involved in the growth-promoting pathways to be overactive or oversensitive.[10] Tumor cells show reduced dependence on stimulation form their normal tissue microenvironment by generating their own GS.[8] In this manner proliferative signaling is sustained.

B) Evading growth suppressors

In a similar manner to stimulatory messages, inhibitory messages are transmitted to the cell's nucleus by tumor-suppressor genes. When these antigrowth signals are not received, the growth promoting pathways operate without restraint, leading to uncontrolled cellular growth.[8, 10]

C) Resisting cell death

Programmed cell death (apoptosis) is crucial when abnormalities are detected. Cancer cells can acquire resistance to apoptosis though a variety of strategies. Mutation of the p53 tumor-suppressor gene which results in functional inactivation of p53 protein is an example of a common strategy for cancer cells to evade death.[10]

D) Enabling replicative immortality

Acquired deregulation of cell-to-cell signaling (abnormal proliferation and apoptosis) does not account for the enormous cell population that makes up macroscopic tumors. This introduces the fourth hallmark known as replicative immortality. Cells carry an intrinsic cell-autonomous program that prevents them from proliferating indefinitely. This system is controlled by a counting device involving DNA segments at the end of chromosomes, known as telomeres. With each chromosome replication the telomeres become shorter and eventually reach a limit that causes the cell to stop dividing, resulting in cellular death. An enzyme known as telomerase, enables cancer cells to proliferate endlessly, by systematically replacing the telomeric segments which restrict replicative immortality.[8, 10]

E) Inducing angiogenesis

The process of angiogenesis generates tumor-associated neovasculature to supply the cancer cells with nutrients and oxygen. In adults, angiogenesis is only transiently turned on, but during tumor progression an "angiogenic switch" remains on to continually sprout new vessels and sustain growth.[9]

This angiogenic switch is governed by counterbalancing positive or negative factors that either encourage or block angiogenesis.[8] Angiogenesis is induced by factors such as vascular endothelial growth factor (VEGF), basic fibroblast growth factor (bFGF) and platelet-derived growth factor (PDGF).

Pericytes which support blood vessel growth express PDGF receptors, while VEGF receptors are expressed on the endothelial cells of tumor vessels. Pericytes produce VEGF and endothelial cells produce both VEGF and PDGF. Each cell type is therefore able to promote proliferation and survival of the other cell type, by producing the specific growth factor.[12] Tumors threaten human life when they invade and disrupt the tissues and organs needed for survival.

F) Activating invasion and metastasis

Malignant tumors are capable of shedding abnormal cells into the blood and lymph systems, establishing new tumors throughout the body. This invasion to adjacent tissue and formation of new cancer colonies is known as metastases and is the cause of 90% of cancer deaths.[8] The mechanisms underlying invasion and metastasis are complex and are not fully understood. Both processes involve changes in the physical coupling of cells to their microenvironment and activation of extracellular protease. The affected proteins include cell-cell adhesion molecules (CAMs) and integrins, which link cells to extracellular matrix substrates. E-cadherin is an example of a CAM which undergoes mutational inactivation when invasion and metastasis is observed.Over the past few years a number of advances have been made in delineating the features of this hallmark, but representation of these advances are yet to be completed.[8-9]

It is believed that almost all cancer cells will acquire these hallmark capabilities in a manner which differs both mechanistically and chronologically.[8] An enabling characteristic associated with the acquisition of these hallmarks is genome instability. Defects in genome maintenance and repair encourage tumor progression, by accelerating the rate of accumulative favorable genotypes in evolving neoplastic cells.[8-9]Another enabling characteristic is contributed to the tumor-associated inflammatory response, which enhances tumerogenesis. Inflammation can supply the tumor microenvironment with bioactive molecules, survival factors, proangiogenic factors, invasion/metastasis and many other hallmark facilitating programs.[9] Recent research suggests two additional emerging hallmarks of cancer. Firstly, deregulating cellular energies involves altering and reprogramming of cellular metabolism to support neoplasmic growth. The second emerging hallmark is the defective immunological monitoring of tumors that evade immunological destruction. This capability involves deficiencies in the development and function of T and B lymphocytes, macrophages, and natural killer cells. A representation of the six hallmarks, the emerging hallmarks and enabling characteristics is displayed below in figure 3.[9]

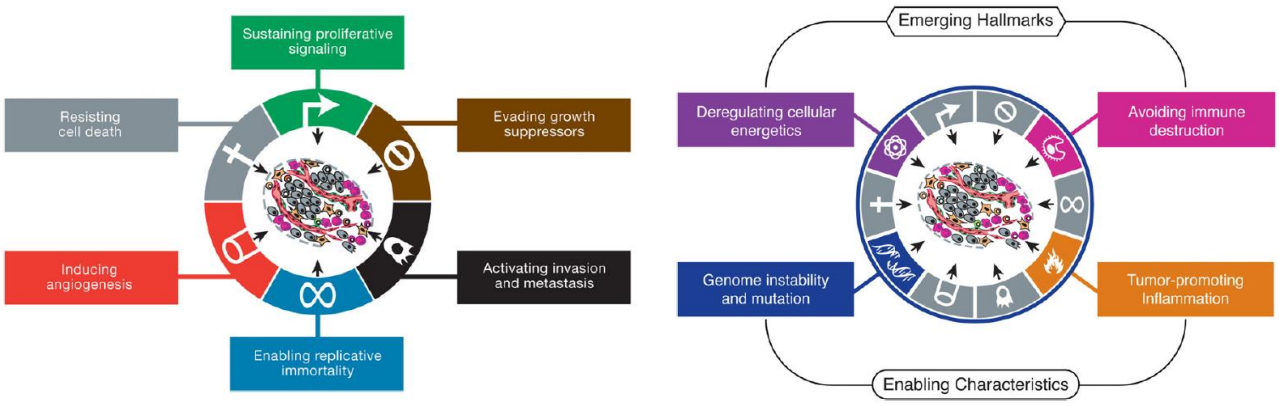

Figure 3

The six hallmarks of cancer are illustrated in the left diagram. Two new emerging hallmarks and enabling characteristics have also been proposed (see diagram on the right). Image reproduced from following reference.[9]

1.2 Treatment

1.2.1 Chemotherapy

The remarkable progress of research into the mechanisms of cancer pathogenesis provided scientists a mode to devise new strategies and generate effective weaponry to combat cancer.[13] In this respect, cancer treatment has evolved from nonspecific, high-dose chemotherapy to targeted treatment.[14] The first tool available for treatment was surgical removal of the tumor. For this method of treatment, the introduction of radical mastectomy and *en bloc* resection in 1894 by William Halsted, had a profound influence, leading to the application of *en bloc* resection to remove all other cancers. Surgery was the only option for cancer treatment in the first era of the 20th century, but only a minority of patients could be cured by this type of treatment alone. Together with the discovery of X-rays came the era of radiation therapy. In 1928, fractional radiation treatments were shown to cure neck and head cancers.The introduction of cobalt teletherapy initiated the modern era of radiation treatments in 1950.[7] Surgery and radiotherapy dominated the field of cancer therapy into the 1960s, but sadly only 33% of all cancers could be cured by these two approaches - alone or combined - due to the presence of micro-metastases.[7, 15]

In the early 1900s, Paul Ehrlich made a concerted effort to develop drugs to treat infectious diseases. His interests involved creating chemicals to cure cancer, a term he coined “chemotherapy”. Another major contribution Ehrlich made to cancer drug development was the discovery of using animal models to screen drugs for their anticancer activity.[15] The first half of the 20th century was dedicated to model development for screening of various drugs for their potential activity against cancer cells.[7]

The start of the modern era of chemotherapy can be traced back to World War II when an accidental spill of sulfur mustards on troops led to depleted bone marrow and lymph nodes of the men exposed to the gases. This observation encouraged Louis Goodman and Alfred Gilman to use nitrogen mustard to treat a patient with non-Hodgkin's lymphoma. For the first time it was proved that chemotherapy could induce tumor regression. Another important event that provided encouragement for the use of anticancer drugs was the use of antifolates by Sydney Farber to induce remission in children with acute lymphoblastic leukemia (ALL).[15-17] These discoveries lead to a national screening effort at the NCI and the use of chemotherapy became more popular.[16] Still, the controversy and hostile attitude towards chemotherapy remained. The main concern was whether the drugs caused more harm than good.[15] A major breakthrough in the mid-1960s gave evidence that combination chemotherapy (combination of drugs, each with a different mode of action) could cure childhood leukemia and Hodgkin's disease. This led to remarkable advances in the field of chemotherapy and the use of combination treatment and chemotherapy as an adjuvant to surgery and radiation therapy.[15-16] The various pivotal events in cancer treatment are represented in the timeline below (figure 4).[7]

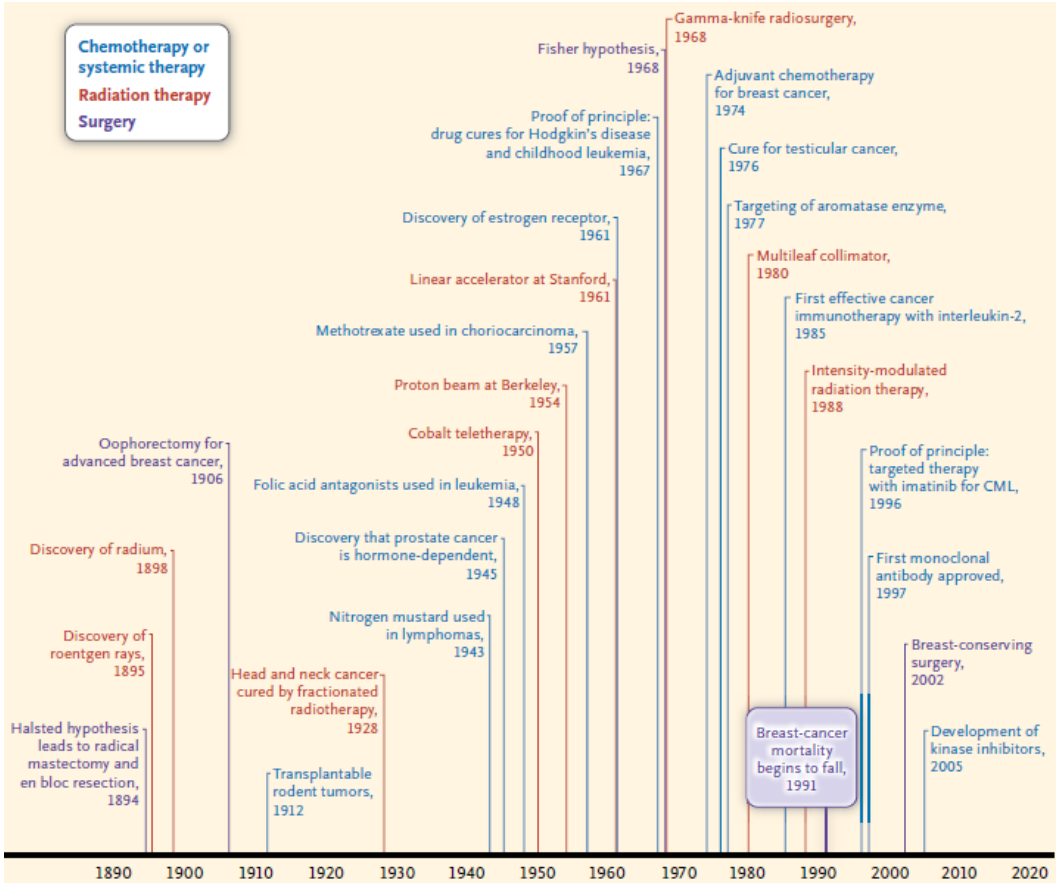

Figure 4
Pivotal events in the treatment of cancer. Image reproduced from following reference.[7]

1.2.2 Targeted treatment

Paul Ehrlich's ideas and bold assumptions inspired generations of scientists to devise powerful molecular cancer therapeutics. His postulate of creating "magic bullets" paved the way for targeted therapy and today Ehrlich's ideal of "aiming precisely" using drugs with high efficacy dominates modern drug discovery.[15] The revolutionary insights in cell biology and the mechanisms associated with the hallmarks of cancer initiated the era of targeted therapy.[9, 16] A milestone in the targeted revolution was the development and clinical success of Imatinib (Gleevec) for chronic myeloid leukemia (CML).[13]

Imatinib inhibits the kinase activity of all proteins that contain ABL, ABL-related genes (ARG) protein, or platelet-derived growth factor receptor (PDGFRs), as well as the KIT tyrosine kinase.[17] The ABL gene is found on chromosome 9 of the Philadelphia chromosome and encodes for a tightly regulated tyrosine kinase. The Philadelphia chromosome is the product of the translocation between chromosome 9 and chromosome 22. Chromosome 22 carries the breakpoint cluster region (BCR) gene. The principle target of Imatinib is this BCR-ABL fusion protein which involves the pathogenesis of CML.[14, 16, 18] Proof-of-principle was now established that targeted therapy towards specific molecular abnormalities could possibly convert certain cancers into manageable chronic illnesses.[7] This led to numerous efforts to develop and test small-molecule inhibitors targeting effectors in the acquired biological capabilities of cancer cells.[15] Most of these hallmark-targeting cancer drugs have been directed towards specific molecular targets as seen in figure 5. This type of specificity was thought to be advantageous as it presents targeted inhibitory activity without harming healthy tissue. Despite the remarkable achievements by targeted treatment the limitations of off-target toxicity and adaptive resistance have been acknowledged.[9, 15]

Clinical responses have frequently been temporary, being followed by almost-inevitable relapse.[9] In the case of Imatinib, in the acute leukemic phase, treatment leads to drug-resistant cells that display mutations in the catalytic kinase domain of ABL. The presence of drug-resistant cells before drug exposure has proven the fact that cancers possess a range of drug-resistant mutant sub-clones, even before treatment.[16] Similarly to the development of resistance, the target protein governs whether the drug will work and which patients will respond to treatment. This is illustrated by the kinase inhibitor, gefitinib, which blocks the activity of epidermal growth factor receptor (EGFR), which is overexpressed in 40-80% of lung cancers. However, gefitinib causes partial remissions in only 10-15% of patients. This response was attributed to the presence of mutations around the ATP binding pocket of the EGFR proteins. Patients that responded to gefitinib tend to carry these specific mutations.[13, 16]

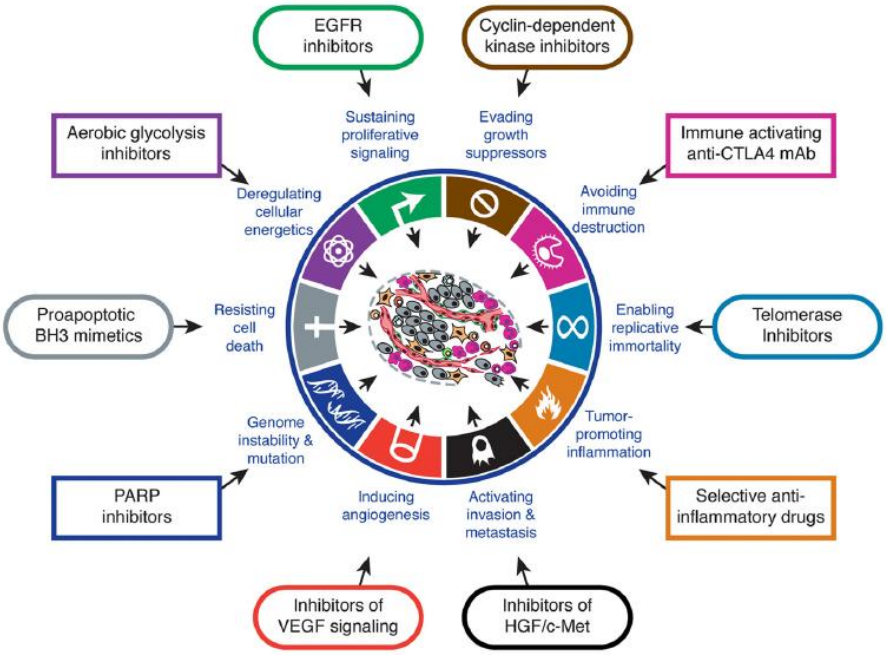

Figure 5

Illustrative examples of inhibitors which target the specific hallmarks of cancer and enabling characteristics. Image reproduced from following reference.[9]

For many years Ehrlich's "magic bullet" was interpreted by scientists as a compound that specifically targets a single oncoprotein. Knowing that cancer is a multi-factorial disease that has a number of parallel signaling pathways which support core hallmark capabilities, has changed the interpretation of Ehrlich's vision to a " multiple magic bullet".[15] Targeting crucial signaling proteins that regulate the hallmarks of cancer cells will potentially result in more effective and durable therapies.[9] Furthermore, as a result of the resistance towards single agents, Ehrlich's idea of combination therapy is essential for tumor eradication.[15-16] Therefore, network-targeted combination therapy is a promising strategy for the future development of more efficacious weaponry against cancer.[15] The discovery of small molecule kinase inhibitors has attracted growing interest for novel drug development and targeting protein kinases has been the subject of intensive study.[19-20] Thus, an understanding of protein kinases is necessary and will be discussed in the following section. It must be noted that small molecule kinase inhibitors are not the only type of targeting therapeutic agent. Numerous drugs have been investigated and developed for targeted therapies and have been approved for the use in cancer treatment. These include monoclonal antibodies, apoptosis-inducing drugs, angiogenesis inhibitors, cancer vaccines and gene therapy.[21-22]

1.3 Kinases

1.3.1 Kinases and their relation to cancer

The reversible phosphorylation of proteins is the most general regulatory device adopted by eukaryotic cells and represents a key step in many crucial cellular processes including metabolism, growth, division, differentiation, motility, organelle trafficking, membrane transport, muscle contraction, immunity, learning and memory.[23-25] Protein phosphorylation is the most prominent post-translational modification to both intracellular and extracellular signals.[20, 24] In addition, perturbed signal transduction is a major cause of deregulated cell growth in both benign and malignant neoplasms.[26] Protein kinases are enzymes that phosphorylate their substrate proteins by catalyzing the transfer of the terminal γ-phosphate of adenosine triphosphate (ATP), to the hydroxyl acceptor group on the side chains of serine, threonine, or tyrosine residues (in eukaryotes) of the substrate protein (Scheme 1).[19] Due to the central involvement of kinases in growth factor signaling, cell cycle control, apoptosis and angiogenesis, they have been linked to cancer development and are attractive drug targets for cancer therapeutics.[19-20]

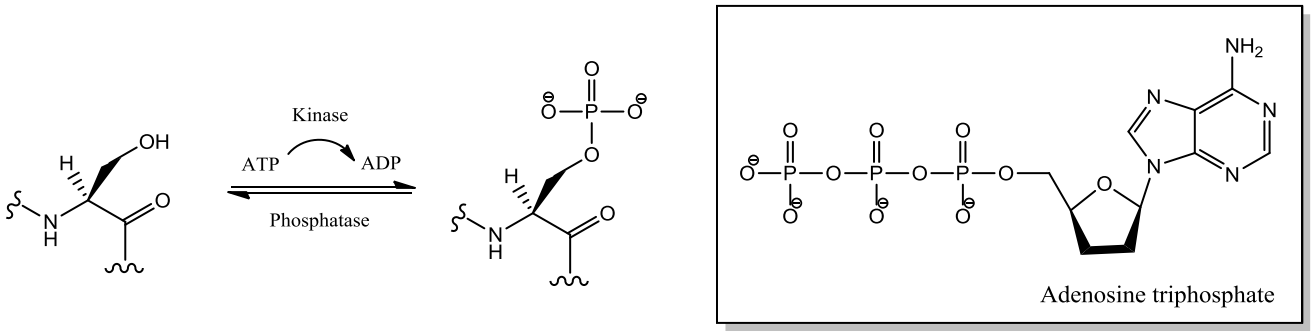

Scheme 1
General scheme for the phosphorylation of a serine residue by a kinase.

1.3.2 The kinase superfamily

An ultimate purpose of research into signal transduction is to obtain a full understanding of protein phosphorylation in normal and disease states.[25, 27] An ambitious goal to achieve this knowledge, pursued by Hanks and Hunter, was to determine the number of protein kinases encoded by eukaryotic genomes and assess the structures, functions and evolutionary relationships.[27-29] The advent of gene cloning and sequencing techniques led to an exponential rise in the number of unique members in the protein kinase family being identified. An immense amount of progress in the pregenomic and genomic era has contributed to the completion of the first draft of the human genome, allowing the identification of almost all human protein kinases. [25, 27-29]

The human kinome comprises of 518 protein kinases (478 eukaryotic protein kinases and 40 atypical protein kinases), approximately 1.7% of all human genes.[27] Protein kinases constitute one of the largest human gene families and the relationships between the members of the complete superfamily is depicted in a phylogenic tree shown in figure 6. The most widely used human protein kinase classification phylogenic tree is constructed based on public and proprietary genomic, complementary DNA, and expressed sequence tag (EST) sequences.[25, 27-28] The tip of each branch represents a kinase and similarity is inversely related to the distance between positions on the tree.[30] This similarity among various kinases is the sequence and structure of their catalytic domain. The feature of a conserved catalytic domain was a main attribute used in the identification of the protein kinase family.[28-29] There are 7 major groups, consisting of smaller kinase families with highly related sequences and biological function. The grey branches in the center of the tree represent other kinases. According to Manning's classification of protein kinases, the major groups are: TK (tyrosine kinases); TKL (tyrosine kinase-like); AGC; CAMK (Calcium/calmodulin-dependant protein kinase); CKI (Casein kinase 1); CMGC; STE (Homologs of yeast Sterile 7, 11, 20 kinases); RGC *(*Receptor Guanylate Cyclases); AK (Atypical kinases) and other.[25]

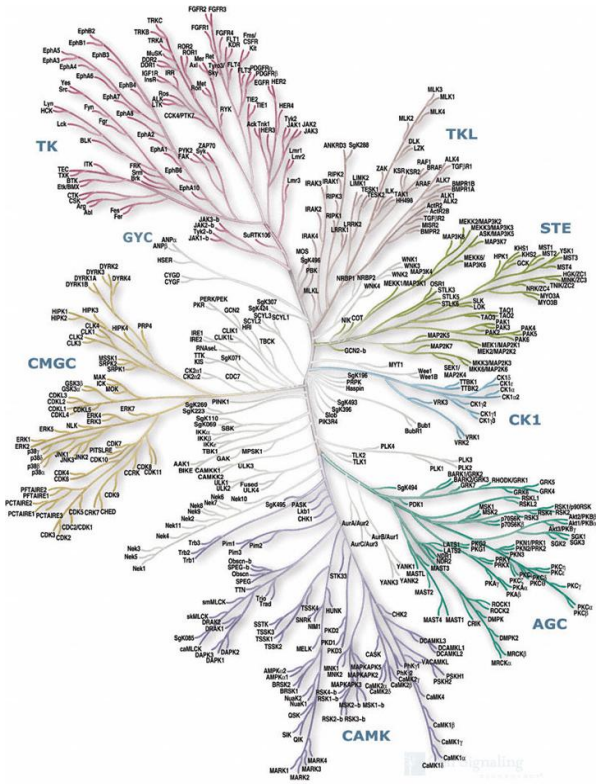

Figure 6

The phylogenic tree depicting the human kinome. Image reproduced from following reference.[31] For enlarged image visit kinase.com/human/kinome/.

One of the most commonly targeted families for the development of cancer therapeutics is the receptor tyrosine kinases (RTKs), which include the epidermal growth factor receptors (EGFRs), the vascular endothelial growth factor receptors (VEGFRs) and the platelet-derived growth factor receptors (PDGFRs).[20] The RTK class comprises 58 known members that are distinguished among 20 subfamilies. The fact that more than half of these cell-surface receptors are known to be mutated or overexpressed in diseases make them attractive candidates as targets. The EGFR family has four members: EGFR, human EGRF-related 2 (HER2) and the kinase impaired HER3 and HER4.[32] For the purpose of this project particular interest is directed towards the inhibition of EGFRs.

Cloning and sequencing of EGFR cDNA in the 1980s provided insight into its molecular architecture. EGFR is a large flexible glycoprotein with a modular structure containing an extracellular ligand-binding domain, a transmembrane region, and a cytoplasmic tyrosine-kinase region flanked by regulatory regions which are non-catalytic (tail).[32] When a ligand binds to this RTK, dimerization occurs. Autophosphorylation of key tyrosine residues in the activation loops of their catalytic kinase domains then follows, resulting in subsequent stimulation of tyrosine-kinase activity.[32] In the case of EGFR, the extracellular region is composed of four articulated domains that recognize the epidermal growth factor (EGF) ligand. On binding of the monomeric ligand to the receptor, the receptor opens up and binds to another copy of itself.[33-34] As seen on the right of figure 7, two ligands (red) bind to an EGF-induced dimer (blue). When EGF is absent the receptor folds back onto itself (left of figure 7).[33] EGFR dimerization is mediated entirely by receptor-receptor interactions and is activated by one of its many ligands, such as EGF or transforming growth factor alpha. Dimerization can either be with another EGFR (homodimerization) or one of the other receptors from the HER family (heterodimerization). This leads to the activation of the catalytic system of the tyrosine kinase, bringing about stimulation of signaling proteins inside the cell and activating multiple pathways (proliferation, angiogenesis, metastasis, etc.).[32, 34-35]

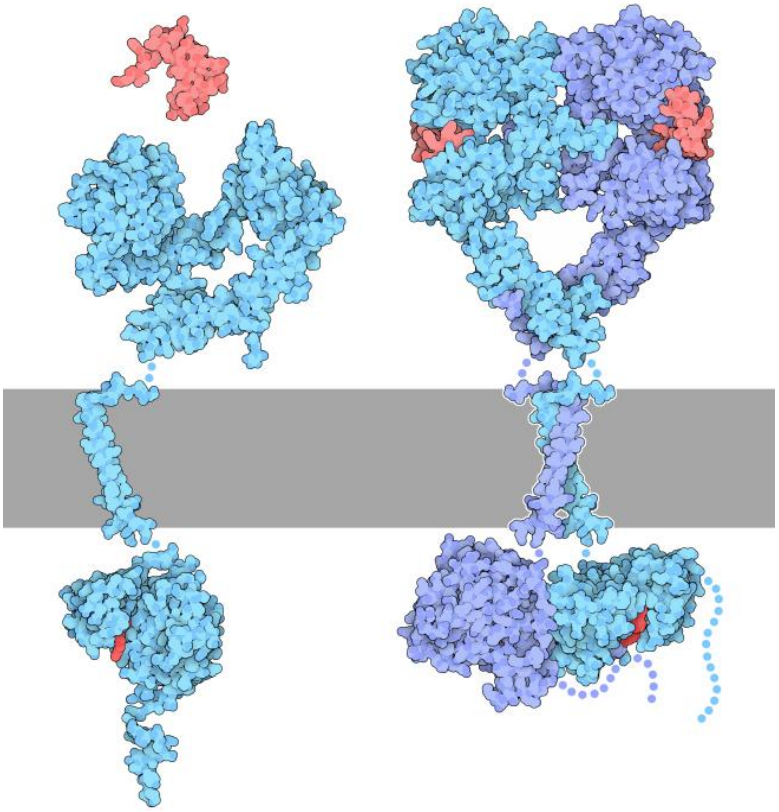

Figure 7
Depiction of the EGF (red) binding to the receptor EGFR (blue), forming a dimeric complex. Image reproduced from following reference.[33]

1.3.3 Kinase architecture

Before addressing the topic of kinase inhibitors, some insight into the architecture of kinases and their functioning is required. Protein kinase catalytic domains range from 250-300 amino acid residues and consist of 12 conserved subdomains of alternating regions of high and low conservation.[28] Hanks and Hunter proposed that the conserved subdomains are either directly involved in the catalytic function or indirectly by contributing to the formation of the active site. On the other hand, the non-conserved regions allow the conserved regions to come together, forming loop structures.[27-28] With technical advances, Hanks and Hunter's findings and proposals have been confirmed and a greater understanding of the internal composition of kinases has been obtained over the years.The structural core of eukaryotic protein kinases is organized in such a way that it contributes in a unique manner to their dynamic regulation and catalysis. This universal regulatory mechanism developed by protein kinases is associated with a large activation segment that can be folded or unfolded in the course of cell functioning. The complex regulatory machinery and their function as molecular switches, distinguish eukaryotic protein kinases from most metabolic enzymes.[36-37]

The catalytic domain contains most of the crucial machinery for catalysis and for scaffolding, to ensure controlled function of downstream signaling. Most protein kinases have a common bi-lobal fold made up of helical and beta subdomains.[37]

The two lobes converge to form a narrow hydrophobic pocket known as the ATP binging site.[38] The smaller N-terminal lobe (N-lobe) consists of five-stranded anti-parallel β-sheet coupled to a helical subdomain. These β-strands are essential for binding of ATP and contain a flexible glycine-rich loop (G-loop/P-loop) which anchors and position the γ-phosphate for phosphate transfer. The larger C-terminal lobe (C-lobe) is highly helical, plus a β-sheet, and is fairly conformationally stable. The helical subdomain forms the core of the kinase and serves as a tethering surface for protein/peptide substrates. The β-sheet resting on the core forms the bottom surface of the active site and consists of four short β-strands which contains much of the catalytic machinery. Between β-strands 6 and 7 lies the catalytic loop which direct the γ-phosphate of ATP to the protein substrate. Between β-strands 8 and 9 is the DFG motif, where a conserved aspartate (Asp) binds to a catalytic magnesium ion and engages in a salt bridge formation. The activation loop, containing threonine, serine or tyrosine residues, lies on the outer surface of the C-lobe and occupies part of the active site when the residues are not phosphorylated. When an upstream kinase activates phosphorylation the activation loop exposes the active site, allowing ATP to bind and transfer its γ-phosphate to a substrate. This substrate can often be a downstream kinase.[36-38]

The flexible hinge region which connects the N-lobe and C-lobe usually has one hydrogen donor with two hydrogen acceptors on one or either side of the donor atom.[38] The hinge region plays an integral role in the design of the kinase inhibitors, as hydrogen interactions to this region are considered vital for kinase recognition.[39] Another residue that plays an important role in protein kinase activation is the gatekeeper (gk) residue.[38] The size/volume of the gatekeeper side chain dictates access into the hydrophobic pocket. 77% of human kinases have relatively large gatekeeper residues (Leu, Met, Phe) while 21% of them (mostly in TK) have smaller gatekeeper residues (Thr, Val). Mutagenesis resulting in a reduction in size/volume of the gatekeeper side chain provides a potential inhibitor selectivity of the ATP site. Conversely, mutations that result in the steric enhancement of gatekeeper side chains have been responsible for drug resistance in certain patients.[36] T790M in EGFR is an example of such a mutation, where the gatekeeper residue threonine 790 is substituted with a much bulkier methionine side chain which interferes sterically with the inhibitor binding and increases ATP affinity.[40] Figure 8 shows ATP bound in a kinase active site, depicting the N-,C-lobe, hinge region and gatekeeper.[38] Although the internal architecture of kinases is similar, they exhibit a variety of conformational states. Since kinase inhibitors target either the active or inactive conformation of kinases, these two distinctive states will be briefly discussed.

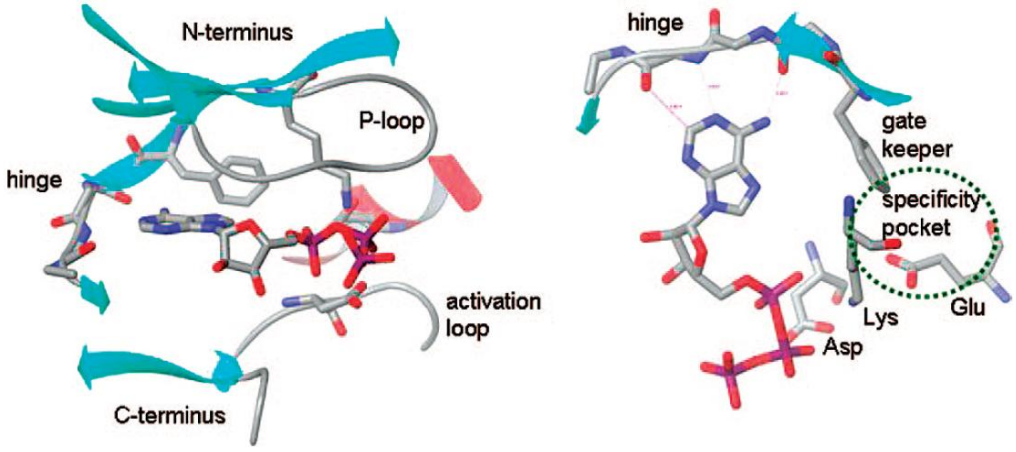

Figure 8
Diagram illustrating ATP bound in the active site between the N- and C-lobe. The hinge region and gatekeeper are depicted on the right. Image reproduced from following reference.[38]

Johnson and co-workers stated that, "All active kinases are alike, but an inactive kinase is inactive after its own fashion."[41] Kinases switch between active and inactive conformations, a process that is highly regulated and complex. Analysis of local spatial pattern (LSP) alignments of kinases has revealed an architecture that is fully assembled in the active conformation of the kinase, but that is broken in the most inactive kinases. The LSP studies further revealed the presence of conserved hydrophobic motifs which contribute to the overall kinase assembly and architecture. These hydrophobic motifs, termed spines, provide a firm, but flexible connection between the lobes and are anchored to the F-helix in the middle of the C-lobe (Figure 9). Two spines, the 'regulatory' spine (R-spine) and 'catalytic spine' (C-spine), have been identified.[36-37]

The R-spine is assembled as a consequence of phosphorylation, and causes the DFG motif to flip so that the phenylalanine is repositioned. This completes the R-spine and reveals the hydrophobic pocket. The movement also leaves the Asp to interact with a magnesium ion. This completed R-spine is referred to as a "DFG-in" conformation. In the inactive kinase state, the R-spine is broken and is referred to as a "DGF-out" conformation. The 180° flip of the highly conserved DFG motif changes the activation loop structurally to an inactive (DFG-out) conformation, resulting in obstruction of ATP binding and exposure of adjacent allosteric sites.[42] However, it is important to evaluate the overall spine configuration before classifying a kinase as active or inactive, since certain DFG-in conformations can be inactive if the R-spine is disrupted in another way. The R-spine is therefore a fundamental feature of the "switch mechanism" and plays a key role in regulation of kinase activity.In a similar manner to the insertion of phenylalanine to complete the R-spine, the C-spine is completed by the adenine ring of ATP.[36-38]

Although the most crucial catalytic machinery is located in the core of the kinase, the presence of flanking regions or domains (linkers and tails) which are anchored to the core, play an essential role in assisting catalysis and regulation.[37] Kinases employ a number of different regulatory mechanisms to tightly regulate their activity. These regulatory mechanisms have been discussed in literature.[20, 43-44] Furthermore, multiple specificity mechanisms including structural features, complex formation and interactions between kinases and substrates, have been evolved by kinases to recognize particular substrates and phosphorylation sites.[24]

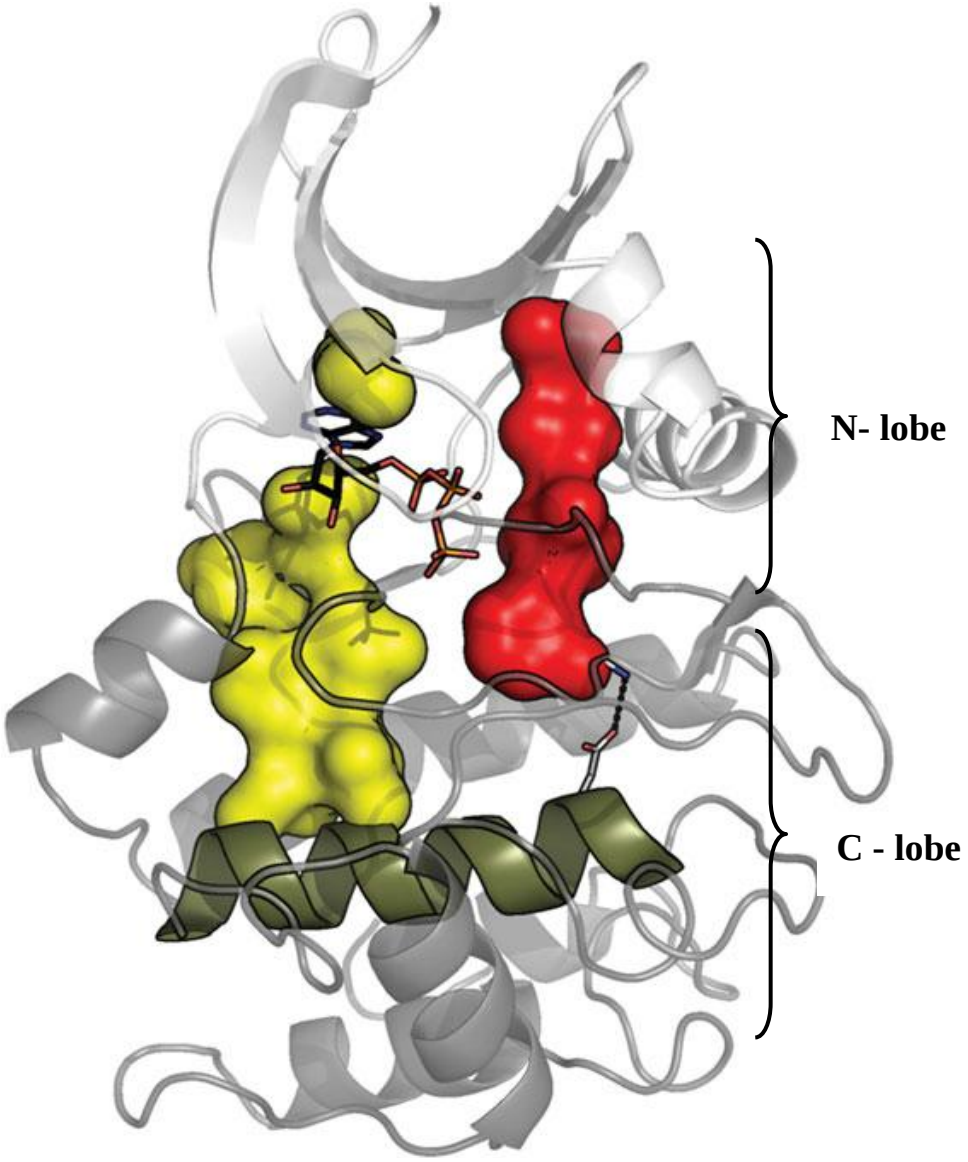

Figure 9
The two hydrophobic spines and F-helix, defining the internal architecture of the protein kinase molecule. The red R-spine and yellow C-spine are anchored to the green F-helix. Image reproduced from following reference.[36]

1.4 Targeting kinases

1.4.1 Types of kinase inhibitors

Protein kinases have developed into one of the more important target class in cancer drug discovery.[45] The first protein-kinase inhibitors were developed by Hidaka in the early 1980s, following the discovery of the first oncogene, vSrc, and its identification as an enzyme with tyrosine kinase activity. Inhibitor development projects were initially met with skepticism but the discovery of staurosporine, with its potent kinase inhibitor activity, made the pharmaceutical industry take notice and initiate drug development efforts. A landmark event occurred in 2001 when Imatinib (Gleevec) was approved for clinical use and provided motivation for the pursuit of kinase inhibitor design. Since then, the pharmaceutical industry has applied a large portion of their resources to the search for small molecule kinase inhibitors as target therapeutic agents.[38, 45-46] Over the past two decades, 23 ATP competitive kinase inhibitor drugs have been approved and a large number of compounds are currently in preclinical and clinical development.[47] Despite the recent successes in targeted therapy and kinase inhibitors, lack of efficacy, drug resistant mutations and inhibitor selectivity persist as fundamental challenges in the development of effective long-term cancer treatments.[42, 48]

Although protein kinases serve as an attractive candidate to target in oncology, their "drugability" is significantly challenging. Three principle ways in which protein kinases can be inhibited exist: ATP-competitive binding, competitive binding to the protein substrate site, and non-competitive binding at a remote site which allosterically disrupts enzyme function.[20] Understanding inhibitor binding modes is very useful for the rational design of drugs. For this reason, the manner in which protein kinases inhibitors bind will be discussed in more detail.[38]

The most commonly observed binding mode involves the inhibitor binding in and around the region occupied by the adenine ring of ATP. These inhibitors are classified as *type I* inhibitors and bind with the activation loop consuming a conformation conductive to phosphate transfer (active conformation).[47, 49] *Type I* inhibitors may form zero to three hydrogen bonds to the kinase hinge segment which often mimic the binding interactions of the adenosine moiety.[20, 47] The region of inhibition is further divided into subregions, namely: the hydrophobic region I and II, the adenine region, the ribose region and the phosphate binding region (figure 10). All *type I* inhibitors occupy the adenine region, but the ability to bind to other regions promote inhibitor selectivity.[49] Classic kinase inhibitors such as staurosporine, dasatinib and gefitinib are examples of *type I* inhibitors shown in figure 11.[42, 47]

Mutations affecting *type I* inhibitors that commonly occur are located at the gatekeeper position in the hinge segment where an enhancement in size/volume of the gatekeeper residue occurs (classically Thr is exchanged for Ile or Met).[42]

Serendipity, combined with structure-activity relationship analysis, particularly when Imatinib was co-crystalized with Abl, led to the discovery of *type II* binding mode. *Type II* inhibitors can also bind to the hinge region, but take advantage of the DFG-out conformation where an additional hydrophobic pocket adjacent to the ATP pocket, referred to as an allosteric site, is available for binding (Figure 10).[42, 49] These interactions in the allosteric site are characteristic of *type II* inhibitors and a hydrogen-bond pair between the inhibitor and the residues in the allosteric site is conserved in all *type II* modes of binding. All *type II* inhibitors also have a hydrophobic moiety, which forms van der Waals interactions with the allosteric site.[49] Three classic examples of *type II* inhibitors include Imatinib, Nilotinib and Sorafenib.[50] Another well categorized class of inhibitors, *type III*, comparing molecules which bind outside the ATP-binding site at an allosteric site and allosterically modulates the kinase enzymatic activity. CI-1040 is an example of a *type III* inhibitor and inhibits MEK1 and MEK2 by occupying a pocket adjacent to the ATP binding site.[50] *Type IV* inhibitors are also classified as allosteric inhibitors, but bind at remote sites on the kinase. GNF-2, GNF-5 and MK-2206 are examples of inhibitors that demonstrate *type IV* binding interactions.[47, 50]

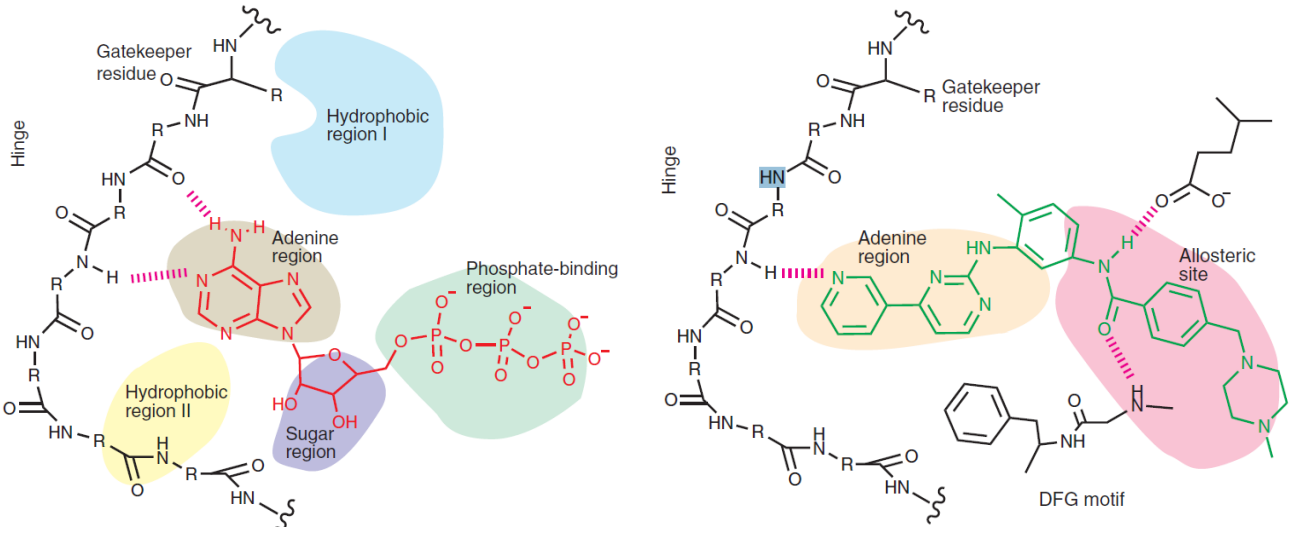

Figure 10
Representation of the ATP binding site divided into subregions (left) and Imatinib binding to an additional allosteric site (right). Image reproduced from following reference.[49]

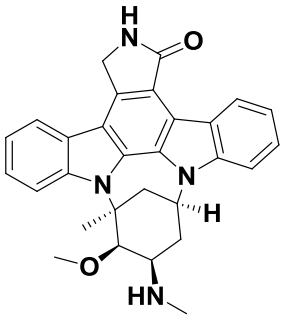

Staurosporine

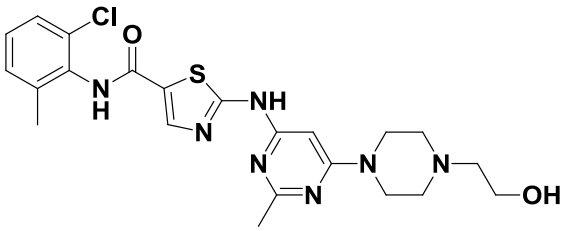

Dasatinib

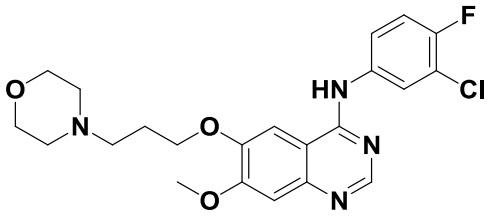

Gefitinib

Figure 11

Examples of *type I* kinase inhibitors.

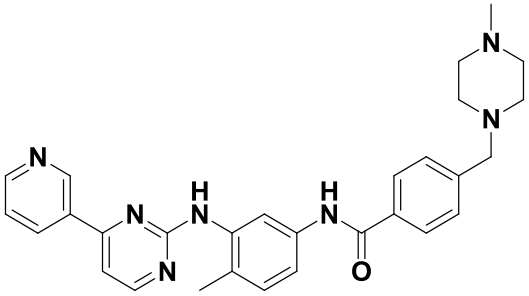

Imatinib

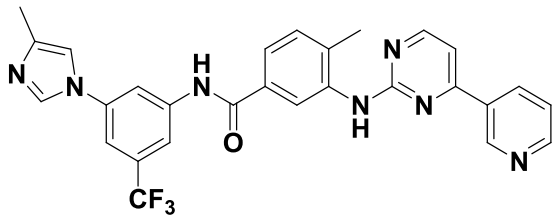

Nilotinib

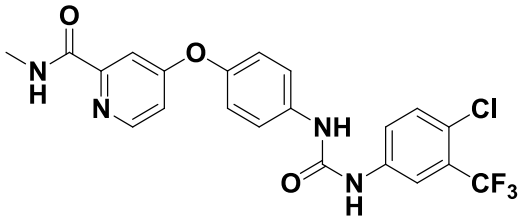

Sorafenib

Figure 12

Examples of *type II* kinase inhibitors.

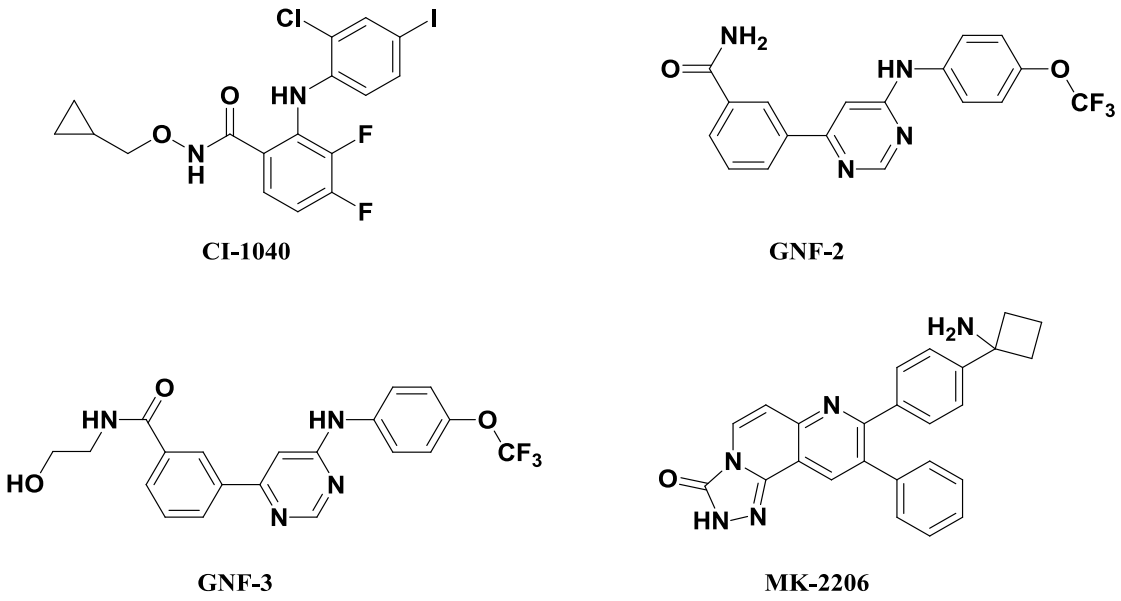

Figure 13

Examples of *type III* and *type IV* kinase inhibitors.

The majority of small molecule kinase inhibitors bind in or around the ATP binding site, thereby preventing ATP from binding.[47] As described before, the catalytic domain in the active conformation is highly conserved throughout the kinase family, and this has been regarded as a major challenge in designing inhibitors with target specificity. Furthermore, potency of inhibitors is crucial to compete with high intercellular ATP concentrations.[20] In addition, improved specificity for the intended target and selective regulation reduces off-target side effects and prevents inhibition of kinases involved in normal physiology.[51]

Although a few examples of highly selective ATP-competitive kinase inhibitors exist, the majority of cases are troubled by selectivity issues, especially in the case of *type I* inhibitors which target the highly conserved active conformation. Targeting alternative sites which become accessible when the kinase adopts the inactive conformation, can address the challenges of selectivity and drug target residence times.[48] *Type II* inhibitors are indirectly ATP-competitive, but since the amino acids in the allosteric pocket are less conserved throughout the kinase family, it has been proposed that kinase selectivity may be more easily achieved.[49] Furthermore, the lower affinity for ATP in the DFG-out conformation, compared to the active conformation, attribute to the potent cellular activity of *type II* inhibitors.[49] *Type III* and *IV* inhibitors have purely allosteric modes of action and tend to exhibit the highest degree of kinase selectivity, as they exploit unique binding sites and regulatory mechanisms of particular kinases or kinase families.[48, 50]

The majority of inhibitors developed thus far are ATP-competitive compounds since they target the ATP binding or surrounding sites. These compounds inhibit protein catalytic activity in a reversible manner by binding through weak interactions (hydrogen bonds, van der Waals forces and hydrophobic interactions).[52] The challenges implicated with these ATP-competitive, reversible drug candidates attributed to the emerging strategy to develop kinase-targeted drugs that are irreversible.[40] Over the past century there have been many examples of medicines that are covalent drugs and some covalent, irreversible inhibitors include the anti-inflammatory drug aspirin and antibiotics such as penicillin.[53-54] The different types of kinase inhibitor binding modes are illustrated in figure 14. The development of irreversible kinase inhibitors began in the late 1990s and will be discussed in the next subsection.[55]

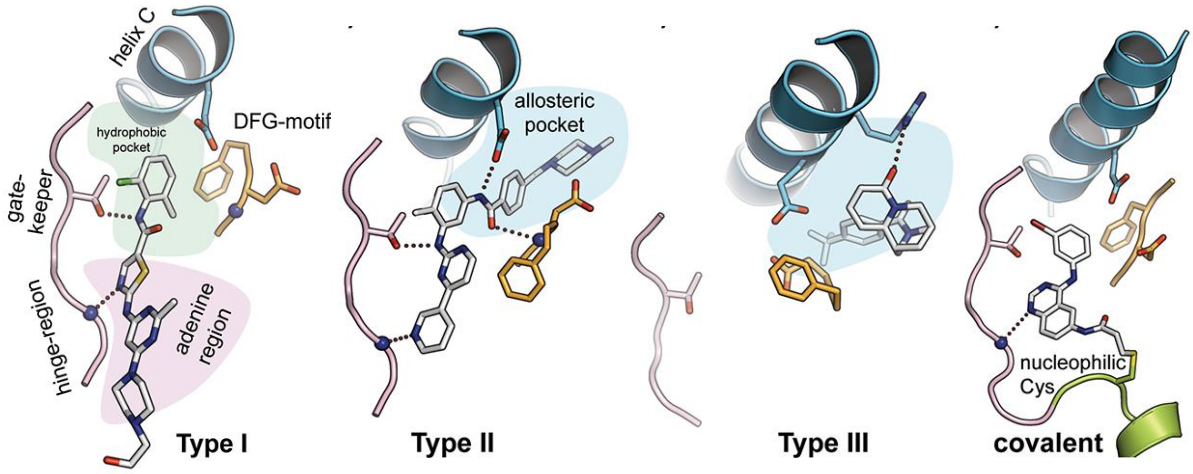

Figure 14
The various modes of binding to the kinase by the different types of inhibitors. Image reproduced from following reference.[48]

1.4.2 Irreversible kinase inhibitors

An important factor for the therapeutic success of protein kinase inhibitors is the amount of time spent by the inhibitor in the kinase nucleotide binding site. This is particularly important since these inhibitors generally compete with high concentrations of intracellular ATP.[56] In this regard, irreversible kinase inhibitors behave in a non-competitive manner to ATP, by binding covalently and shifting the physiological equilibrium between ATP and the target kinase. Hereby, the catalytic activity of the kinase is permanently inhibited by remaining bound to the kinase active site, even when the level of the drug administered is lowered.[55] Since covalency inactivates the enzyme and biological effects persist even after the inhibitor has left the circulation, in principle there is no need to maintain high levels of drug concentration to achieve continuous target engagement.[52-53]

In addition, irreversible inhibitors have the potential to overcome resistance due to the fact that they are less affected by changes in the ATP binding affinity, which can occur with mutant forms of the kinase.[52] The aggressive relapse of 50% of non-small cell lung cancer (NSCLC) patients treated with the ATP-competitive, reversible inhibitors erlotinib and gefitinib is a classic example of the emergence of a secondary drug-resistant mutation.[55] This mutation at the gatekeeper residue (T790M in EGFR) is a common mechanism of acquired resistance to kinase inhibitors and was discussed earlier (see section 1.3.3). Irreversible inhibitors have shown to overcome this drug resistance and a number of irreversible drug candidates have progressed to late stage clinical development.[40, 57-58]

Another major advantage of irreversible inhibitors is improved selectivity, since only the kinases involved in the covalent interaction with the inhibitor will be inactivated.[52] Most covalent inhibitor strategies target a highly nucleophilic cysteine thiol present in the target protein. Structural analysis of different conformations of the protein kinases, have revealed a thorough landscape of cysteine positions that can be harnessed for irreversible inhibition. As mentioned before, the shape of the ATP binding pocket has been classified as three conformations (active, inactive C-helix-out and inactive DFG-out) and the number of cysteine positions shared between kinases have been grouped accordingly.[56] Liu *et al.* performed an informatics study in which 442 kinases were superimposed and their ATP-binding sites were evaluated to construct a graphical image of the accessible cysteines in the kinome. Figure 15 shows the representative positions of the accessible cysteines in the active site, as constructed by Liu *et al*.[53]

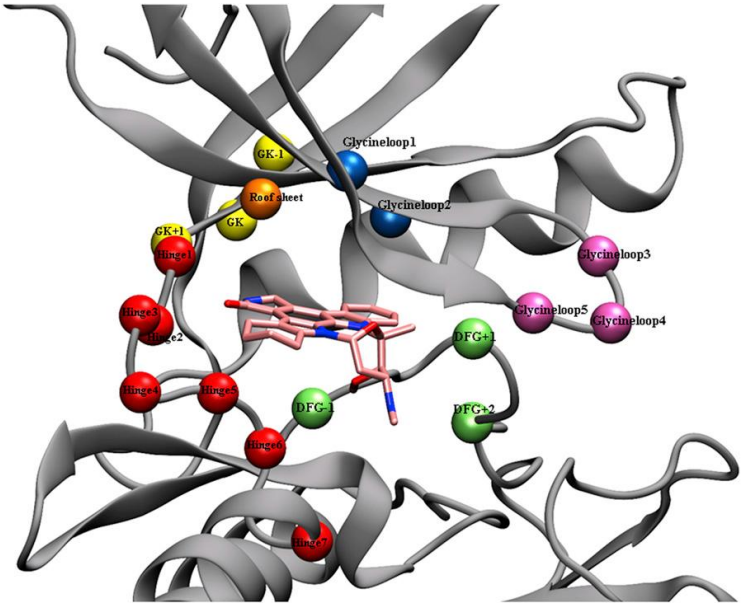

Figure 15
Depiction of staurosporine in the kinase domain, displaying the various accessible cysteine positions in the kinome, as constructed by Liu *et al*. Image reproduced from following reference.[53]

Many protein kinases possess cysteine residues in and around the ATP-binding site, but only a very small fraction of these kinases (20 kinases) have been targeted by currently available irreversible inhibitors. To date, only six distinct cysteine positions have been targeted. Due to the fact that the main focus of this project is directed towards EGFR inhibition, the cysteine target (Cys797) for EGFR irreversible inhibitors is important. Cys797 is located at the lip of the ATP binding site (just after the hinge region) and is present in 11 kinases.[52-53] Harnessing very particular cysteine positions shared between only a few kinases illustrates the opportunity to enhance selectivity for target kinases. The reactivity of the cysteine thiol varies according to the protein microenvironment (chemical and location), which allows for additional fine tuning (selectivity and specificity) of the inhibitor.[56] Furthermore, the identification of more accessible cysteine residues in different kinase conformations, unlocks tremendous potential to develop new irreversible inhibitors.[52, 56]

Covalent irreversible kinase inhibitors have typically been developed by incorporating an electrophilic moiety to a noncovalent inhibitor which already possesses submicromolar binding affinity for the kinase targeted.[53] Irreversible TK inhibitors are generally characterized by a heterocyclic core structure known as a driving portion. This driving portion docks into the active site of the kinase domain and resembles features of reversible inhibitors. The core structure carries, at a particular position, an electrophilic functionality known as a "warhead". It is this "warhead" which covalently interacts with a nucleophilic cysteine residue in or near the ATP-binding site.[52] The irreversible covalent bond is mostly achieved through a Michael reaction (Scheme 2). Functional groups typically used as Michael acceptors (warheads) in irreversible kinase inhibitors are illustrated in figure 16.[53]

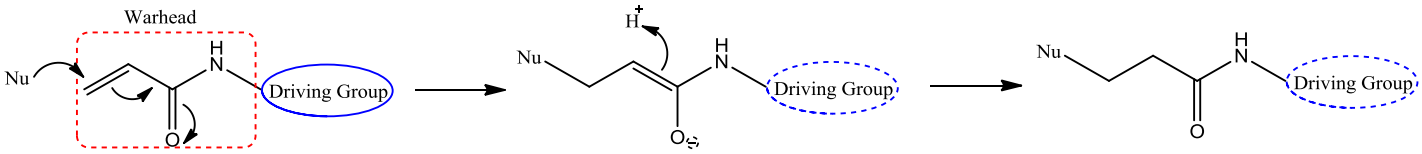

Scheme 2

Conjugate addition of the nucleophile to the β-carbon forms a covalent bond in irreversible inhibition.[52]

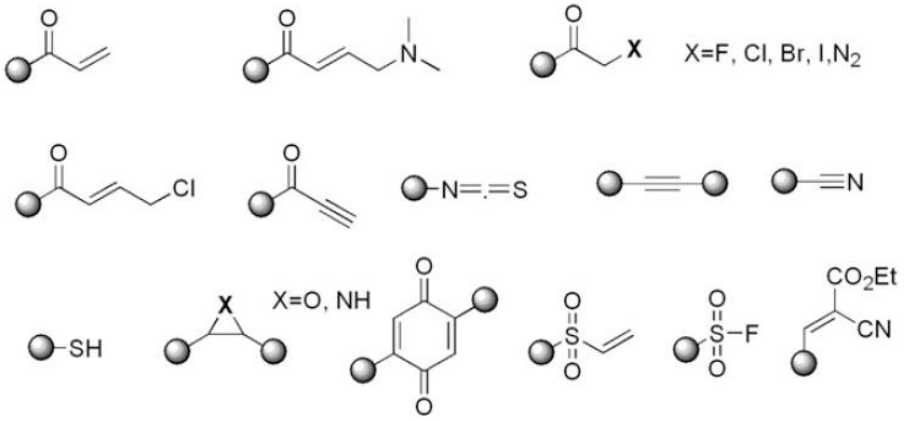

Figure 16
Electrophilic "warheads" used in irreversible kinase inhibitors. The black spheres represent the driving portions or other pharmacophore structures. Image reproduced from following reference.[53]

A drawback of covalent irreversible inhibitors is promiscuity and the risk of covalently binding to other solvent exposed thiol groups. This leads to non-selective reactions with off-target proteins and increased toxicity. [52, 55] An integral part of drug optimization is to design compounds with a suitable driving portion, having at a particular position a low intrinsic reactive electrophilic warhead. The covalent reaction between the cysteine residue and inhibitor can only occur once the driving portion reversibly docks into the active site, interacts with the hinge region, and presents the reactive counterparts at a favourable distance and orientation.[40, 52] In order for the driving portion to present a suitable "platform" to incorporate the electrophilic "warhead" at the proper trajectory, the less flexibility there is between the target cysteine and the electrophile, the more encouraging the chances that only a single cysteine residue will be targeted.[53]

Lung cancer is the most common cause of cancer related deaths worldwide. NSCLC accounts for almost 85% of all lung cancers. EGFR is the focus of many new treatment strategies and has become a well-established target for the treatment of patients with NSCLC.[58-59] Oncogenic activating mutations of EGFR result in abnormal signaling for 10-30% of NSCLC patients. In 2000, two first generation inhibitors - gefitinib and erlotinib - moved from the bench to the clinic. These inhibitors act in a reversible manner and are ATP competitive. [35] NSCLC patients with the most common EGFR mutations respond well to therapy with gefitinib and erlotinib, but unfortunately 50% of these patients develop a secondary drug-resistant mutation (T790M).[55, 60]

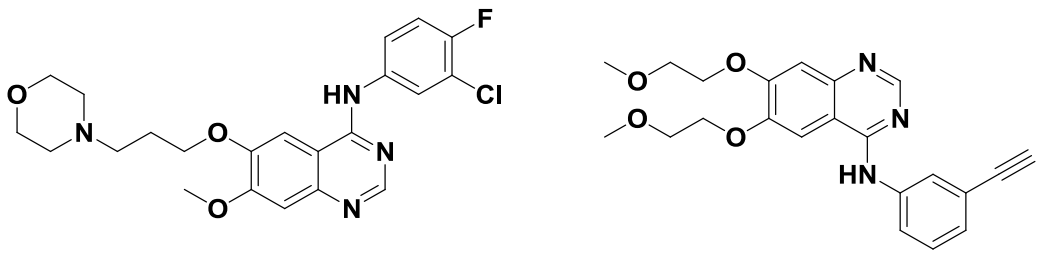

Gefitinib **Erlotinib**

Figure 17
Structures of the first generation inhibitors gefitinib and erlotinib.

The advantages associated with covalent irreversible inhibitors have sparked a growing interest in their development and number of effective second generation irreversible EGFR inhibitors have progressed to late stage clinical development (figure 18).[52, 58, 61-62] Clinical evidence suggests that superior performance of these drugs relative to reversible inhibitors is evident, but the emergence of drug resistance is also limiting their activity. Mechanisms of drug resistance include reversible cysteine-inhibitor warhead interactions and specific cysteine oxidation, which are currently under investigation.[58, 60] The ongoing war on cancer and pursuit to develop more efficient, potent and safe therapeutic agents is an essential part of oncology research, particularly when the enemy is of such a complex and deadly nature.

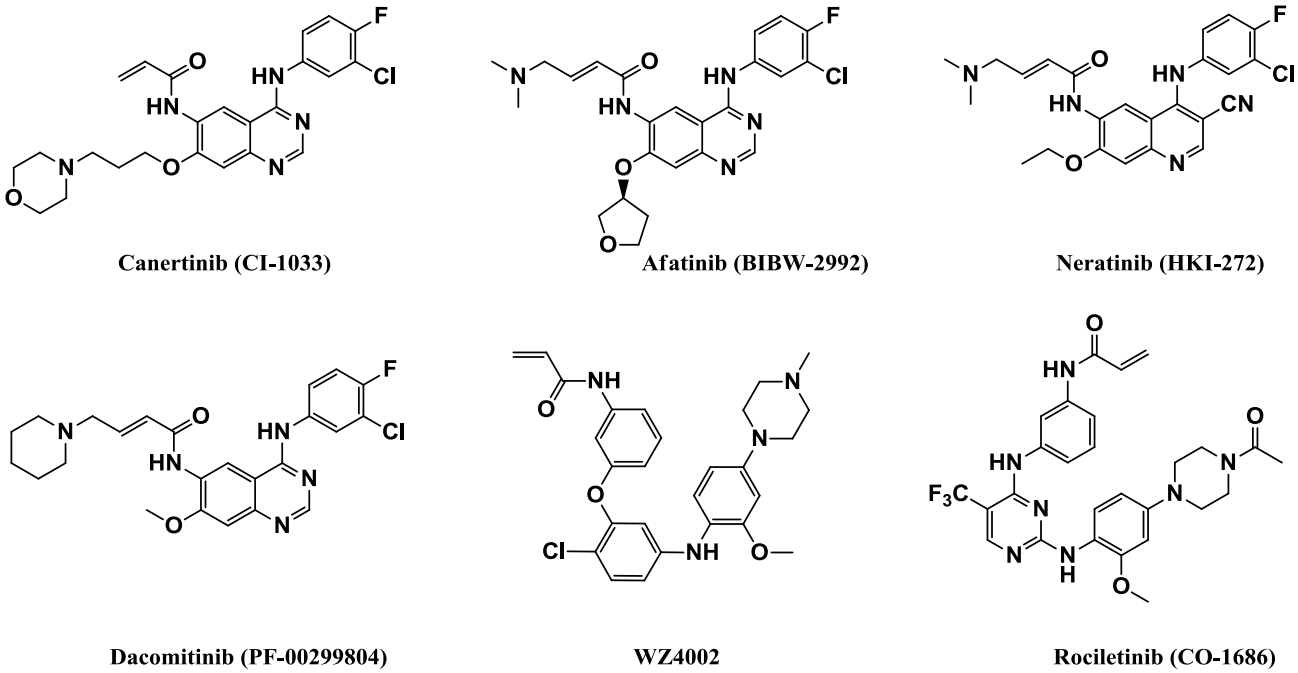

Canertinib (CI-1033) **Afatinib (BIBW-2992)** **Neratinib (HKI-272)**

Dacomitinib (PF-00299804) **WZ4002** **Rociletinib (CO-1686)**

Figure 18
Irreversible EGFR inhibitors in clinical trials.[52-53]

1.5 Natural products

1.5.1 The inspiration from natural products and chemical space

Aristotle stated that "Nature creates nothing without purpose or uselessly".[63] Nature's symphonic processes have inspired human creation in fields such as science, arts and architecture for millennia.[64] Throughout the ages people have relied on natural products for the treatment of a wide spectrum of diseases with some of the earliest records dating from around 2600 BC.[65]They form the basis of most early medicines and have played an essential role in drug discovery, particularly in the development of chemotherapy and oncology.[66] The complex and diverse secondary metabolites (natural products) are formulated within an organism - through interactions with the environment - to enhance their survival and competitiveness.[67] Natural products have evolved to interact with multiple proteins, displaying a variety of biological activities and being effective modulators of almost all basic cellular processes.[68] The scaffolds of these compounds are thought of as evolutionary-chosen "privileged structures", positioning them as pre-validated starting points for library design.[69-70] Today, natural products remain a major source of inspiration in drug development and often serve as a structural 'muse' for the design of new biologically active small molecules.[69]

In the 1980s and 1990s, with the emergence of combination therapy, the focus of drug discovery shifted from Nature to the laboratory bench. However, synthetic chemists soon realized that new libraries lacked the "complexity" associated with natural products and this led to a shortage of lead compounds progressing into clinical trials.[66, 71] The decade of 2000s witnessed a recovery in natural product drug discovery. Between 2005 and 2010, a total of 19 natural product based drugs were approved for marketing worldwide.[67] An analysis of sources of new drugs over a certain period (1981-2010) indicated that only 36% of the 1073 chemical new entities can be classified as truly synthetic – i.e. with no natural product conception. The various classes are represented in a pie chart (figure 19), illustrating the immense contribution of natural products.[65] Furthermore, of the 115 small molecules approved as anticancer drugs (1940s–2006), 73% are naturally derived agents, including 47% either being natural products or derivatives thereof.[72]

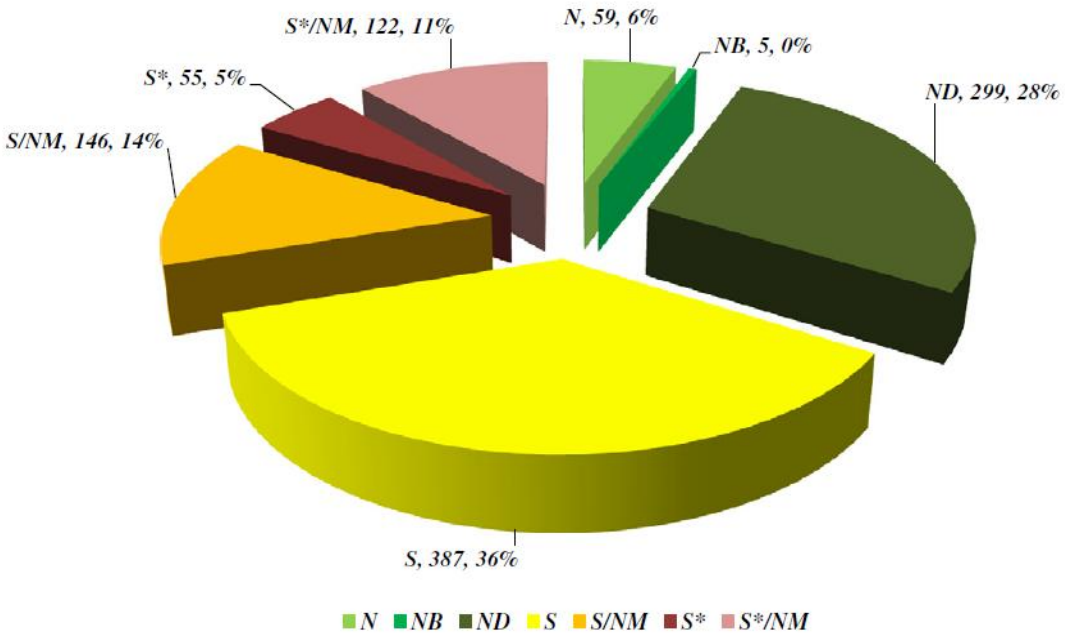

Figure 19

Classification of new drug sources. Keys: N (natural product unmodified); NB (natural product botanical); ND (natural product modified); S (purely synthetic); S/NM (synthetic compound showing competitive inhibition of natural product substrate); S* (synthetic compound with natural product pharmacophore); S*/NM (synthetic compound with natural product pharmacophore showing competitive inhibition).Image reproduced from following reference.[65]

Chemical space is enormous with estimates of 10^{63} small molecules populating drug-like chemical space. It should thus be obvious that is impossible to investigate all these opportunities by means of synthetic efforts. Therefore, a key challenge in chemical biology research and drug discovery is to identify, map and navigate biologically relevant chemical space.[69-70] Several different approaches, in particular ones employing evolutionary arguments (sequence homology), mechanistic considerations, and the generation of chemical diversity (diversity-orientated synthesis, DOS), have been developed in the quest to identify these biologically relevant areas in chemical space.[73-75] Natural products can display a vast range of biological activities when their common shared scaffold differs only in substitution pattern. Of significance is that only a tiny fraction of chemical space based on natural product scaffolds has been exploited. In fact, both protein folds and natural product scaffolds are highly conserved in nature. For this reason, only a limited number of small-molecule binding sites inspire rational approaches to inhibitor and ligand development.[73, 75] As mentioned earlier, natural products have been regarded as biologically pre-validated since they were chosen by evolution to interact with their biological targets. This fact, together with their particular molecular properties which encode architecture for substance recognition by enzymes and proteins, has led to the concept of biology-orientated synthesis (BIOS).[70, 76]

BIOS employ chem- and bio-informatics methods for mapping biologically relevant chemical space and protein space to generate hypotheses for compound collection design and synthesis.[73] This strategy therefore builds on the inspiration given by nature through natural products, exploiting their structural conservatism and diversity.[75-76] BIOS makes use of a hierarchical organization concept named "structural classification of natural products" (SCONP). This concept is based on a set of defined rules derived from organic and medicinal chemistry, to step-wise deconstruct the larger natural product scaffolds (child scaffolds) into smaller parent structures. This approach led to the SCONP scaffold tree where each chemical entity is a substructure of the original natural product, providing a way to reduce molecular complexity while retaining bioactivity. An illustration of the SCONP scaffold tree is depicted in figure 21.[70, 73, 75] Another concept used in BIOS is the protein structure similarity cluster (PSSC), which identifies ligand binding sites with high subfold similarity and attempts to link them to new potential biological targets of small molecules.[73] The merging of SCONP and PSSC led to the BIOS approach which serves to identify new starting points in chemical space for the design and synthesis of small-molecule libraries, in order to find new ligands for particular protein domains (figure 21). [73, 75] Small molecules synthesized according to BIOS are enriched in bioactivity and the synthesis of natural products has inspired compound collections with high scaffold, substituent and stereochemical diversity.[73, 75] However, it is often necessary to improve selectivity and potency of these protein ligands in subsequent optimization studies, since many compounds in BIOS libraries show limited selectivity.[73]

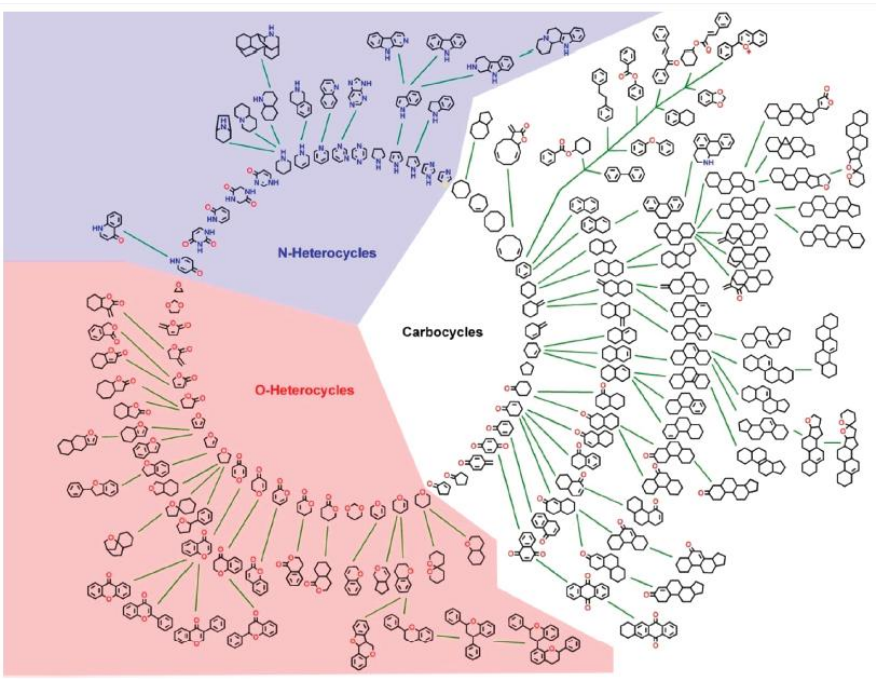

Figure 20
SCONP scaffold tree of natural products. Image reproduced from following reference.[69]

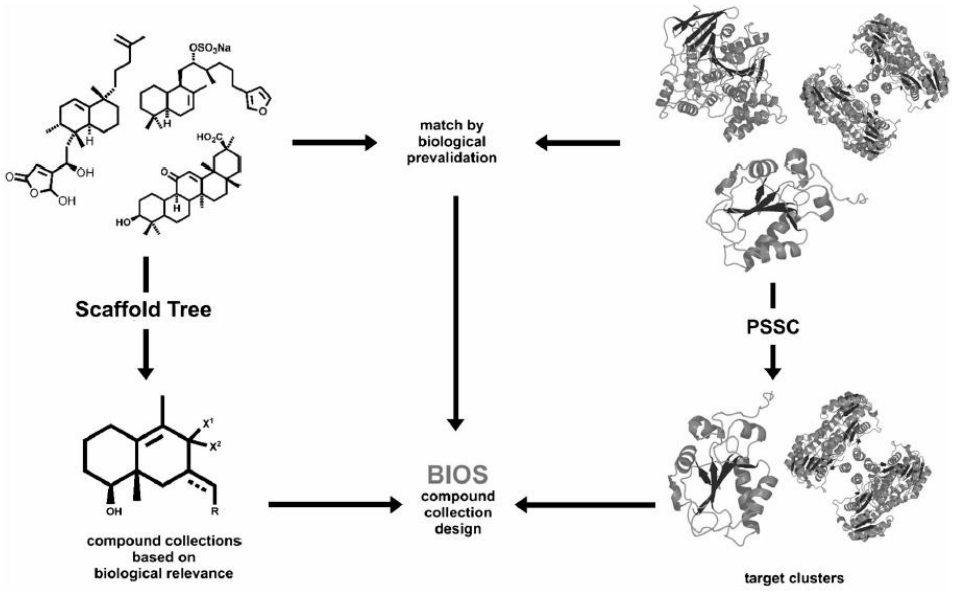

Figure 21

BIOS connects chemical and biological space by using the SCONP and PSSC approach. Image reproduced from following reference.[70]

Plants have been used for the treatment of cancer throughout history and have formed the basis of sophisticated traditional medicine systems.[65, 77] Almost all of the current drugs derived from natural products are of terrestrial origin.[78] Natural products from marine organisms do not have a significant history in traditional medicines and their investigation was limited before the mid-1960s. The development of scuba diving, improved technology for deep-sea collections and large-scale aquaculture production opened the world's oceans as an enormous resource for the discovery of potential chemotherapeutic agents.[65, 78] The diversity of marine habitats and unique environmental conditions of the sea, offers mostly untapped sources of potential drugs with superior chemical novelty compared to terrestrial natural products. More than 20000 natural products have been isolated from marine life-forms. The review by Bharate and co-workers discusses and analyzes various marine-derived kinase inhibitors that are currently in various stages of clinical development.[78]

Microorganisms of both terrestrial (plants and soil) and aquatic origin have provided some of the key drugs for cancer chemotherapy.[77] They are either used directly for cancer treatment or modified to modulate activities against tumor cell growth. The bacteria from the order, *Actinomycetales* have produced some of the most impressive compounds directly from nature or semi-synthetic modifications. These bacteria have been the leading producers of medically useful drugs and introduce the natural product of interest for this project, called staurosporine.[79]

1.5.2 Staurosporine

The discovery of staurosporine was made in 1977, when it was isolated from the bacterium *Streptomyces staurosporeus*, while screening for microbial alkaloids in a culture of soil. [80] Over the past few decades, staurosporine and related natural indolocarbazole compounds (more than 50) have been isolated from various *Actinomycetes*, slime molds, cyanobacteria and marine invertebrates.[78, 81] The structure of staurosporine is shown in figure 22. A decade after the isolation of staurosporine, its potent kinase activity was identified.[82] This discovery offered tremendous promise for drug development and stimulated a variety of medicinal programs aimed at synthesizing staurosporine analogues based on this compound. Numerous pharmaceutical companies pursued the search for selective kinase inhibitors by screening natural products and through chemical synthesis.[46, 81, 83]

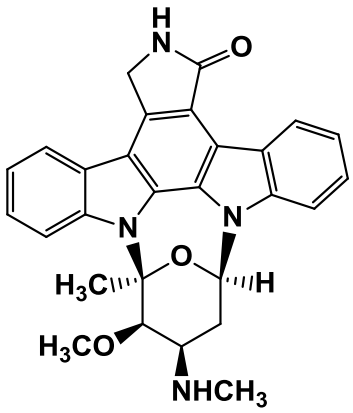

Figure 22
The natural product staurosporine.

Initially, staurosporine was shown to be a nanomolar inhibitor of protein kinase C (PKC), but further investigation showed that staurosporine inhibited a "cocktail" of kinases.[83] In fact, staurosporine inhibits the majority of human protein kinases and it is as a result of this promiscuity that staurosporine itself is not a viable option as an effective anticancer agent. The lack of selectivity demonstrated by staurosporine has been shown to lead to toxic, off-target activities.[84] However, this natural product has been widely used in research as a universal kinase inhibitor and serves as a "structural muse" to design protein kinase inhibitors with improved specificity and selectivity.[78, 84-85]

Staurosporine possesses all the elements that define an ATP-competitive inhibitor and numerous co-crystal structures with various kinases reveal a common binding mode. The structure consists of a hydrogen bond donor/acceptor pair, a large rigid planar structure, and an aromatic ring system to complement the ATP binding pocket.

All of these structural features ensure that staurosporine mimics the natural binding interactions that provide the recognition and orientation of ATP in protein kinases. This explains why staurosporine interacts with such a wide range of serine/threonine and tyrosine kinases. Staurosporine docks into the ATP binding pocket with the planar indolocarbozole sandwiched between the N-lobe and C-lobe, oriented by hydrogen bonds to the hinge region. This mimics the adenine base of ATP. In addition, the indolocarbozole and sugar ring form a boat-shaped conformation within the kinase active site. Another hydrogen bond is formed between the methyl amino group on the sugar ring and a largely hydrophilic residue which normally stabilizes the ATP ribose hydroxyl moiety. These electrostatic interactions are illustrated as dashed lines in figure 23. Staurosporine is further stabilized by van der Waals interactions between the aromatic plane of staurosporine and the side chains of amino acids lining the ATP pocket. Many CH-π interactions between the conjugated indolocarbazole and CH moieties of these side chains have also been identified.[20, 78] Molecular modelling of staurosporine within the EGFR kinase domain is illustrated in figure 24. The hinge region interactions between staurosporine amide and residues Met793 and Gln791in the EGRF domain are highlighted on the right.

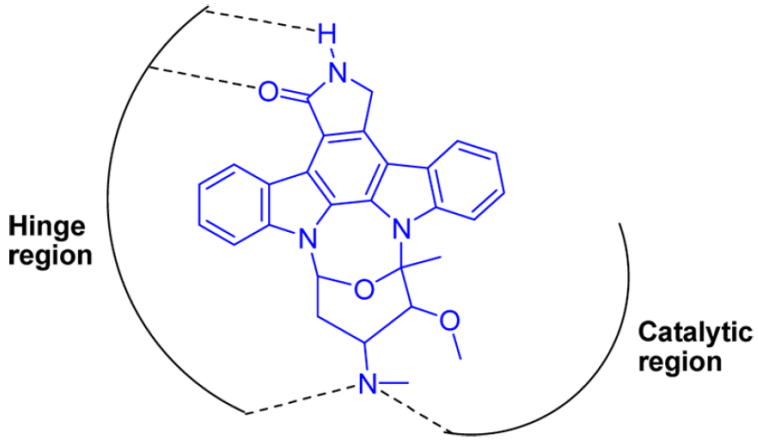

Figure 23
Important interactions (dashed lines) of staurosporine in a protein kinase. Image reproduced from following reference.[78]

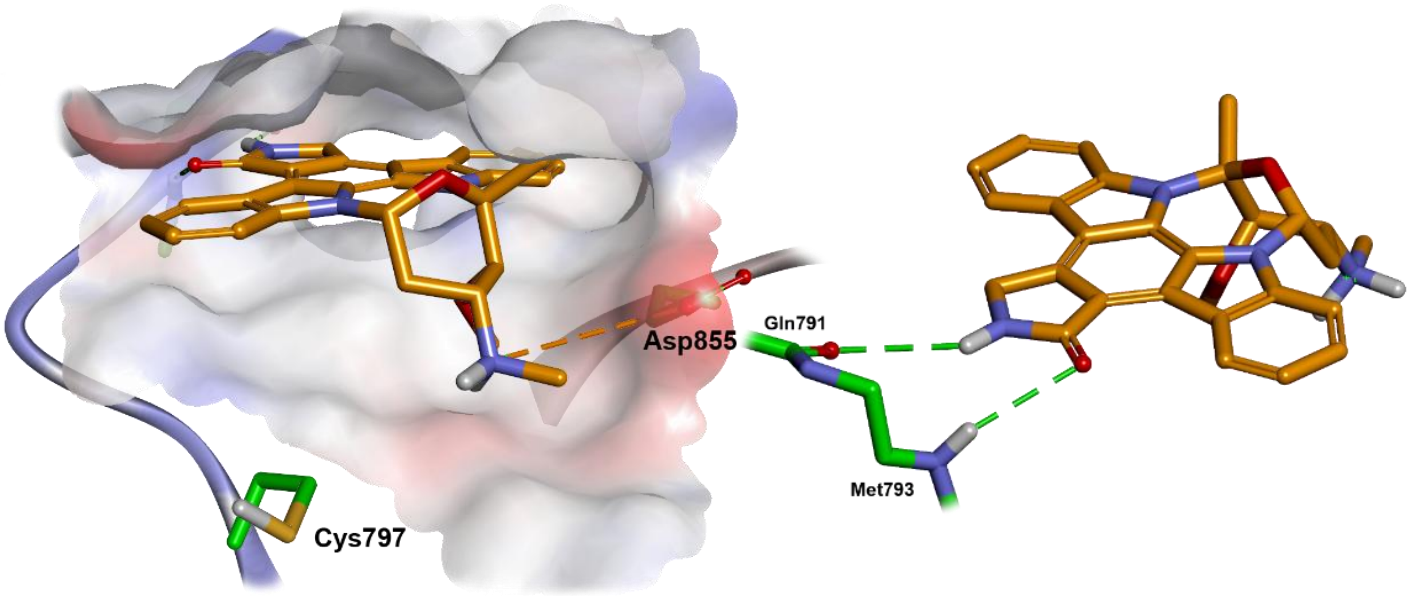

Figure 24

Illustration of staurosporine in the EGFR kinase domain. The important hydrogen interactions between the amide of staurosporine and residues Met793and Gln791 in the EGFR protein are highlighted in the image on the right.

As mentioned previously, natural products were among the first protein kinase inhibitors discovered and several natural product derived kinase inhibitors have entered clinical trials over the past decade.[68] Staurosporine is an intriguing natural product and many of its analogues have been evaluated against various human cancer cell lines, some showing promising therapeutic activity.[78-79, 83, 85]A major focus in the design and synthesis of these staurosporine derivatives has been to develop agents with improved selectivity, while retaining the potency associated with staurosporine.[84] A few staurosporine inspired drug candidates, which demonstrate protein kinase inhibitory activity, and that are currently in active development, are show in figure 25. In addition, bisaryl maleimide derivatives (such as enzastaurin), which are considered as the "open" form of the indolocarbazole, have also demonstrated improved selectivity.[86]

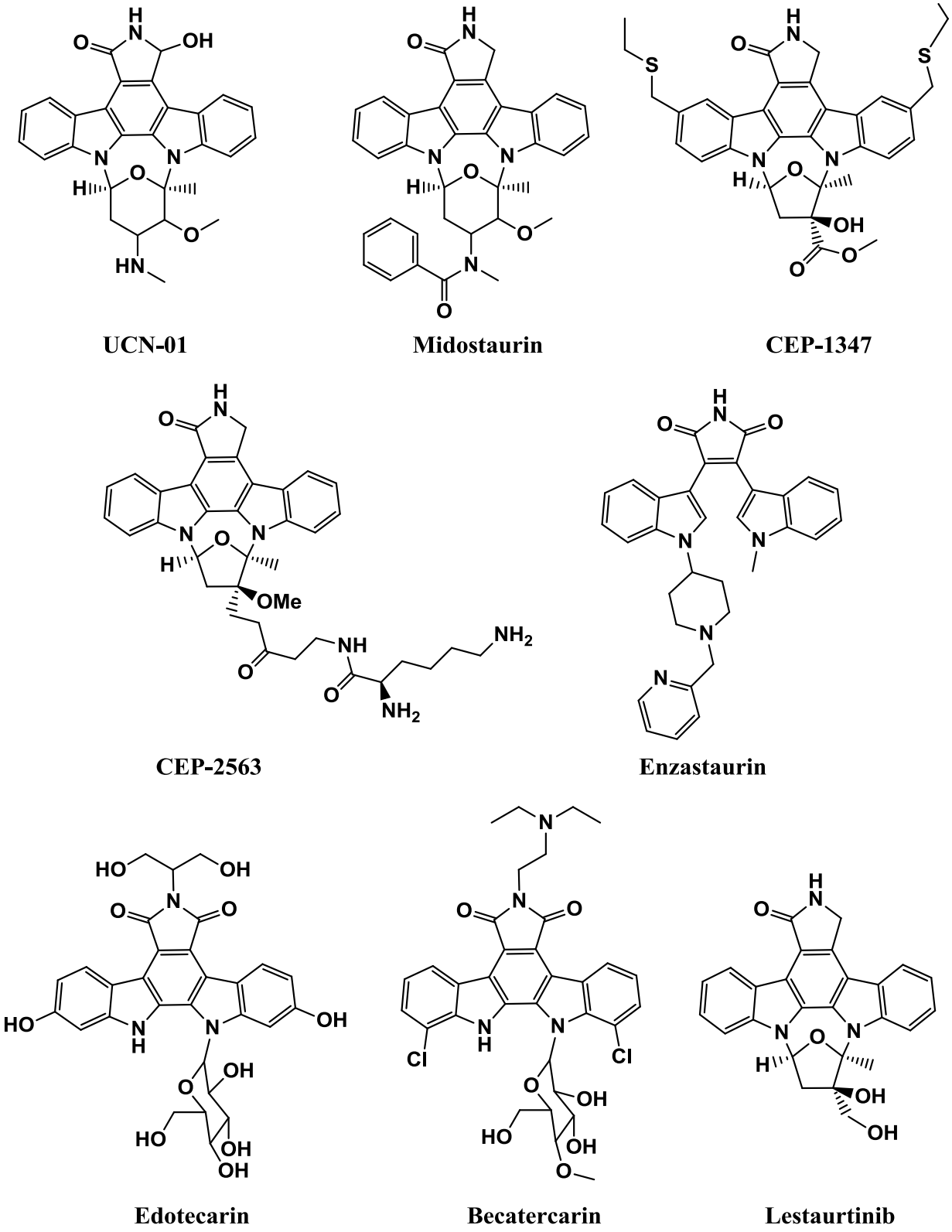

Figure 25
Staurosporine analogues as promising kinase inhibitors.[78]

CHAPTER 2 – CLICK CHEMISTRY AND KINASE INHIBITORS

2.1 The impact of click chemistry on kinase inhibitors

2.1.1 An introduction to click chemistry

The chemist, George S. Hammond, stated that: "The most fundamental and lasting objective of synthesis is not production of new compounds, but production of properties."[87] In the case of the pharmaceutical industry, these useful properties are represented by aiming to synthesize more effective therapeutic drugs. The manner in which the organic synthesis is done has extensive impact on the entire process of drug discovery, development, and manufacture.[87] In other words, a major objective is the development of an efficient synthetic strategy. In recent years, combinational chemistry has been introduced in the hope to improve the amount and rate of lead compound discovery and optimization. Unfortunately, combinational chemistry proved to be more dependable on individual reactions to generate the new network of chemical bonds compared to the 'traditional' synthetic chemistry, leading to a shortage of new lead compounds entering clinical trials.[66, 88] Natural products have had an immense impact on drug discovery, but the intricate architecture of these secondary metabolites often result in slow and complex syntheses.[87-88] Furthermore, as mentioned earlier, the enormous available chemical space has staggering implications on drug discovery and a vast majority of molecules with useful properties remain to be discovered.[70, 88] The way Nature performs her own type of combinational chemistry, achieving astonishing diversity and modularity from less than 40 monomers to make the macromolecules which are central to life processes, has inspired synthetic organic chemists.[87] An investigation of the bioactivity of molecules created by nature, has revealed an overall preference for carbon-heteroatom bonds over carbon-carbon bonds.[89] For example, all proteins arise from 20 building blocks that are joined via reversible heteroatom links (amides).[87] Following Nature's inspiration, and limiting the search for new structures to those that can easily be synthesized through joining small units through heteroatom links, led to the powerful strategy defined by Sharpless and co-workers as "Click Chemistry".[89]

A set of stringent criteria has been defined that a process must meet to earn the click chemistry status. For the criteria to be met, the reaction must be "modular, wide in scope, high yielding, create only inoffensive by-products (that can be removed without chromatography), be stereospecific, simple to perform, and require benign or easily removed solvent, readily available starting materials and reagents, and require simple product isolation."

In this regard, the readily available, high energy olefins and acetylenes are useful reactive building blocks, ideal for the fast, irreversible assembly of diverse molecules with drug-like structural features. Several processes have been identified which meet the requirements to match the Click Chemistry criteria (figure 26). These reactions are exothermic and thought of as being "spring loaded" for a single trajectory. This approach thus provides rapid synthesis from a set of powerful, highly reliable and selective reactions, to develop new useful compounds.[87]

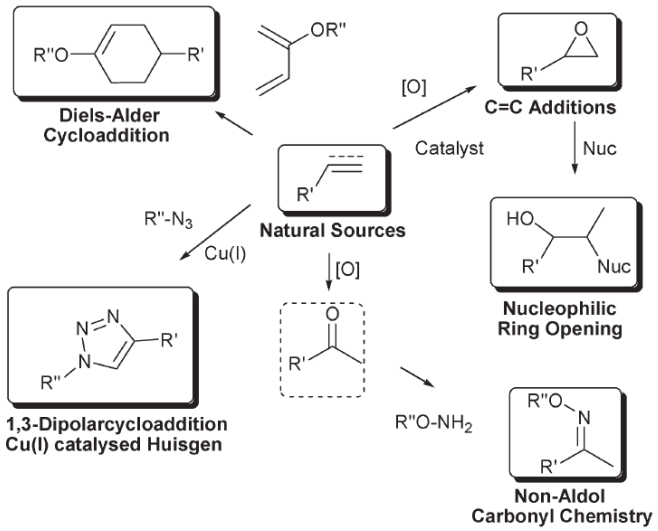

Figure 26
Examples of reactions which have earned the "click chemistry" status. Image reproduced from following reference.[89]

Of these reactions, the premier example of a click reaction is the copper (I) catalyzed variant of the Huisgen 1,3-dipolar cycloaddition of alkynes and azides to yield 1,2,3-triazoles.[88, 90] In 2001, Meldal and co-workers reported the discovery of a novel regiospecific copper(I) catalyzed 1,3-dipolar cycloaddition of terminal alkynes to azides.[91] Sharpless and Meldal laboratories independently realized that the introduction of the copper(I) catalysis lead to a dramatic rate acceleration of the coupling reaction.[90, 92] This finding, together with the discovery of the beneficial effects of water, placed the Cu(I) catalyzed Huisgen reaction at the center stage of click chemistry.[88-89] This particular copper-catalyzed azide-alkyne cycloaddition (CuAAC) is a 'near perfect' reaction according to the criteria defined by Sharpless and is often referred to as "The" click reaction.[89] Azide and alkyne functionalities are easy to install, and although they are amongst the most energetic species known, they are kinetically stable. These two attractive complementary coupling partners are inert to most biological and organic conditions, including molecular oxygen, water and the majority of reaction conditions in organic synthesis, and functional groups.[89-90] Uncatalyzed Huisgen cycloadditions are slow, require elevated temperatures and often result in a mixture of products (1:1 1,4- and 1,5-regioisomer).

Besides the fact that the reaction rate increases up to 10^7 times under Cu(I) catalyzed conditions, the regioselectivity is dramatically improved, affording the 1,4-regioisomer exclusively (figure 27).[90, 93] In 2005, Sharpless and co-workers, reported that ruthenium-catalyzed azides-alkynes cycloaddition (RuAAC) gave the 1,5-regioisomer product exclusively. Another advantage of RuAAC is that both terminal and internal alkynes can be utilized.[94] However, for the purpose of this project, particular interest was directed towards CuAAC.

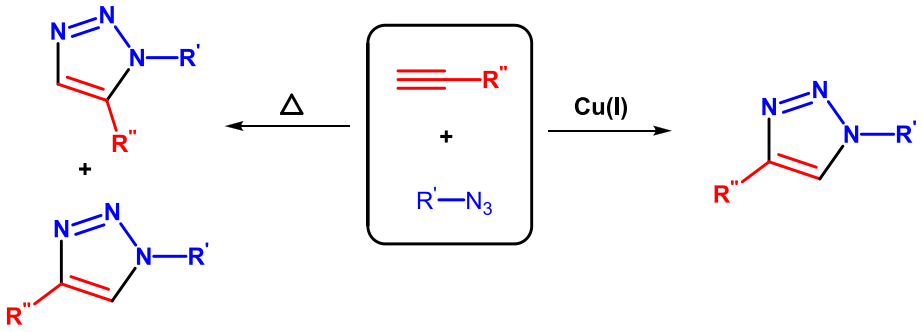

Figure 27

The CuAAC results in exclusive formation of the 1,4-disubstituted-1,2,3-triazole, while the thermally induced Huisgen cycloaddition results in the formation of a 1:1 mixture of 1,4-disubstituted-1,2,3-triazole and 1,5-disubstituted-1,2,3-triazole.[89]

Since the discovery of the CuAAC approach, various sources of copper and reaction conditions (solvents, temperatures and pH range) have been tested.[93] The robustness of the reaction is supported by the high yield of triazole formation under a variety of conditions.[90] Meldal and co-workers initially described the use of Cu(I) salts in the solid phase, while Sharpless and co-workers reported solution-phase in-situ reduction of Cu(II) salts or comproportionation of Cu(0) and Cu(II).[90-91, 93] It should be noted that the role of copper in this catalysis has been subject to many disputes and revisions.[92] The mechanism has remained difficult to establish as a result of the multiple equilibria between several reactive intermediates involved during the reaction. Examination of the mechanism, although daunting, has been a pursuit of organic chemists to have a better understanding of the fundamental reactivity and to be able to optimize the reaction parameters.[95] With this aim, the analysis of catalytic systems relies on one or a combination of methods. Some of these methods include the application of computational studies, initial rate studies, the study of isotope crossover and kinetic isotope effect, reintroduction of an intermediate in a reaction mixture to prove its involvement in the catalytic cycle, and analysis of stereoelectronic effects. Throughout the years, several possible mechanisms have been proposed, but despite the number of studies, the elucidation of the exact mechanism remains complex.[92, 95-96] Fokin and co-workers have reported the latest plausible mechanism, which is supported by various theoretical studies.

The experiments were carried out by real-time monitoring of a cycloaddition reaction via heat-flow reaction calorimetry and crossover experiments with isotopically enriched exogenous copper source.[95] This proposed catalytic model for CuAAC, involving two copper atoms, is represented below (figure 28).

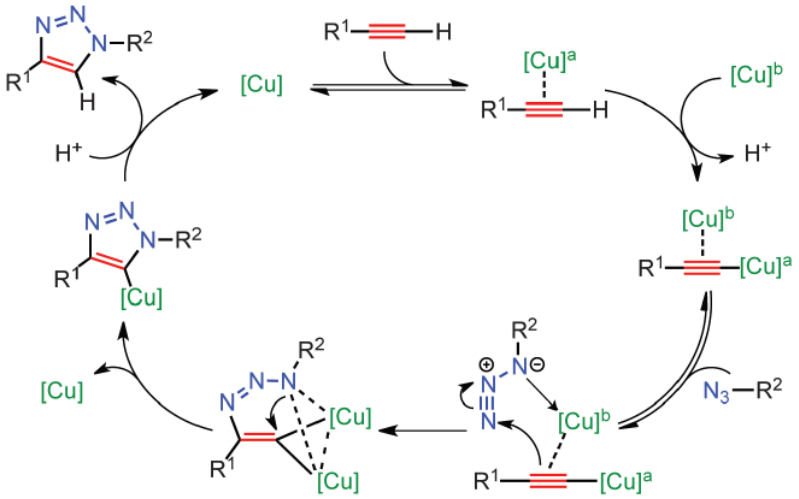

Figure 28

CuAAC mechanism as proposed by Fokin and co-workers. Image reproduced from following reference.[95]

Click chemistry uses the most practical and reliable chemical transformations, and its applications in chemistry, biology, and material sciences are extensive. In drug discovery, the applications range from lead finding through combinational chemistry and target template *in situ* chemistry, to proteomics and DNA research using bio-conjugation reactions.[88, 96] CuAAC has been referred to as the gold standard of click chemistry, exhibiting remarkably broad scope and exquisite selectivity.[96-97] The triazole products are more than just linkers, they associate with biological targets through hydrogen bonds and dipole interactions, acting as a pharmacophore in the field of medicinal chemistry. Besides being attractive connecting units and pharmacophores, the 1,2,3-triazole moieties are stable to metabolic degradation, and are capable of forming hydrogen bonds which can improve solubility and bind biomolecular targets.[97] Click chemistry, and in particular CuAAC, accelerates lead discovery and optimization, due above all to its broad scope, modular design, and its reliance on short sequences of near-perfect reactions.[88]

2.1.2 The application of click chemistry in kinase inhibitor development

A particular focus of this project was to develop kinase inhibitors *via* click chemistry. For this reason, an outline will be given on the topic of various kinase inhibitors synthesized by the click approach.

The 1,2,3-triazole scaffold has been associated with several advantages in the development of kinase inhibitors, namely: (i) the 1,2,3-triazole ring can act as a mimic of the ATP purine that targets the ATP-

binding site; (ii) the triazole ring can also function as a bioisostere of flat heteroaromatic rings (purine, pyrazole and imidazole) which are frequently present in kinase inhibitor structures; (iii) the 1,2,3-triazole can be easily assembled by click chemistry; (iv) a diverse group of structures can easily be generated by attaching commercially available alkynes and to a much lesser extent, azides. [98] Therefore, various examples in literature employing click chemistry to design kinase inhibitors are described in this section.

The design of kinase inhibitors that exploit less conserved substrate-binding/allosteric pockets, is an attractive approach to enhance inhibitor selectivity. The fact that the majority of kinase inhibitors bind to the ATP-binding site is problematic, since the binding pocket is highly conserved throughout the kinase superfamily.[48, 99] Drug development strategies to produce selective kinase inhibitors remain an active area of research. One such strategy is the rational design of bisubstrate inhibitors. This type of inhibitor consists of two conjoined inhibitor scaffolds, one binding to the ATP-binding site, while the other targets the allosteric/substrate-binding site. In these structures, the ATP-binding part affords affinity and the allosteric/substrate-binding part affords selectivity. Therefore, bisubstrate kinase inhibitors can be designed to impart improved selectivity and potency. A number of successful examples based on this approach have been demonstrated, showing improved selectivity and affinity for kinase inhibitors.[99-100]

For example, Kalesh *et al.* developed an efficient method for the construction of small-molecule based bisubstrate inhibitors of Abl kinase using click chemistry.[99] In their approach, two clickable warheads were designed to effectively bind to the ATP-binding site. The two scaffolds were based on the Imatinib core structure by replacing the piperazine-linked benzene ring with an alkyne group (figure 29). A small library of short chain azides was then subjected to click reactions with the two Imatinib-based warheads. In this manner, the warheads were able to project the diversity element (the azide chain) into the secondary binding site of the kinase. One example of this approach is represented in figure 30.

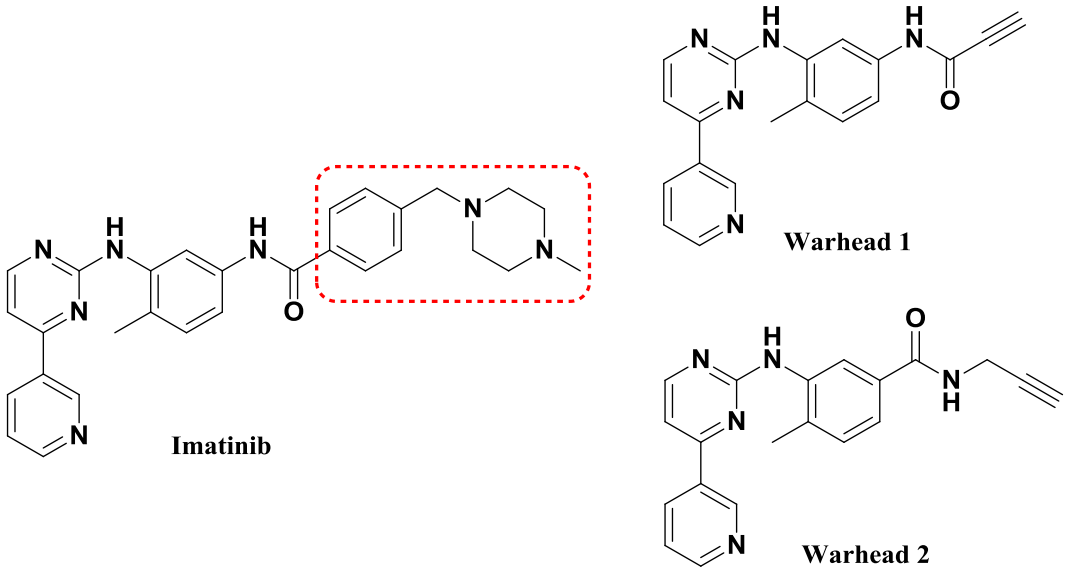

Figure 29

Warheads based on Imatinib for the construction of the bisubstrate inhibitors. The red box indicates the part of the structure which is replaced by a terminal alkyne.[99]

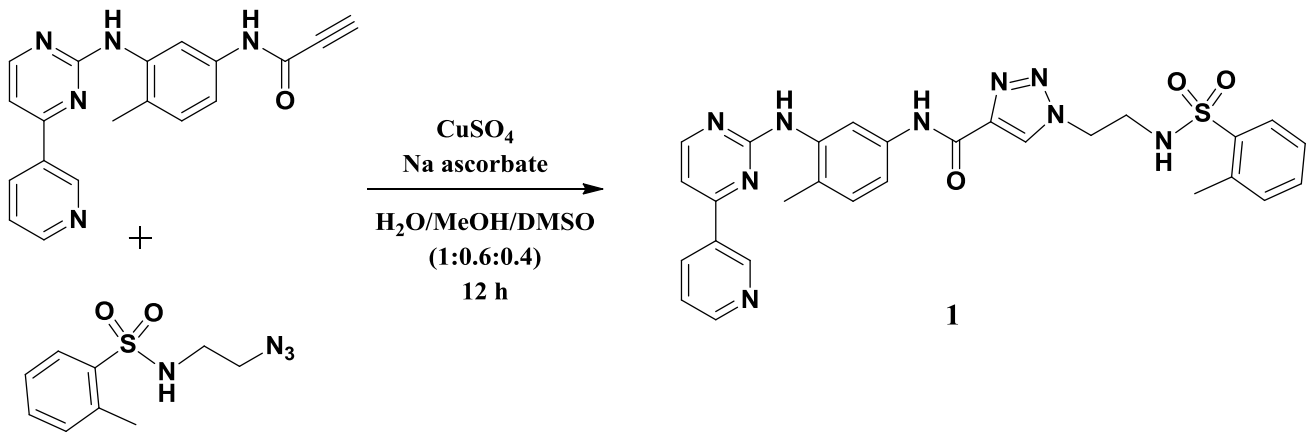

Figure 30

An example of the click chemistry approach used to generate the bisubstrate kinase inhibitor **1**.[99]

This method led to the synthesis of 90 inhibitors, with the majority displaying better inhibition against Abl over Src kinase. Quantitative inhibition assays were carried out for 11 of these inhibitors to obtain their IC_{50} values against Abl kinase. A few moderately potent inhibitors were identified, some of which are comparable to the potency of Imatinib. The two most potent inhibitors of the various warheads (W1 and W2) are represented below in figure 31. Although these compounds showed only a marginal improvement over Imatinib, the utility of the strategy as a tool in the field of kinase research is demonstrated.[99]

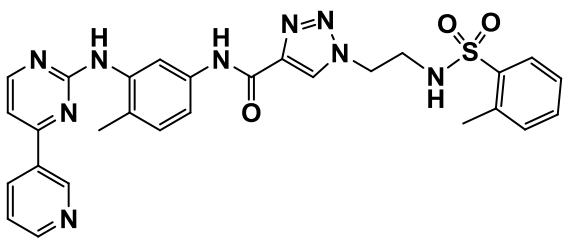

1

IC_{50} = 704 nM against Abl

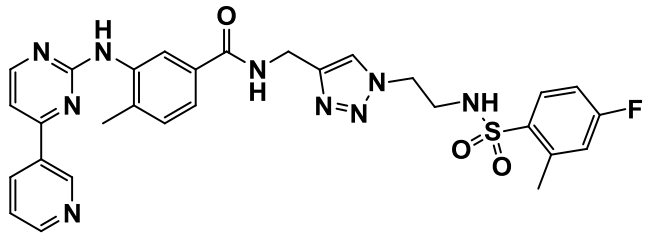

2

IC_{50} = 1123 nM against Abl

Figure 31

Imatinib based bisubstrate inhibitors of Abl kinase.[99]

Similarly, the bisubstrate strategy was employed by Poot *et al.* to develop kinase inhibitors against PKC isozymes.[100] In this approach, novel bisubstrate structures were generated by linking peptide-binding site inhibitors to ATP-binding site scaffolds through click chemistry. Initially, peptide microarrays were used to identify peptide substrates with large affinity differences within a given set of kinases. Three PKC isozymes, each from one of the subfamilies PKCα, PKCθ and PKCζ, were selected for substrate profiling. The peptide selected for this study was the peptide EILSRRPSYRKIL, derived from the cAMP-responsive element binding protein. Peptide EILSRRPSYRKIL was then transformed into two pseudosubstrates and linked to the ATP-binding site inhibitor. A functionalized bisindolyl maleimide was next selected as the ATP-binding site scaffold. Through click chemistry, two novel bisubstrate-based inhibitors (**3** and **4**) were synthesized and their structures are shown in figure 32. They displayed improved potency and selectivity compared to their constituent parts. Compound **(3)** showed similar inhibition of PKCα compared to its respective bisindolyl maleimide constituent part, but its inhibition of PKCθ-mediated phosphorylation was significantly better. In addition, a fourfold reduction of its IC_{50} was observed (0.6-0.9 μM). Compound **(4)** did not inhibit PKCα, but showed excellent isozyme selectivity for PKCθ amongst the three isozymes evaluated. Its inhibition for PKCθ (IC_{50} = 0.4 - 0.8 μM) was similar to that of compound **(3).**

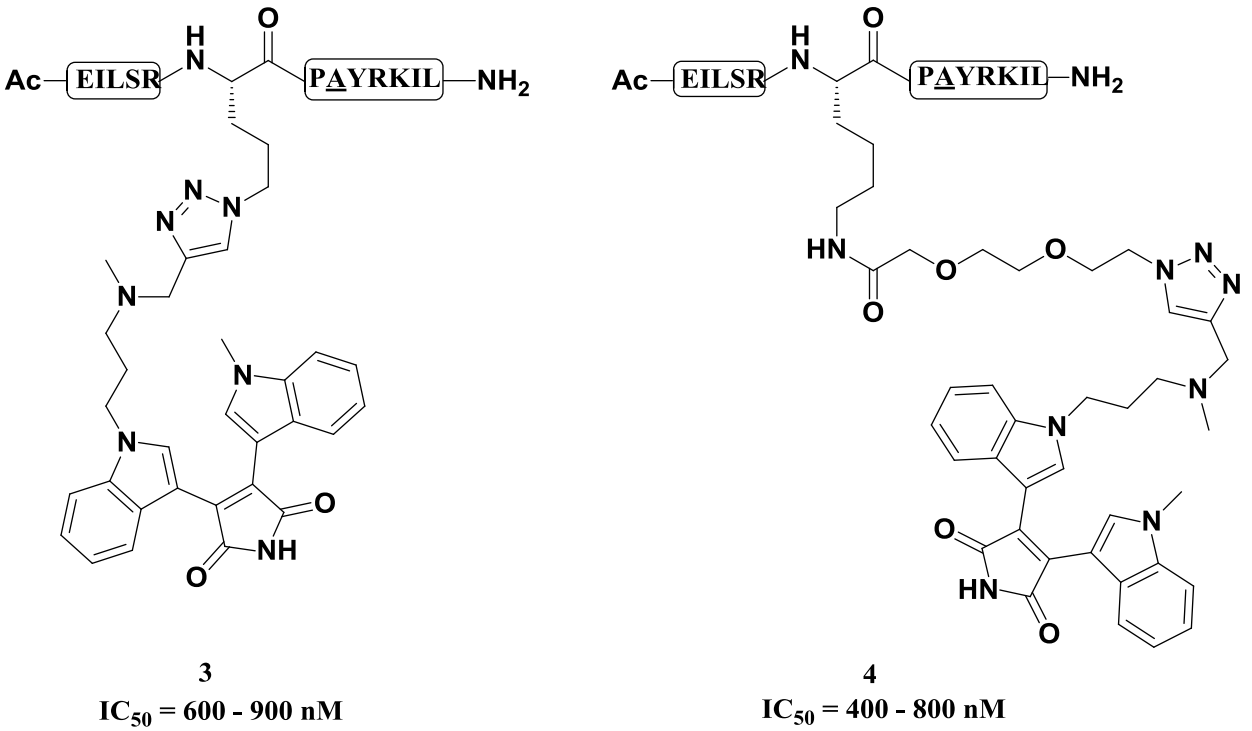

3
IC_{50} = 600 - 900 nM

4
IC_{50} = 400 - 800 nM

Figure 32
Bisubstrate inhibitors constructed from pseudosubstrates (transformed from peptide EILSRRPSYRKIL) and functionalized bisindolyl maleimide.[100]

Over the past decade, advances in the development of active compounds have been made to selectively inhibit Bcr-Abl kinase activity. Imatinib, the most well-known of these inhibitors, currently represents the first line treatment of CML. Resistance to Imatinib has led to a growing interest in developing second-generation small-molecule inhibitors that are able overcome Imatinib-resistant CML.[46] Arioli *et al*. attempted this by developing potential inhibitors of Bcr-Abl through the design of *N*-[2-methyl-5-(triazol-1-yl)phenyl]pyrimidin-2-amine derivatives.[101] The strategy was based on substituting the amide bond in the Imatinib structure with a 1,2,3-triazole ring, utilizing the bioisosterism between an amide group and a 1,2,3-triazole ring. Six novel compounds were synthesized and their potency was assessed by evaluating their effects on enzymatic activity, cell proliferation, phosphorylation, cdc25A expression, and pro-apoptotic activity. One particular compound (**5**) showed potent anti-enzymatic activity against recombinant Abl kinase (figure 33).Its efficacy was demonstrated by its antiproliferative activity in the low micromolar range with an IC_{50} value of 0.9 ± 0.1 μM against the K-562 cell line. Unfortunately, **5** showed decreased activity against the Imatinib-resistant mutant Abl T3151. Furthermore, **5** had the ability to decrease the phosphorylation of Bcr-Abl, c-Abl, STAT-5, Scr, and was an active inhibitor of cdc25A in two different cell lines.

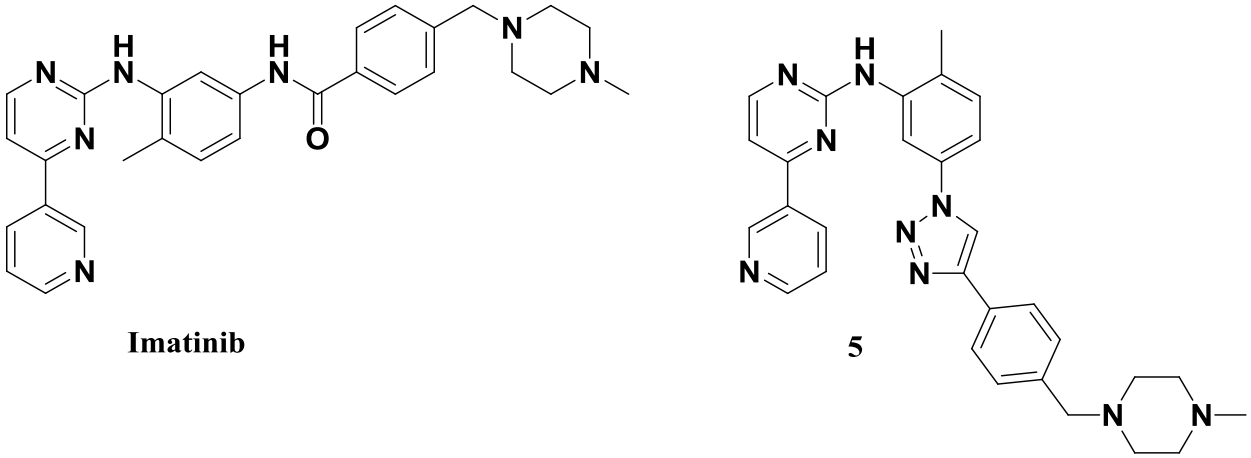

Figure 33
Compound **5**, a triazole-based Imatinib analogue demonstrating inhibitory activity against recombinant Abl kinase.[101]

Aurora kinases are members of serine/threonine kinases. Many Aurora-selective small-molecule inhibitors have been developed, but none have been approved by the FDA. Song *et al.* developed a series of 1,2,3-triazolylsalicylamide derivatives via (CuAAC) click chemistry and evaluated their inhibitory activity against Aurora kinases.[102] Their strategy was inspired by a previously identified antiproliferative agent **6**, which exhibited very good selectivity for the Aurora A kinase. The antiproliferative agent was modified as illustrated in figure 34. A variety of substituents were readily installed through CuAAC, thereby generating a number of different compounds which were tested against Aurora A and Aurora B.

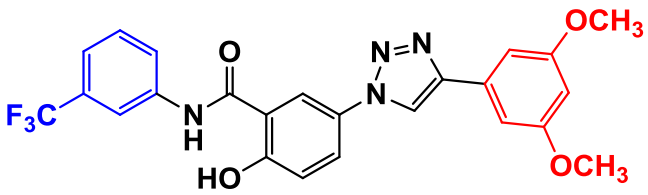

6

Antiproliferative Agent 1,2,3-triazolylsalicylamide

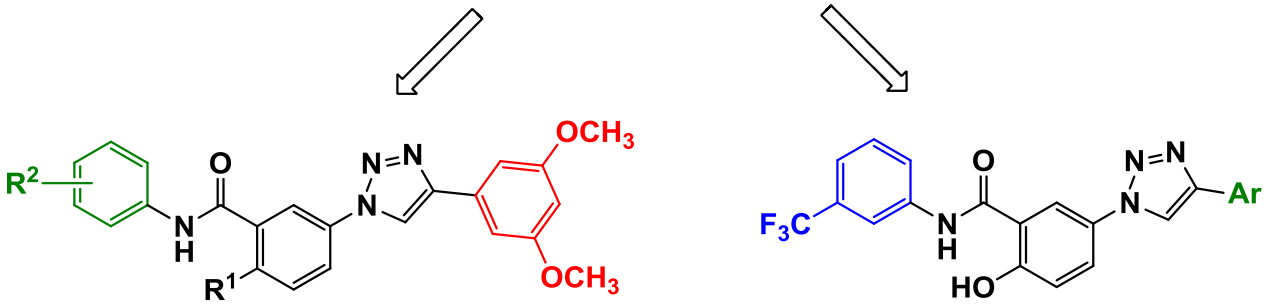

1,2,3-triazolylsalicylamide derivatives

Figure 34

Design of 1,2,3-triazolylsalicylamide derivatives for the inhibition of Aurora kinases.[102]

Most of the compounds showed some selectivity towards Aurora A and 5-50 times more strongly inhibited Aurora A over Aurora B. In addition, a few compounds inhibited Aurora A with IC_{50} values in the low micromolar to nanomolar range. Compound **7** (figure 35), the best among the series, showed inhibitory activity with an IC_{50} value of 0.37μM.[102]

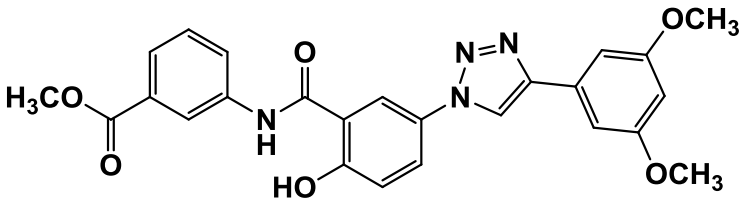

7

IC_{50} = 370 nM against Aurora A Kinase

Figure 35

Compound **7** exhibiting the best inhibitory activity, amongst the series, for Aurora A.[102]

Another protein kinase which has been implicated in the development of a variety of cancers, and the subject of major interest in recent years, is the non-receptor tyrosine kinase Src. Src kinase is a key modulator of cancer cell invasion and metastasis, and several structural motifs have been reported to target this kinase.[103-106] Dasatinib and Bosutinib have been approved to use in patients with CML, after Imatinib treatment as it is a dual Src/Abl inhibitor.[104, 107-108] Kumar, A and Kumar, D *et al.* have independently reported two studies in which they attempt to synthesize inhibitors which target the Src kinase by using click chemistry.[106, 109] Previous studies have shown that 3-phenylpyrazolopyrimidines bind to the ATP-binding pocket in such a manner that the hydrophobic interaction between the phenyl group and hydrophobic pocket is crucial. Furthermore, the pyrazolopyrimidine resembles the purine core of ATP and binds in a similar manner as the adenine base of ATP. A cavity which is usually occupied by the carbohydrate moiety and the triphosphate group of ATP, is left unfilled in the case of 3-phenylpyrazolopyrimidine (figure 36), due to the smaller *tert*-butyl group.[105-106, 110]

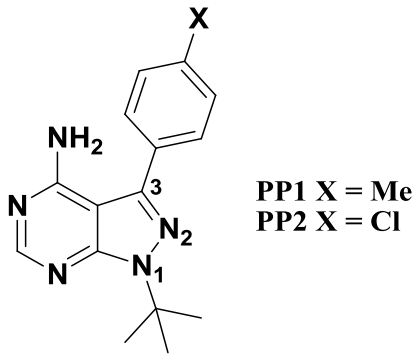

Figure 36
General structure of 3-phenylpyrazolopyrimidines.[106, 109]

In the first study, Kumar and co-workers synthesized and evaluated 1,4-disubstituted 1,2,3-triazoles as a novel template for Src kinase inhibition. They hypothesized that substitution at N_1 and position 4 of the triazole with hydrophobic residues would display similar binding compared to 3-phenylpyrazolopyrimidine and enhance the potency against Src kinase.[109] To this end, two classes of compounds were synthesized by means of a one-pot click reaction . The first class of compounds included R_1 as phenyl, substituted phenyl, coumarinyl, 2-thienyl, or other nonaromatic substituents on the 1,2,3-triazole. Class 2 compounds included cyclopentanone-2-yl, cyclohexanone-2-yl, or cycloheptanone-2-yl as R_1, which are represented as a circle in figure 37. For both classes, position 4 (R_2) was phenyl, substituted phenyl, short alkyl, or a heteroaromatic.

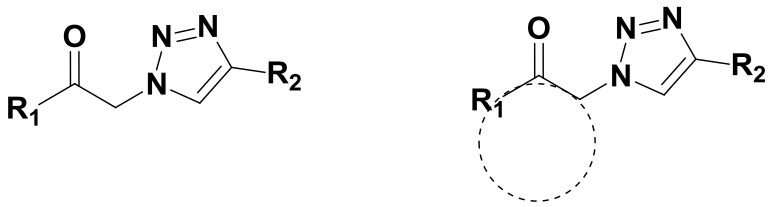

Figure 37

General structure of the class 1 and class 2 1,4-disubstituted 1,2,3-triazoles.[109]

The 1,4-disubstituted 1,2,3-triazole compounds were tested against Src kinase and a number of observations were made regarding the nature of substituent R_1 and R_2 on the inhibitory activity of the compounds. In general, the compounds exhibited weak Src kinase activity, but five of the compounds displayed modest inhibitory activity with the IC_{50s} ranging from 32 - 43 μM. Of interest was compound **8**, which demonstrated selectivity towards Src kinase when compared to other kinases (figure 38). The study provided insight into optimization of the scaffold and fragment-based discovery of Src kinase inhibitors.[109]

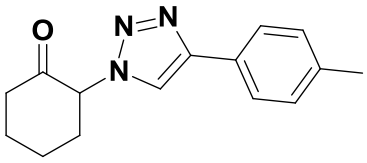

8

IC_{50} = 33.9 μM against Src kinase

Figure 38

Structure of compound **8** exhibiting modest inhibitory activity and selectivity against Src kinase.[109]

In continuation of their efforts to develop Src kinase inhibitors, Kumar, A. *et al.* investigated whether the empty cavity formed, when 3-phenylpyrazolopyrimidines binds to the Src kinase, can be occupied when 1,2,3-triazoles containing hydrophobic residues are substituted at the N_1 position - thereby enhancing inhibitor potency.[105-106] In this study, two classes of 3–phenylpyrazolopyrimidines (PhPP)-1,2,3-triazole conjugates were synthesized via click chemistry.[106] The general structures obtained are illustrated in figure 39.

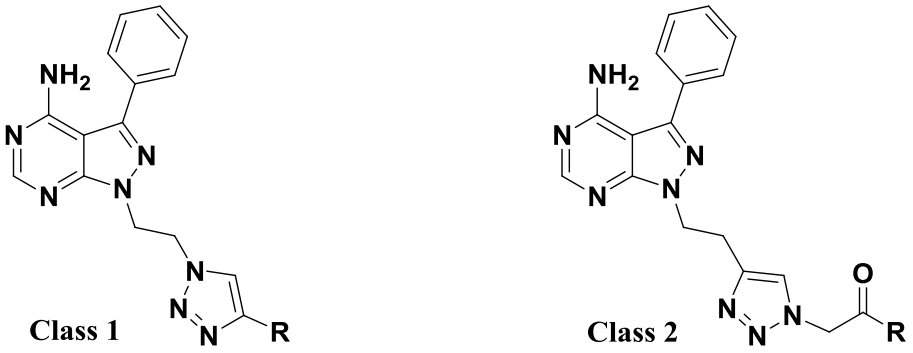

Figure 39

General structures of 3-phenylpyrazolopyrimidines (PhPP)-1,2,3-triazole conjugates where R = alkyl, aryl, or heteroaryl.[106]

In total, 20 final compounds were synthesized and tested against Src kinase. The compounds from class 1 showed less inhibitory activity than PP2, although a number of compounds exhibited modest inhibitory activity in the IC_{50} range 5.6 – 29.6 μM. The data further revealed that the cavity cannot accommodate bulky groups attached to the triazole with an ethylene linker to PhPP. The class 2 compounds showed more diverse inhibitory activity, with some compounds exhibiting modest inhibition (IC_{50} = 9.1 – 23.1 μM). Overall, the data suggested that incorporating a bulky group at position N_1 was not tolerated very well. Compound **9** from class 1 and **10** from class 2 showed the best inhibitory activity amongst the group of 3-phenylpyrazolopyrimidines (PhPP)-1,2,3-triazole conjugates synthesized (figure 40).[106]

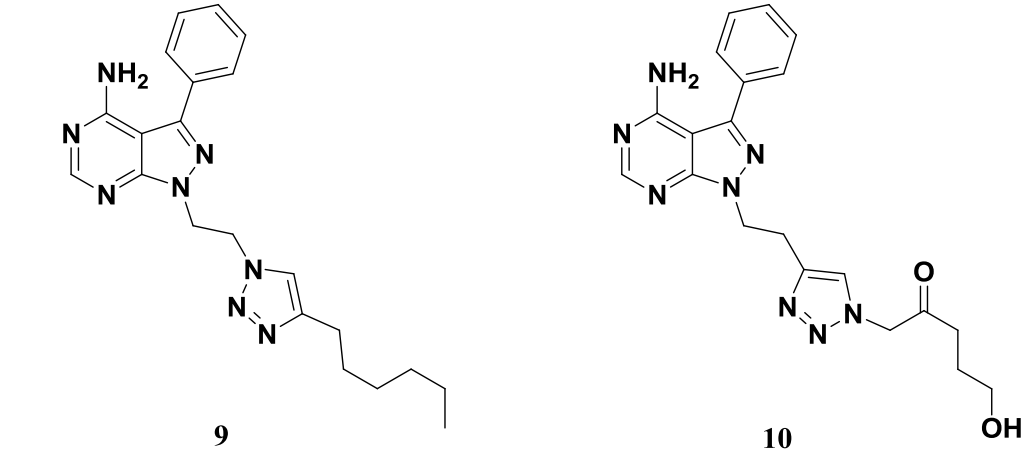

9
IC_{50} = 5.6 μM against Src kinase

10
IC_{50} = 9.1 μM against Src kinase

Figure 40

Compound **8** and **9** exhibiting modest inhibitory activity against Src kinase.[106]

The Met kinase belongs to the receptor tyrosine kinase (RTK) family and plays a central role in signaling pathways. The progression of a malignant tumor involves cell scattering, which is induced by hepatocyte growth factor (HGF)/scatter factor (SF).

The Met kinase binds the HGF ligand and triggers signaling. HFG/Met alterations lead to deregulated downstream signaling contributing to tumorigenesis and cancer progression. Oncogenic Met is also responsible for oncogene addition and drug resistance. [111-112] Furlan *et al*. recently synthesized a compound, triflorcas, which successfully targets cancer cells dependent on oncogenic Met. [113] The amide present in triflorcas, and its bioisosterism to 1,2,3-triazole, inspired Colombo and co-workers to synthesize a triazole-based analogue of triflorcas.[114] As can be seen in figure 41, a 1,2,3-triazole ring (red) was incorporated into triflorcas in place of the amide (blue) functionality by way of CuAAC click chemistry. The triazole-based analogue (**11**) was evaluated and maintained good inhibitory activity compared to the lead compound, triflorcas. **11** efficiently inhibited Met-triggered biological activities, including cell scattering and tumorigenicity.[114] Their study further demonstrates how click chemistry can be utilized to exploit the bioisosterism between amides and 1,2,3-triazole rings to develop new analogues from inhibitors containing amide groups.

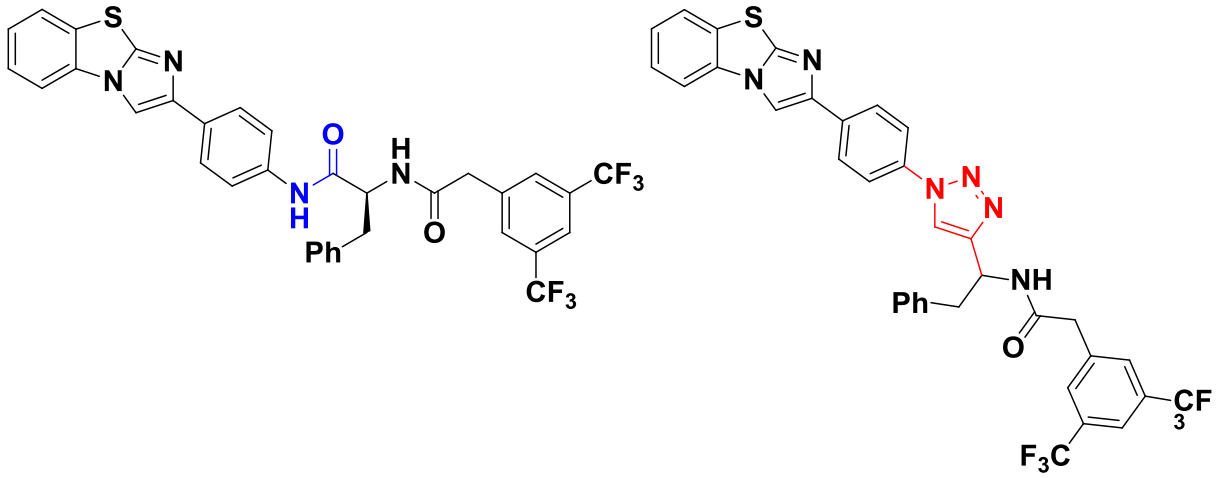

Triflorcas
IC_{50} = 200 nM against Met kinase

11
IC_{50} = 600 nM against Met kinase

Figure 41
Lead compound triflorcas and its triazole-based analogue **11**.[114]

Casein kinase II (CK2), a serine/threonine protein kinase, has been afforded the status "master regulator".[115] This is ascribed to its global role in activities related to cell growth, cell death, and cell survival.CK2 is a potent suppressor of apoptosis, making it an attractive target to avoid tumor cells escaping death through an alternative pathway. Various cancers have demonstrated elevated levels of CK2 and a number of CK2-directed compounds have been generated to inhibit its activity.[115-116]

Swider and co-workers synthesized and evaluated 4,5,6,7-tetrabromobenzotriazole (TBB)-based derivatives, capable of acting as multisite-directed inhibitors toward protein kinase CK2. These compounds were designed to occupy the ATP-binding site, and to interact with the protein substrate binding residues, as well as the Mg^{2+}- chelating residues. The synthesis involved CuAAC of three alkylated TBB compounds with a series of azides to generate a small library of 14 compounds. These compounds were then tested against CK2, and compound (**12**) exhibited the best inhibitory activity with an IC_{50} of 44.5 μM. The structure of this compound is represented in figure 42. Molecular modeling identified the CK2-inhibitor interactions and could be useful in future optimization and development of multisite-directed inhibitors.[116]

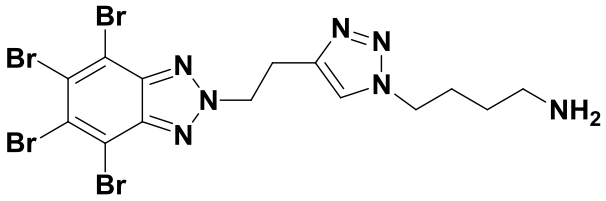

12

IC_{50} = ± 44.5 μM against CK2 kinase

Figure 42

The TBB-based CK2 inhibitor (**12**) exhibiting the best inhibitory activity, amongst the family synthesized.[116]

Members of the transforming growth factor-β (TGF-β) superfamily, signal through a combination of transmembrane serine/threonine kinases (type II and type I receptors), and play a crucial role in development and disease.[98] TGF-β is a member of the TGF-β superfamily, along with bone morphogenic proteins (BMPs), growth and differentiation factors (GDFs), activins, inhibins, nodal and anti-Müllerian hormone. In humans, three isoforms of TGF-β have been described. Active TGF-β binds selectively to the membrane-spanning serine/threonine kinase receptorII (TβRII), which then activatesTGF-β receptor type I (TβRI) - also known as activin receptor-like kinase 5 (ALK5). The activated TβRI/ALK5 interacts and phosphorylates downstream Smad effectors, which eventually lead to complexation with a Smad mediator and translocation to the nucleus. TGF-β overproduction is commonly observed in a number of solid tumors when the TGF-β suppressive effects are lost. Inhibition of the protein kinase ALK5 could therefore effectively disrupt the mechanism of action, and prevent tumor growth.[98, 117-118]

Attempts to block the TGF-β effect have been investigated, with particular focus on targeting the ALK5 kinase. A number of potent imidazole and pyrazole inhibitors have been developed, which display anticancer activities.

In continuation with their efforts to develop 1,2,3-triazole anticancer agents, and studying the current ALK5 inhibitors - with particular interest in the binding interaction of compound **IN-1166** - Li and co-workers designed and synthesized 1-(6-methylpyridin-2-yl)-5-(quinoxalin-6-yl)-1,2,3-triazoles as novel ALK5 inhibitors (figure 43).[98]

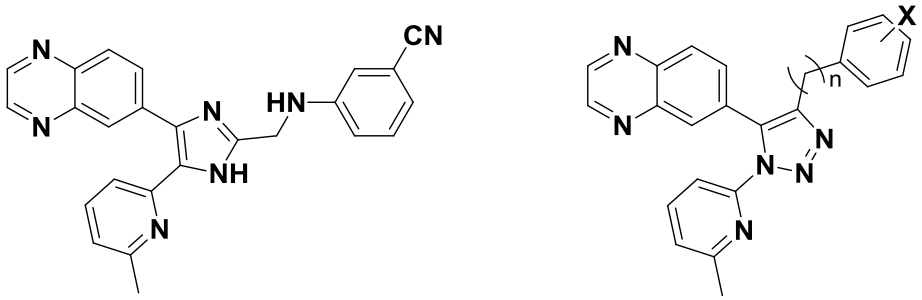

IN-1166 **1,2,3-triazole ALK5 inhibitors**

Figure 43

Design of 1-(6-methylpyridin-2-yl)-5-(quinoxalin-6-yl)-1,2,3-triazoles based on the AKL5 inhibitor IN-1166.[98]

The synthetic strategy, shown in scheme 3, was straightforward and applied click chemistry (CuAAC) for the combination of 2-azido-6-methylpyridine and various alkynes (R). The resulting compounds of 1-(6-methylpyridin-2-yl)-1,2,3-triazoles was subsequently coupled with 6-bromoquinoxaline to afford the final compounds. The inhibitory activity of these compounds was then evaluated against AKL5 and p38α MAP kinase (to produce a selectivity profile). The synthesized 1-(6-methylpyridin-2-yl)-5-(quinoxalin-6-yl)-1,2,3-triazoles exhibited modest to significant AKL5 inhibitory activity and displayed good selectivity differences versus p38α MAP. Overall, compound **13** shown in figure 44, demonstrated the best selectivity and inhibitory activity against AKL5, and served as a valuable lead for optimization studies.[98]

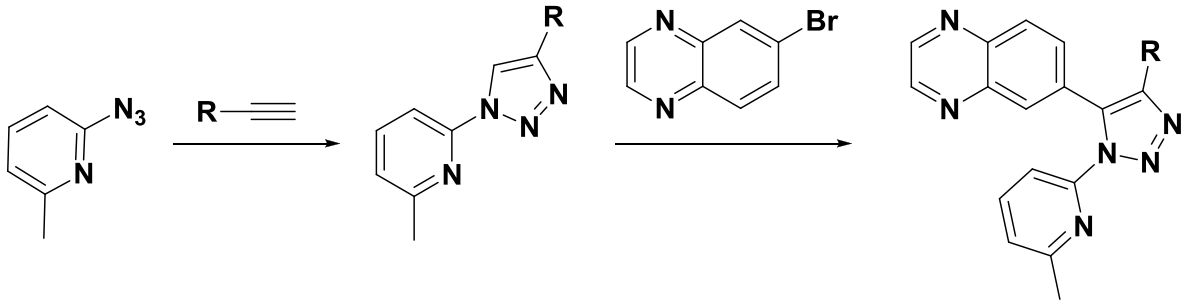

Scheme 3

General strategy utilized to synthesize the 1-(6-methylpyridin-2-yl)-5-(quinoxalin-6-yl)-1,2,3-triazoles.[98]

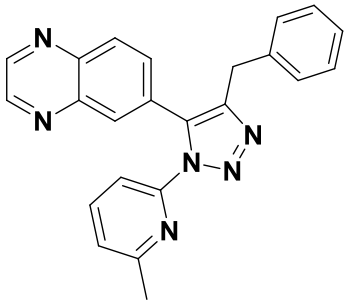

13
IC_{50} = 4.69 μM against AKL5 kinase

Figure 44
The benzyl 1,2,3-triazole 13 exhibiting the best inhibitory activity and selectivity for AKL5, amongst the series of compounds.[98]

3-Phosphoinositide-dependant protein kinase 1 (PDK1) is a serine/threonine kinase that belongs to the AGC family. PDK1 is responsible for regulating the activity of at least 23 other AGC kinases by phosphorylating a specific threonine or serine residue within the activation loop (T-loop). Downstream signaling of these kinases has often been implicated in cancer development.[119-120] The work of Merkul *et al*. has led to the effective synthesis of 7-azaindole analogues, which display inhibitory activity against PDK1 kinases. Indoles and their aza analogues play an important role as scaffolds for biologically active molecules. The ability of 7-azaindoles to bind to the hinge region of the kinase domain, makes its structure of particular interest for kinase inhibitors. The simplified synthetic analogues of marine natural products variolin B, known as meriolins, are prominent examples of azaindoles having a heterocyclic substituent at the C-3 position (figure 45).[121]

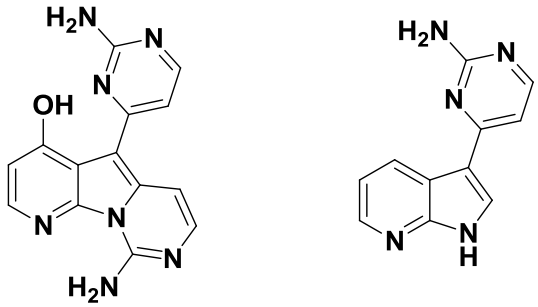

Variolin B **Meriolin 1**

Figure 45
Structure of the natural product variolin B and the synthetic analogue meriolin 1.[121]

Upon investigating the binding features of previously synthesized 7-azaindole analogues, Merkul and co-workers decided to continue their study by incorporating 1,2,3-triazoles into the structures. In their research, they reported a diversity-orientated synthetic approach to generate 3-triazolyl-substituted (aza)indole scaffolds. The strategy involved a one-pot synthetic procedure, including a Sonogashira coupling and CuAAC reaction, to generate several triazolyl NH-heterocycles. The kinase inhibitory activity of these synthesized compounds was then tested against a broad panel of kinases (95-121 kinases).It was found that a few of these compounds, represented in figure 46, exhibited inhibition against PDK1 kinases with IC_{50} values in the low micro molar region (< 1μM). Furthermore, it was shown that the 1,2,3-triazole ring acts as more than just a linker but displays biological activity. This observation was made by the significantly reduced inhibitory activity exhibited by a compound, when the triazole ring was replaced with a pyrazolyl group. A crystal structure obtained for one of the compounds with PDK1, demonstrated the important binding interactions. This information obtained can be used to design more potent kinase inhibitors that target PDK1.[121]

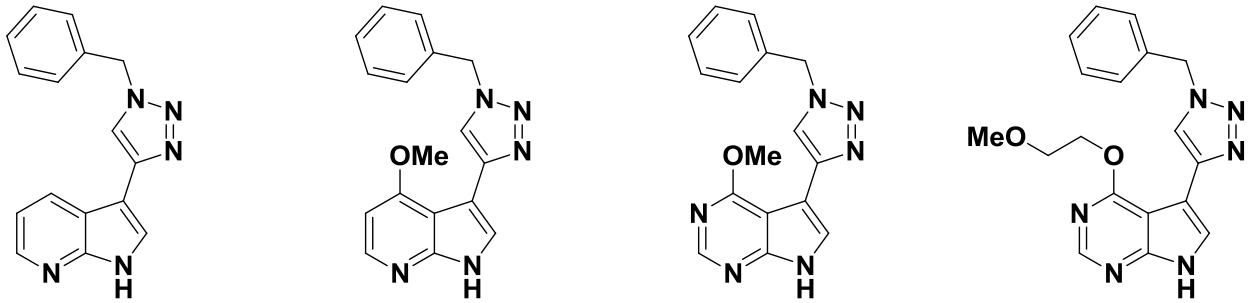

14 IC_{50} = 800 nM

15 IC_{50} = 100 nM

16 IC_{50} = 200 nM

17 IC_{50} = 300 nM

Figure 46

Triazolyl substituted NH heterocyclic inhibitors for PDK1 kinase.[121]

The serine/threonine family of Pim (proviral integration site for Moloney murine leukemia virus) kinases is involved in the regulation of important proliferation and survival pathways in cancer cells. The Pim family consists of three members (Pim1-3) and forms part of a sub-family within the CAMK (calcium/calmoduli-dependant protein kinase) group. These enzymes have been found to be over-regulated in solid tumors and hematological malignancies. Pim kinases are therefore relevant targets for the development of new anticancer drugs.[122-123] Letribot and co-workers demonstrated that pyrrolo[2,3-*a*]carbozole-3-carbaldehydes are potent Pim kinase inhibitors.[124] By studying the binding interactions of pyrrolocarbozole-3-carbaldehyde (figure 47) in the ATP-binding site of the protein kinase Pim, they envisioned to synthesize new pyrrolocarbazoles substituted at the N-10 position via click chemistry.

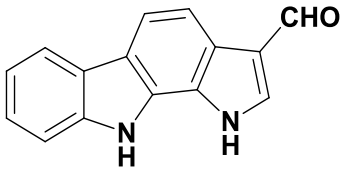

Figure 47
Structure of the reference compound pyrrolocarbozole-3-carbaldehyde.

This particular position was shown not to be directly involved in the interaction within the ATP-binding site, and could serve as a promising site to introduce a group to improve water solubility of the compound, or to introduce a fluorescent moiety to aid in detection.[123]

The azide was introduced to the pyrrolocarbazole backbone over four steps, followed by CuAAC reaction with several alkynes bearing hydroxymethyl, choline (ammonium) and dansyl groups to obtain the final compounds **18**, **19**, and **20**, represented in figure 48. The kinase inhibitory activity of these compounds was tested against Pim1-3, and the pyrrolocarbozole-3-carbaldehyde was used as a reference. The results indicated that the 1,2,3-triazole compounds (**18-20**) inhibited Pim-1 in the same concentration range as the reference compound, whereas they were less active towards Pim-3. Letribot and co-workers thus showed that the N-10 position can be substituted without losing Pim-1 and Pim-3 inhibitory activities. Furthermore, compounds **18** and **19** showed improved aqueous solubility compared to pyrrolocarbozole-3-carbaldehydeand compound **20** demonstrated that fluorescent labels could be added without significant loss of inhibitory potency against Pim-1.[123]

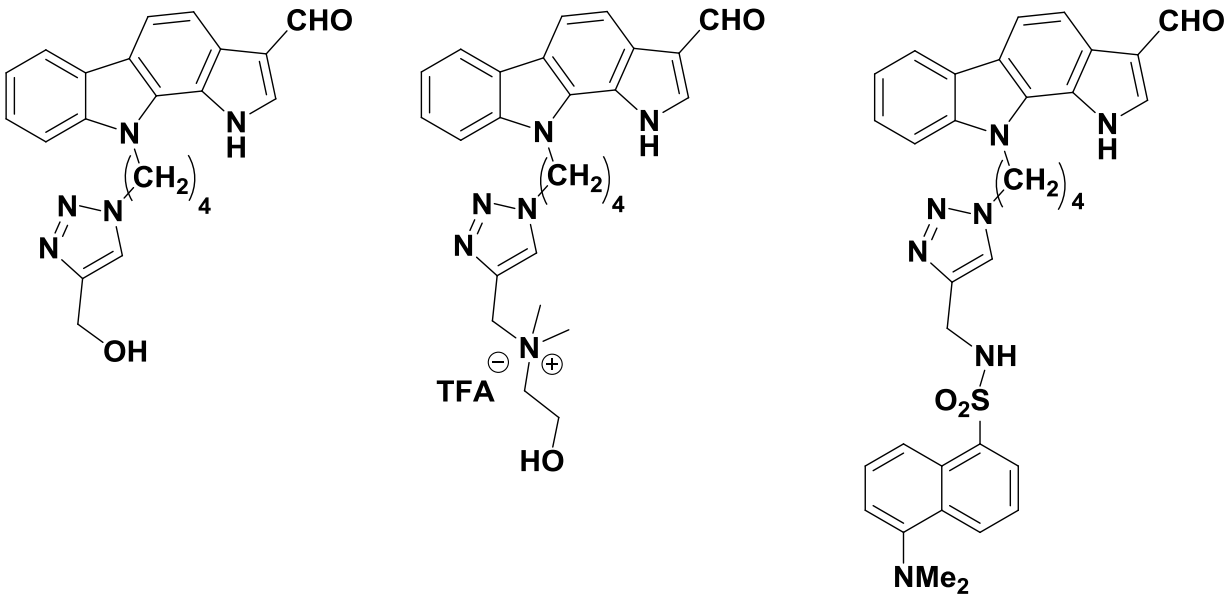

18
IC_{50} = 315 nM against Pim-1
235 nM against Pim-3

19
IC_{50} = 327 nM against Pim-1
490 nM against Pim-3

20
IC_{50} = Not determined

Figure 48
Synthesized analogues substituted at position N-10 via CuAAC.[123]

The fibroblast growth factor receptor (FGFR) family includes four homologous receptor members (FRGR1-4) that are involved in wound healing, development and inflammation. Eighteen FGF ligands have been identified that bind to these types of receptor tyrosine kinases (RTKs). Aberrant FGFR signaling results in the activation of mutations, leading to ligand-independent firing or overexpression of the receptor itself.FGFR3 has been identified as an oncogene in bladder cancers, multiple myeloma, cervical and prostate cancers.[125] An inhibitor (PD173074), exhibiting high potency against FGFR1, VEGFR2 and FGFR3, sparked the interests of Le Corre *et al.* to develop a library of pyrido[2,3-d]pyrimidines using click chemistry. Their efforts were based on the investigation of the binding interactions of the two FGFR-3 inhibitors, PD173074 and SU5402, co-crystallized with FGFR1. Their work involved the synthesis of PD173074 analogues bearing substituents at position 2. By using click chemistry, biologically active triazoles were introduced into the compounds and a small library of inhibitors was quickly obtained (Figure 49).[126]

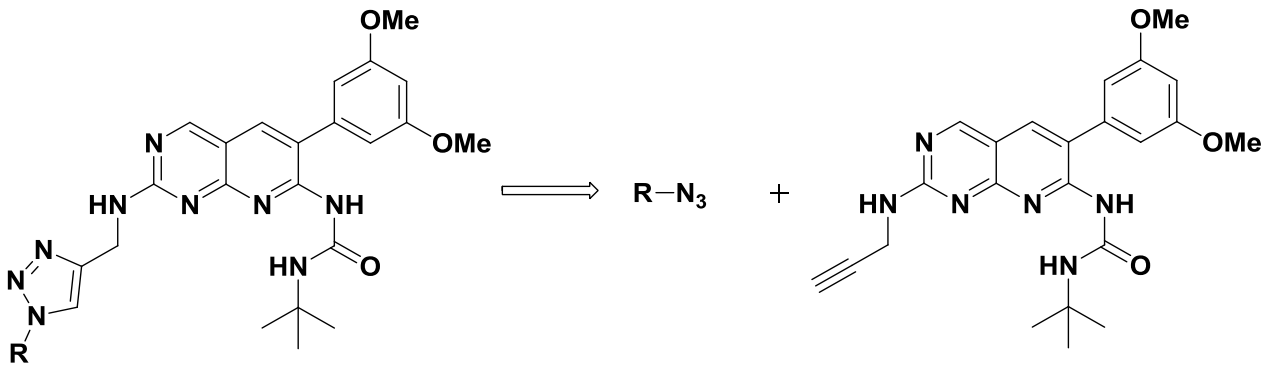

Figure 49
Rationale for the synthesis of "click" pyrido[2,3-d]pyrimidines analogues.[126]

The synthetic strategy employed generated three series of diverse structures. Upon biological evaluation of the compounds, a number of useful observations were made. Among the 27 analogues synthesized more than half exhibited 55-89% inhibition of *in vitro* FGFR3 kinase activity at 2 μM. Introduction of the 1,2,3-triazole moiety at position 2 of the pyridopyrimidine scaffold had no significant negative effect on potency, but the triazole geometry was shown to be crucial for biological activity. For example, compound **21** was found to inhibit auto-phosphorylation of mutant FGFR3-K650M in transfected HEK cells (figure 50).[126]

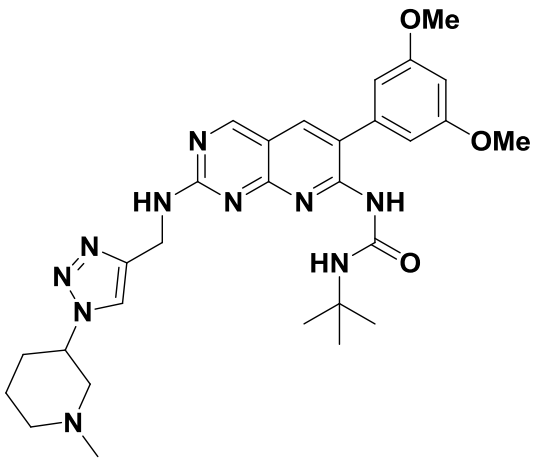

21
Exhibited 89% inhibition of *in vitro* FGFR3 activity at 2 μM

Figure 50
Compound **21** exhibited the most potent inhibitory activity for FGFR3 amongst the library of analogues.[126]

Over the past decade, a useful approach for lead generation, known as fragment-based lead discovery, has emerged.[127] In this strategy, small fragments are identified as starting points to be optimized, and generate lead compounds in subsequent synthetic steps. Efficient potency (affinity) of the initial fragment simplifies the optimization step to deliver potential novel lead compounds for kinase targets.

In the work of Irie and co-workers, it was demonstrated that a kinase focused evolved fragment (KFEF) library could be generated using click chemistry to identify an evolved fragment compound as lead candidate. The design concept of the KFEF library involves the combinatorial assembly of kinase privileged-alkyne fragments and a diverse group of azide fragments as shown in figure 51. The kinase privileged fragments were chosen from kinase inhibitors in the literature to incorporate the crucial hinge binding interactions into the KFEF library. Two different click reactions were then used to generate a diverse library of 1,2,3-triazole compounds. The Cu-catalyzed click reaction were used to synthesize the 1,4-disubstituted 1,2,3-triazoles, while the Ru-catalyzed click reaction was used to construct the 1,5-disubstitued 1,2,3-triazoles.[39]

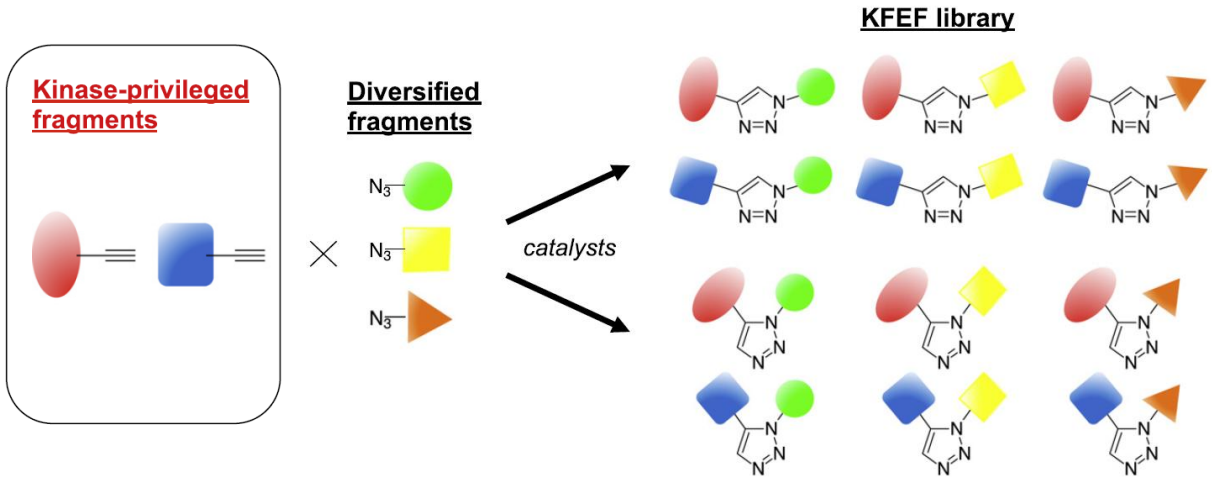

Figure 51
Design of the KFEF library using copper and ruthenium catalyzed click chemistry. Image reproduced from following reference.[39]

In this way a KFEF library of 76 compounds was successfully synthesized and screened against protein kinases FLT3 and GSK3β to identify promising lead compounds. Furthermore, the binding efficiencies, and binding modes of the most potent candidates were evaluated. The KFEF synthesis and screening approach successfully identified two hit compounds shown in figure 52: **22** which exhibited selective inhibitory activity (IC_{50} = 1.1 μM) for FLT3 with excellent binding efficiencies (BEI = 25.2), and **23** which exhibited selective inhibited selective inhibitory activity (IC_{50} = 0.49 μM) for GSK3β, also displaying excellent binding efficiencies (BEI =26.7).

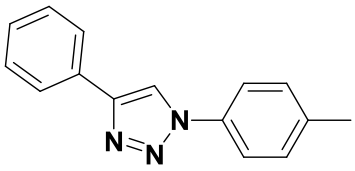

22
IC_{50} = 1.1 μM against FLT3

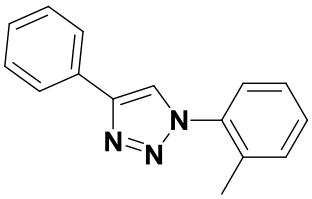

23
IC_{50} = 0.49 μM against GSK3β

Figure 52
Two most promising selective lead compounds (**22** and **23**) selected from the KFEF library. Both compounds are based on the CuAAC approach to afford the regioselective 1,4-disubstituted 1,2,3-triazole structures.[39]

Hereby, Irie and co-workers proved that the KFEF library showed great potential in fragment-based drug discovery, and that click chemistry is a simple but useful strategy to generate large libraries with diverse structures.[39]

For the purpose of this project, specific focus is aimed towards cancer drug discovery and protein kinase inhibitors. However, abnormal protein kinases have been implicated in various diseases and are presented as attractive drug-targets in several fields of medicinal research. Malaria is a major threat to world health, and parasitic protein kinases are suitable targets for drug development. Many of these kinases display profound structural and functional divergence from the human host counterparts. *Plasmodium falciparum* protein kinase 7 (PfPK7) is an "orphan" kinase (non eukaryotic-like protein kinase) which offers promising *P. falciparum* specific drug targets. The organism *P. falciparum* is responsible for the most virulent form of malaria.[128-129]

Purines are involved in many metabolic processes which play significant roles in cell signaling and other fundamental biological processes. This important heterocycle is also the core structure of adenine and guanine in nucleic acids. To design selective kinase inhibitors, the independent work of Shokat and Pan *et al*., showed that non-ATP binding pockets (less conserved) are targeted by 4-aminopyrazolo[3,4-*d*]pyrimidine scaffolds with a "bent" geometry of the substituents in the 3-position of the pyrazole ring.[130-131] Klein and co-workers were motivated by these findings, to develop new 4-aminopyrazolo[3,4-*d*]pyrimidines, by using click chemistry to introduce a bent geometry triazole ring at position 3 of the pyrazole ring. Two efficient routes, involving a one-pot two-step reaction, were used to obtain compounds (**24** and **25**) with both 1- and 4-substituted triazole rings in the 3-position of the pyrazole ring as illustrated in figure 53.[132]

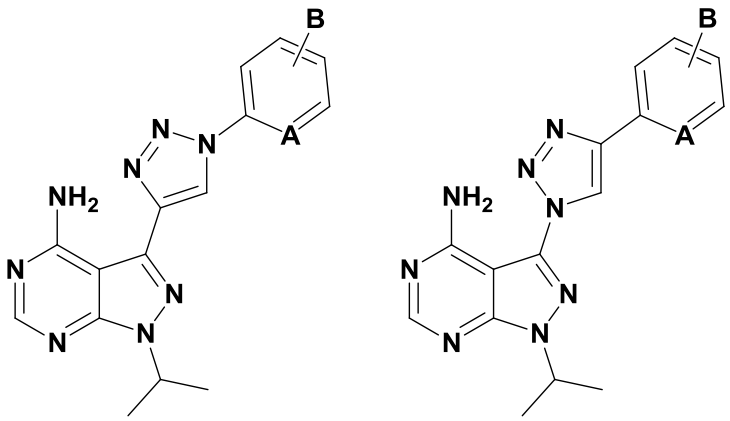

24 **25**

Figure 53

General structures of 3-(1,2,3-triazol-4-yl)-substituted pyrazolo[3,4-*d*]pyrimidin-4-amines (**24**) and 3-(1,2,3-triazol-1-yl)-substituted pyrazolo[3,4-*d*]pyrimidin-4-amines (**25**).[132]

Upon investigation of X-ray studies of PfPK7 kinase with different known inhibitors, Klein *et al*. observed that the structures of the inhibitors were based on the same pyrazolopyrimidine scaffold as those synthesized in their work. Therefore, the 4-aminopyrazolo[3,4-*d*]pyrimidine analogues synthesized via the click chemistry approach were tested against recombinant PfPK7 kinase. These tests involved an inhibition assay that measured the efficacy of compounds at decreasing myelin basic protein (MBP) phosphorylation. A significant decrease in MBP phosphorylations was observed with compounds **26** and **27** (IC_{50} = 20 μM and 10μM, respectively) as shown in figure 54. The binding mode of **26** in docking studies revealed that the compound binds in the ATP-binding site of the kinase and not in an allosteric site, as was desired. Although the compounds were able to decrease the activity, complete inhibition of the kinase was not successful. However, the study identified some of the very few inhibitors that target the PfPK7 kinase and can be useful in developing lead compounds.[132]

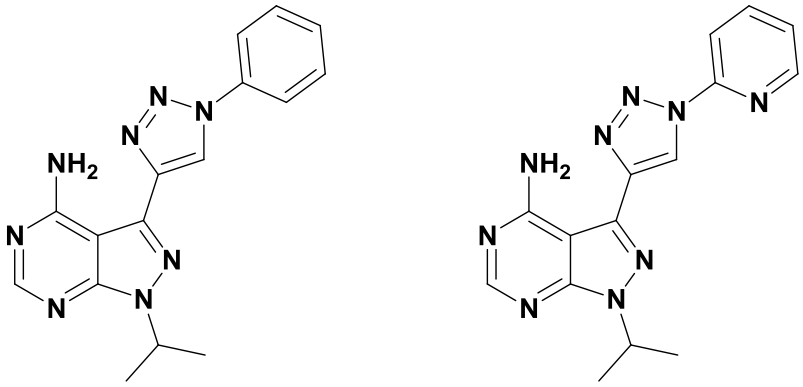

26
IC_{50} = 20 μM against PfPK7

27
IC_{50} = 10 μM against PfPK7

Figure 54
Compounds **26** and **27** exhibiting inhibitory activity against PfPK7.[132]

As previously stated, (See section 1.5.2) the natural product staurosporine has been an inspiration for the design of various therapeutic agents.[83] In addition, the "open" form of the natural indolocarbazole scaffold has exhibited improved selectivity as demonstrated by the two PKC selective kinase inhibitors, Enzastaurin and Ruboxistaurin, currently under clinical trials.[133-134] The enhanced selectivity of these structures, together with the fact that click chemistry has become a major tool in hit discovery, motivated Gu and co-workers to develop novel bisaryl maleimides through the CuAAC approach. A general structure of the click bisaryl maleimides is shown in figure 55. In this study, seven structurally diverse click bisaryl maleimides were generated and evaluated against four cancer cell lines. One compound (**28**), shown in figure 56, was selected as a representative to enter into kinase inhibitor assay, and proved to be a highly selective hit compound. In a panel of 124 kinases, the hit compound **28** only showed high potency against three kinases (GSK-3β, CLK2 and VEGFR2). From the kinase inhibitory activity data, the best inhibitory potency was against protein kinase GSK-3β.[86]

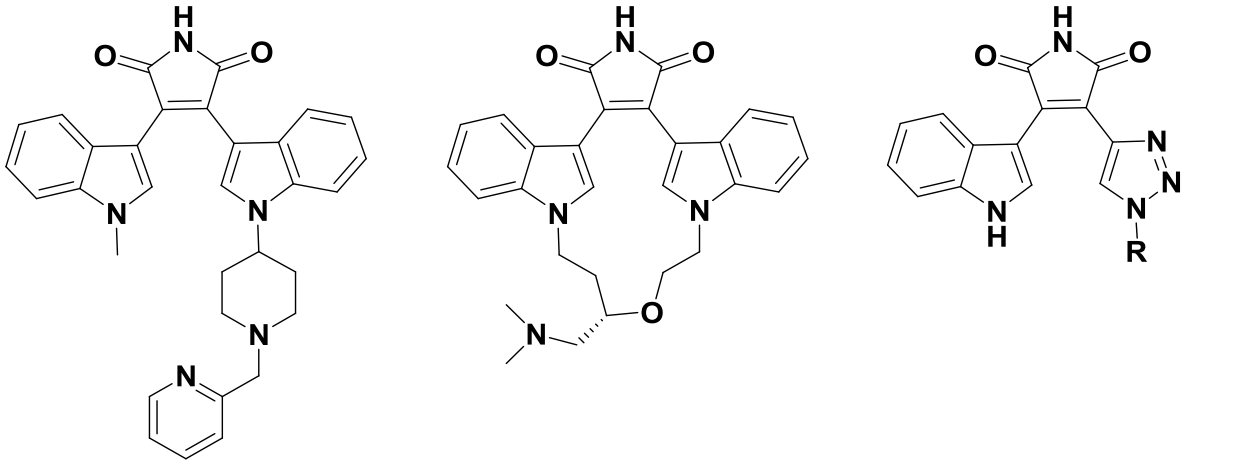

Enzastaurin **Ruboxistaurn** **"Click" bisaryl maleimides**

Figure 55

The design of bisaryl maleimides *via* click chemistry. These structures are based on the "open", selective indolocarbazoles, Enzastaurin and Ruboxistaurin.[86]

To understand the high selectivity demonstrated by compound **28**, its structural features were investigated. An ATP-competitive experiment confirmed that **28** is an ATP competitive inhibitor and docking studies involving the GSK-3β crystal structure identified further interactions (figure 56). An interesting observation, to explain the mechanism of selectivity, was the distinct inward flip of Phe67 in the active site. In this way, Phe67 was presented at a suitable distance to the phenyl group of **28** to form π-π interactions. The inward flipping of Phe67 caused a conformational change of the P-loop and thereby a dramatic topological change of the ATP binding site. The authors proposed that the deformed P-loop may account for the high selectivity of **28** in the 124-kinase assay. In addition, the triazole ring, introduced by the click reaction, allowed for additional π-π stacking interactions within the binding pocket. The work of Gu *et al*. showed that the combination of click chemistry and rational design can be a powerful approach for hit discovery.[86]

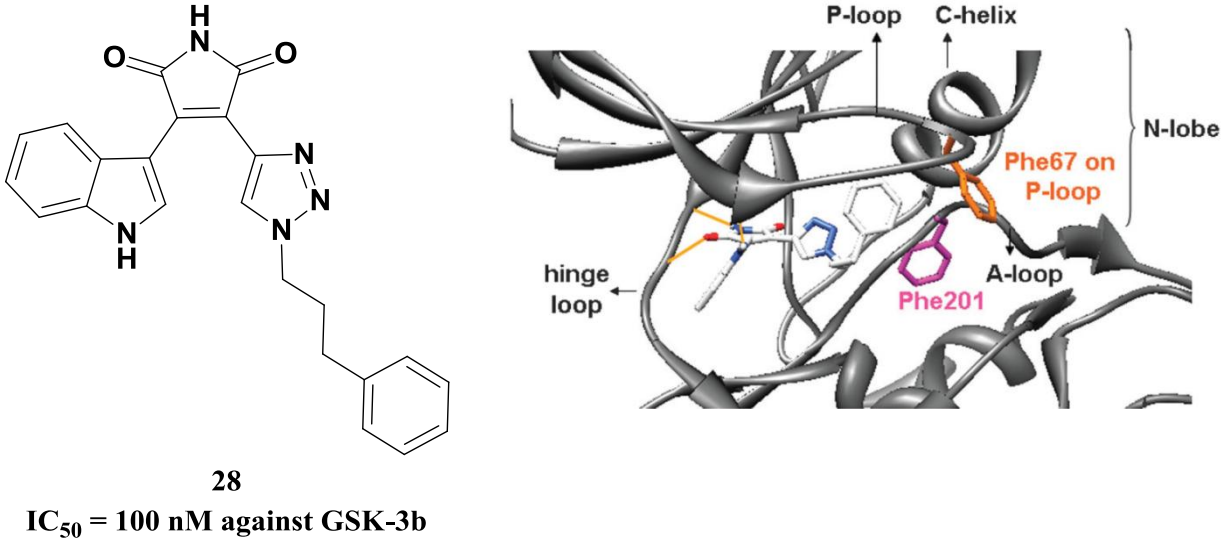

28

IC_{50} = 100 nM against GSK-3b

Figure 56

The selective bisaryl maleimide **28** and a representation of its docking within the ATP-binding site of GSK-3β kinase. The inward flipping of the Phe67 (orange) on the P-loop is illustrated. Image reproduced from the following reference.[86]

Click chemistry has proven to be a powerful tool in biomedical research, and the importance of triazole compounds is undeniable.[88, 97] The various examples given in this section illustrate the use of the click approach, particularly CuAAC, in the development of kinase inhibitors. The work undertaken by these research groups is also current (published between 2009 and 2014), demonstrating the potential of utilizing click chemistry as a promising approach to develop new effective kinase inhibitors.

2.2 Aims

In this project we envisaged to develop potential kinase inhibitors that would selectively target EGFR. Exploiting the attractive features demonstrated by the natural product staurosporine, the design was based on a staurosporine scaffold. The project was composed of two parts. The first part involved the synthesis of compounds having the closed pyrrolocarbazole core, while the second part focused on the synthesis of compounds resembling an "open" form of indolocarbazole derivatives (figure 57).

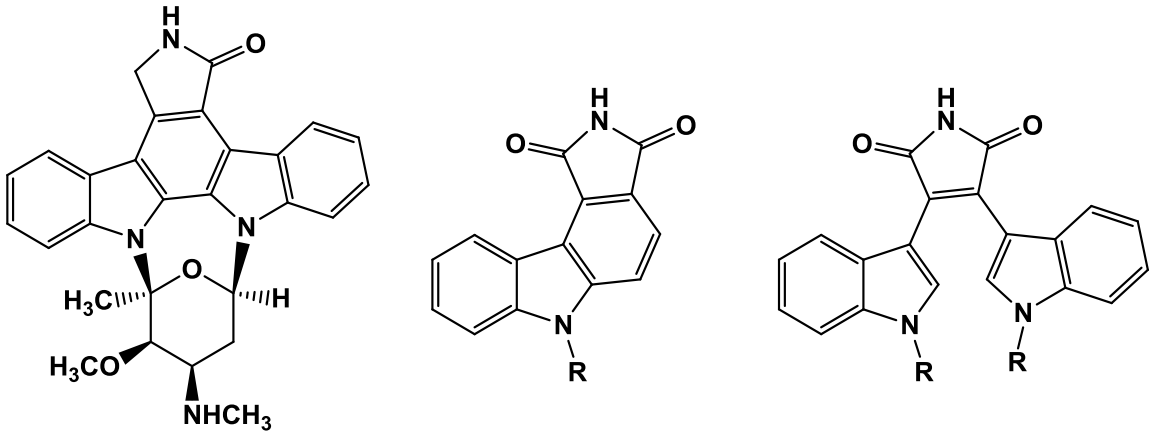

Figure 57
Staurosporine inspired pyrrolocarbazole and "open" indolocarbazole compounds.

The pyrrolocarbazole scaffold could act as a driving portion that would present a suitable platform to incorporate various warheads **(R)** at a proper trajectory (figure 58). Displaying the warhead at a particular distance and orientation, a potential covalent interaction to cysteine 797 could form in the kinase active site.

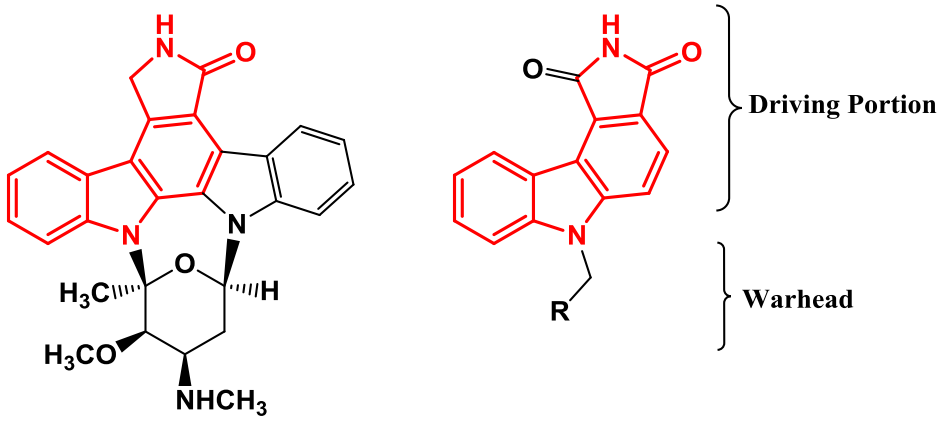

Figure 58
Pyrrolocarbazole driving portion with warhead.

The second part of this project was mainly motivated by the success of the "open" indolocarbazole derivative, enzastaurin, which has demonstrated kinase inhibitory activity with enhanced selectivity. A major source of inspiration in the design of these "open" structures is based on click chemistry to generate bisaryl maleimide derivatives, as well as bisamino maleimides as seen in figure 59. Incorporating a warhead **(R)** is also crucial in this strategy to afford potential kinase inhibitors. It must be noted that the warhead **(R)** can be a functionality that either acts in a reversible, or irreversible manner.

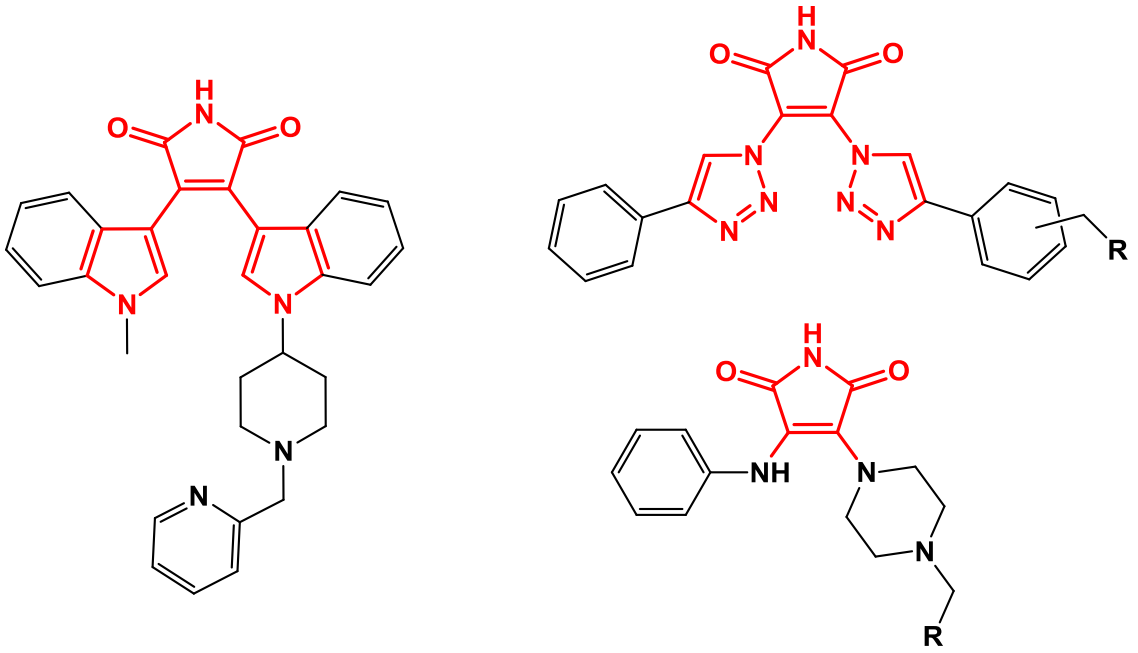

Figure 59

The staurosporine muse enzastaurin (left structure), an inspiration for the design of the click- and bisamino products.

In the following chapters, we discuss the research strategies undertaken to generate the desired compounds. A detailed description of the synthesis is given, including the challenges encountered and decisions taken to successfully obtain the final products.

CHAPTER 3 –PYRROLOCARBAZOLE ANALOGUES

3.1 Towards the pyrrolocarbazole kinase inhibitors

The initial focus of this project was towards the synthesis of staurosporine-inspired pyrrolocarbazole compounds as kinase inhibitors. Incorporating various groups onto the pyrrolocarbazole scaffold would allow for the prospect of developing both reversible and irreversible inhibitors. In the following section, the research strategies employed will be described, as well as the reactions used to design the staurosporine analogues as potential EGFR kinase inhibitors.

3.1.1 Motivation from previous research

The design of these compounds was motivated by previous research undertaken in our group. In this regard, compound 29 demonstrated encouraging results upon biochemical screening against the wild type (WT) and mutant strains of EGFR. A favorable selectivity profile towards the mutant strains was exhibited with very little inhibitory activity for the normal EGFR WT. Good inhibition for the single mutant EGFR was shown (IC_{50} = 1320 nM), while a better inhibitory activity (IC_{50} = 1190 nM) was demonstrated for the double mutant strain of EGFR (figure 60). Compared to the FDA approved EGFR inhibitor, Gefitinib (see section 1.4.2, figure 17), compound **29** exhibits an inhibitory activity approximately twice as potent against the double mutant strain, and 0.5 fold more potent against the single mutant strain. These promising results, together with the practicable synthetic procedures, inspired the development of various derivatives based on the pyrrolocarbazole scaffold.

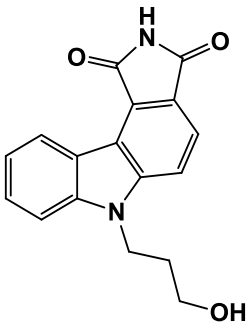

29

IC_{50} = 1320 nM against L858R
IC_{50} = 1190 nM against L858R-T790M

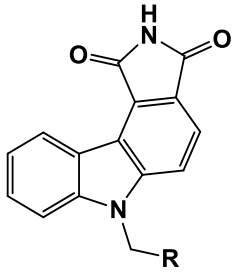

Pyrrolocarbazole Derivatives

R = Warhead for reversible or irrevesible inhibition

Figure 60
Compound **29** activity against single and double mutations and the general structure of the pyrrolocarbazole derivatives synthesized in this project.

3.2 Strategy pertaining to the synthesis of *N*–acryloyl target compound 30

In order to build the pyrrocarbazole backbone, a proposed synthetic strategy was considered, as outlined in scheme 4. The linear synthesis involved a number of steps including protection, reduction, oxidation, Wittig reaction, Diels-Alder reaction, aromatization and finally the introduction of a possible warhead. A particular concern was the outcome of the exposed acidic indole amine proton during the Wittig reaction. In addition, the 2-vinyl-1*H*-indole could have posed a possible threat to instability and caused the product to undergo polymerization. For this reason, we proposed that the introduction of an electron withdrawing protecting group on the indole amine, prior to the Witting reaction, could circumvent these potential problems. Once the alkene product was generated, a Diels-Alder reaction, using maleimide as the dienophile, could be performed. Following aromatization, the pyrrolocarbazole scaffold would then be available for further modification.

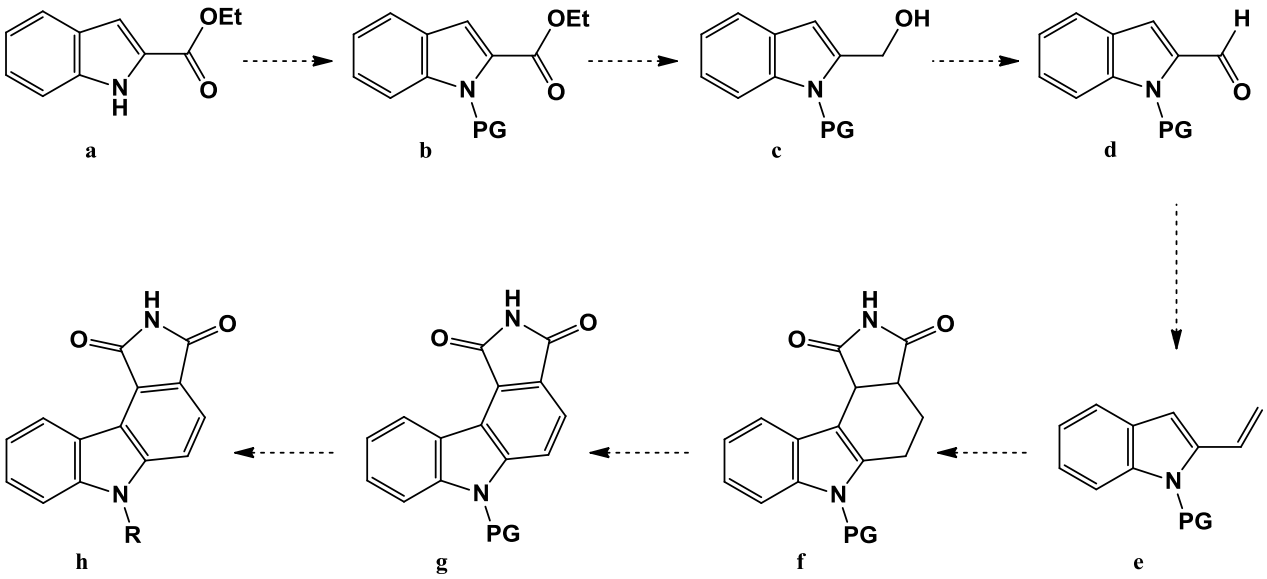

Scheme 4

Outline of strategy towards the pyrrolocarbazole backbone**.**

The initial target compound [6-acryloylpyrrolo[3,4-c]carbazole-1,3(2*H*,6*H*)-dione] (**30**), was devised to incorporate a Michael acceptor functionality, namely the acryl amide group, in the pyrrolocarbazole scaffold (figure 61). The acryl amide group has been involved in numerous investigations as an electrophilic warhead in the design of irreversible kinase inhibitors.[40,54,135-136] By integrating this functionality into an appropriate driving portion, such as the pyrrolcarbazole scaffold, the potential to form a covalent interaction with an appropriate cysteine residue present in the kinase, was expected to be enhanced (see section 1.4.2).

***N*-acryloyl target compound**

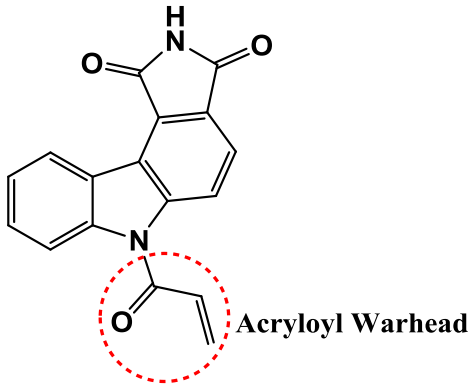

30

Figure 61

Structure of N – acryloyl target compound as a potential irreversible kinase inhibitor.

Molecular modeling analysis for this target compound was performed previously in the group and the docking studies revealed an appropriate orientation and distance (2.9 Å) of the potential inhibitor warhead (β carbon of the acryloyl group) to the nucleophilic thiol of cysteine 797 (Cys797) (figure 62). A major goal in the design of the target compound was to improve kinase selectivity (by introducing the irreversible warhead), while maintaining the potency of staurosporine. With this aim in mind, the synthesis of the pyrrolocarbazole scaffold (driving portion) was embarked.

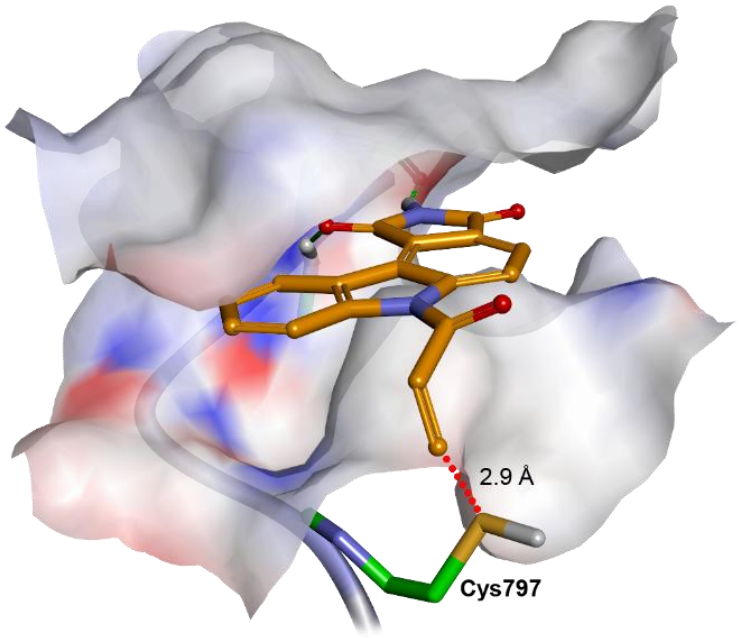

Figure 62

Representation of the target compound 30 in the EGFR domain. The close proximity (2.9 Å) between the β carbon of the acryloyl group and Cys797 is demonstrated.

3.3 Towards *N*-acryloyl target compound 30

3.3.1 Synthesis of 1-*tert*-butyl 2-ethyl 1*H*-indole-1,2-dicarboxylate (32)

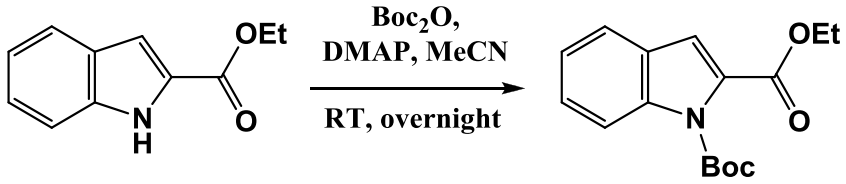

31 **32**

Scheme 5

The first step of the synthesis involved conversion of **31** into **32**. This was done to avoid possible polymerization of the impending vinyl indole. The electron-withdrawing ability of this carbamate group was envisioned to stabilize the Wittig product. Following a procedure in literature, the reaction proceeded smoothly as shown in scheme 5.[138] Upon treating a solution of ethyl indole-2-carboxylate (**31**) in MeCN with Boc_2O and DMAP, the product was obtained and purified by means of column chromatography. The pure compound (**32**) was afforded in a good yield of 85%.

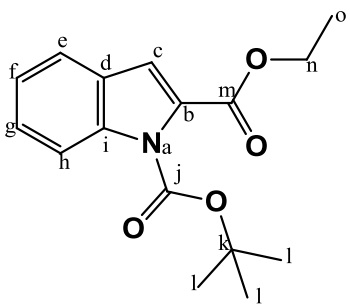

The ^1H NMR spectrum of the product **32** corresponded well to that reported in literature.[138] A clear indication that the Boc protection was carried out successfully was demonstrated by the absence of the broad signal for the –NH indole group, and the formation of a new singlet at 1.64 ppm. The singlet integrated for nine and was assigned to H_l. The remainder of the proton signals corresponded to the starting material and could all be accounted for in the spectrum.

3.3.2 The reduction and oxidation reactions

A number of reducing and oxidizing agents are capable of generating the 1*H*-indole-2-carbaldehyde required for the Wittig reaction. One option was to use the reducing agent DIBAL, which is known to reduce esters into aldehydes in a single step, but risks the formation of a mixtures of products.[139] It was decided to synthesize the indole aldehyde in two separate controlled steps. Firstly, the reactive hydride reducing agent, $LiAlH_4$, would be used to form the alcohol, followed by oxidation using MnO_2, to generate the desired aldehyde species. This approach was motivated by the high yields reported in literature and the accessibility of the reagents.[140-145]

3.3.2.1 Reduction using $LiAlH_4$

$LiAlH_4$ is a powerful reducing agent, which reduces a vast number of different functional groups. Its discovery was made in 1947 by Finholt, Bond and Schlesinger.[146] The presence of a polar metal hydrogen bond makes $LiAlH_4$ a strong reducing agent, serving as a source of hydride for reduction.[147] This reaction is one of the best ways of making alcohols from esters.[148] The reactive $LiAlH_4$ hydride attacks the carbonyl of the ester, forming an aldehyde. This aldehyde is even more reactive than the ester starting material, and readily undergoes a second attack from the $LiAlH_4$ hydride, forming an alkoxide anion. Following hydrolysis by H_2O, the primary alcohol product is generated. The general mechanism is illustrated in scheme 6.[148]

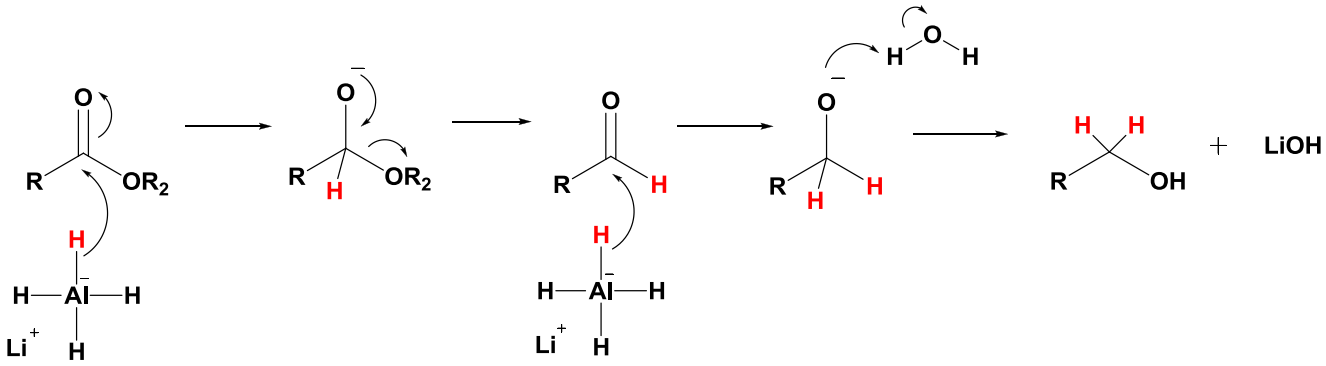

Scheme 6

General mechanism for the reduction of an ester using $LiAlH_4$.[148]

3.3.2.2 Attempted synthesis of *tert*-butyl 2-(hydroxymethyl)-1*H*-indole-1-carboxylate (33)

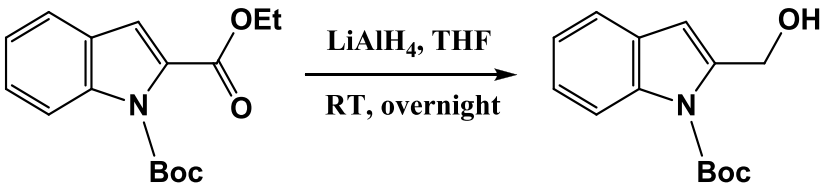

32 **33**

Scheme 7

Direct $LiAlH_4$ reduction of the Boc product **32**, resulted in numerous products (as per TLC) and the reaction was attempted without the Boc-protecting group.

3.3.2.3 Synthesis of (1*H*-indol-2-yl)methanol (34)

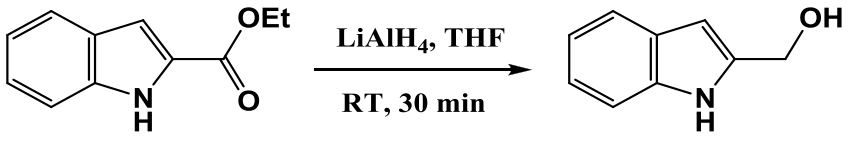

31 **34**

Scheme 8

Subsequently, the reduction of commercially available ethyl indole-2-carboxylate (**31**), was carried out successfully by using the same procedure as described in section 3.3.2.2. and in literature.[143] The reaction was completed within 30 minutes when stirred at room temperature. Upon completion the excess $LiAlH_4$ was quenched with H_2O and NaOH (1M) and stirred for a further 30 minutes. Following filtration, a workup was performed. The crude product was purified by column chromatography, affording the pure product (**34**) in an excellent yield of 93%.

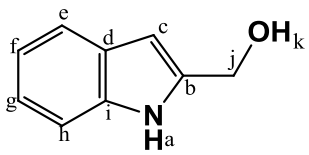

The ^{1}H NMR spectrum of the product (**34**) corresponded well to that reported in literature.[149] The reduction of the ester group to a primary alcohol functionality was clearly evident by the presence of a broad $-OH_k$ signal at 1.99 ppm. Further evidence was obtained by the singlet of H_j at 4.80 ppm, integrating for two. The absence of the triplet and quartet signals, which belonged to the ester functionality, was another indication that the reduction was successful.

3.3.2.4 Oxidation using MnO_2

MnO_2 is one of the most attractive inorganic materials due to its extensive range of applications, its low cost, and environmentally benign nature. MnO_2 is a widely used standard oxidant, employing very mild conditions and simple work-up procedures.[150-151] The oxidative ability of MnO_2 has been known since the 1870's. [151] The first publication of active MnO_2 as organic oxidant was reported in 1948 by *Ball et al*. for the oxidation of vitamin A to retinene.[150,152] The oxidizing power of this reagent depends largely on its preparation and reaction temperature. MnO_2 is able to oxidize a large number of functionalities and perform selective oxidation, provided that the reaction temperature is not too high. [147,151] Mechanistic studies involving the oxidation of alcohols with MnO_2 have met a number of difficulties and uncertainties regarding the chemical nature of the real reagent in the excess of MnO_2.

The mechanism involves complexation of the alcohol on the surface of MnO_2 particles, followed by oxidation and desorption of the carbonyl compound. The complexation may be aided by the presence of foreign particles in the large amount of MnO_2. A number of mechanistic proposals have been made which correspond with experimental data.

Pratt and van de Castle suggested a radical mechanism as shown in scheme 9. In combination with the work of Hall and Story, a refined radical mechanism involving an intermediate manganese ester, was proposed by Goldman (Scheme 9). Kwart and George also proposed a mechanism whereby hydrogen transfers via a cyclic five-membered transition state as seen in Scheme 9.[151]

Radical mechanism

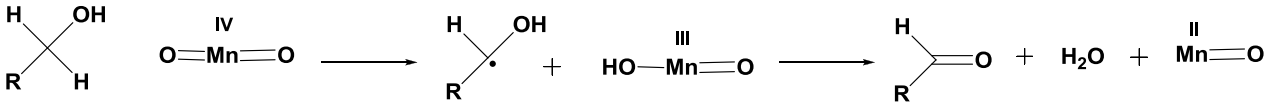

Refined radical mechanism

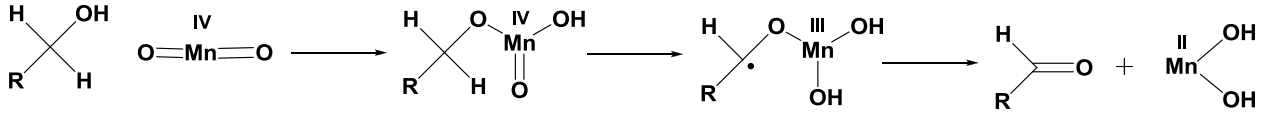

Hydrogen transfer by cyclic transition state mechanism

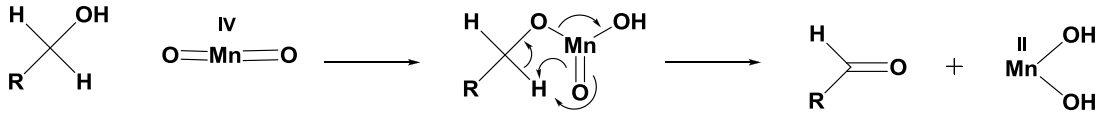

Scheme 9
Proposed mechanisms for MnO_2 oxidation.[151]

3.3.2.5 Synthesis of 1*H*-indole-2-carbaldehyde (35)

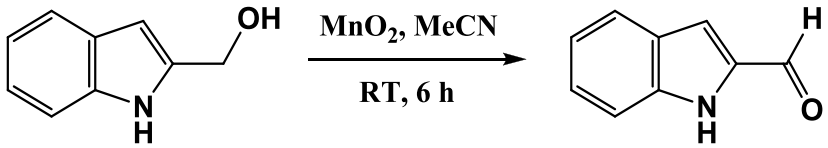

34 **35**

Scheme 10

Another effective reaction in our synthetic route was the oxidation of the primary alcohol (**34**) to the aldehyde (**35**). This reaction proceeded smoothly without any difficulties. MnO_2 was employed as oxidizing agent and led to the procedure being very simple. Prior activation of the MnO_2 was achieved by placing a beaker of MnO_2 in an oven at 120 ° C for 24 hours.

The activation step was a crucial preliminary measure taken to ensure the oxidation reaction succeeded. Upon completion of the reaction, the product (**35**) was afforded in a good yield of 76%. This allowed for subsequent Boc-protection compound **36**.

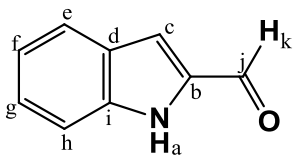

The ^{1}H NMR spectrum of the product (**35**) compared well to that found in literature.[139,149] The loss of the signal at 4.80 ppm, which belonged to the methylene group of the primary alcohol, and the formation of the distinctive H_k aldehyde singlet at 9.86 ppm, was an indication that the product formed was in fact the 1*H*-Indole-2-carbaldehyde. In addition, the remainder of the aromatic peaks and the amine –NH_a were all accounted for.

3.3.3 Synthesis of *tert*-butyl 2-formyl-1*H*-indole-1-carboxylate (36)

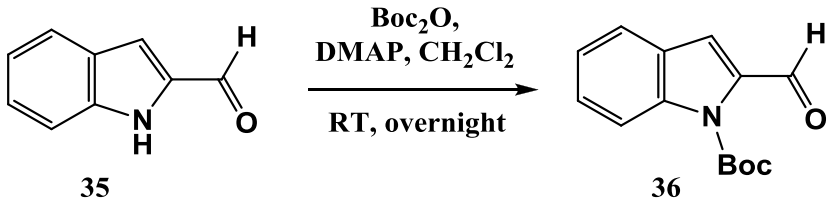

Scheme11

The Boc-protection of the 1*H*-Indole-2-carbaldehyde (**35**) followed a similar method to the protection reaction of the indole ester (**31**) utilized earlier (see section 3.3.1), shown in scheme 11, affording the pure compound (**36**) in a good yield of 88%.

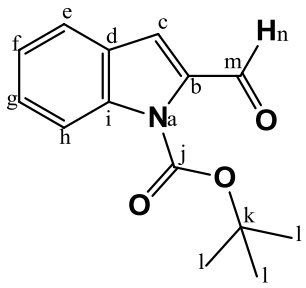

The ^{1}H NMR spectrum of the product (**36**) compared well to that in literature.[149] The absence of the indole –NH_a broad signal and the presence of the new singlet (H_l) at 1.72 ppm, which integrated for nine, was proof that the Boc-protection had been successful.

3.3.4 The Wittig reaction

The impact of the Wittig reaction on synthetic organic chemistry has been monumental. This reaction between phosphorus ylids and aldehydes/ketones has been referred to as "the most important practical method for the construction of carbon-carbon double bonds." [153,154] The first ylid was synthesized more than a century ago, but ylid chemistry did not flower until the Nobel-Prize-winning work of Wittig in 1953.

The Wittig reaction was born in 1919-1921, when Staudinger and coworkers, prepared, isolated and recognized the first ylid. However, the significance of this discovery and its versatility as a synthetic tool for olefination of carbonyl compounds was only established by George Wittig a few decades later. [154-155]

One of the main virtues of the Wittig reaction is its complete structural specificity. The formation of *Z* or *E* alkenes can be controlled by the selection of the type of ylid, the type of carbonyl compound, or the reaction conditions – all of which have been the subject of intense study.[154] The mechanism of the Wittig reaction has been investigated for more than 40 years and a total of eight mechanisms have been proposed since 1953.[153] Detailed studies led to the currently accepted mechanisms which can be described separately according to the nature of the ylid.[154] Stabilized ylids characteristically have conjugating or anion-stabilizing substituents adjacent to the negative charge, whereas non-stabilized ylids do not possess these functionalities. The general rule states that stabilized ylids are selective for the formation of (*E*)-alkenes, while non-stabilized ylids favour the formation of (*Z*)-alkenes.[148] Although no single mechanism exists, a "general mechanism" - as represented in scheme 12 - does encompass the behaviour of the different ylids. Two major aspects of the ylids, which account for the stereochemical outcome, includes differences in the rate-determining step and structure detail of the transition state to the oxaphosphatanes.[153]

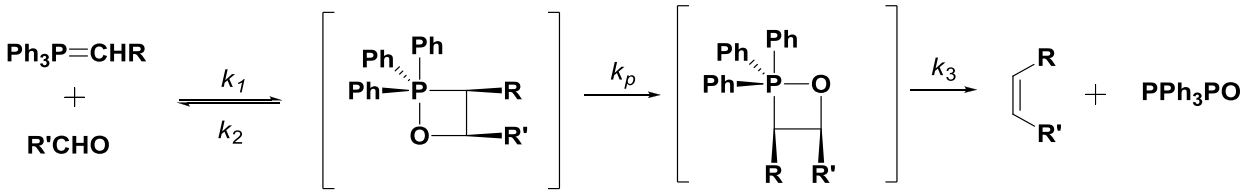

Scheme 12

General mechanism of the Wittig reaction involving oxaphosphatanes and different rate-determining steps.[153]

For the purpose of this project, the Wittig reaction product required to build the pyrrolocarbazole backbone may demonstrate instability and risk polymerizing as shown in figure 63. To circumvent this potential problem, the introduction of an electron withdrawing protecting group could offer stabilization to the vinyl indole and avoid polymerization.

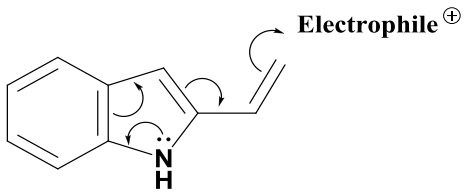

Figure 63

Possible polymerization of the vinyl indole.

3.3.4.1 Attempted synthesis of *tert*-butyl 2-vinyl-1*H*-indole-1-carboxylate (37)

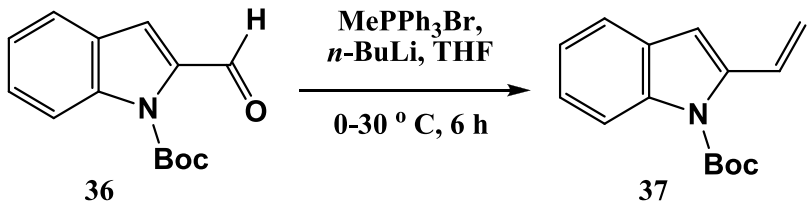

36 37

Scheme 13

Having the Boc-protected 1*H*-indole-2-carbaldehyde (**36**) in hand, the Wittig reaction was performed as shown in scheme 13, with the aim of synthesizing the stabilized vinyl indole (**37**). Unfortunately, this reaction was unsuccessful. The procedure initially involved the generation of the ylid, by treating $MePPh_3Br$ with *n*BuLi in dry THF. The yellow/orange colour change of the reaction was a good indication of ylid formation. The ylid was then reacted with the Boc-protected 1*H*-Indole-2-carbaldehyde (**36**), but resulted in most of the starting material remaining unreacted. Upon increasing the temperature and the concentration of the ylid, multiple spots were observed (as per TLC), and it was suspected that the Boc-protecting group was not stable enough to withstand these reaction conditions.

3.3.5 Use of an alternative protecting group

The problems associated with the Wittig reaction led to the belief that the Boc-carbamate was not the correct choice of protecting group for the strategized synthesis. Sulfonamides are amongst the most stable of the nitrogen protecting groups.[156] For this reason, it was decided to devise an alternative route using a benzenesulfonyl protecting group. Not only would it serve as a good protecting group, but additionally, it would facilitate a directed *ortho*-lithiation reaction to incorporate the desired aldehyde functionality.The synthetic strategy is outlined below in Scheme 14.

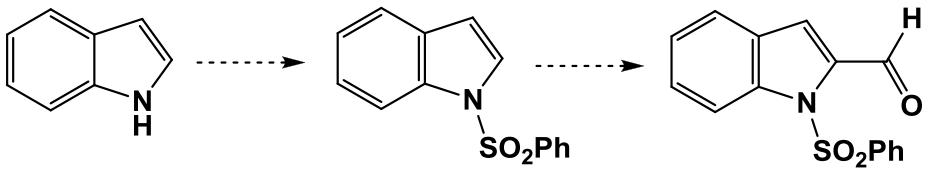

Scheme 14

Outline of strategy to use benzenesulfonyl as an alternative protecting group.

3.3.5.1 Synthesis of *tert*-butyl 2-formyl-1*H*-indole-1-carboxylate (39)

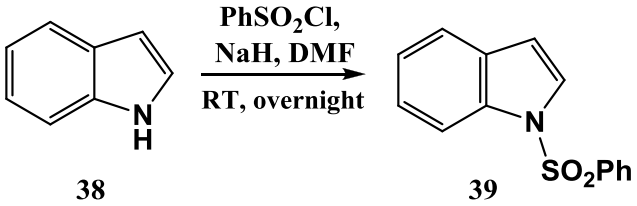

38 **39**

Scheme 15

The synthetic route was embarked by firstly introducing the benzenesulfonyl group to the indole (**38**). This was accomplished by treating indole, dissolved in dry DMF, with NaH, followed by the drop-wise addition of benzenesulfonyl chloride. The reaction mixture was stirred at room temperature overnight. Upon completion, a workup was performed, and no further purification was required. In this manner, the crude product (**39**) was obtained in a yield of 55%.

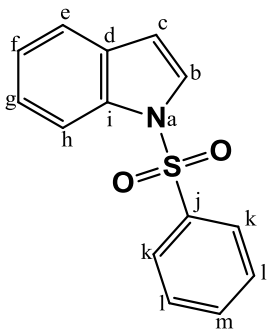

The ^{1}H NMR spectrum of the product (**39**) was compared to that in literature and corresponded well.[157] The absence of the broad signal of the indole –NH_a and the clear increase of aromatic signals (H_k, H_l, H_m), was indicative of the benzenesulfonyl indole product formed during the reaction.

3.3.5.2 Synthesis of 1-(phenylsulfonyl)-1*H*-indole-2-carbaldehyde (40)

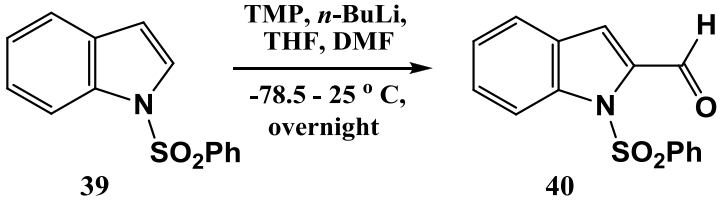

39 **40**

Scheme 16

Having synthesized the benzensulfonyl indole (**39**), the next reaction involved a directed ortholithiation using a large bulky base (TMP), *n*-BuLi and DMF as shown in scheme 16. A proposed mechanism of the reaction is shown in scheme 17. The manner in which the reaction was carried out is briefly explained. Formation of the non-nucleophilic base LiTMP was performed *in situ* by treating a solution of TMP, in dry THF, with *n*-BuLi at -78 °C. The reaction flask was transferred to an ice bath and stirred at 0 °C, for 30 minutes. The indole was then added to the LiTMP solution and stirred for an hour at -78 °C, following an extra 20 minutes of stirring at 0 °C. At this stage we had hoped to form the aryllithium species.

The presence of the sulfonyl functionality was critical for this step, since the sulfonyl oxygen guides the LiTMP to attack the adjacent proton, by forming a complex with the Lewis-acidic lithium atom.[148]

The next step of the reaction was to introduce the aldehyde functionality by using DMF. This was achieved by adding DMF to the reaction mixture at -78 ° C, and allowing the reaction temperature to increase to room temperature. The progress of the reaction was monitored by TLC, and it was observed that some of the benzenesulfonyl indole (**39**) remained unreacted. For this reason, the reaction was left to stir overnight. Unfortunately, the reaction did not progress to completion. The mixture was then quenched with saturated NH_4Cl and a workup was performed. The product (**40**) was purified by means of column chromatography and was obtained in a rather low yield of 36%. The low yield can be ascribed to the reaction not proceeding to completion. This may be as a result of the aryllithium species formation not being completely successful.

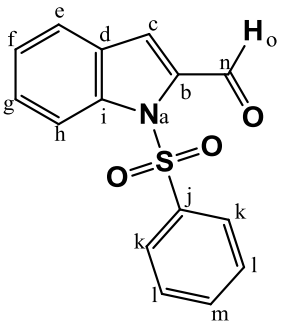

The ^1H NMR spectrum of the product (**40**) was compared to that found in literature and corresponded well.[158] The formation of a new singlet at 10.53 ppm which integrated for one, was indicative of the characteristic aldehyde signal of H_o. The rest of the aromatic signals were all accounted for in the spectrum, and agreed with the expected integration.

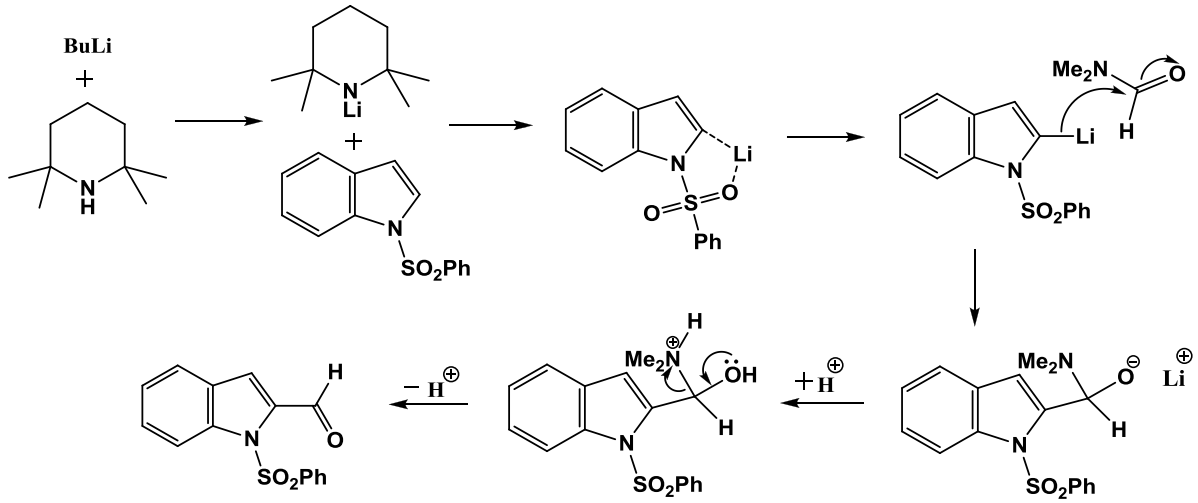

Scheme 17
Proposed ortholithiation mechanism to generate the benzensulfonyl indole aldehyde.[148]

3.3.6 Use of the unprotected indole system

In addition to the anticipated problems regarding vinyl indole polymerization (see figure 63), another reason for incorporating a protecting group was not only to obtain the desired products, but also to synthesize these compounds in high yield. Previous studies have shown that the pyrrolocarbazole demonstrates poor solubility – a factor which becomes rather problematic, especially when performing subsequent reactions.[159] This establishes another motive for introducing a protecting group - to provide the pyrrolocarbazole with a more organic character and enhance solubility. Unfortunately, both the Boc-protecting group and benzenesulfonyl group did not meet the requirements to a satisfactory level - the Boc-carbamate resulted in multiple products during the Wittig reaction, while the route incorporating the benzenesulfonyl group rendered low yields. A concurrent synthetic strategy was undertaken, involving a procedure in which a protecting group was omitted, as demonstrated by Tao *et al*.[160] The previous premonition of 2-vinyl-1*H*-indole instability was reconsidered, and the unprotected route was attempted. Furthermore, we envisioned that the pyrrolocarbazole would be soluble in DMF, which is a suitable solvent to carry out the final step (an alkylation reaction), to introduce the acryloyl moiety.

3.3.6.1 Synthesis of 2-vinyl-1*H*-indole (41)

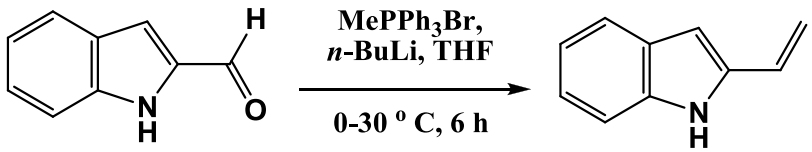

35 **41**

Scheme 18

This reaction was performed in the same manner as the initial Wittig reaction (see section 3.3.4.1) as shown in scheme 18. The ylid generation was carried out exactly the same, but with a higher concentration relative to the indole aldehyde (**35**). A number of optimization reactions were carried out in which the equivalents of ylid used was varied. Once the ylid was formed, a solution of compound **35** was added in a drop-wise manner at 0 °C, and stirred for 6 hours at room temperature. To our delight, TLC monitoring indicated full consumption of the starting material and conversion to the product. Upon completion, a workup was performed and the compound was purified by column chromatography. The pure product (**41**) was afforded in a satisfactory yield of 74%, and was stored in a dark environment, and under an inert atmosphere to prevent potential polymerization.

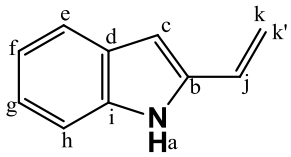

The ^{1}H NMR spectrum of the product (**41**) was compared to that reported in literature and corresponded well.[139] The vinyl protons, H_k and $H_{k'}$, were present as two doublets at 5.55 ppm and 5.27 ppm, respectively. In addition, the doublet of doublets integrating for one at 6.75 ppm was assigned to H_j. The rest of the aromatic signals and indole $-NH_a$ were all accounted for and matched the expected integration.

3.3.7 The Diels-Alder reaction

In 1928, Professor Otto Diels and his research student, Kurt Alder, identified the products arising from the reaction of cyclopentadiene with quinone (Scheme 19).[161] This historic event in the field of chemistry led to the birth of the Diels-Alder reaction, rewarding the namesakes with the Nobel Prize in 1950.[162] The true power and effectiveness of this pericyclic reaction began to be realized in the 1950s and 1960s when it was applied to the total synthesis of many complex natural compounds. An example includes the work of Woodward and co-workers, who adopted the Diels-Alder reaction as a key step in the synthesis of cortisone, cholesterol and reserpine.[161] To date, the Diels-Alder reaction remains one of the most important and fascinating transformations in chemistry.[162]

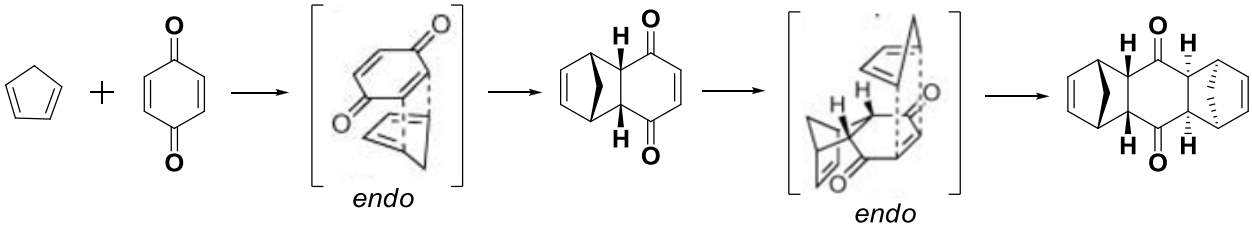

Scheme 19

Reaction products of cyclopentadiene with quinone, as identified by Diels and Alder.[161]

The Diels-Alder reaction is the most famous example of the pericyclic reactions.[148] This particular pericyclic reaction forms part of the class known as cycloadditions and is a special case which involves the combination of conjugated dienes with an alkene (4 + 2). A six-membered ring is created by the formation of two new σ-bonds at the expense of two π-bonds.[163] In order for the reaction to be successful and avoid dimerization, the alkene must possess a conjugated electron-withdrawing group, or some sort of extra conjugation. This group is known as the dienophile.[148] Dienes on the other hand can have different kinds of substituents, and can be open-chain or cyclic. Many dienes can occur in two conformations (s-*trans*/s-*cis*) since they are capable of rotating about the single bond, between the conjugated double bonds. A requirement for the Diels-Alder reaction is that the diene must have the s-*cis* conformation.[163]

The Diels-Alder reaction has a regioselective and stereospecific nature and the stereochemistry of the product depends on that of the diene and dienophile. An important feature of Diels-Alder reaction, recognized in 1934 by Alder and Stein, is that the product predominantly or exclusively leads to the formation of the *endo* cycloadduct and not the *exo* diastereoisomer. This observation is illustrated in the most famous Diels-Alder reaction of all time – that between cyclopentadiene and maleic anhydride (Scheme 20).[148] The preference for the more sterically crowded and less thermodynamically stable transition state, was explained by Hoffmann and Woodward and ascribed to secondary orbital interactions.[161, 164] In the example below, these secondary orbital interactions are formed between the carbonyl groups of the dienophile and the developing π-bond at the back of the diene.[148] Many experimental and theoretical arguments have been proposed to explain the formation of the endo product. Besides the secondary orbital theory, other explanations include stabilization of the endo orientation by inductive, charge-transfer, or CH-π interactions. However, the exact factors controlling the endo [4 +2] cycloaddition reactions are still not completely understood and remain a pursuit of researchers.[164]

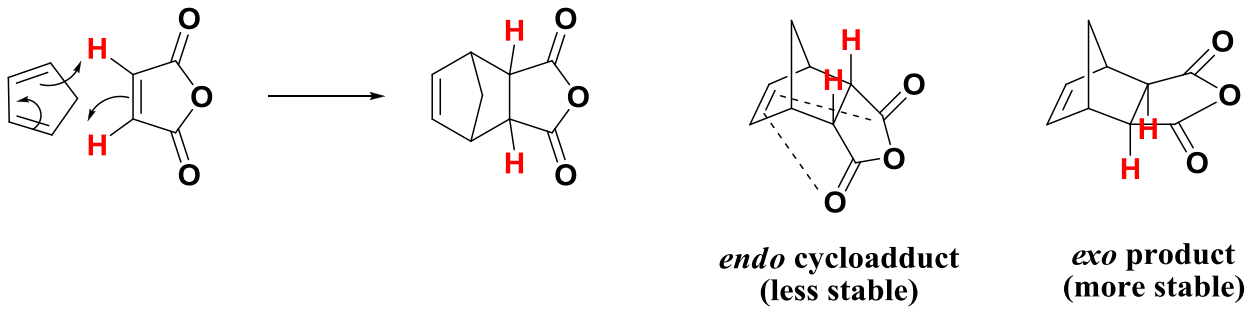

Scheme 20

The reaction between cyclopentadiene and maleic anhydride forming the less stable endo cycloadduct.[148]

For the purpose of this project, the conjugated diene required for the Diels-Alder reaction is obtained following the Wittig reaction. The choice of the dienophile is based on the crucial hydrogen bond interactions between the amide functionality of staurosporine and the hinge region of the EGFR kinase domain. Furthermore, investigating the structures of the staurosporine-derived analogues as promising kinase inhibitors (see section 1.5.2), it was noted that almost all the compounds possess an unsubstituted −NH amide/imide group. We proposed that the –NH is essential for the formation of hydrogen bond interactions in the hinge region, and was thus included in the design strategy of our compounds. For this reason, maleimide was chosen as the dienophile. The Diels alder reaction between the indole alkene and maleimide is represented below in scheme 21. It must be noted that the newly formed π-bond rearranges to reconstruct the conjugated system of the compound.

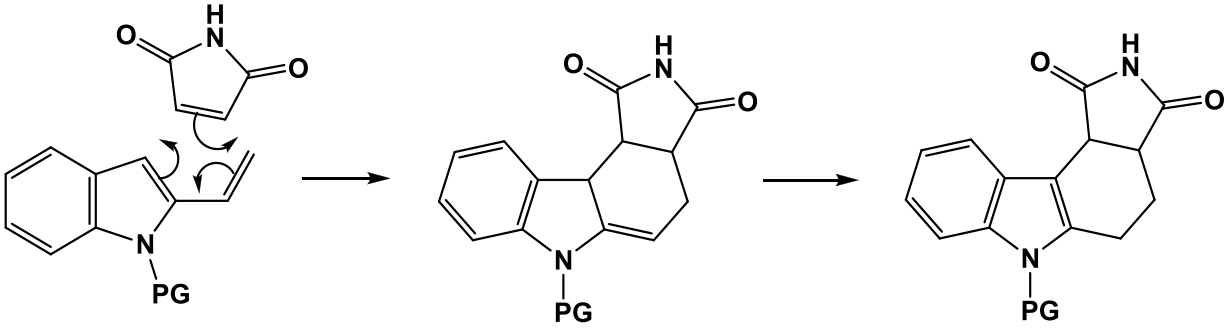

Scheme 21

Diels-Alder reaction between indole alkene (diene) and maleimide (dienophile).

3.3.7.1 Synthesis of 4,5,6,10c-tetrahydropyrrolo[3,4-*c*]carbazole-1,3(2*H*,3a*H*)-dione (42)

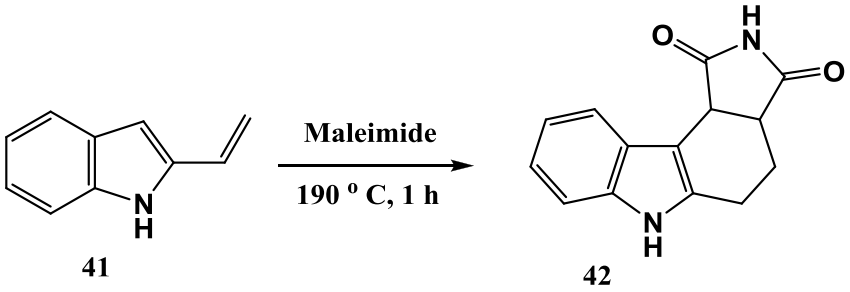

41 **42**

Scheme 22

The Diels-Alder reaction is a key tool in organic chemistry to increase the molecular complexity (molecular size, stereochemistry, functionality) in a single step, and has been widely utilized in the synthesis of complex natural products. [162,164] As stated in section 3.3.7, the choice of our dienophile was maleimide. The reaction was performed as shown in scheme 22. The reagents were heated together, upon which they melted, fused and solidified. The crude product formed was highly insoluble, which led to challenges and complications in purification by crystallization or column chromatography. For this reason, the crude compound (**42**) was utilized directly in the following synthetic step.

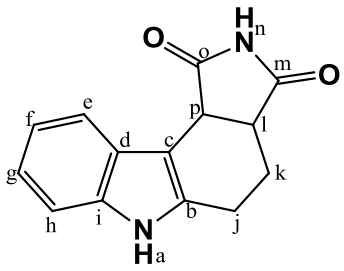

The ^{1}H NMR spectrum of the crude product (**42**), although a bit unclean, did reveal indicative signals. Unfortunately, only one broad peak of $-NH_a$ was found. We suspect that the maleimide $-NH_n$ may have been shadowed by an impurity. The four multiplets for the diastereotopic protons of H_k and H_j were found upfield and integrated for one each. H_p and H_l were located at 4.17 ppm and 3.17 ppm respectively, and each integrated for one proton. The aromatic peaks could all be accounted for.

3.3.8 The aromatization of the pyrrolocarbazole scaffold

MnO_2 has been widely used for dehydrogenation and aromatization reactions. [147] In addition to the vital role of this reagent for the synthesis of the indole aldehyde in this project, MnO_2 is also used for the aromatization step required to generate the conjugated pyrrolocarbazole system.

Another powerful oxidant employed in the design strategy is DDQ. DDQ is a versatile quinone reagent, combining high oxidation ability with relative stability.[147] In this project DDQ was used as an alternative reagent for the aromatization step. The reagent has proven useful for a wide range of reactions, including dehydrogenation, oxidation and selective deprotection.[151] DDQ's mechanism of dehydrogenation is believed to involve an initial rate-determining transfer of a hydride ion from the hydrocarbon to the quinone oxygen atom - forming a phenolate anion and a carbocation as shown in scheme 23. The following step is rapid, and involves the carbocation of the product losing a proton (forming a double bond in the process) and generating hydroquinone. The degree of stabilization of the carbocation is essential for dehydrogenation to occur. The presence of functionalities (alkene or aromatic moieties) capable of stabilizing the transition state is therefore necessary to initiate hydrogen transfer. [147,165] An example of the mechanism is shown in scheme 23.

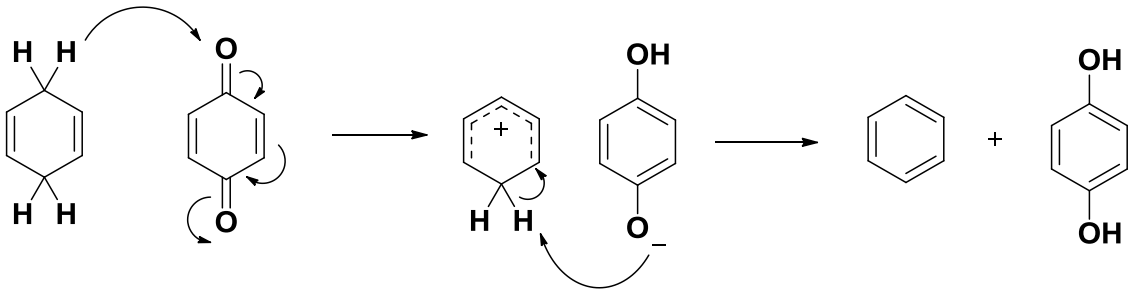

Scheme 23
Mechanism of dehydrogenation by DDQ.[165]

3.3.8.1 Synthesis of pyrrolo[3,4-*c*]carbazole-1,3(2*H*,6*H*)-dione (43)

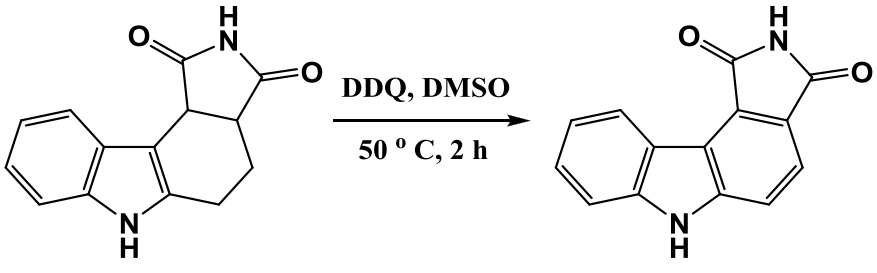

42 **43**

Scheme 24

Following the Diels-Alder reaction, the final step to build the pyrrolocarbazole backbone (**43**) required the aromatization of the compound (scheme 24). This reaction was carried out by dissolving the solid Diels-Alder product (**42**) in DMSO and treating the solution with DDQ. The reaction mixture was stirred for 2 hours at 50 °C. Cold H_2O was then added drop-wise to the reaction mixture, which led to formation of a precipitate. The precipitate was collected and no further purification was required. The product (**43**) was obtained as a brown solid with a yield of 40%, which corresponded with that found in the literature.[160]

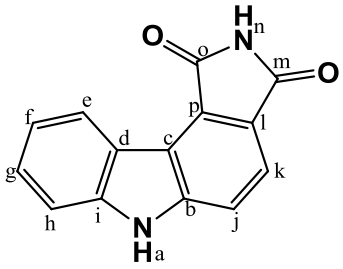

The ^{1}H NMR spectrum of the product (**43**) was evaluated and all six aromatic protons (H_e, H_f, H_g, H_h, H_j, H_k) were identified. The two distinctive broad signals of the indole amine $–NH_a$ and the imide $–NH_n$, were also present in the spectrum. Evaluation of the ^{13}C NMR spectrum revealed all the carbon signals as expected. For example, the two carbonyl signals (C_o and C_m) were clearly evident at 170.4 ppm and 170.3 ppm. Finally, the IR spectrum showed the presence of the 2° amine stretch at 3186 cm^{-1} and the imide stretch at 3057 cm^{-1}, as well as the carbonyl stretch at 1697 cm^{-1}.

3.3.9 Attempted synthesis of (6-acryloylpyrrolo[3,4-*c*]carbazole-1,3(2*H*,6*H*)-dione) (30)

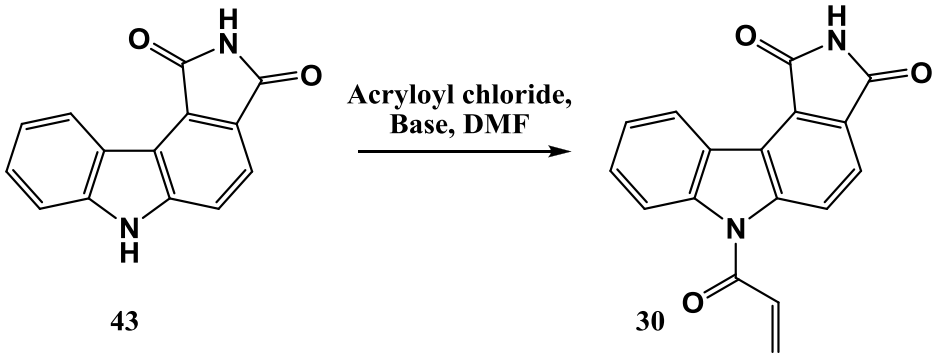

43 **30**

Scheme 25

Numerous attempts were made towards the final step of the synthesis. Despite the various efforts, the reactions performed to incorporate the acryloyl moiety were unsuccessful. Firstly, the reaction was carried out without the use of a base. The acryloyl chloride (diluted in DMF) was added drop-wise to a solution of compound **43** in DMF at 0 °C. The reaction mixture was then stirred at 80 °C, under N_2 gas, for 2 days. While monitoring the progress of the reaction by TLC, it was observed that compound **43** remained unreacted. The same reaction was then performed, after initial treatment of compound **43** with NaH (scheme 25).

The colour of the reaction mixture changed from yellow to purple once the NaH was added. Upon addition of the diluted acryloyl chloride, a colour change back to yellow was observed. The reaction was again monitored by TLC, but unfortunately showed no product formation over a period of 4 days. Fearing that the maleimide –NH might be the reason for the problems, an alternative approach to introduce the acryloyl group, which utilizes a protected maleimide was attempted (scheme 26). In this manner possible regioselectivity problems between the nucleophilic indole amine and acidic maleimide imide present in (**43**), could be avoided.

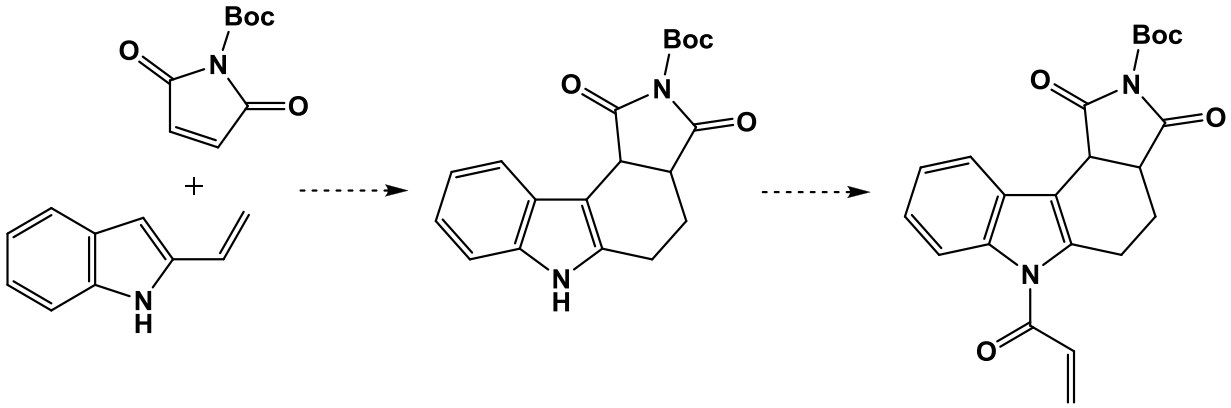

Scheme 26

Outline of strategy using Boc-protected maleimide as an alternative approach to introduce the acrolyl moiety.

3.3.9.1 Synthesis of *tert*-butyl 2,5-dioxo-2,5-dihydro-1*H*-pyrrole-1-carboxylate (45)

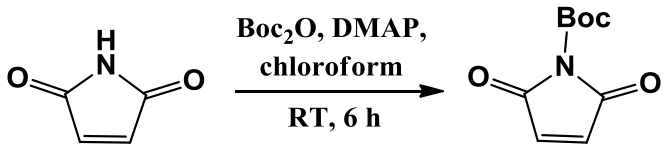

44 **45**

Scheme 27

The reaction to protect maleimide (**44**) was carried out smoothly, following a procedure in literature to afford the pure compound (**45**) in a yield of 67%.[166]

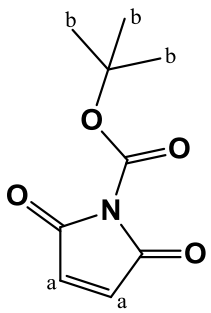

The ^{1}H NMR spectrum of the product (**45**) was evaluated and showed the presence of two signals. The singlet at 6.78 ppm, integrating for two, was assigned to H_a. The Boc group (H_b) integrated for nine, and was located at 1.57 ppm. The absence of the broad signal of –NH was another indication that the Boc-protection reaction was a success.

3.3.9.2 Synthesis of *tert*-butyl 1,3-dioxo-1,3,3a,4,5,10c-hexahydropyrrolo[3,4-*c*]carbazole-2(6*H*)-carboxylate (46)

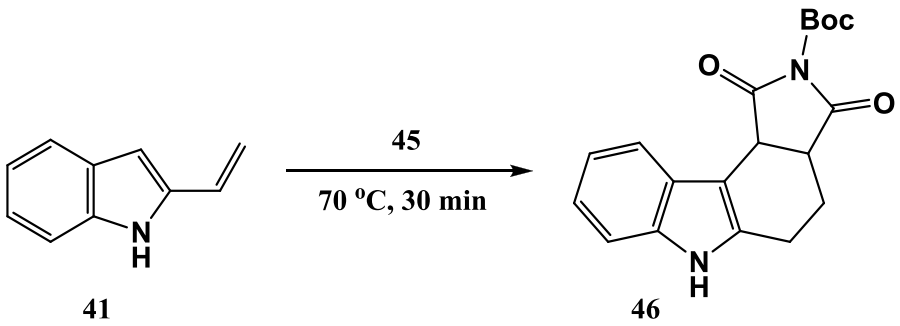

41 46

Scheme 28

The Diels-Alder reaction was performed, as shown in scheme 28, by adding the Boc-protected maleimide (**45**) and 2-vinyl-1*H*-indole (**41**) neat to a reaction flask. The reaction temperature was kept at 70 °C, since higher temperatures resulted in protecting group cleavage. Unfortunately, complete consumption of **41** was not observed, even when increasing the equivalents of protected maleimide (**45**). This result could be ascribed to improper mixing of the starting materials in the melt. After the reaction, the crude product was purified by column chromatography to afford the pure compound **46** in a yield of 59%.

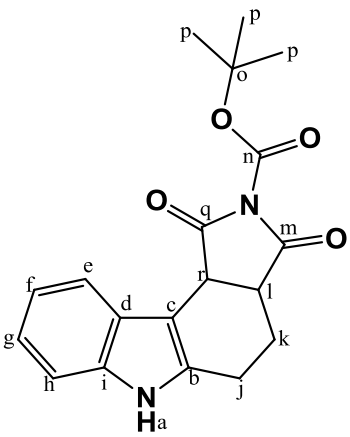

In the ^{1}H NMR spectrum of the product (**46**), the singlet (H_p) from the Boc group was evident at 1.45 ppm. The diastereotopic protons of H_j and H_k were present as four distinct signals in the range between 2.80 – 1.86 ppm, each integrating for one. A single broad signal for –NH_a was identified at 11.07 ppm. The ^{13}C NMR spectrum showed the carbonyl signals (C_q and C_m) at 175.7 ppm and 173.4 ppm, while that of the Boc group (C_n) was located at 147.1 ppm. Finally, the results of the mass spectral analysis of 363.1321amu correlated with the expected mass of 363.1321 amu.

3.3.9.3 Attempted synthesis towards *tert*-butyl 6-acryloyl-1,3-dioxo-1,3,3a,4,5,10*c*-hexahydropyrrolo[3,4-*c*]carbazole-2(6*H*)-carboxylate (47)

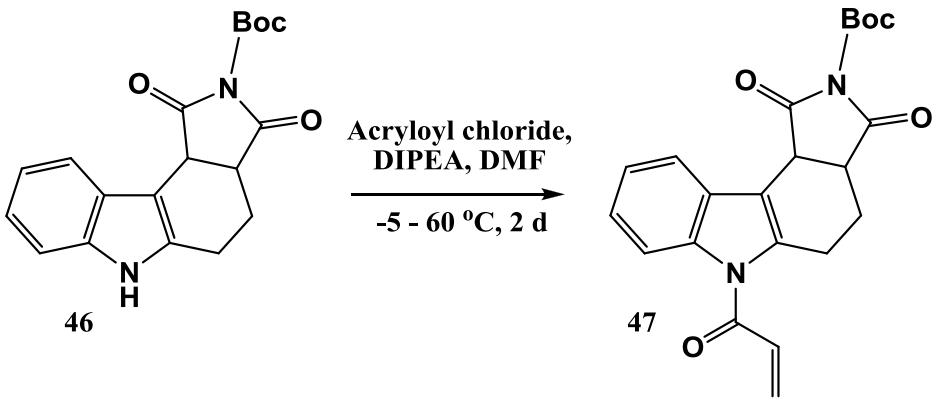

Scheme 29

The Boc-protected Diels-Alder product (**46**) was dissolved in DMF in a reaction flask and treated with DIPEA. The mixture was cooled to - 5 °C and a solution of acryloyl chloride in DMF was added drop-wise. The reaction temperature was then increased to 60 °C and stirred for 2 days. Unfortunately, the Boc group was cleaved with the reaction conditions and the product was not formed. Another reaction involving aromatization of compound **46** was also attempted prior to the acryloyl introduction. Unfortunately, both DDQ and MnO_2 oxidants did not succeed in the aromatization of the Boc-protected Diels-Alder product (**46**), since the heat required during these reactions led to the Boc group being cleaved. The inability to install the acryloyl functionality onto the indole amine therefore required a modification of the project targets.

3.4 New target compounds

The challenges experienced thus far led the synthesis of target compound **30** being discontinued. The focus was directed towards the design of different target compounds shown in figure 64. It must be noted that particular interest was directed towards the activity of the unaromatized compounds compared to their aromatized partners. The pyrrolocarbazole has a rigid scaffold relative to the unaromatized Diels-Alder product which displays a more flexible nature. The envisaged strategy of these new target compounds are discussed in detail in the following sections. The aim was to synthesize potential kinase inhibitors by utilizing the pyrrolocarbazole (aromatized and unaromatized) scaffold and introducing the various warheads (hydroxyl, propargyl and nitrile) onto the structure. As discussed earlier (see section 1.4.2, figure 16), the propargyl and nitrile moieties have the ability to form covalent interaction and could demonstrate irreversible inhibition.

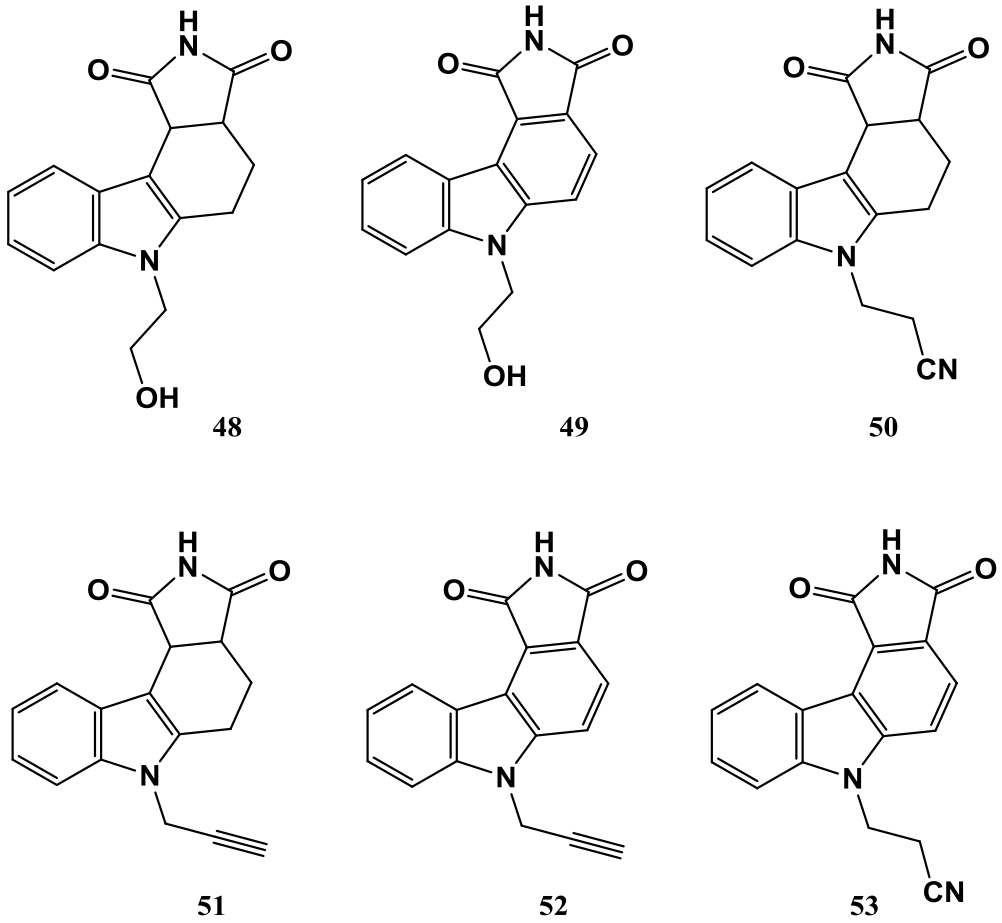

Figure 64
Illustration of the new target compounds.

3.5 Synthesis of *N*–tether hydroxyl target compounds 48 and 49

The promising results demonstrated by compound **29** (see page 63), encouraged the synthesis of a similar compound, having one less carbon in the chain linking the hydroxyl functionality. The envisaged strategy required the introduction of a silyl-protected 2-bromoethoxy group to the commercially available indole ester (**31**). The various reactions highlighted earlier (reduction, oxidation, Wittig, Diels-Alder, aromatization) were once again included in the strategy as shown in scheme 30. Together with a silyl-deprotection reaction, these procedures were utilized to generate target compounds **48** and **49**.

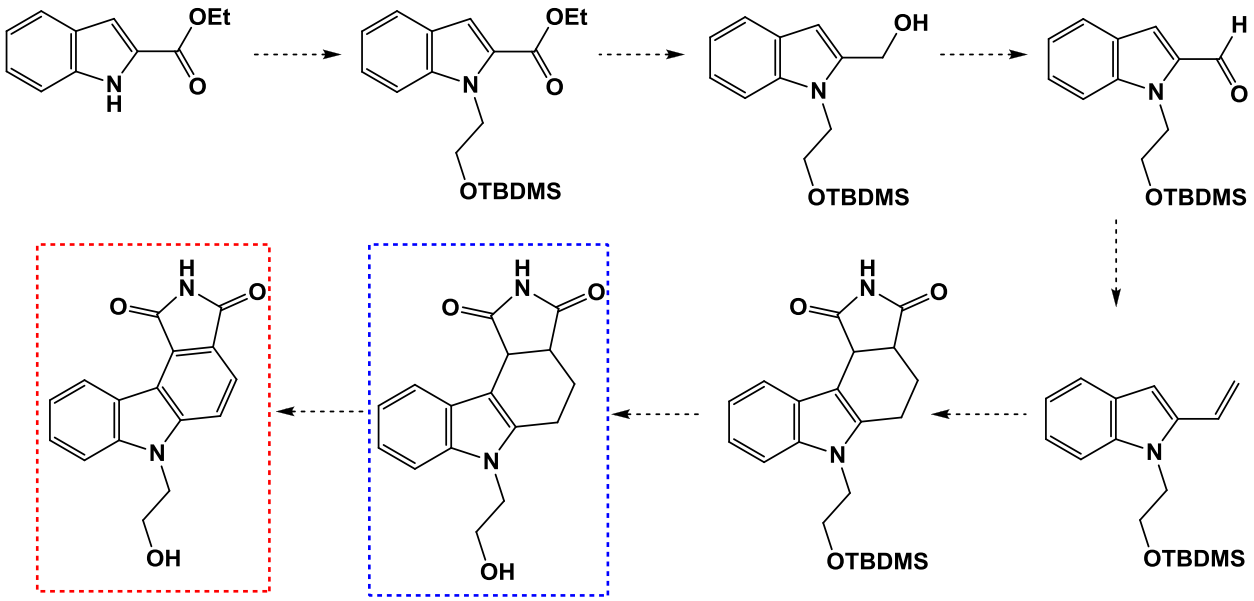

Scheme 30

Outline of strategy towards target compounds **48** and **49**.

3.5.1 Synthesis of (2-bromoethoxy)(*tert*-butyl)dimethylsilane (55)

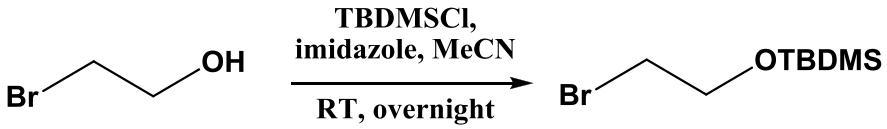

54 **55**

Scheme 31

The first step in the synthetic route was to generate the silyl-protected 2-bromoethoxy group (**55**). The reaction was carried out successfully by treating a solution of imidazole and MeCN with 2-bromoethanol (**54**) and TBDMSCl at 0 °C (scheme 31). The product (**55**) was afforded as an oily liquid in a satisfactory yield of 74% and no further purification was required.

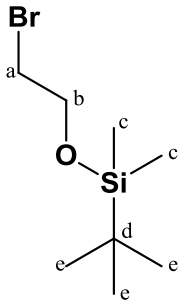

The ^{1}H NMR spectrum of the product (**55**) was compared to that reported in literature and corresponded well.[167] The singlet located at 0.90 ppm integrated for nine, and was identified as H_e. In addition, the upfield singlet at 0.09 ppm was assigned to the protons (H_c) of the Si-C bond and integrated accurately for six protons. Finally, the signals of H_a and H_b were also clearly evident at 3.39 ppm and 3.89 ppm, respectively.

3.5.2 Synthesis of ethyl 1-{2-(*tert*-butyldimethylsilyloxy)ethyl}-1*H*-indole-2-carboxylate (56)

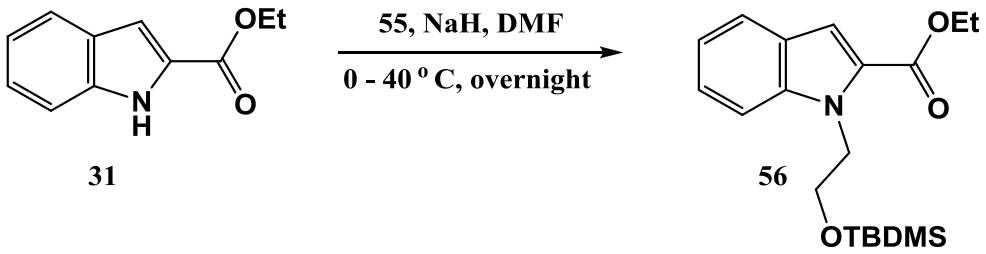

31 56

Scheme 32

Having synthesized compound **55**, it could be introduced to the commercially available ethyl indole-2-carboxylate (**31**) in the reaction shown in scheme 32. This reaction was carried out by treating a solution of **31** in DMF with NaH, followed by 2-bromoethoxy silyl (**55**). Upon completion of the reaction, the product was purified by column chromatography to obtain compound **56** an acceptable yield of 73%.

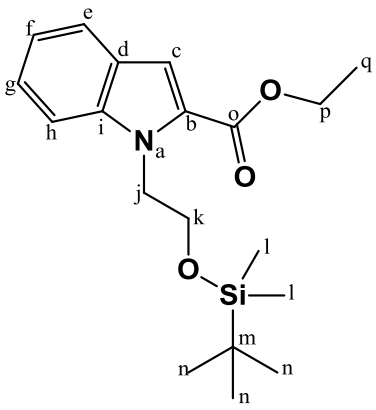

The ^{1}H NMR spectrum of the product (**56**) was evaluated and all the expected signals could be identified. The absence of the broad indole – NH_a signal, together with the location of all the peaks identified earlier for the 2-bromoethoxy silyl protecting group, confirmed the formation of the desired product. Finally, the results of the mass spectral analysis of 348.2007 amu correlated with the expected mass of 348.1995 amu.

3.5.3 Synthesis of [1-{2-(*tert*-butyldimethylsilyloxy)ethyl}-1*H*-indol-2-yl]methanol (57)

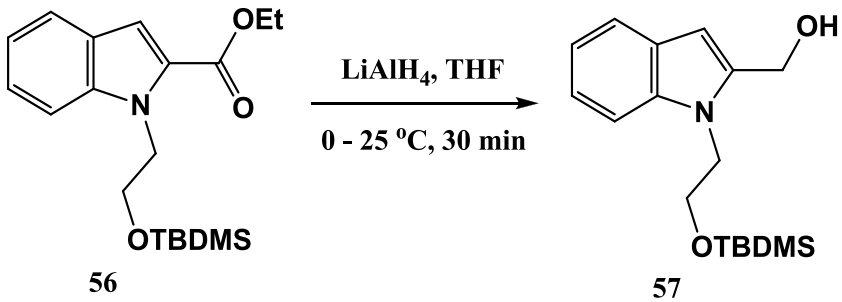

56 57

Scheme 33

The reduction reaction using $LiAlH_4$ was performed similarly to that in section 3.3.2.2. The only slight, but crucial difference, was that the reaction temperature was kept at 0 °C, once the solution of the compound **56** was added to the $LiAlH_4$.

It should be noted that removal of the ice bath during this step led to the loss of the ethoxy silyl group from the indole alcohol product. After the reaction, the product (**57**) was purified by column chromatography to afford a white solid in an excellent yield of 97%.

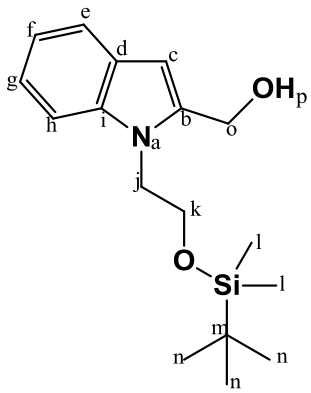

The ^{1}H NMR spectrum of the product (**57)** was similar to that of the starting material, except for the absence of the ester signals. The loss of the quartet and triplet of the ethyl ester group was replaced by a broad singlet at 3.23 ppm for H_p, and a singlet belonging to the methylene H_o integrated for two at 4.78 ppm. The loss of two carbon signals in the ^{13}C NMR spectrum of the product (**57**) was also indicative for the successful formation of the indole alcohol from the indole ester. IR analysis showed the hydroxyl stretch at 3258 cm^{-1}. The results of the mass spectral analysis of 306.1889 amu correlated with the expected mass of 306.1889 amu.

3.5.4 Synthesis of 1-{2-(*tert*-butyldimethylsilyloxy)ethyl}-1*H*-indole-2-carbaldehyde (58)

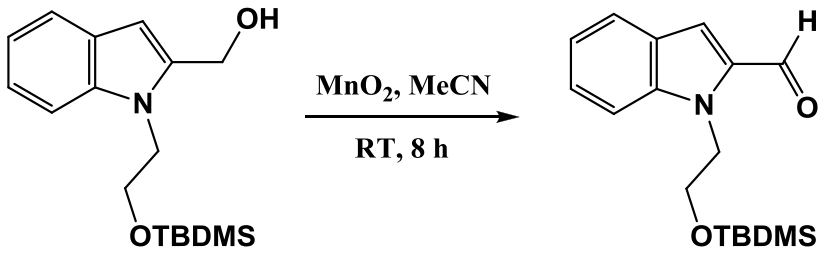

57 **58**

Scheme 34

The oxidation reaction was performed exactly according to the procedure in section 3.3.2.5, but required a longer reaction time. Once completed, the product (**58**) required no further purification, and was afforded in a very good yield of 83%.

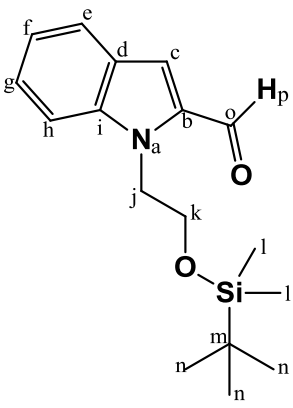

The ^{1}H NMR spectrum of the product (**58**) revealed the distinctive aldehyde H_p singlet located downfield at 9.88 ppm, which integrated for one. Furthermore, the carbonyl C_o signal in the ^{13}C NMR spectrum was identified at 182.7 ppm. The rest of the aromatic and ethoxy silyl group were all present in the spectra and integration corresponded accurately. Lastly, the results of the mass spectral analysis of 304.1730 amu correlated with the expected mass of 304.1733 amu.

3.5.5 Synthesis of 1-{2-(*tert*-butyldimethylsilyloxy)ethyl}-2-vinyl-1*H*-indole (59)

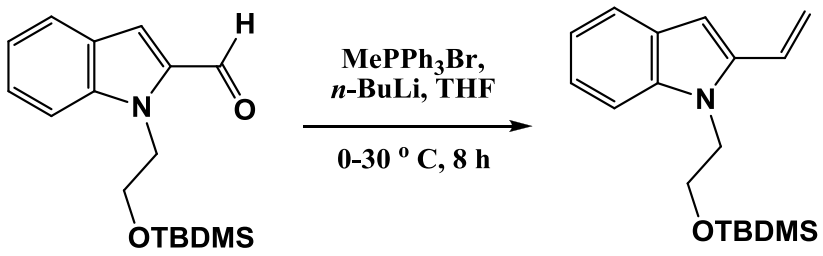

58 **59**

Scheme 35

The Wittig reaction was carried out with the same conditions as the procedure used in section 3.2.4.6, with the difference allowing for a longer reaction time (scheme 35). The crude product was purified by means of column chromatography, which afforded the pure product (**59**) in a satisfactory yield of 79%.

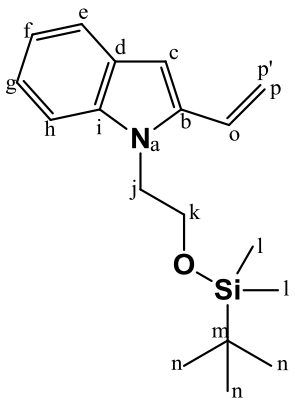

The vinyl protons H_p and $H_{p'}$ were clearly present in the ^{1}H NMR spectrum of the product **59**. They were identified as doublet of doublets at 5.26 ppm and 5.76 ppm respectively, and each integrated for one. H_o was located at 6.77 ppm as a doublet of doublets, with coupling constants corresponding to the respective vinyl protons. An extra carbon signal for C_p, was shown in the ^{13}C NMR spectrum of the product (**59**). The remaining signals in the spectra were all accounted for, and matched the expected integration for the ^{1}H NMR spectrum.

3.5.6 Synthesis of 6-{2-(*tert*-butyldimethylsilyloxy)ethyl}-4,5,6,10*c*-tetrahydropyrrolo[3,4-*c*]carbazole-1,3(2*H*,3a*H*)-dione (60)

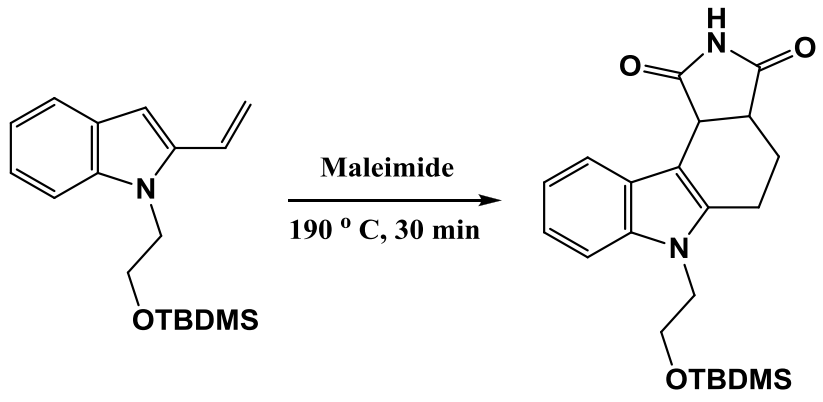

59 **60**

Scheme 36

The Diels –Alder reaction, shown in scheme 36, was carried out neat with compound **59** and maleimide – similarly to that performed in section 3.3.7.1. However, TLC monitoring revealed that some of the starting material **59** remained unreacted – a result observed even when the equivalence of the maleimide was increased. The incomplete reaction of compound **59** could be ascribed to the way in which the starting reagents mixed in the melt, not being in complete contact throughout the mixture. The crude product appeared as a combination of a highly insoluble solid and an oily solid. The insoluble solid was used in the following synthetic step without further purification, while the oily solid could be purified by column chromatography. Taking into account the recovered starting material (**59**), the yield of the product (**60**) was calculated as 78%.

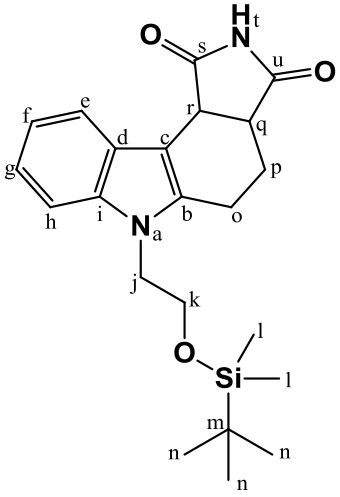

The ^{1}H NMR spectrum of the product (**60**) was evaluated and showed the presence of a new broad signal for the maleimide –NH_t. A number of new multiplets were also observed. The signals of H_o and H_p were identified as four multiplets for the diastereotopic protons, integrating for one each. These signals were located upfield between 2.92 – 1.69 ppm. The multiplets of H_r and H_q were also present, close to the methylene (H_j/H_k) protons. Four new carbon signals were identified in the ^{13}C NMR spectrum of the product, including the 2 distinctive carbonyl signals (C_s/C_u) at 180.3 ppm and 178.6 ppm. The results of the mass spectral analysis of 399.2109 amu correlated with the expected mass of 399.2104 amu.

3.5.7 Synthesis of 6-(2-hydroxyethyl)-4,5,6,10c-tetrahydropyrrolo[3,4-*c*]carbazole-1,3(2*H*,3a*H*)-dione (48)

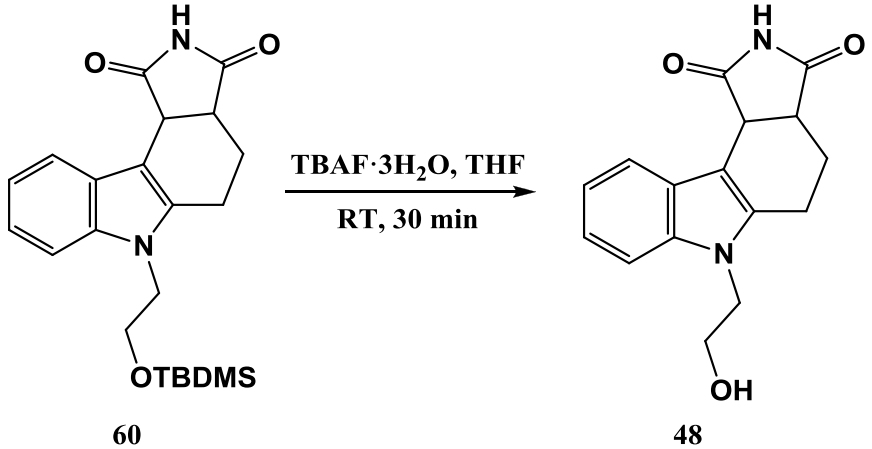

60 **48**

Scheme 37

The next step in the proposed synthetic route was to remove the silyl-protecting group to expose the hydroxyl functionality, thus generating target compound **48**. The deprotection reaction was performed by treating compound **60** with TBAF·$3H_2O$, as shown in scheme 37. The reaction proceeded smoothly within 30 minutes at room temperature. Upon completion, a workup was performed and the compound was purified by means of column chromatography, to afford the pure product (**48**) in an excellent yield of 86%.

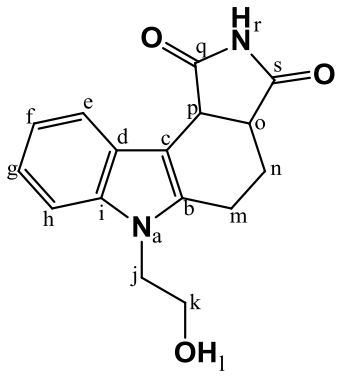

Evaluating the ^{1}H NMR spectrum (figure 65) of the product (**48**), it was clearly visible that the deprotection reaction was successful. The intense proton signals of the tert-butyl and dimethyl groups of the silyl protecting group disappeared, while a broad peak for the newly formed hydroxyl group –OH_l was present at 4.84 ppm. The ^{13}C NMR spectrum also revealed the absence of the three carbon signals belonging to the silyl-protecting group. IR analysis showed the hydroxyl stretch at 3421 cm^{-1}. Finally, the results of the mass spectral analysis peak at 285.1246 amu correlated with the expected mass of 285.1239 amu.

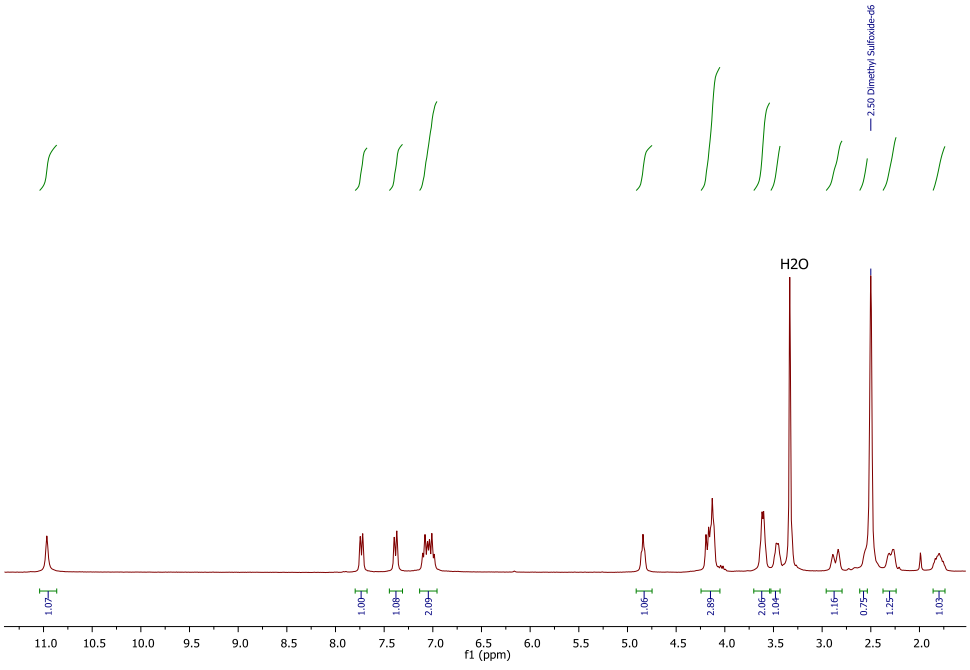

Figure 65
^{1}H NMR of target compound **48**.

3.5.8 Synthesis of 6-(2-Hydroxyethyl)pyrrolo[3,4-*c*]carbazole-1,3(2*H*,6*H*)-dione (49)

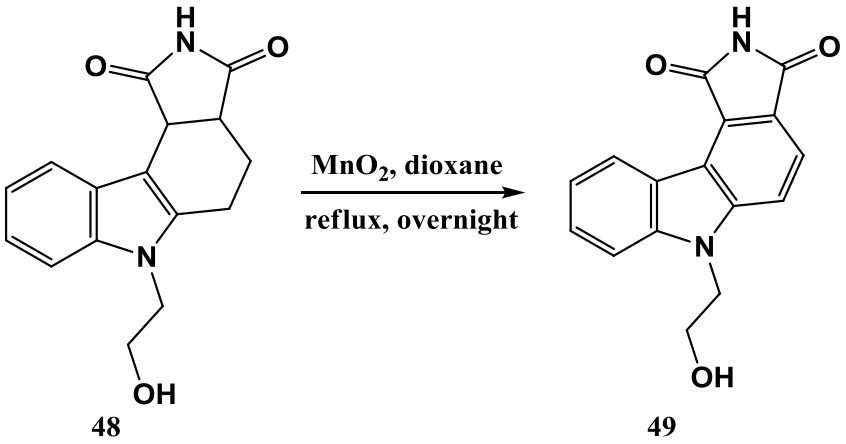

48 **49**

Scheme 38

The final step in the route towards target compound **49** was to perform an aromatization reaction as seen in scheme 38. The previous aromatization reaction (section 3.3.8.1) made use of the quinone DDQ. However, as a result of the availability of MnO_2, it was decided to use this oxidant instead. Compound **48** was dissolved in dioxane in a reaction flask and treated with an excess of MnO_2. As for the previous oxidation reactions, the MnO_2 was activated beforehand. The compound was finally purified by column chromatography to afford the final product (**49**) in a moderate yield of 53%.

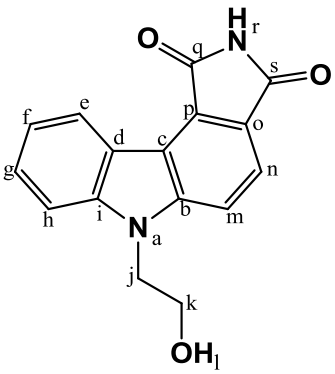

The ^{1}H NMR spectrum of the final aromatized product **49** (figure 66) was evaluated and displayed six signals in the aromatic region. The newly formed doublets of H_m and H_n, integrated for one each. The $-OH_l$ signal is no longer just a singlet – a result ascribed to long range coupling to H_k.The ^{13}C NMR spectrum also revealed a shift of some of the carbon signals to the aromatic region. Finally, the results of the mass spectral analysis of 281.0937 amu correlated with the expected mass of 281.0926 amu.

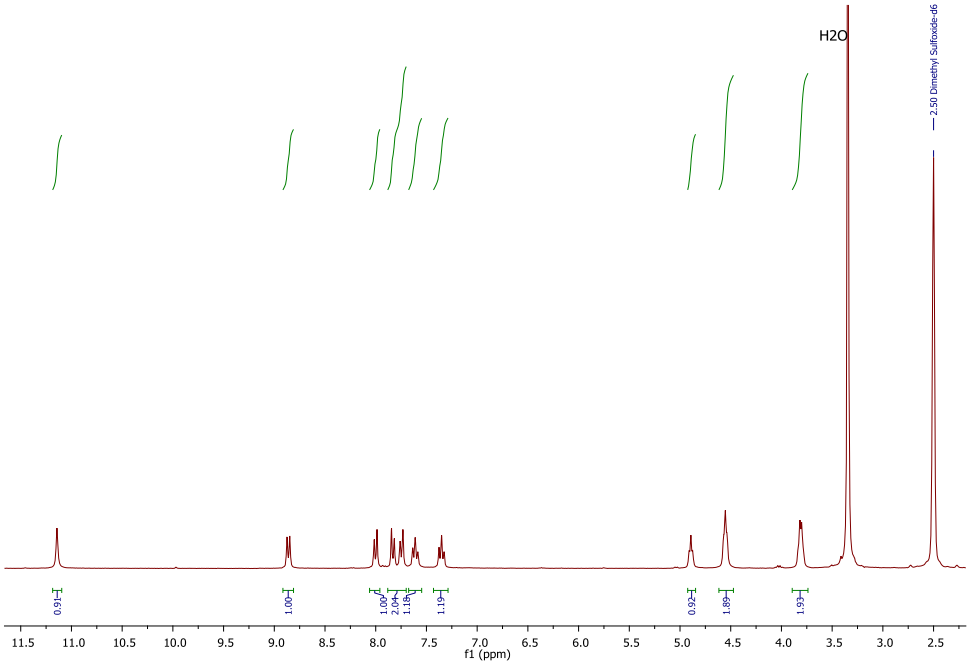

Figure 66
^{1}H NMR of target compound **49**.

3.6 Synthesis of *N*–propargyl target compounds 51 and 52

The design strategy of compounds **51** and **52** was based on the fact that the propargyl group could be introduced to the indole alkene, as shown by the reaction performed by Perez-Serrano and co-workers.[168] The 2-vinyl-1*H*-indole adds to the propargyl bromide by means of a nucleophilic substitution reaction. A Diels-Alder cycloaddition and aromatization reaction would then be able to afford the respective target compounds. An outline of this envisaged route is shown in scheme 39.

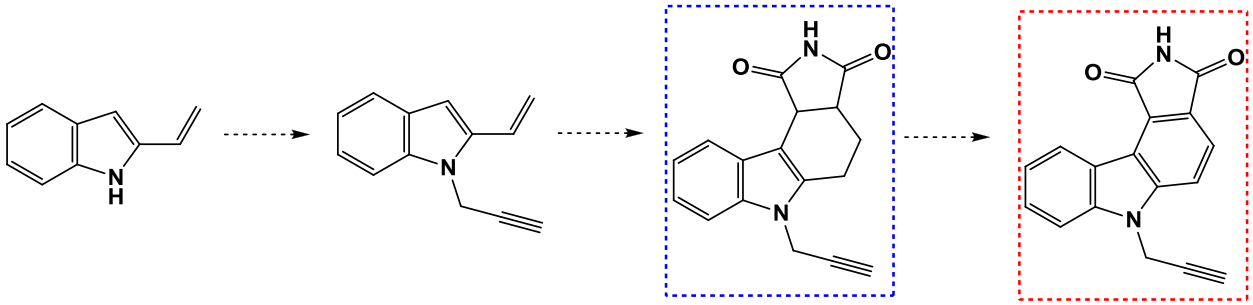

Scheme 39
Outline of strategy towards target compounds **51** and **52**.

3.6.1 Synthesis of 1-(2-propynyl)-2-vinyl-1*H*-indole (61)

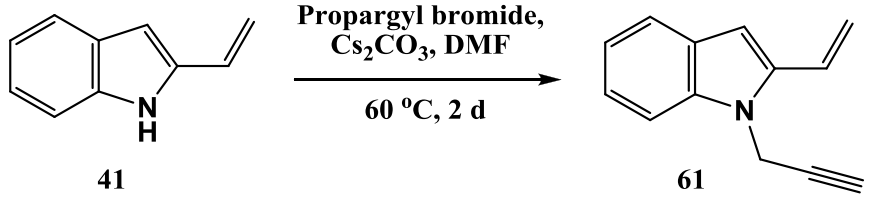

41 **61**

Scheme 40

The propargyl group was introduced to the previously synthesized 2-vinyl-1*H*-indole (**41**) by a nucleophilic substitution reaction. A literature procedure was followed and the reaction proceeded smoothly.[168] Compound **41**, dissolved in dry DMF, was treated with Cs_2CO_3 and propargyl bromide as shown in scheme 40. After a work-up, the compound was purified by means of column chromatography, affording the product (**61**) in a yield of 45%. The low yield could probably be ascribed to polymerization side reactions.

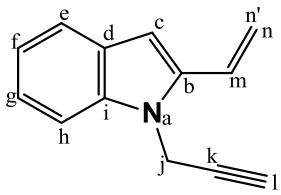

The ^{1}H NMR spectrum of the product (**61**) was compared to that reported in literature and corresponded well.[168] The absence of the broad singlet of $-NH_a$, together with the formation of the new doublet (H_j) and the triplet (H_l), confirm the successful synthesis of the product. The signal assigned to H_j integrated for two, while H_l had an integration of one. The splitting pattern of H_j and H_l was ascribed to long range coupling. The rest of the proton signals were all accounted for and corresponded well with the expected integration.

3.6.2 Synthesis of 6-(2-propynyl)-4,5,6,10*c*-tetrahydropyrrolo[3,4-*c*]carbazole-1,3(2*H*,3a*H*)-dione (51)

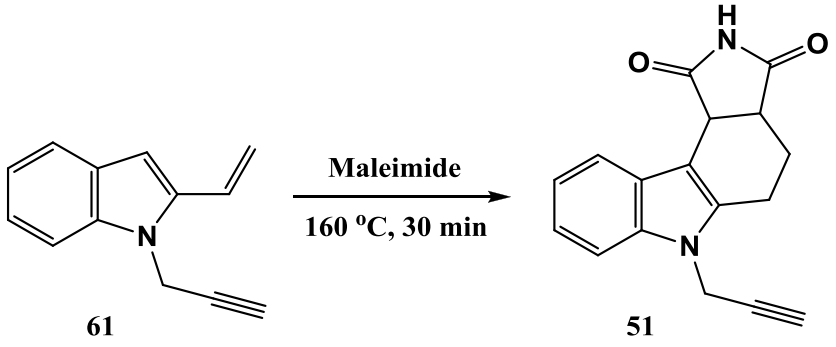

61 **51**

Scheme 41

In order to obtain target compound **51**, the Diels-Alder reaction was performed in the same manner as that in section 3.3.7.1, with the only difference being a lower reaction temperature (160 °C) as shown in scheme 41. Similarly, starting material (**61**) did not react to completion.

The crude product was purified by column chromatography. The yield of the pure product (**51**) was calculated to be in a range of 35-58%, taking into account the recovered starting material (**61**).

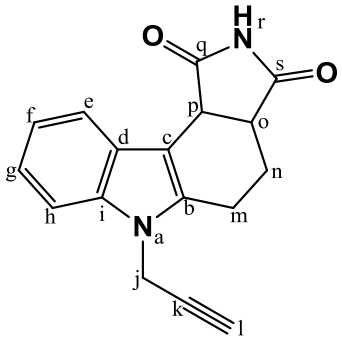

The ^{1}H NMR spectrum of the product (**51**) (figure 67) was evaluated and showed the formation of a number of new signals. The broad peak of –NH_r was located at 11.03 and integrated for one. Four signals were identified for the diastereotopic methylene protons (H_m/H_n) between the range 2.93 – 1.85, each integrating for one. The signals of H_p and H_o were also clearly evident at approximately 3.48 ppm and 4.21 ppm. The ^{13}C NMR spectrum of the product (**51**) showed the formation of four new carbon signals, including the distinctive carbonyl (C_q/C_s) peaks at 180.7 ppm and 1789.0 ppm. Lastly, the results of the mass spectral analysis of 279.1126 amu correlated with the expected mass of 279.1134 amu.

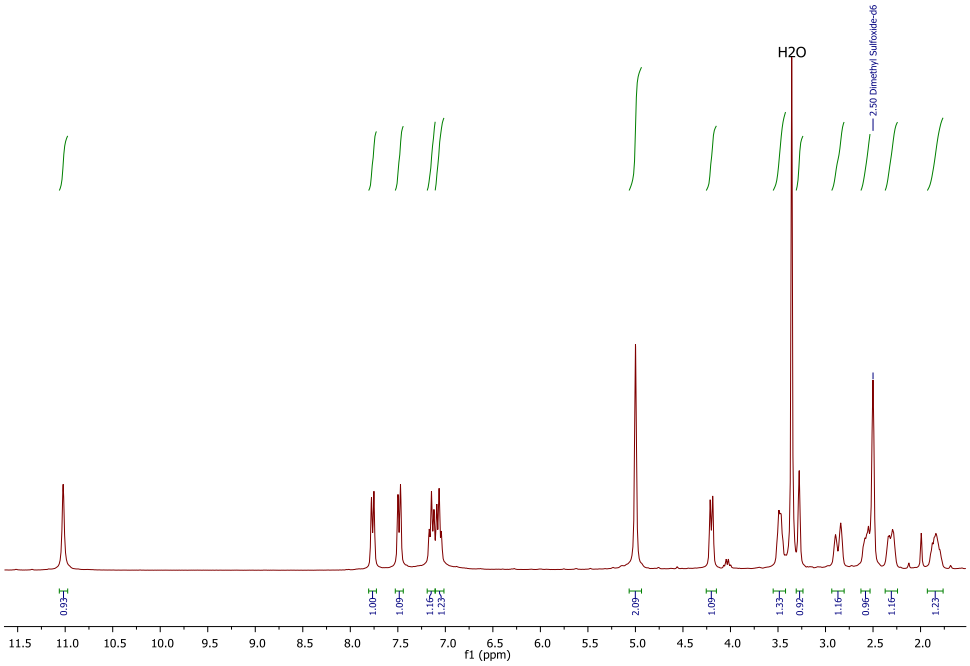

Figure 67
^{1}H NMR of target compound **51**.

3.6.3 Synthesis of 6-(2-propynyl)pyrrolo[3,4-*c*]carbazole-1,3(2*H*,6*H*)-dione (52)

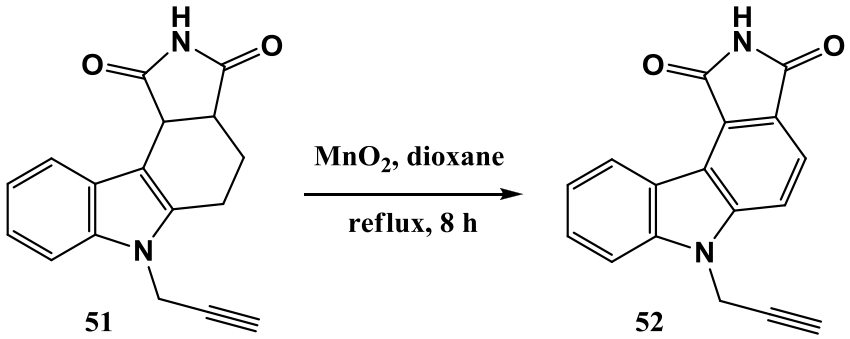

Scheme 42

The final step to synthesize target compound **52** was an aromatization reaction. This reaction was performed, as shown in scheme 42, using an excess of MnO_2, and heating compound **51** to reflux in dioxane for a minimum of 8 hours. Upon completion, the crude product was obtained as a highly insoluble compound and could not be purified by column chromatography. Triturating the crude product with CH_2Cl_2 and acetone afforded the final product (**52**) in a good yield of 72%.

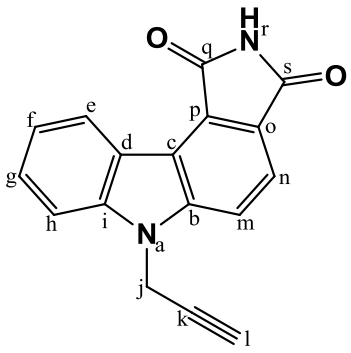

The ^{1}H NMR spectrum of the product (**52**) (figure 68) showed six signals located in the aromatic region – each integrating for one. The newly aromatized protons, H_m and H_n, were identified as doublets at 8.08 ppm and 7.90 ppm. The carbon signals of the carbazole were all accounted for in the ^{13}C NMR spectrum of the product (**52**), and were located in the region between 143.6 ppm and 110.3 ppm. Analysis of the IR spectrum showed the presence of the alkyne stretch at 657 cm^{-1}. Finally, the results of the mass spectral analysis of 275.0316 amu correlated with the expected mass of 275.0821 amu.

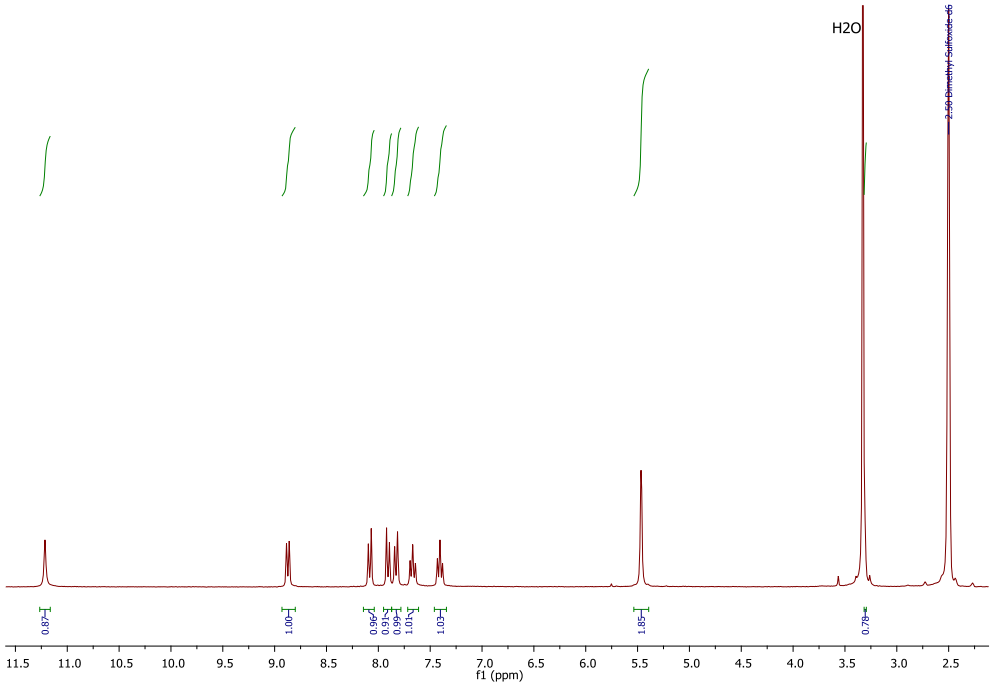

Figure 68
^{1}H NMR of target compound **52**.

3.7 Towards N–tether nitrile target compounds 50 and 53

Studies by Smaill *et al*. suggested that the introduction of side chains on the amine of the carbazole structure, were best implemented on the 2-vinyl-1*H*-indole prior to the construction of the pyrrolocarbazole backbone (**43**). [169] In this manner, regioselectivity problems are prevented, since the imide of the maleimide is frequently the preferred site of alkylation. Their work served as a motivation for our envisioned strategy outlined in scheme 43. This route involved a Michael addition to incorporate the cyanoethyl group, followed by a Diels-Alder cycloaddition (**50**), and finally an aromatization reaction to afford the compound **53**.

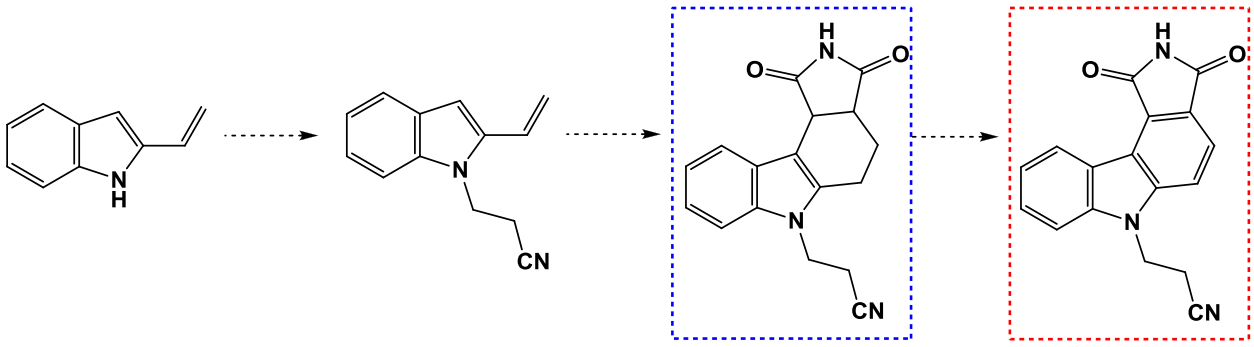

Scheme 43
Outline of strategy towards target compounds **50** and **53**.

3.7.1 Synthesis of 3-(2-vinyl-1*H*-indol-1-yl)propanenitrile (62)

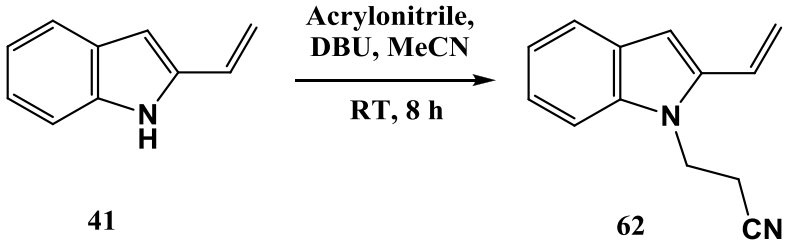

Scheme 44

To introduce the nitrile group to the compound, a Michael addition between the 2-vinyl-1*H*-indole (**41**) and acrylonitrile was performed (scheme 44). Compound **41** was dissolved in MeCN, and treated with acrylonitrile and DBU. Acrylonitrile is a conjugated nitrile and a good Michael acceptor. In this reaction, the Michael addition using acrylonitrile introduced a β-cyanoethyl group to the structure, a process known as cyanoethylation.[148,170] A proposed mechanism of the reaction is given in scheme 45. DBU has been used as a powerful catalyst in Michael additions, and allowed the use of mild conditions.[171] For this reason we decided to employ DBU and avoid the side-reactions associated with strongly basic conditions of classic base catalysis. The indole amine attacked the alkene (conjugate addition) to yield a stable delocalized anion. Protonation at the carbon restored the cyanide functional group and afforded the product. The base catalyst DBU was able to facilitate this process.

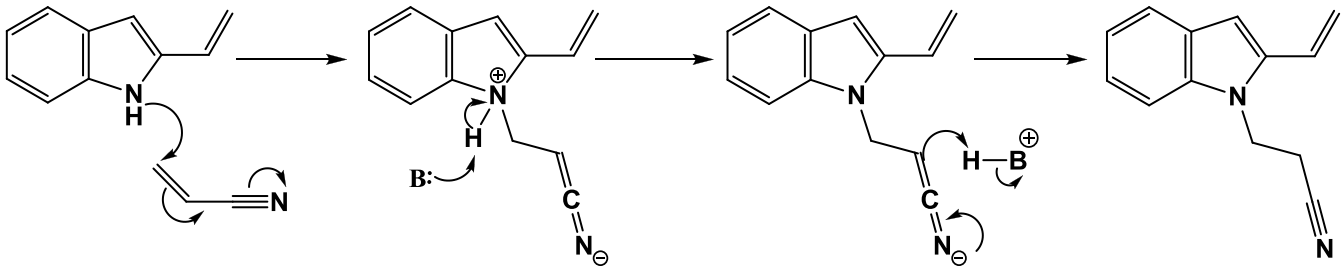

Scheme 45

Proposed Michael addition mechanism to introduce the cyanoethyl group. DBU acts as the catalytic base during the reaction.

The reaction proceeded smoothly at room temperature within 8 hours. Unfortunately, the reaction did not reach completion, even with increased equivalents of reagents. In addition, the reaction temperature was kept at room temperature to prevent possible polymerization of acrylonitrile and 2-vinyl-1*H*-indole (**41**). After the reaction, the crude product was purified by means of column chromatography. Taking into account the recovered 2-vinyl-1*H*-indole starting material (**41**), the yield was calculated to be 84%.

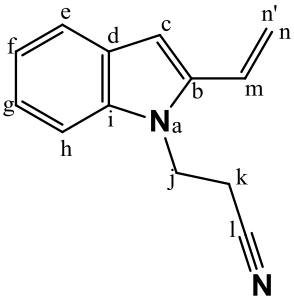

The ^{1}H NMR spectrum of the product (**62)** showed the loss of the broad indole -NH_a signal, which was replaced by new signals of the cyanoethyl group. The diastereotopic protons of H_j and H_k were located at 4.47 ppm and 2.73 ppm, respectively. They appeared as two separate doublet of doublets, each integrating for two. Analysis of the ^{13}C NMR spectrum of the product (**62**) revealed the presence of three new carbon signals. The IR spectrum showed a clear nitrile stretch at 2247 cm^{-1}. Lastly, the results of the mass spectral analysis of 197.1072 amu correlated with the expected mass of 197.1079 amu.

3.7.2 Synthesis of 3-{1,3-dioxo-1,2,3,3a,4,5-hexahydropyrrolo[3,4-*c*]carbazol-6(10c*H*)-yl}propanenitrile (50)

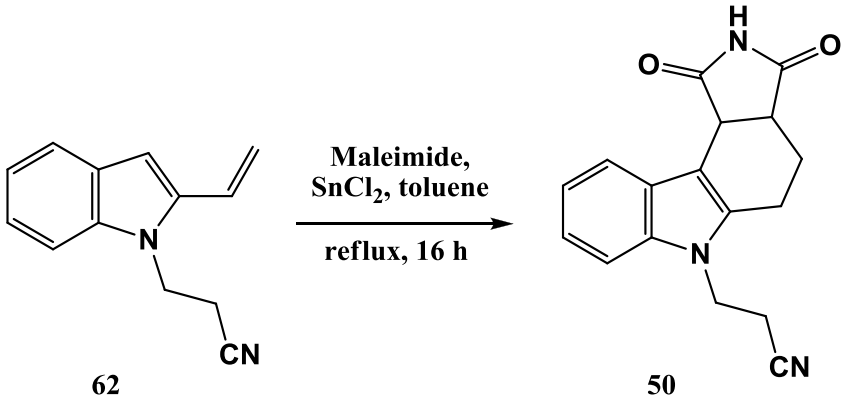

Scheme 46

The addition of a Lewis acid to a Diels-Alder reaction can catalyze the process by interaction of this Lewis acid with the dienophile. Numerous Lewis acid catalysts have been identified, and the manner in which they enhance regioselectivity in Diels-Alder reactions has been a subject of interest for many years.[161-162] In this case, $SnCl_2$ was used as a Lewis acid and was able to complex to the carbonyl of maleimide, thereby increasing the electron withdrawing ability of the dienophile and promoting the reaction. In this reaction, compound **62**, maleimide and the Lewis acid $SnCl_2$, were added to a reaction flask and heated to reflux in toluene (scheme 46). The reaction mixture was then stirred for 16 hours. As witnessed in the previous Diels-Alder reactions, this reaction did not reach completion, even when left for longer reaction times or increasing the equivalents of starting material added. The crude product was purified by column chromatography to obtain the pure target compound **50**. The yield for the reaction was calculated to be 71%, taking into account the recovered starting material.

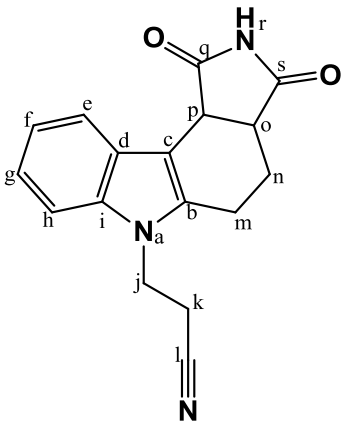

The ^{1}H NMR spectrum of the product (**50**) (figure 69) was evaluated and a number of new signals supported the success of the reaction. The diastereotopic methylene protons H_m and H_n appeared as four individual multiplets, each integrating for one, located in the region between 2.88 – 1.75 ppm. The presence of a broad maleimide $–NH_r$ was identified at 11.02 ppm. Four new carbon signals were located in the ^{13}C NMR spectrum, including the distinctive carbonyl peaks at 180.3 ppm and 178.5 ppm. IR analysis showed the presence of the nitrile stretch at 2246 cm^{-1}. The results of the mass spectral analysis of 294.1253 amu correlated with the expected mass of 294.1243 amu.

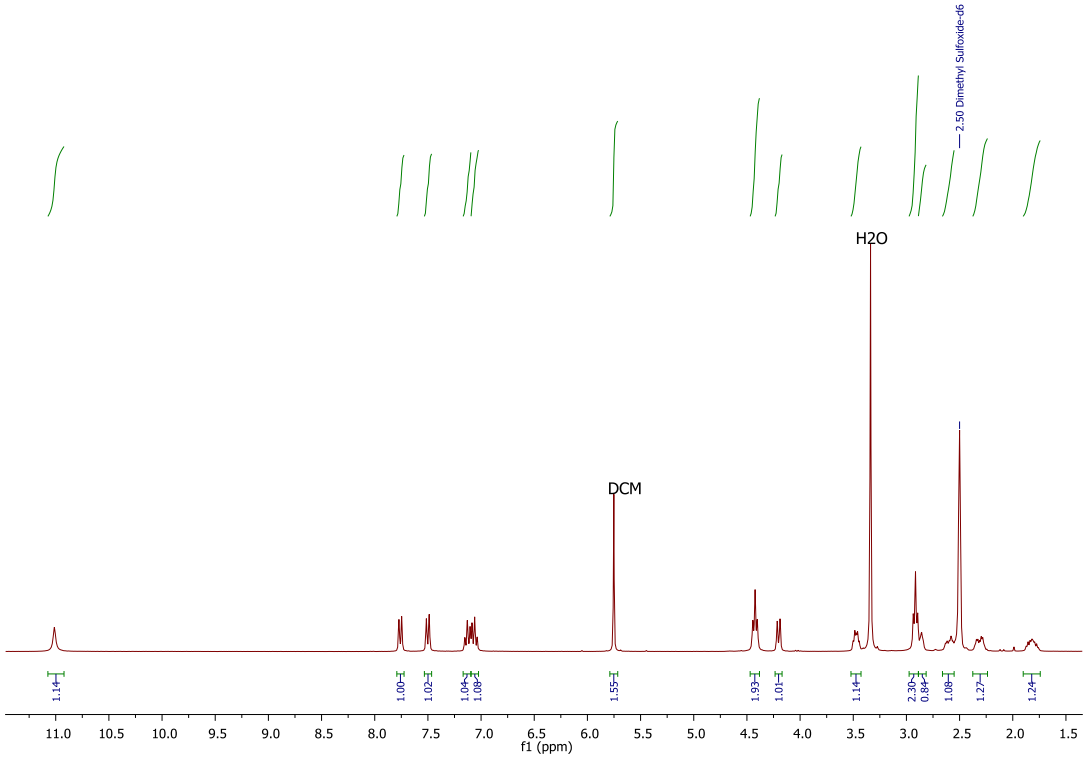

Figure 69
^{1}H NMR of target compound **50**.

3.7.3 Synthesis of 3-{1,3-dioxo-2,3-dihydropyrrolo[3,4-*c*]carbazol-6(1*H*)-yl} (propanenitrile (53)

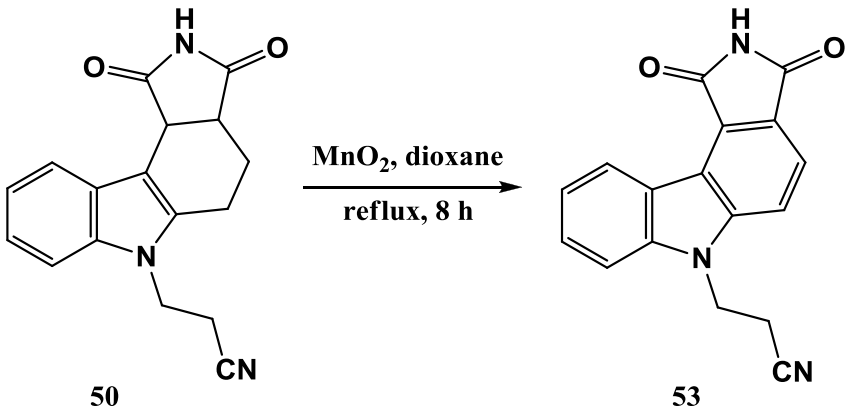

50 **53**

Scheme 47

The final aromatization step to synthesize the target compound **53** was performed in exactly the same manner as that in section 3.3.2.3. As a result of the insolubility of the crude product, column chromatography was not employed as a purification technique. Recrystallization from DMF was thus used to obtain the product as a pure compound (**53**) in a yield of 30%. It is suspected that the yield is not a true representation of the reaction, since recrystallization using DMF as solvent was found to be challenging.

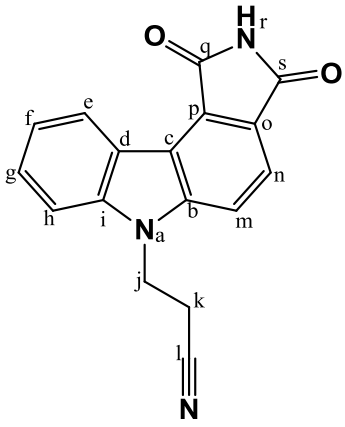

In the ^{1}H NMR spectrum of the product (**53**) (figure 70), six signals in the aromatic region were identified. Each of these signals integrated for one and was assigned to the aromatic protons H_e, H_f, H_g, H_h, H_m and H_n. The number of carbon signals in the ^{13}C NMR spectrum of the product (**53**) corresponded with the expected amount. The nitrile stretch was evident at 2251 cm^{-1} in the IR spectrum. Finally, the results of the mass spectral analysis of 290.0928 amu correlated well with the expected mass of 290.0930 amu.

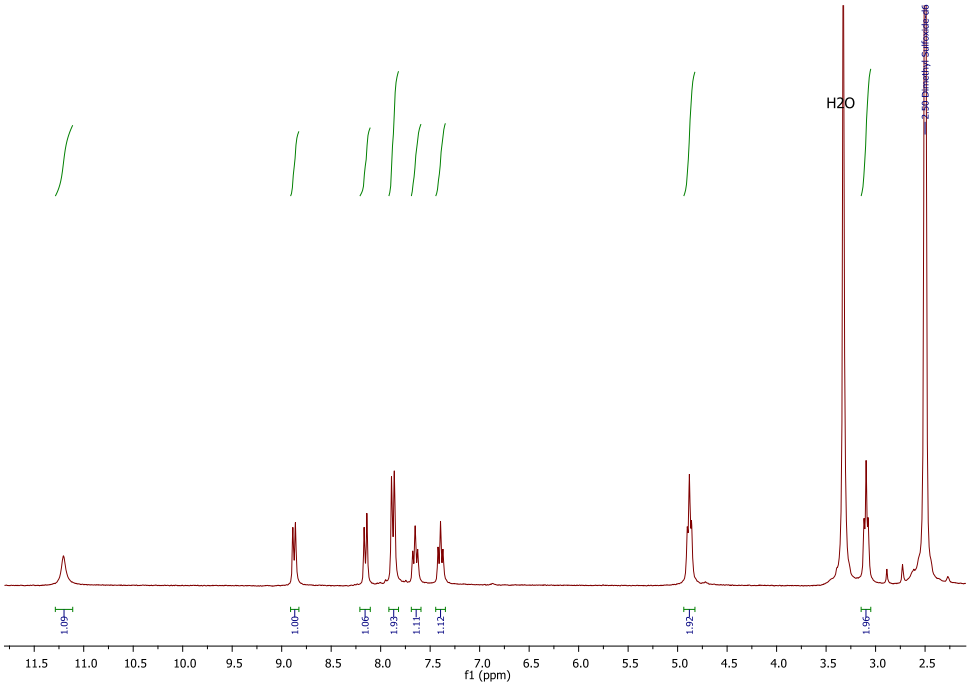

Figure 70
^{1}H NMR of target compound **53**.

3.7.4 Alternative approach attempted towards target compound 54

While the envisioned strategy towards target compounds **50** and **53**, following the route depicted in scheme 43 was under way, another strategy to generate target compound **53** was being applied. The route of this alternative strategy is outlined in scheme 48. The design of this synthesis involved introducing the cyanoethyl group to the already built pyrrolocarbazole scaffold. To avoid the challenges associated with the unprotected pyrrolocarbazole experienced in section 3.3.9, it was decided to protect the maleimide with a group that could withstand the reaction conditions. The protecting group would then finally be removed to expose the crucial imide –NH group. Furthermore, this route would allow for a more divergent synthesis, since the ability to introduce other functionalities, by *N*-alkylation of the protected pyrrolocarbazole structure, would permit the generation of several pyrrolocarbazole analogues. For this route we decided to use benzylamine as a protecting group. The approach described was motivated by the work of Caballero *et al*. [172]

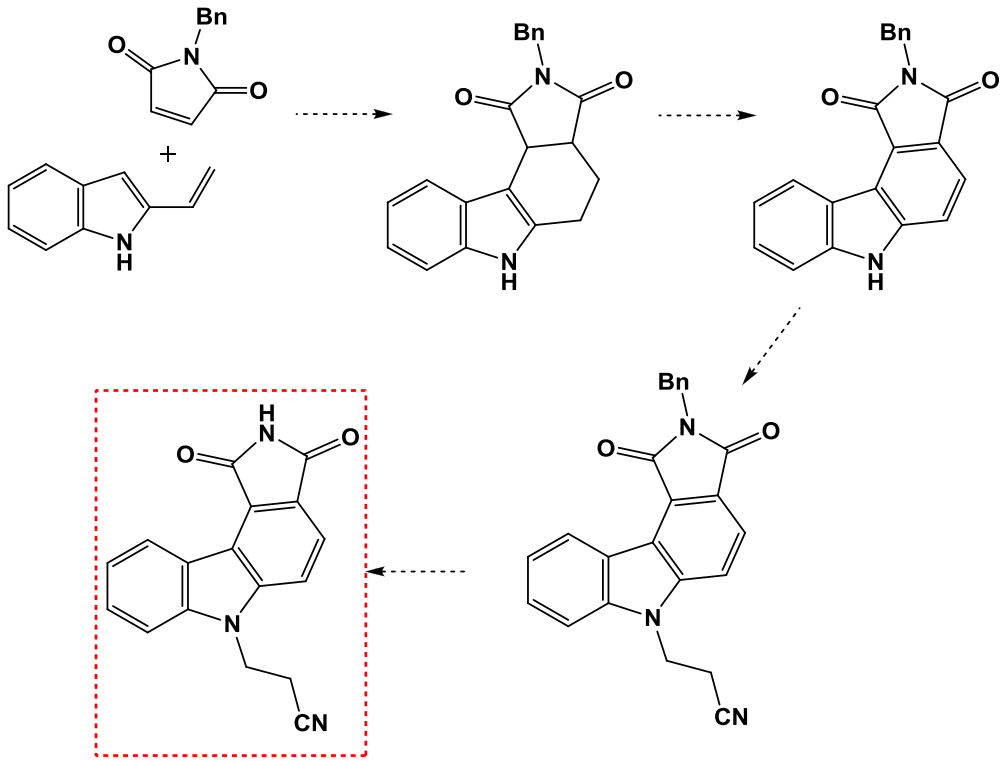

Scheme 48

Outline of alternative strategy towards target compound **53**.

3.7.4.1 Synthesis of 1-benzyl-1*H*-pyrrole-2,5-dione (64)

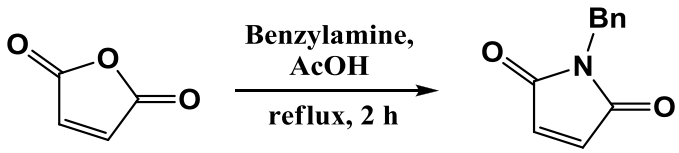

63 **64**

Scheme 49

This strategized route began with the synthesis of benzyl maleimide (**64**) as shown in scheme 49. The reaction was carried out smoothly, following a procedure described in literature.[173] Maleic anhydride (**63**) and benzylamine were added to a reaction flask and dissolved in AcOH. The reaction mixture was heated to reflux for 2 hours. Upon completion, the product was purified by column chromatography to afford the pure compound (**64**) in a yield of 62%.

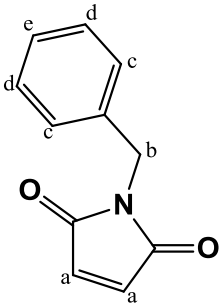

The ^{1}H NMR spectrum of the product (**64**) was compared to that in literature and corresponded well.[173] The compound contains symmetry and three signals were identified in the spectrum. The aromatic protons (H_c, H_d and H_e) were found as a multiplet integrating for five at 7.24 ppm. The H_b signal was located as a singlet at

4.61 ppm and integrated for two.The chemically equivalent H_a protons were also identified as a singlet, integrating for two at 6.64 ppm.

3.7.4.2 Synthesis of 2-benzylpyrrolo[3,4-*c*]carbazole-1,3(2*H*,6*H*)-dione (65)

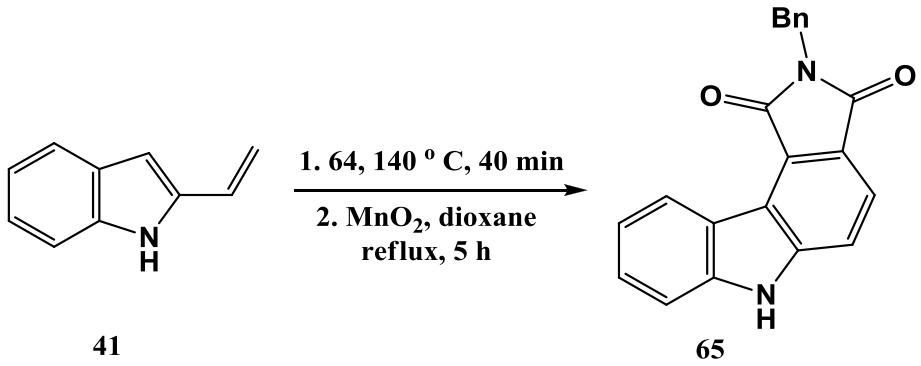

41 **65**

Scheme 50

The synthesis of the benzyl-protected pyrrolocarbazole scaffold (**65**) involved a one pot procedure of the Diels-Alder cycloaddition and MnO_2 aromatization reactions. Having the 2-vinyl-1*H*-indole (**41**) in hand, the Diels-Alder reaction could easily be performed in a melt at 140 °C with the previously synthesized benzyl maleimide (**64**). After 40 min, the crude product was dissolved in dioxane and treated with an excess MnO_2. The reaction mixture was then heated to reflux for 5 hours. Following filtration through Celite, the product was purified by column chromatography to afford the pure compound (**65**) in a satisfactory yield of 84% over the two steps.

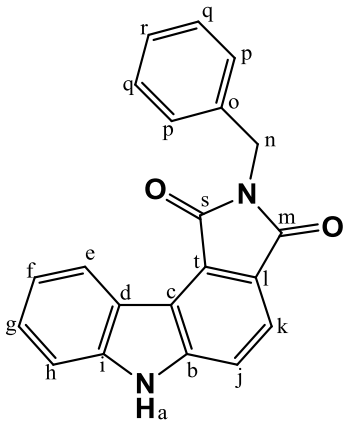

The ^{1}H NMR spectrum of the product (**65**) was evaluated and a number of multiplet signals in the aromatic region were identified – these signals were assigned to the carbazole protons (H_e, H_f, H_g, H_h, H_j, H_k) and the phenyl ring protons (H_p, H_q, H_r). The integration of the aromatic multiplets summed to 11. Furthermore, a broad signal for $–NH_a$ was identified at 12.10 ppm, and the methylene H_n integrated for 2 at 4.82 ppm. The ^{13}C NMR of the product showed the distinctive carbonyl signals (C_s, C_m) at 169.4 ppm and 169.3 ppm. Lastly, the results of the mass spectral analysis of 327.1131 amu correlated with the expected mass of 327.1134 amu.

3.7.4.3 Synthesis of 3-{2-benzyl-1,3-dioxo-2,3-dihydropyrrolo[3,4-*c*]carbazol-6(1*H*)-yl}propanenitrile (66)

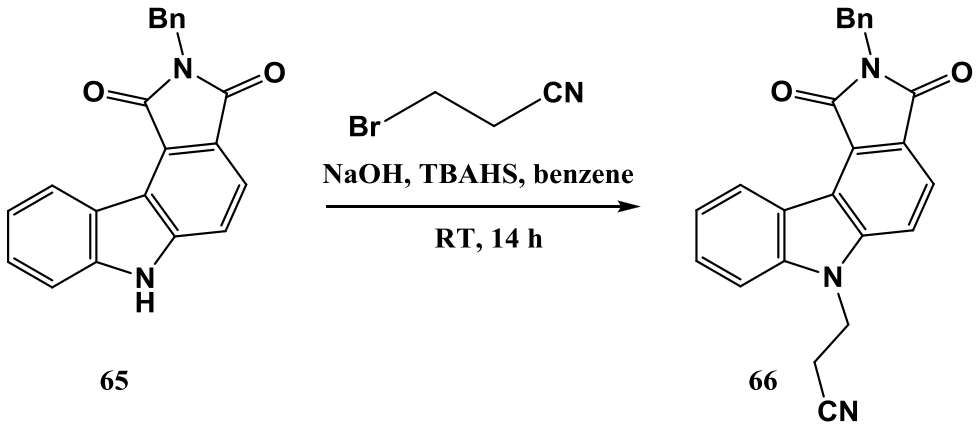

65 66

Scheme 51

The cyanoethyl group was next incorporated into the pyrrolocarbazole scaffold (**65**), as shown in scheme 51, in a similar manner as the procedure described by Caballero *et al.*[172] For this reaction, 3-bromopropionitrile was used as the alkylating agent. A suspension of compound **65** in benzene was treated with NaOH (50%) and TBAHS. The TBAHS acted as a phase transfer agent to catalyze the nucleophilic substitution reaction. 3-bromopropionitrile was then added to the reaction mixture and it was stirred at room temperature for 14 hours. The product was purified by means of column chromatography to afford the pure compound (**66**) in a yield of 60%.

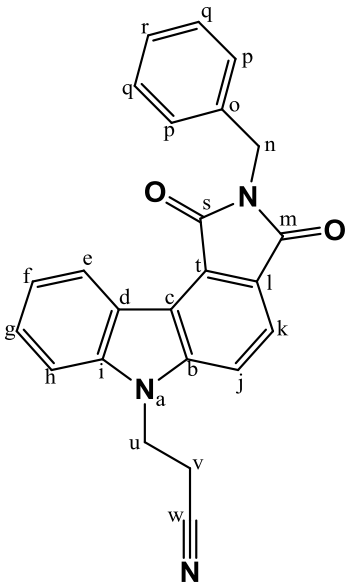

The ^{1}H NMR spectrum of the product (**66**) revealed the absence of the broad -NH_a signal and newly formed multiplet peaks belonging to the cyanoethyl group. H_v showed a doublet of doublets at 3.08 ppm and integrated for two. The signals of H_u and H_n overlapped and formed a multiplet at 4.76 ppm, integrating for four. Three extra carbon signals were evident in the ^{13}C NMR spectrum of the product (**66**). IR analysis showed the nitrile stretch at 2251 cm^{-1}. The results of the mass spectral analysis of 380.1401 amu correlated with the expected mass of 380.1399 amu.

3.7.4.4 Attempted synthesis of 3-[1,3-dioxo-2,3-dihydropyrrolo[3,4-*c*]carbazol-6(1*H*)-yl]propanenitrile (67)

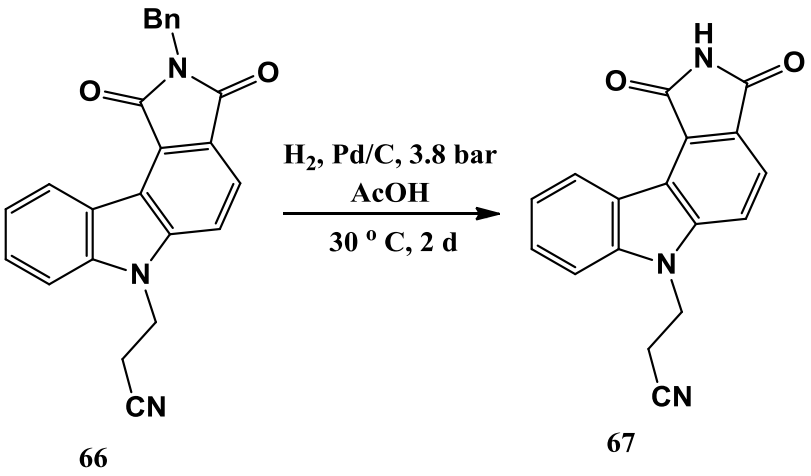

Scheme 52

A method for removing a benzyl protecting group from an amide is to perform a hydrogenation reaction using Pd/C as catalyst, in AcOH.[174] We attempted using a similar approach to deprotect the benzyl group from the pyrrolocarbazole scaffold (scheme 52). In our case, the debenzylation was not successful and the starting material remained unreacted (**66**). Transfer hydrogenation is a more promising approach to remove a benzyl from an imide, and is an alternative approach that could be employed.[175] Unfortunately, the limited availability of compound **66**, together with the time constraints, resulted in the approach being aborted. Fortunately, the success from the approach utilized in section 3.7.3. was able to generate target compound **53**.

3.8 The six final compounds

In summary, the six target compounds represented in figure 63 were successfully synthesized using the various envisaged design strategies. Three respective warheads (hydroxyl, propargyl and nitrile functionalities) were incorporated into the unaromatized and aromatized pyrrolocarbazole scaffold. These final compounds were subsequently sent to Germany to test their inhibitory activity against EGFR kinases. The biochemical assay results are discussed in detail in Chapter 5.

CHAPTER 4 – STAUROSPORINE INSPIRED 'OPEN' ANALOGUES

4.1 Towards novel bisaryl maleimide kinase inhibitors

The second part of this project focused on the synthesis of bisaryl maleimide derivatives as potential kinase inhibitors of EGFR. As mentioned previously (see section 2.2), the staurosporine inspired "open" form of the natural indolocarbazole scaffold, has demonstrated better selectivity in terms of kinase inhibition. Enzastaurin and Ruboxistaurin, are two examples of bisindole maleimide as selective kinase inhibitors undergoing clinical trials (figure 71).

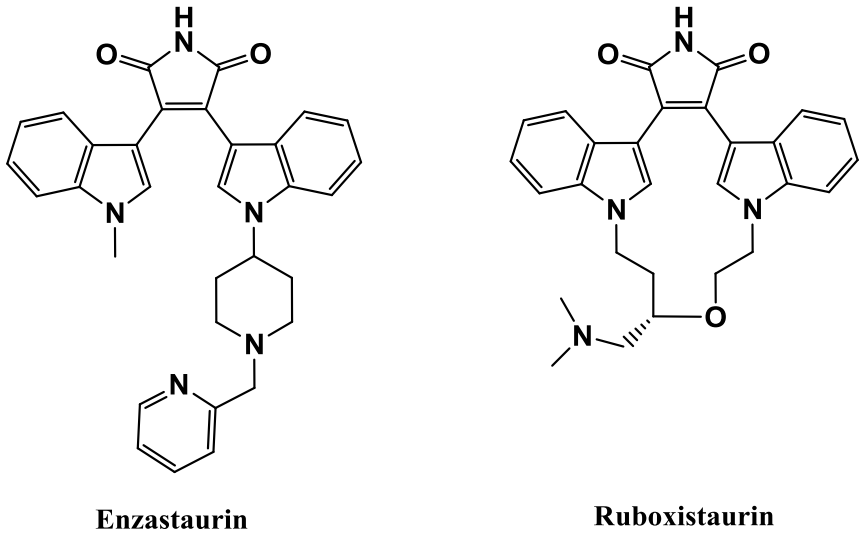

Enzastaurin **Ruboxistaurin**

Figure 71
Bisaryl maleimides as PKC selective kinase inhibitors

4.1.1 Motivation from literature

The rationale behind the design strategy was based on the independent work of the researchers Souffrin and Gu. Souffrin and co-workers applied the Sonogashira cross-coupling reaction to synthesize disubstituted maleimides. Their main interest was to couple various terminal alkynes to the maleimide scaffold.[176] The research of Gu *et al.* implemented Cu(I) click chemistry to generate bisaryl maleimides as kinase inhibitors.[86] This work was discussed in more detail in section 2.1.2. The general structures of the 'click' bisaryl maleimide and dialkynylated maleimide, of Gu and Souffrins work respectively, are illustrated in figure 72.

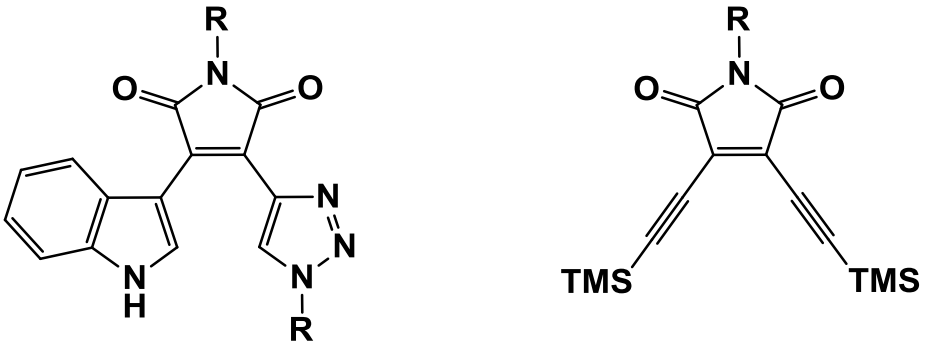

Figure 72
Structures of 'click' bisaryl maleimide and Sonogashira coupled dialkynylated maleimide.

Together, this research motivated and inspired the design of disubstituted maleimide structures resembling the 'open' form of staurosporine. This chapter constitutes 3 main sections. The first section pertains to the synthesis of bisaryl maleimides by employing a 'double click' approach. Thereafter, the following section involves indolylmaleimde click products, and finally, the last section aims to synthesize bisaminated maleimide derivatives. Having described the objective for the second part of the project, we now endeavor to synthesize the various compounds. A discussion of the different envisaged research strategies, reactions and problems encountered is given in the remainder of this chapter.

4.2 The bisaryl maleimide double click compounds

The initial focus of this chapter was towards the synthesis of bisaryl maleimide scaffolds by attempting a 'double click' approach. Incorporating a 'warhead' (R), such as an acryloyl group, into the structure would permit the compound to behave as a potential irreversible kinase inhibitor. The Cu(I) click reactions can be performed by utilizing either the disubstituted azide or disubstituted alkyne maleimide starting material, generating the respective products as shown in figure 73.

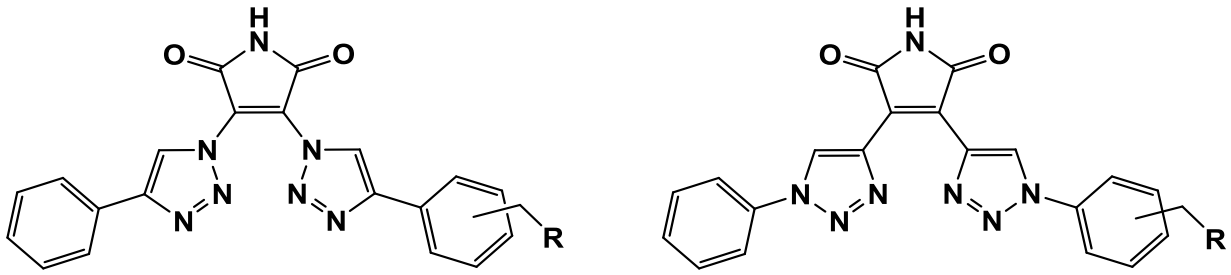

Figure 73
Structures of the 'double click' products following the addition of a warhead (R).

4.2.1 Strategy pertaining to the bisaryl maleimide 'double click' compounds

The design strategy started with the chlorination of the commercially available maleic anhydride, followed by the subsequent transformation to the maleimide. The significance of the –NH imide has been discussed in section 3.7.4. Thereafter, a substitution reaction of the chloro atoms with sodium azide prepared both the mono- and diazido maleimide compounds. An outline of the strategy, to determine the effectiveness of a simple 'double click' reaction, is shown in scheme 53. Once the 'double click' reaction proof of concept could be established, a scope of opportunities would be available to perform click reactions simultaneously with aryl groups, having a pre-installed warhead (acryloyl group), as shown in Figure 74.

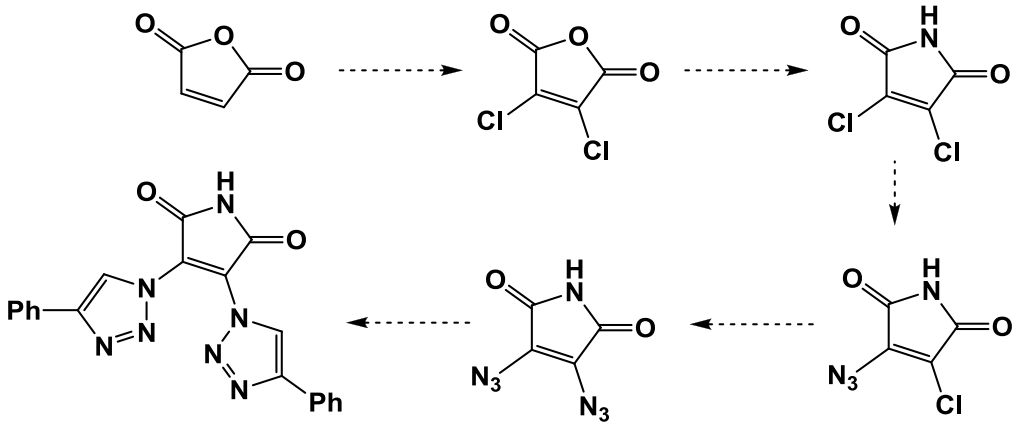

Scheme 53
Outline of strategy towards the bisaryl maleimide compound.

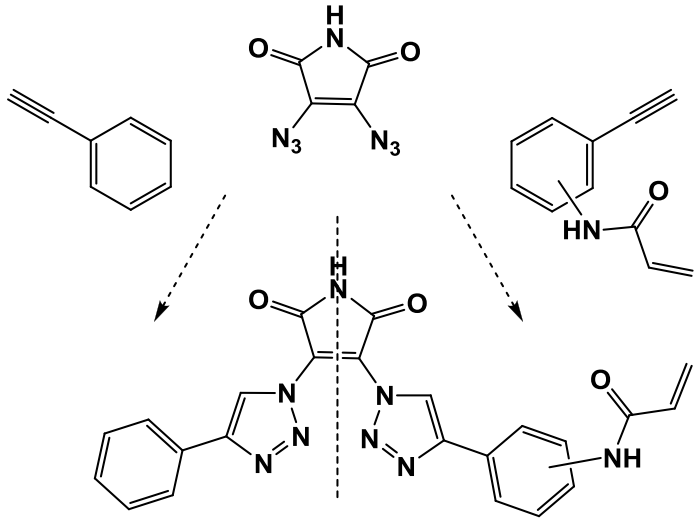

Figure 74
'Double click' approach to introduce 'warhead' (acryloyl group) pre-installed in an aryl group.

4.2.2 Synthesis of bisaryl maleimide 'double click' compounds

4.2.2.1 Synthesis of 3,4-dichlorofuran-2,5-dione (69)

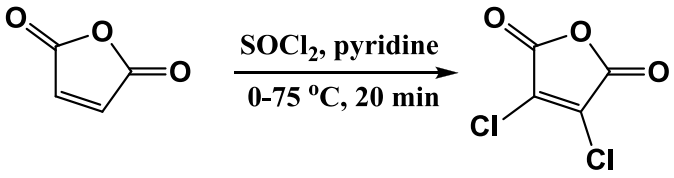

68 **69**

Scheme 54

The first reaction pertaining to the strategy involved the chlorination of maleic anhydride (**68**), as shown in scheme 54. The synthesis was carried out smoothly, following a procedure described in literature which utilized a thionyl chloride-pyridine method.[177] The manner in which the reaction progressed did not follow a simple replacement of hydrogen by chlorine, and the mechanism was investigated and described in detail by Relles.[177] The reaction was performed by treating a solution of maleic anhydride (**68**) and $SOCl_2$ with pyridine, afforded compound **69** in a yield of 70% in sufficient purity.

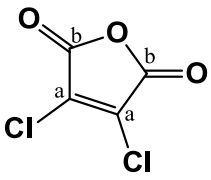

The ^{1}H NMR spectrum showed no proton signals present for the product (**69**). Two carbon signals were identified in the ^{13}C NMR spectrum owing to the symmetrical structure of the product. The carbonyl carbon (C_b) was located at 162.0 ppm, while C_a was found at 130.4 ppm.

4.2.2.2 Synthesis of 3,4-dichloro-1*H*-pyrrole-2,5-dione (70)

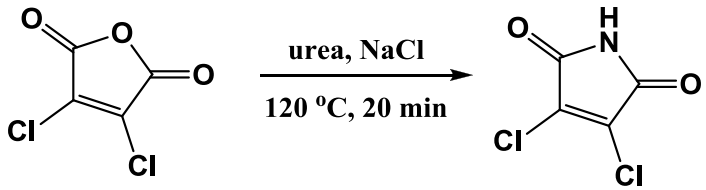

69 **70**

Scheme 55

The important imide functionality was introduced by following a simple procedure described in the literature.[178] In the reaction the solids dichloro-maleic anhydride, urea and NaCl were ground together and reacted at 120 °C for 20 minutes (Scheme 55). The reaction mixture was then recrystallized from methanol-water (2:1 v/v), affording the product (**70**) in a yield of 57%. The yield corresponded to that in literature.[178]

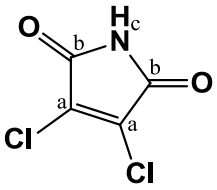

The ^{1}H NMR of the product showed the characteristic imide –NH_c broad signal at 11.71 ppm.

4.2.2.3 Synthesis of 3-azido-4-chloro-1*H*-pyrrolo -2,5-dione (71) and 3,4-diazido-1*H*-pyrrolo -2,5-dione (72)

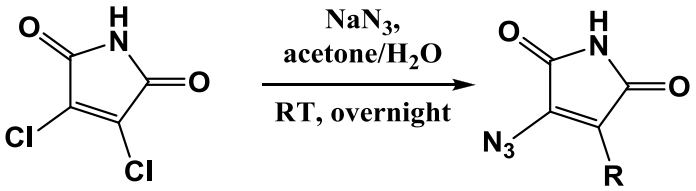

70 **71** **72**

Scheme 56

In order to perform the click reactions, we decided to synthesize both the mono- and diazido maleimide compounds. The substitution reactions were carried out smoothly, generating the respective products depending on the equivalents of azide added (Scheme 56). A solution of NaN_3 dissolved in H_2O was then prepared and added to the reaction flask. The addition of 1 equivalent of NaN_3 formed the 3-azido-4-chloro-1*H*-pyrrolo -2,5-dione product (**71**), while 3 equivalents gave the 3,4-diazido-1*H*-pyrrolo -2,5-dione product (**72**). It must be noted that the diazido compound (**72**) could also be prepared from the mono-azido compound (**71**). The reaction mixture was stirred overnight at room temperature. Upon completion, a workup was carried out and the products were purified by column chromatography. The monoazido product (**71**) was afforded as a light yellow solid in a yield of 79%. When 3 equivalents of NaN_3 was used the diazido product (**72**) was afforded as a bright yellow solid in a yield of 66%.

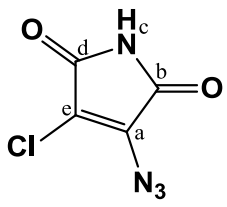

The ^{1}H NMR spectrum of the product (**71**) showed the presence of the broad –NH_c signal at 11.46 ppm. Four carbon signals were identified in the ^{13}C NMR spectrum of the product. The carbonyl signals (C_b and C_d) were located at 165.05 ppm and 164.89 ppm. The signal of C_a was found most upfield at 111.0 ppm, while C_e was found at 136.7 ppm. Importantly, the IR spectrum revealed a clear azide stretch at 2149 cm^{-1}. The results of the mass spectral analysis of 172.9700 amu correlated with the expected mass of 172.9866 amu.

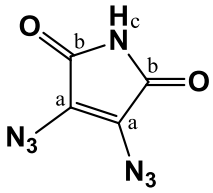

A distinctive feature of the diazido product (**72)**, is that it is symmetrical, while the monoazido compound clearly is not. For this reason, the ^{13}C NMR of the product revealed only two carbon signals – C_b located at 166.4 ppm and C_a at 112.0 ppm. The ^{1}H NMR of the product showed the presence of the broad $–NH_c$ signal at 11.28 ppm. Furthermore, a strong azide stretch at 2088 cm^{-1} could be identified in the IR spectrum. The MS technique utilized did not result in detection of the molecular ion of compound **72**.

4.2.2.4 Attempted synthesis of 3,4-bis(4-phenyl-1*H*-1,2,3-triazol-1-yl)-1*H*-pyrrole-2,5-dione (73)

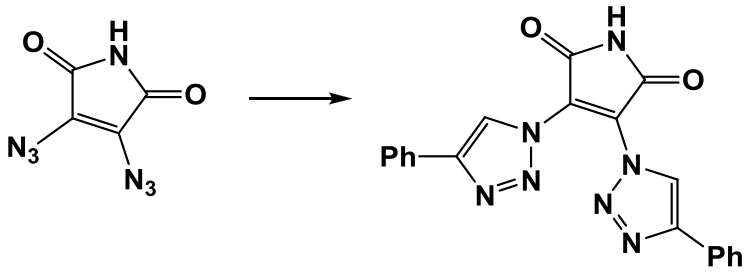

72 **73**

Scheme 57

As mentioned before, a simple 'double click' reaction was initially carried out to investigate and determine the most optimal reaction conditions (scheme 57). Since phenyl acetylene was readily available, it was chosen as the alkyne counterpart for this click reaction.The 'double click' reaction proved to be very challenging. Various reaction conditions were attempted as shown in table 1. Different sources of copper, solvent, temperature, reaction time and equivalents of phenyl acetylene were tested, without any success. The reactions were monitored by TLC, and the starting material remained unreacted, with no new spot formation being observed. A trace amount of what seemed to be the product was obtained from the reaction conditions highlighted in table 1. This particular reaction was performed by treating compound **72** in MeOH with a mixture of $CuSO_4$•$5H_2O$ and sodium ascorbate dissolved in H_2O. The reaction mixture was then left to stir at 40 °C for 4 days. After this time, it seemed as if the reaction had reached its completion, with some starting material (**72**) remaining unreacted. Following a workup and purification by column chromatography, only a trace amount of the product (**73**) was obtained. Unfortunately, due to the small amount of product available - and DMSO required as NMR solvent - the product was not recovered and full characterization was not possible.

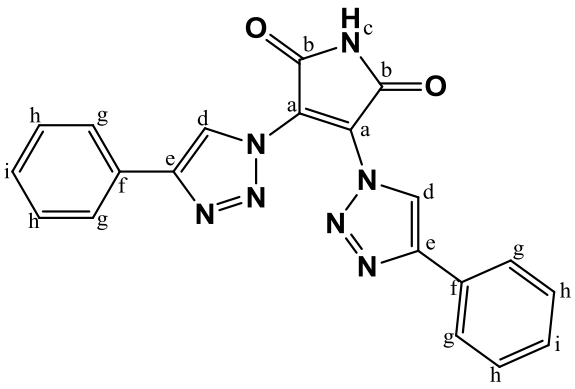

The ^{1}H NMR spectrum of the product (**73**) showed a broad signal for -NH_c at 11.28 ppm. Structural symmetry allowed for several protons to be chemically equivalent, which corresponded with the expected integration. The indicative proton signal of the triazole ring (H_d) was located at 8.75 ppm and integrated for two. The H_g signal appeared as a doublet at 7.93, integrating for four. The rest of the phenyl proton signals (H_h and H_i) appeared as a multiplet at 7.84-7.28 ppm with an integration of six.

Table 1
Reaction conditions for the 'double click' reaction

Phenyl acetylene (equiv)	Solvent	Catalyst (equiv)	Reductant (equiv)	Temperature (°C)	Time	Yield
2.2	MeCN	0.1 CuI	2.2 DIPEA	RT	24 h	0
4	H_2O: MeOH (1:4)	0.1 $Cu(AcO)_2$	none	RT	3 d	0
2.4	H_2O: MeOH (1:1)	0.02 $CuSO_4$•$5H_2O$	0.2 Na ascorbate	RT	24 h	0
2.4	H_2O: MeOH (1:2)	0.1 $CuSO_4$•$5H_2O$	1 Na ascorbate	40	4 d	trace amount

4.2.3 Tackling the first possible obstacle

The challenges associated with the 'double click' reaction, led us to question the viability of this approach, and to target the possible problems which may attribute to its limited success. The initial rationalization was that the close proximity of the azide groups altered the electronics in such a manner that the 'double click' was prohibited. To verify this point, a click reaction was carried out using the mono-azido maleimide (3-azido-4-chloro-1*H*-pyrrolo-2,5-dione) (**71**) as shown in scheme 58. This reaction was performed in a similar manner as that described in the previous click reaction (subsection 4.2.2.4). Similarly, TLC monitoring revealed that the starting material (**71**) remained unreacted with no new spot formation. Hence, the electronic nature of the diazido maleimide (**72**) was excluded as a possible reason for the 'double click' approach not working.

4.2.3.1 Attempted synthesis of 3-chloro-4-(4-phenyl-1*H*-1,2,3-triazol-1-yl)-1*H*-pyrrole-2,5-dione (74)

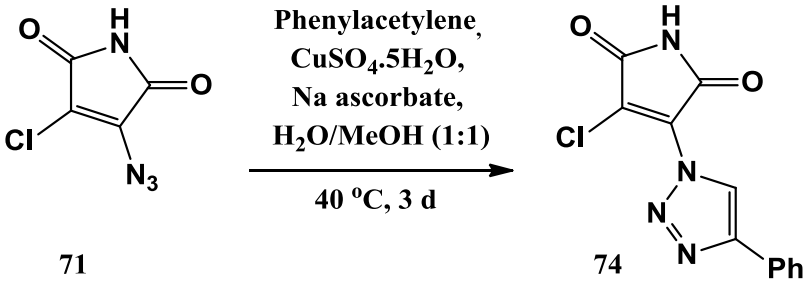

Scheme 58

4.2.4 Tackling the second possible obstacle

Another plausible explanation for the 'double click' reaction being unsuccessful was that the imide –NH group may be troublesome - possibly acting as a good ligand for complexation to the copper ion. For this reason we attempted a strategy in which a methyl group was incorporated into the maleimide structure. An outline of the strategy is illustrated in scheme 59.

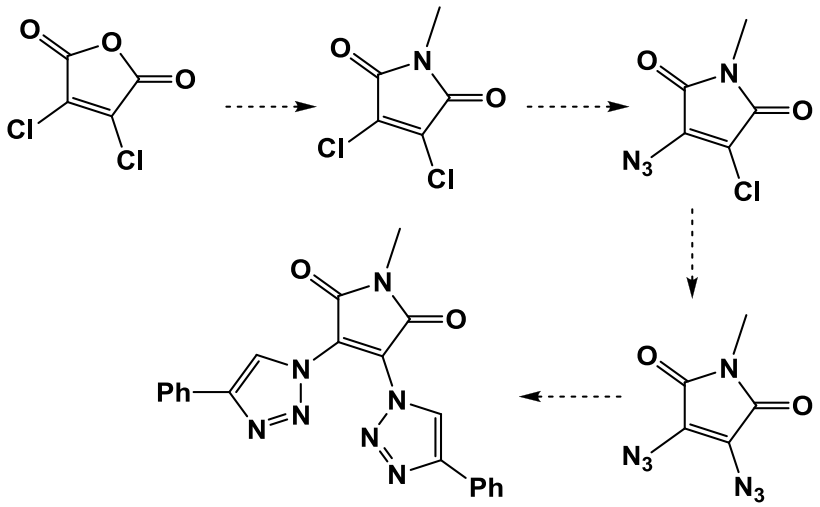

Scheme 59
Outline of strategy incorporating a methyl to the maleimide.

4.2.4.1 Synthesis of 3,4-dichloro-1-methyl-1*H*-pyrrole-2,5-dione (75)

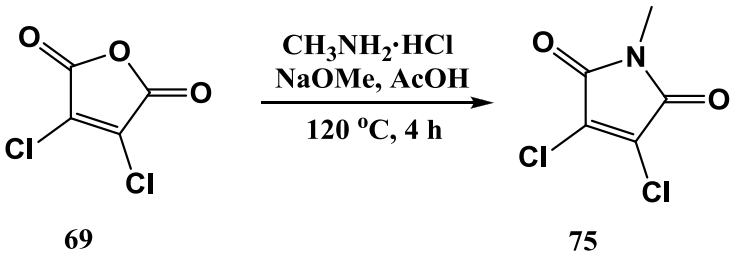

69 **75**

Scheme 60

The methyl group was introduced onto the dichloromaleic anhydride (**69**) by following a procedure described in literature.[179] The reaction was carried out smoothly by adding compound **69** and AcOH to a reaction flask, and treating the solution with CH_3NH_2·HCl and NaOMe at 0 °C. The reaction mixture was then heated to reflux for 4 hours. It has been shown that this reaction does not proceed in the absence of a base, even at high temperatures. The required base must be stronger than methylamine, such as methoxide. The NaOMe acts by liberating the nucleophilic CH_3NH_2 gas *in situ*. Upon completion, a workup was carried out, and the product was purified by means of column chromatography, affording the pure product (**75**) in a yield of 62%.

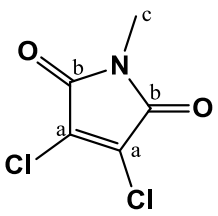

The ^{1}H NMR spectrum of the product (**75**) was compared to that in literature and corresponded well.[180] The signal of the methyl group protons (H_c) was located at 2.95 ppm.

4.2.4.2 Synthesis of 3-azido-4-chloro-1-methyl-1*H*-pyrrole-2,5-dione (76) and 3,4-diazido-1-methyl-1*H*-pyrrole-2,5-dione (77)

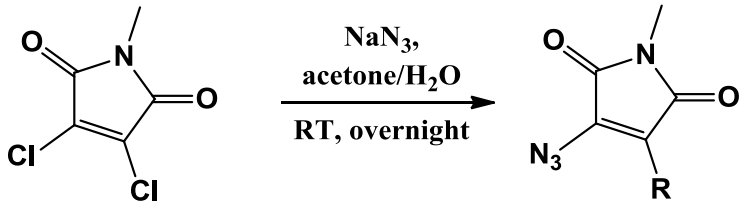

75

R = Cl or N_3

76 **77**

Scheme 61

The substitution reaction to introduce the azide/s to compound **75**, was performed in exactly the same manner as the reactions in subsection 4.2.2.3. Both the mono-and diazido product were synthesized as shown in scheme 61.

As mentioned previously, the various products could be generated from compound **75** depending on the equivalents of NaN_3 added. Column chromatography was used to purify the products synthesized by each reaction. 3-azido-4-chloro-1-methyl-1*H*-pyrrole-2,5-dione (**76**) was afforded as an off-white solid in an excellent yield of 98% and the pure product of 3,4-diazido-1-methyl-1*H*-pyrrole-2,5-dione (**77**) was obtained in a yield of 68%.

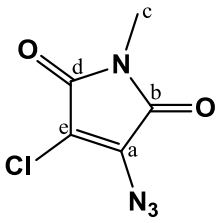

The ^{1}H NMR spectrum of the product (**76**) showed the –NMe (H_c) signal at 3.07 ppm. Five carbon signals were identified in the ^{13}C NMR of the product. The two carbonyl signals (C_d and C_b) were found at 164.21 ppm and 164.12 ppm. The signal of C_e was identified at 135.79 ppm, while that of C_a was found more upfield at 113.14 ppm. The IR spectrum revealed the distinctive azide stretch at 2115 cm^{-1}. The MS technique utilized did not result in detection of the molecular ion of compound **76**.

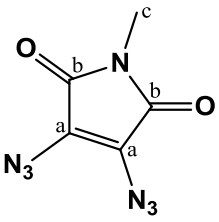

The ^{1}H NMR spectrum of the product (**77**) showed the –NMe (H_c) signal at 3.02 ppm. The structure contains symmetry and revealed three carbon signals in the ^{13}C NMR. The carbonyl C_b was identified at 164.8 ppm, and C_a at 119.8 ppm. The results of the mass spectral analysis ($-2N_2$) of 138.0315 amu correlated with the expected mass of 138.0304 amu.

4.2.4.3 Attempted synthesis of 1-methyl-3,4-bis(4-phenyl-1*H*-1,2,3-triazol-1-yl)-1*H*-pyrrole-2,5-dione (78)

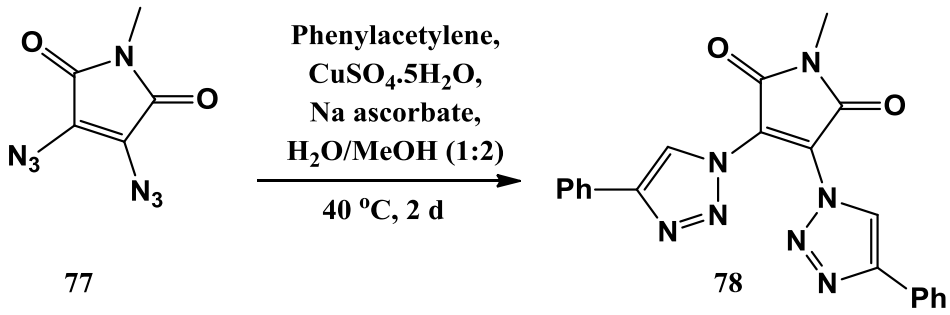

Scheme 62

The 'double click' reaction, as shown in scheme 62, was performed in a similar manner as that in subsection 4.2.2.4. Unfortunately, the reaction did not proceed as hoped. TLC monitoring indicated that most of compound **77** remained unreacted, with only a faint product spot being identified on the TLC plate. No further product formation was observed at a longer reaction time.

The product was purified by column chromatography, affording a trace amount of the pure compound (**78**). The small amount of product obtained, limited the full characterization of the 'double click' compound.

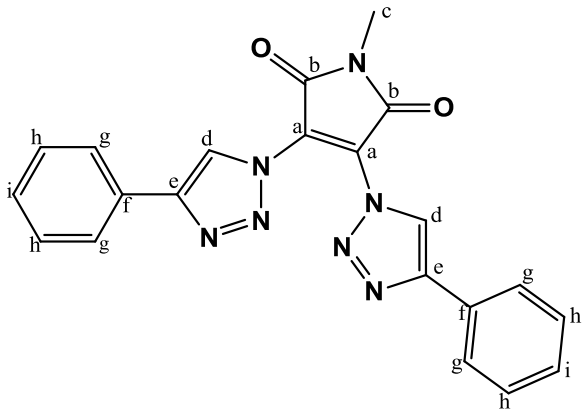

The ^{1}H NMR spectrum of the product (**78**) revealed the indicative triazole singlet (H_d) at 8.75 ppm, integrating for two (structural symmetry). Furthermore, all the signals of the phenyl ring could be accounted for. H_g and H_h were located at 7.94 ppm and 7.47 ppm, respectively. The signal of H_g appeared as a doublet, and H_h as a multiplet, both integrating for four. H_i integrated for two and was located at 7.37 ppm as a multiplet. The -NMe (H_c) was identified most upfield at 2.94 ppm and integrated for three.

4.2.5 Tackling the third possible obstacle

The unsatisfactory outcome of the 'double click' reactions thus far, challenged us to attempt a different strategy whereby the alkyne/azide counterparts are switched for the click reaction – i.e. a click reaction was to be performed between a dialkynylated maleimide and the azide fragments. An outline of this strategy is shown in scheme 63. The rationalization behind this approach was in continuation to the idea that the electronics of the azide-maleimide system were perhaps not suitable for effective triazole ring formation. The inspiration for this strategy was acquired from the work of Souffrin *et al*. in which they implemented a double Sonogashira cross-coupling reaction to incorporate acetylene groups onto the maleimide structure.[176]

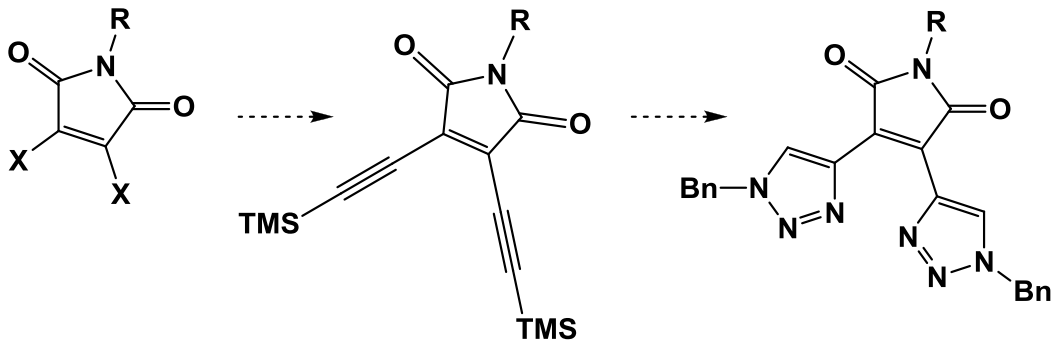

Scheme 63

Outline of strategy whereby a click reaction is performed with a dialkynylated maleimide.

4.2.5.1 Sonogashira cross-coupling reaction

Metal-catalyzed cross-coupling reactions have grown into a powerful strategy and are considered cornerstones in the field of organic chemistry.[181] These reactions have found application in a vast scope of synthetic procedures, including the total synthesis of natural products, pharmaceuticals, and molecular organic materials. Methodologies based on metal catalysis, particularly palladium, have been a major source of stimulation in maleic anhydride/imide chemistry.[181-182]

The Sonogashira reaction is the most popular palladium-catalyzed cross-coupling reaction for the alkynylation of aryl or alkenyl halides.[181] The C-C bond formation involves a terminal sp hybridized carbon from an alkyne with a sp^2 carbon of an aryl or vinyl halide (or triflate).[183] The reaction was discovered in 1975 by Sonogashira, Tohda, and Hagihara, and was an extension of the independent work of Heck and Cassar.[184] The mild conditions of the Sonogashira reaction made it an attractive synthetic procedure compared to the high temperatures required by the palladium-catalyzed Heck and Cassar reactions. The successful alkynylation at room temperature, achieved by the Sonogashira reaction, was ascribed to the already known Stephans-Castro coupling between copper acetylides and phenyl or vinyl halides.[185] Combining the copper-mediated transmetalation of alkynes with a powerful and versatile catalyst such as palladium, greatly increased the reactivity of the system.[184]

Sonogashira's insight of using a co-catalytic amount of CuI together with a Pd(0) catalyst has afforded remarkable success in diverse areas of chemistry.[181,183] An excess amount of amine is required for the Sonogashira reaction and may even be used as the solvent. A stable and soluble Pd(II) derivative, such as $Pd(PPh_3)_4$ or $PdCl_2(PPh_3)_2$, is often employed and reduced *in situ* to the catalytically active Pd(0) species.[148] A general procedure of the Sonogashira reaction is illustrated in scheme 64. A drawback of using a copper co-catalyst is that undesirable alkyne homocoupling (Glaser coupling), can occur upon exposure to air or oxidative agents.[181] For this reason, researchers now pursue the development of coupling procedures that are copper-free, which are still considered as Sonogashira reactions, regardless of the absence of the copper species.[183]

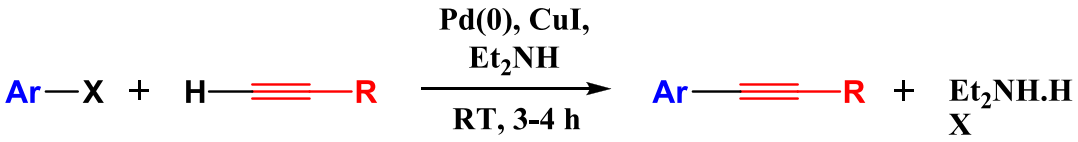

Scheme 64

Generalized procedure of a Sonogashira reaction coupling an aryl halide and terminal alkyne.[148]

Uncertainties pertaining to the exact mechanism of the Sonogashira reaction continue.[183] However, a proposed mechanism for the Pd(0)/Cu(I) catalyzed reaction involves the interaction between two independent catalytic cycles as shown in figure 75. Cycle A, known as the palladium-cycle, is a classical form of C-C coupling and includes oxidative addition, transmetalation and reductive elimination, to afford the coupled product and regenerating the Pd(0) catalyst. Cycle B, is known as the copper-cycle, which generates the alkynyl copper used for the transmetalation step. It is suggested that the base plays an important role in alkynyl copper formation by interacting with the acidic terminal proton of the π-alkyne copper complex.[181,183,185]

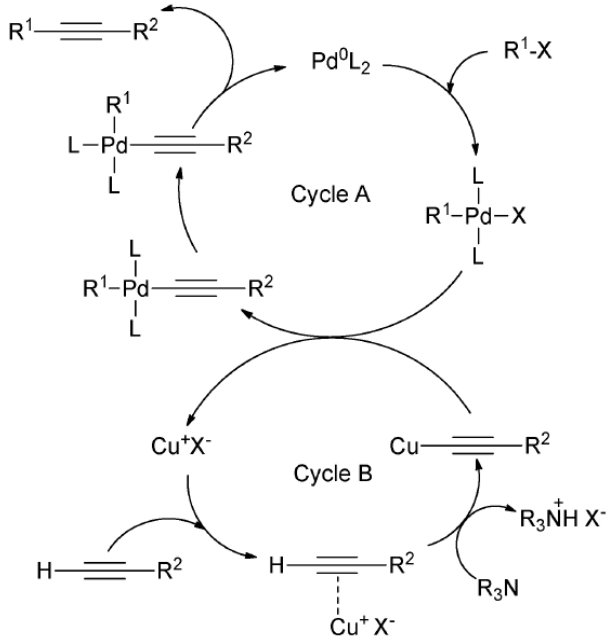

Figure 75

Proposed mechanism for the Sonogashira cross-coupling reaction using Cu(I) as co-catalyst. L represents phosphane, base, solvent or alkyne. Image reproduced from following reference.[183]

4.2.5.2 Synthesis of 3,4-dibromomaleic anhydride (79)

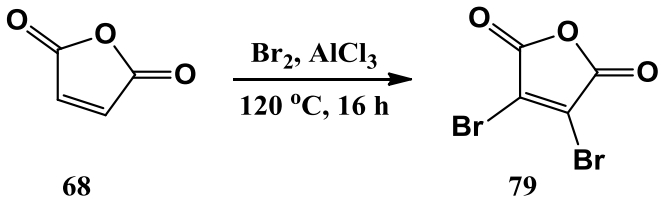

68 **79**

Scheme 65

Regarding the Sonogashira reaction, the bromide sp^2 species is generally more reactive than the chlorine version.[181] For this reason, it was decided to incorporate the dibromo atoms onto the maleimide group. The first step in this strategy involved the bromination of maleic anhydride (**68**) as shown in scheme 65.

The reaction proceeded smoothly, following a procedure described in literature.[186] The procedure involved heating a mixture of compound **68** with Br_2 and a catalytic amount of $AlCl_3$ and the product (**79**) was afforded in a good yield of 72%.

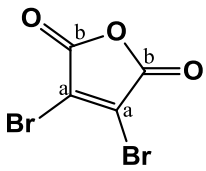

The ^{1}H NMR spectrum of the product (**79**) showed the absence of the proton signal present in the maleic anhydride starting material (**68)**. Two chemically equivalent carbon signals were identified in the ^{13}C NMR spectrum of the product (**79**). The carbonyl C_b was located at 167.6 ppm and C_a at 163.2 ppm.

4.2.5.3 Synthesis of 1-benzyl-3,4-dibromo-1*H*-pyrrole-2,5-dione (80)

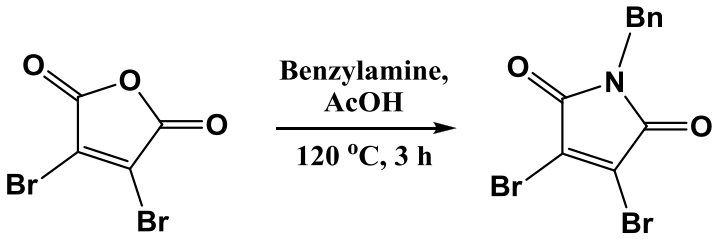

79 **80**

Scheme 66

Following the strategy used by Souffrin *et al*, we decided to synthesize the benzyl-protected dibromo maleimide (**80**). The reaction was carried out according to a procedure described in literature, in which a solution of compound **79** in AcOH, was treated with benzylamine.[187] The product (**80**) was purified by column chromatography, and obtained in a yield of 55%.

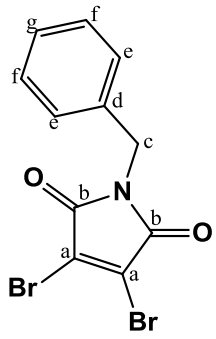

The ^{1}H NMR spectrum of the product (**80**) showed two signals assigned to the benzyl group and corresponded to that reported in literature.[187] The aromatic protons (C_e, C_f, C_g) were located as a multiplet at 7.4-7.3 ppm, and integrated for five. The methylene signal of C_c was located as a singlet at 4.8 ppm, integrating for two. Furthermore, the IR spectrum of the product revealed the presence of the carbonyl stretch at 1707 cm^{-1}, and the C-Br stretch at 697 cm^{-1}.

4.2.5.4 Synthesis of 1-benzyl-3,4-bis{(trimethylsilyl)ethynyl}-1*H*-pyrrole-2,5-dione (81)

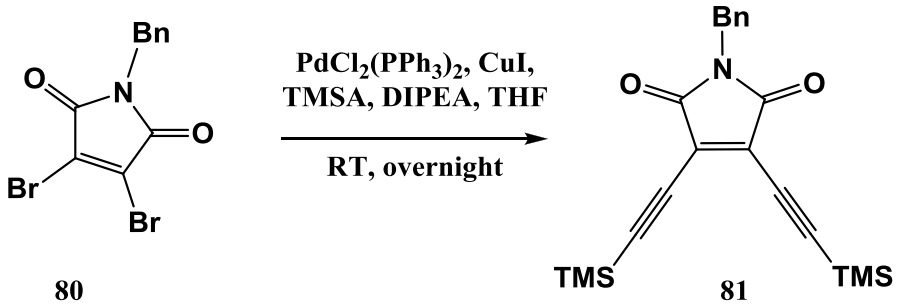

Scheme 67

The Sonogashira reaction was performed as described by Souffrin and co-workers and the synthesis of the dialkynylated maleimide product (**81**) was carried out successfully as shown in scheme 67.[176] The procedure utilized the Pd(0)/Cu(I) catalytic system, with DIPEA as amine base. Since the Cu(I) click reaction requires a terminal alkyne, we envisaged using TMSA for the double Sonogashira reaction. Standard freeze-pump-thaw techniques were employed to ensure an inert, O_2-free environment, and to prevent undesirable alkyne homocoupling. Upon completion and following a workup, the product (**81**) was purified by means of column chromatography and obtained in a yield of 68%.

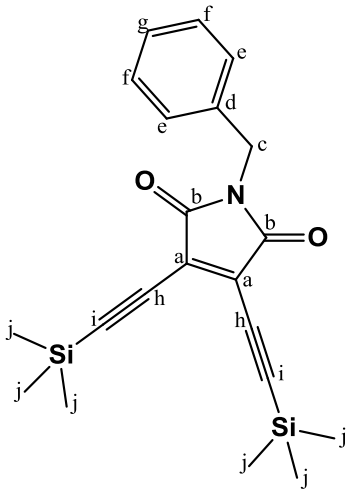

The ^{1}H NMR spectrum of the product (**81**) was compared to that in literature and corresponded well.[176] The successful coupling of the TMSA group was supported by the presence of the new signal of C_j, located at 0.3 ppm, integrating for eighteen. The rest of the benzyl proton signals were all accounted for, and corresponded well to the expected integration.

4.2.5.5 Attempted synthesis of 1-benzyl-3,4-diethynyl-1*H*-pyrrole-2,5-dione (82)

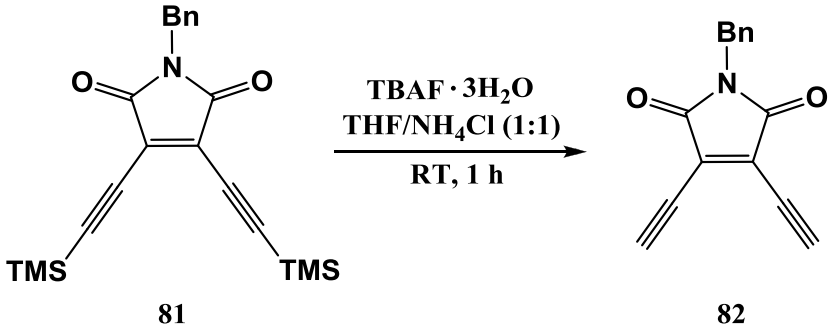

81 **82**

Scheme 68

Removal of the TMS group proved to be problematic and the procedure shown in scheme 68 was not successful. Compound **81** was dissolved in a mixture of THF and saturated NH_4Cl, and treated with $TBAF{\cdot}3H_2O$. The NH_4Cl was included in the hope of quenching the anion formed upon deprotection. It must be noted that maleimide-based enediynes have been reported as good systems for cycloaromatization at low temperatures. The carbonyl groups of maleimide are able to lower the energy barrier of Bergman cyclization, allowing the reaction to proceed at moderate temperatures.[188] For this reason, the reaction was performed in the dark at room temperature. This precaution was taken to avoid any possibility of cycloaddition occurring in the reactive system. The progress of the reaction was monitored by TLC, and it was detected that all the starting material was consumed within the first hour. Two new spots were formed, including one on the baseline. Unfortunately, the product formed was unstable and complete degradation took place upon purification by column chromatography. TLC indicated that the new spot disappeared, and was replaced by one spot on the baseline. Since the product was lost upon purification, we decided to follow a similar strategy, circumventing the degradation problem by attempting a one pot deprotection/ 'double click' reaction. Having 3,4-dichloro-1-methyl-1*H*-pyrrole-2,5-dione (**75**) in hand, we utilized this starting material in the strategy.

4.2.5.6 Synthesis of 1-methyl-3,4-bis{(trimethylsilyl)ethynyl}-1*H*-pyrrole-2,5-dione (83)

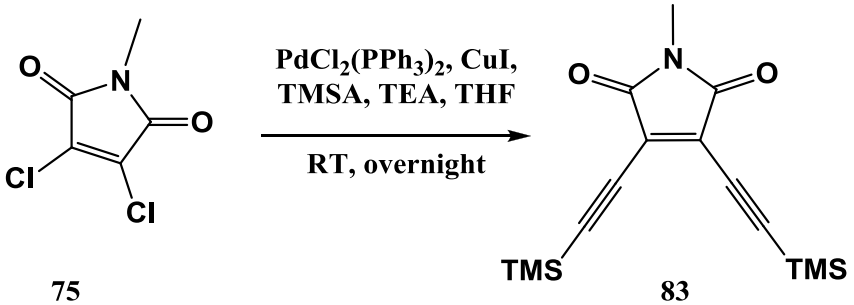

75 **83**

Scheme 69

The Sonogashira reaction was performed in exactly the same manner as that described in subsection 4.2.5.4, with the only difference being the amine base used (TEA), as shown in scheme 69. The product (**83**) was purified by column chromatography and obtained in a rather low yield of 43%.

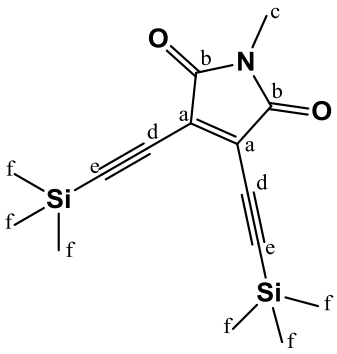

The ^{1}H NMR spectrum of the product (**83**) showed a clear signal for the TMSA group coupled to the starting material. The singlet assigned to H_f integrated for eighteen, and was located at 0.26 ppm. Three additional carbon signals were found in the ^{13}C NMR spectrum of the product (**83**), compared to that of the starting material (**75**). C_f was located at -0.6 ppm, while C_e and C_d were located at 117.1 ppm and 94.4 ppm respectively.

4.2.5.7 Synthesis of 3,4-bis(1-benzyl-1*H*-1,2,3-triazol-4-yl)-1-methyl-1*H*-pyrrole-2,5-dione (84)

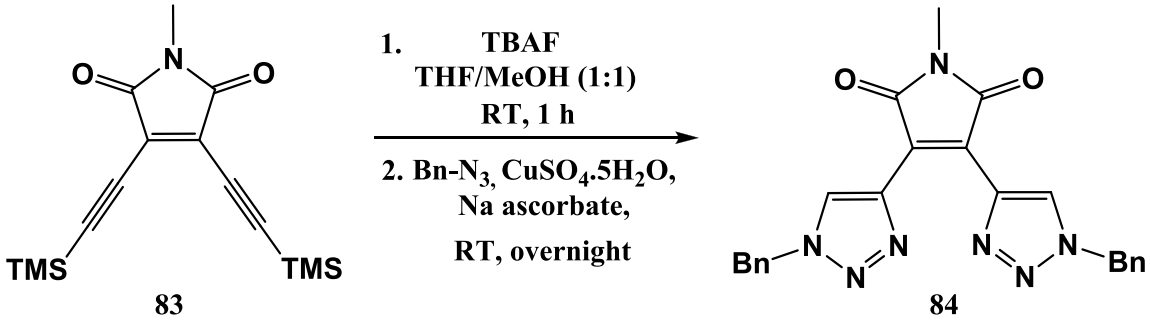

Scheme 70

The one pot reaction was carried out by first performing a deprotection reaction, followed by a 'double click' reaction. The reaction conditions were similar to those utilized by Gu *et al.*[86] Compound **83** was dissolved in a mixture of THF and MeOH, and then treated with TBAF (1M in THF).

The reaction was monitored by TLC and showed the formation of two new spots (product and baseline spot). Benzyl azide, $CuSO_4 \cdot 5H_2O$ and sodium ascorbate were then added the reaction mixture and it was stirred overnight at room temperature in the dark. TLC indicated the formation of a faint new spot, together with an intense spot on the baseline. Following the workup, the product was purified by column chromatography, affording the pure compound (**84**) in a very low yield of 5%. The low yield was ascribed to the degradation of the product following the deprotection step – as indicated by an intense spot on the baseline. It is therefore difficult to determine the effectiveness of the double click reaction in this situation. Unfortunately, as a result of the low yield and the fact that the NMR spectrum samples were performed in DMSO, the product could not be recovered and full characterization was not possible.

The product **84** could only be tentatively characterized by the ^{1}H NMR spectrum, due to the small amount obtained.

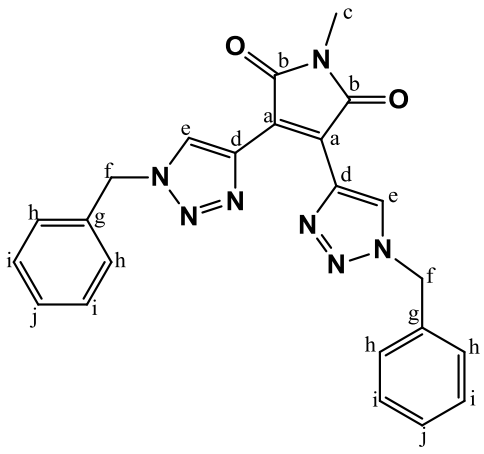

The structure of the product has symmetry and a number of proton atoms were therefore chemically equivalent. The ^{1}H NMR spectrum of the product (**84**) revealed the indicative triazole proton H_e at 8.62 ppm, integrating for two. The proton signals of the benzyl group were all accounted for. H_f was located at 5.64 ppm and integrated for four. The aromatic proton H_i was found as a doublet at 7.84 ppm (integrated four), while the rest of the aromatic signals (H_h, H_i, H_j) were identified in the range 7.46 – 7.29 ppm as a multiplet and integrated for six. The methyl protons H_c, could not be seen in the spectrum and we suspect the singlet is masked by the H_2O present in the DMSO solvent. The number of carbon signals in the ^{13}C NMR spectrum of the product (**84**) corresponded with the expected number of carbon atoms (ten) in the structure, taking symmetry into account.

4.2.6 Remarks about the 'double click' strategy

In summary, the overall results obtained for the 'double click' reactions were disappointing. Although the yields were very low and in some cases only trace amounts were obtained, the fact that the products did form was a hopeful indication for possible optimization. In particular, the dialkynylated maleimide appears to be a more suitable and promising system for the 'double click' reaction. Provided the degradation of the deprotected TMSA maleimide moiety can be avoided or overcome, it is suspected the double click reaction could afford the desired products in higher yields. Unfortunately, due to time constraints, it was decided to abandon this route and focus the attention to the synthesis of bisaryl maleimide derivatives, employing click chemistry.

4.3 Bisaryl maleimide click products

In the next section, the synthesis of the bisaryl maleimide click products as demonstrated by Gu *et al*. was endeavored.[86] The reader is reminded that several bisindolylmaleimide analogues have shown promising activity as kinase inhibitors.[189-190] The purpose of this area of work in the project was to determine the effectiveness of the simple click reaction on an indolylmaleimide system. The strategy is outlined in scheme 71 and includes a condensation, Sonogashira and click reaction.

Upon accomplishing the click reaction with a simplified moiety, such as benzyl azide, the next attempt would be to perform a click reaction with a pre-installed warhead functionality (for example an acryloyl group).

It must be noted that the focus of this section of research was towards investigative purposes, and unfortunately the low yields afforded by the click reactions did not generate enough material for full characterization. Furthermore, DMSO was used as NMR spectrum solvent and the products were therefore not recovered for further analysis.

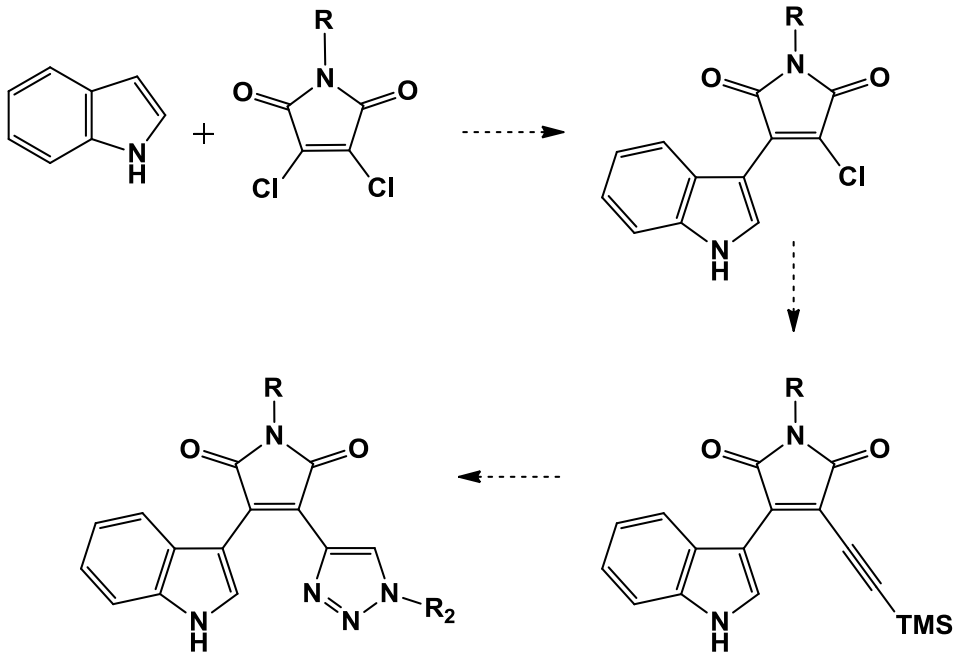

Scheme 71
Outline of strategy towards bisaryl maleimide click products, where R is a methyl or benzyl group.

4.3.1 Indole Grignard Reagents

The first reaction performed in this strategy involves a condensation reaction between *N*-substituted dichloromaleimide and indolyl-MgBr. Grignard reagents have been the most widely used organometallic reagents over the past century.[191] Since their discovery in 1900, these organomagnesium reagents display a broad range of applications in both organic and organometallic synthesis. Their contribution to synthetic chemistry earned Victor Grignard the Nobel Prize in Chemistry in 1912.[191-192] A decade after the discovery of alkylmagnesium halides, Oddo reported that indole reacted in diethyl ether with the Grignard reagent, ethylmagnesium iodide, producing the indole Grignard reagent (indolylmagnesium iodide) with the evolution of ethane.

To date, the procedure described by Oddo is still commonly employed for the preparation of indole Grignard reagents.[193-194] The general structure of the indole Grignard reagent is represented in figure 76.

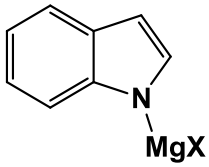

Figure 76
Indole Grignard reagent, where X is usually iodide or bromide.

The indole Grignard reagent has been widely utilized as an intermediate in synthetic work and undergoes many reactions characteristic of simple alkylmagnesium halides. Their widespread use is ascribed to the selective substitution predominately at the 3-position of the indole ring.[193] When dealing with Grignard reagents, care should be taken to avoid exposure to air or water, which may destroy the reagent by protonolysis or oxidation. The choice of solvent is another important factor which affects the yield, stereo-, and regiochemistry of reactions with Grignard reagents. In this regard, ethereal solvents such as diethyl ether and THF are the most commonly used solvents.[192,194]

A variety of approaches have been reported for the synthesis of indolylmaleimides, but one of the more common approaches for preparing mono- and bisindolylmaleimides involves the condensation of an indole Grignard reagent with a dihalomaleimide.[195,198] In our case, a similar strategy was employed to couple the indole to the *N*-substituted-dichloromaleimide. The initial step of the reaction involved the generation of the indole Grignard reagent (indolylmagensium bromide) *in situ*. The work by Brenner *et al.* demonstrated that the solvent used strongly affects the outcome of the reaction. When using toluene, the bisindolyl product forms, whereas the monosubstituted product is obtained when THF is the chosen solvent.[198] For this reason, it was deemed crucial that the reaction was performed in a THF solution to prevent a disubstitution reaction from occurring. A proposed mechanism for the synthesis of this compound is illustrated in scheme 72.

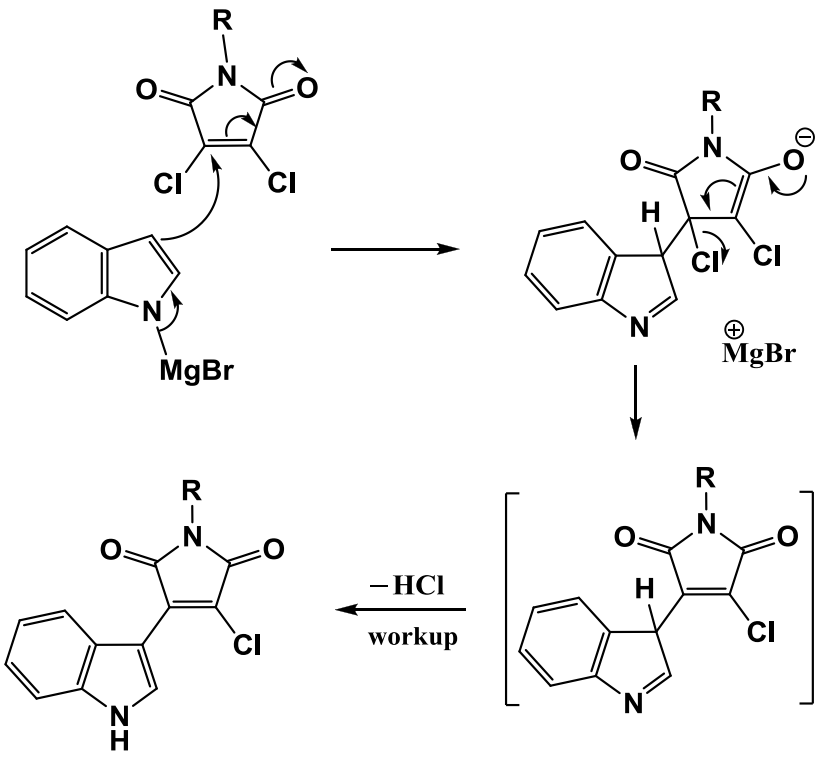

Scheme 72
Proposed mechanism for the synthesis of monoindolyl maleimide compound.

Here follows the synthesis of the various compounds illustrated in the outline, represented in scheme 71. For comparative reasons, both the methyl and benzyl moieties were incorporated into the indolylmaleimide system. Since the procedures employed were the same for both protecting groups, the reaction schemes of only the *N*-Me-indolylmaleimide compound are shown, followed by the individual characterization for the methyl and benzyl indolyl maleimide products.

4.3.2 Synthesis of 1-benzyl-3,4-dichloro-1*H*-pyrrole-2,5-dione (85)

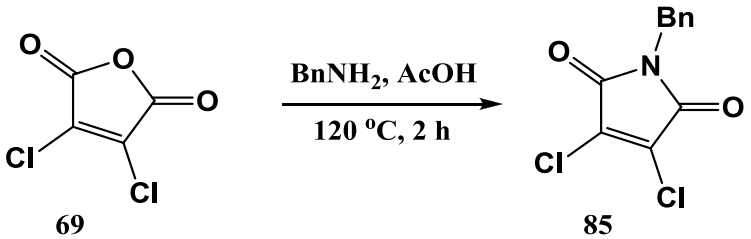

Scheme 73

The route incorporating a benzyl-protected maleimide was carried out, and its effectiveness was compared to the route involving the methyl-protected maleimide as utilized by Gu and coworkers.[176] The first step was to generate the benzyl-protected dichloromaleimide species (**85**).

The reaction was carried out smoothly as shown in scheme 73, by simply heating compound **69** and benzylamine in AcOH to reflux. Upon completion, a workup was carried out, and the crude product was purified by column chromatography. The pure compound (**85**) was afforded in a good yield of 76%.

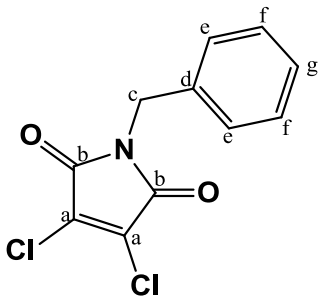

The ^{1}H NMR spectrum of the product (**85**) was compared to that in literature and corresponded well.[199] The benzyl methylene protons H_c were located at 4.73 ppm, as a singlet and integrated for two. The aromatic protons (H_e, H_f, H_g) integrated for five, and were found as a multiplet in the range 7.40-7.23 ppm.

4.3.3 Synthesis of 3-chloro-4-(1*H*-indol-3-yl)-1-methyl-1*H*-pyrrole-2,5-dione (86) and 1-benzyl-3-chloro-4-(1*H*-indol-3-yl)-1*H*-pyrrole-2,5-dione (87)

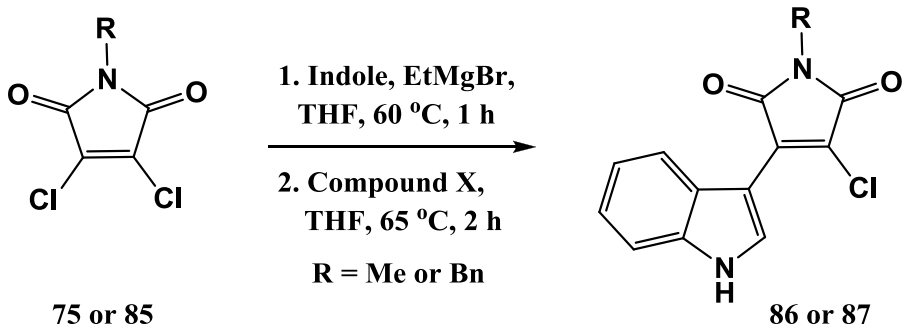

75 or 85 **86 or 87**

Scheme 74

The indole Grignard was prepared *in situ* by treating indole with EtMgBr. The THF used was freshly distilled and degassed to prevent the reaction of H_2O and O_2 with the Grignard reagent.The reaction flask containing the indole solution was then transferred to an ice bath and EtMgBr was added drop-wise. The temperature was increased to 60 °C and stirred for 1 hour. Thereafter, a solution of the respective protected dichloromaleimide (**75** or **85**) in THF was added to the indole Grignard reagent and the reaction was heated to reflux for a further 2 hours. Upon completion, a workup was carried out and the product was purified by column chromatography. The pure product of **86** was afforded in a yield of 57%. The synthesis of **87** was performed according to the exact same procedure, and obtained in a yield of 43%.

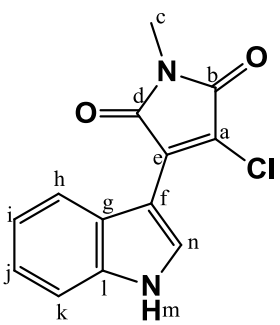

The ^{1}H NMR spectrum of the product (**86)** was compared to that in literature and corresponded well.[176] Upon inspection, the spectrum revealed the presence of both the *N*-Me-maleimide and indole signals, proving the success of the coupling reaction.

The broad signal of the $–NH_m$ peak was located at 12.14 ppm, while H_n was found as a singlet at 8.08 ppm. The aromatic protons H_h and H_k, were identified as doublets at 7.93 ppm and 7.52 ppm. H_i and H_j were found at 7.23 ppm and 7.16 ppm, both as multiplets. All the aromatic signals integrated for one each. The methyl group protons (H_c) were located at 3.00 ppm, as a singlet, and integrated for three.

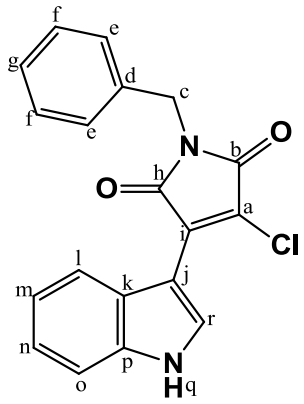

The ^{1}H NMR spectrum of the product (**87**) showed the presence of the indole- and benzyl aromatic proton signals, confirming that the coupling was a success. The broad $–NH_q$ signals was located at 12.18 ppm, and the singlet of the methylene benzyl protons H_c were found at 4.73 ppm, integrating for two. The benzyl aromatic protons (H_e, H_f, H_g) were identified in the range 7.38-7.27 ppm as a multiplet and integrated for 5. H_l and H_o were located at 7.95 ppm and 7.52 ppm as doublet of doublets, both integrating for one. Two multiplets were found at 7.25-7.21 ppm and 7.20-7.13 ppm, which were assigned to H_m and H_n. The two carbonyl carbon signals (C_b, C_h) were located at 168.4 ppm and 165.9 ppm in the ^{13}C NMR spectrum of the product. Furthermore, all the carbon signals of the indole group and benzyl moiety were accounted for. The IR spectrum revealed the amine (-NH) stretch at 3279 cm^{-1}, the carbonyl (C=O) stretch at 1696 cm^{-1},and the C-Cl stretch at 696 cm^{-1}.

4.3.4 Synthesis of 3-(1*H*-indol-3-yl)-1-methyl-4-{(trimethylsilyl)ethynyl}-1*H*-pyrrole-2,5-dione (88) and 1-benzyl-3-(1*H*-indol-3-yl)-4-{(trimethylsilyl)ethynyl}-1*H*-pyrrole-2,5-dione (89)

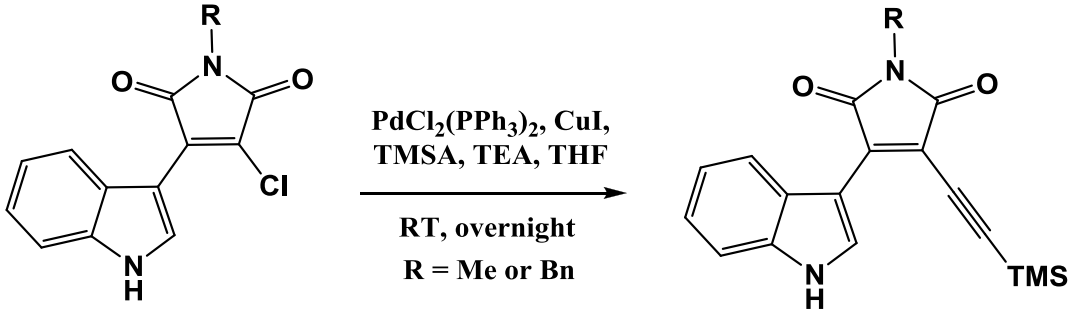

86 or 87 **88 or 89**

Scheme 75

The next reaction in the strategy was a Sonogashira reaction, performed in a similar manner to that in section 4.2.5.4.In this manner, the pure product of **88** was obtained in an excellent yield of 87%. The synthesis of **89** was performed according to the exact same procedure, and the desired product was obtained in a good yield of 83 %.

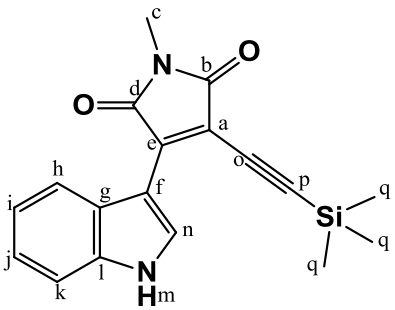

The ^{1}H NMR spectrum of the product (**88**) was compared to that in literature and corresponded well.[176] The presence of the TMSA moiety was confirmed by the presence of the trimethylsilyl protons H_q, which integrated for nine, and was located as a singlet at 0.23 ppm.

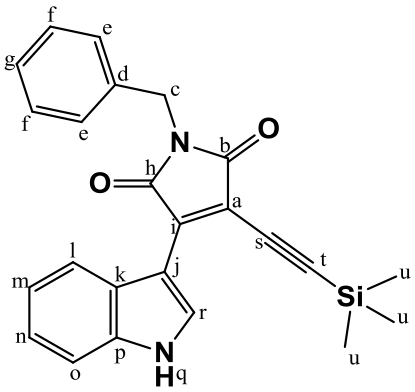

The ^{1}H NMR spectrum of the product (**89**) revealed the presence of the methyl silyl protons H_u at 0.09 ppm as a singlet, integrating for nine. The ^{13}C NMR of the product (**89**) also showed three additional carbon signals, which were not present in the starting compound carbon spectrum. The results of the mass spectral analysis of 399.1528 amu correlated with the expected mass of 399.1529 amu.

4.3.5 Synthesis of 3-(1-benzyl-1*H*-1,2,3-triazol-4-yl)-4-(1*H*-indol-3-yl)-1-methyl-1*H*-pyrrole-2,5-dione (90) and 1-benzyl-3-(1-benzyl-1*H*-1,2,3-triazol-4-yl)-4-(1*H*-indol-3-yl)-1*H*-pyrrole-2,5-dione (91)

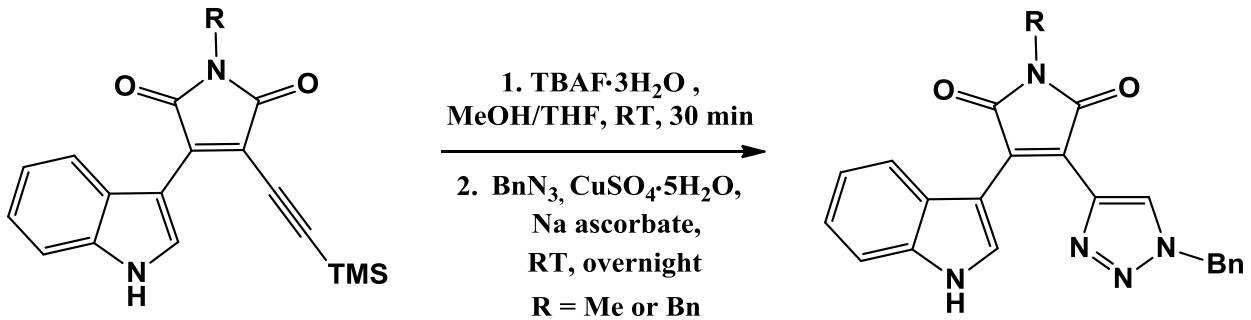

88 or 89 **90 or 91**

Scheme 76

To confirm the effectiveness of the click reaction on the indolylmaleimide system, it was initially carried out using the simple benzyl azide, which was available. The procedure followed by Gu *et al*., involved a silyl deprotection and click reaction in one pot, as shown in scheme 76. The deprotection step showed a clear transformation to one new product spot, and no additional degradation spots were observed on the baseline of the TLC. The click reaction TLC showed that there was incomplete consumption of the alkyne compound (**88** or **89**), and multiple new spots were observed.

Following a workup, the crude product was purified by column chromatography, which afforded the product **90** in a low yield of 19%. The synthesis of **91** was performed according to the exact same procedure, and the product **91** was obtained in a yield of 20 %.

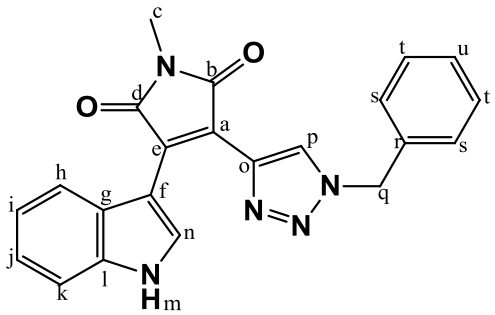

The ^{1}H NMR spectrum of the product (**90**) revealed the indicative triazole H_p signal at 8.20 ppm (or masked by the protons in the aromatic region). The benzyl group was also clearly present in the spectrum, as the number of multiplet signals in the aromatic region increased. The methylene H_q was located at 5.70 ppm and integrated for two. The remainder of the indole and *N*-Me-maleimide proton signals could all be accounted for. The ^{13}C NMR spectrum of the product (**90**) showed the carbonyl signals (C_d/C_b) at 170.9 ppm and 170.8 ppm. The symmetrical aromatic carbons C_s and C_t were found at 128.8 ppm and 127.7 ppm. Furthermore, C_q and C_c could be identified at 52.8 ppm and 24.1 ppm respectively. The rest of the carbon signals proved to be difficult to assign, but were present in the spectrum.

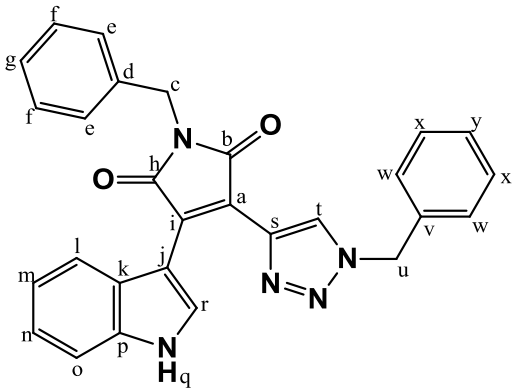

The ^{1}H NMR spectrum of the product (**91**) revealed the indicative triazole proton signal H_t and indole H_r at 8.58 ppm and 8.23 ppm. Both singlets integrated for one and their assignment could not be distinguished. The methylene protons (H_u and H_c) of the benzyl moieties were located at 5.69 ppm and 4.75 ppm. Both appeared as singlets, integrating for two. The broad –NH_q was identified at 11.97 ppm. The remainder of the aromatic signals could all be located as multiplets.

4.3.6 Synthesis of 3-ethynyl-4-(1*H*-indol-3-yl)-1-methyl-1*H*-pyrrole-2,5-dione (92) and 1-benzyl-3-ethynyl-4-(1*H*-indol-3-yl)-1*H*-pyrrole-2,5-dione (93)

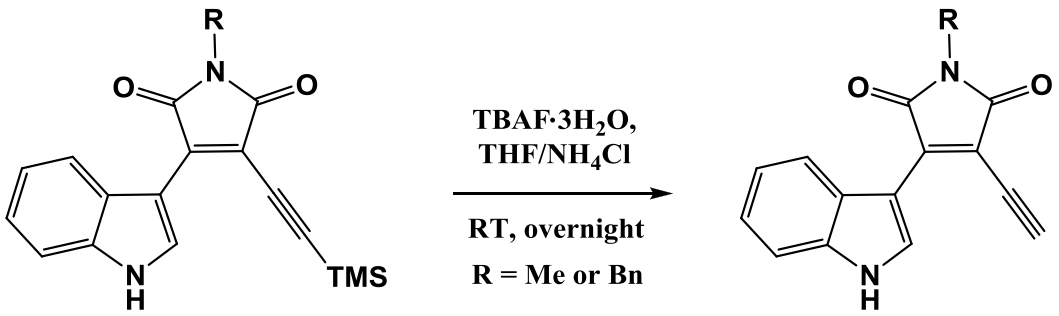

88 or 89 **92 or 93**

Scheme 77

Due to the fact that the one pot deprotection/click reaction made it difficult to distinguish the cause of the low yield, and the effectiveness of the actual click reaction, it was decided to perform these two reactions individually (scheme 77). The TMSA deprotection reaction was initially performed in a similar manner to the previous deprotection in THF/MeOH, using TBAF·$3H_2O$ instead of TBAF. The TLC revealed the formation of a new spot (product), as well as a spot on the baseline within 1 hour. Again, upon purification, the product (**92**) was obtained in a very poor yield of 14%. It was then decided to use a different solvent mixture (THF and saturated NH_4Cl), and stir the reaction overnight in the dark. The TLC showed that the reaction lacked complete consumption of the starting material. In addition to the product spot, a spot on the baseline was observed. This time column chromatography afforded the pure product (**92**) in an increased yield of 44%. The synthesis of **93** was performed according to the exact same procedure, and obtained in an improved yield of 59 %.

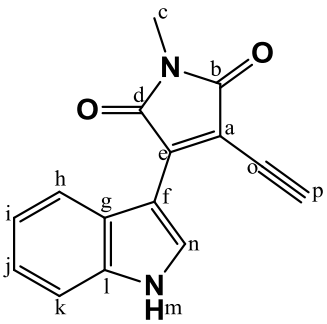

The ^{1}H NMR spectrum of the product (**92**) confirmed the TMSA deprotection. The trimethylsilyl signal was replaced by a singlet for H_p, integrating for one, and located at 5.10 ppm. The number of carbon signals in the ^{13}C NMR spectrum corresponded to the number of carbon atoms of the product. The terminal alkyne carbon peak could not be clearly identified in the ^{13}C NMR spectrum.

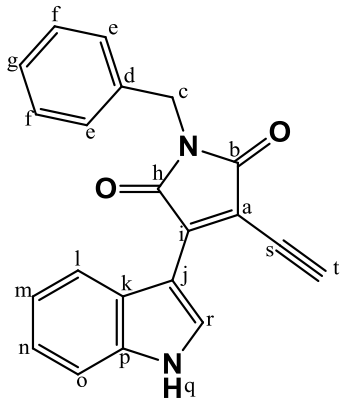

The ^{1}H NMR spectrum of the product (**93**) revealed all the proton signals of the starting material, together with the loss of the methyl silyl singlet. The new signal at 3.80 ppm was assigned to H_t, integrating for one.

4.3.7 Synthesis of *N*-(4-[4-{4-(1*H*-indol-3-yl)-1-methyl-2,5-dioxo-2,5-dihydro-1*H*-pyrrol-3-yl}-1*H*-1,2,3-triazol-1-yl]phenyl)acrylamide (94)

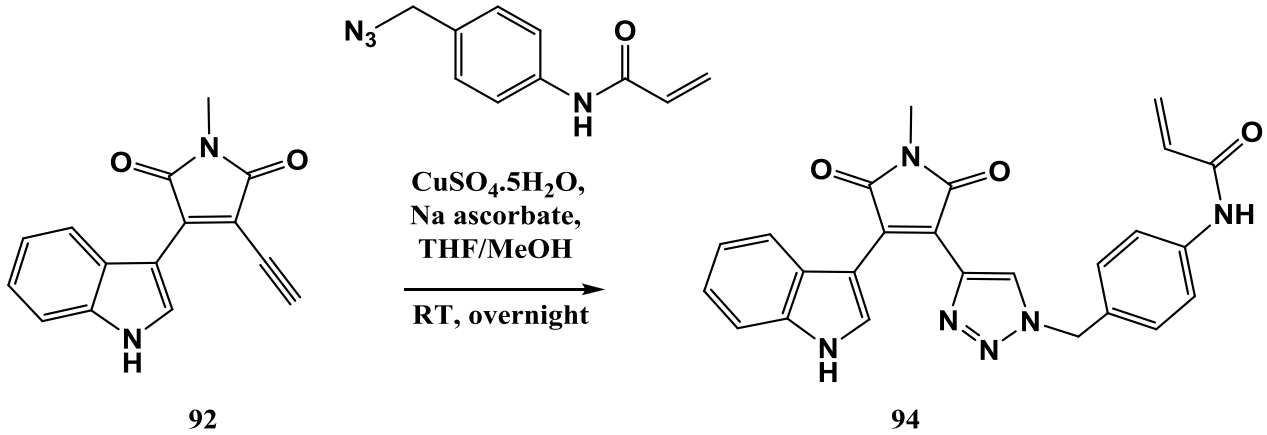

92 **94**

Scheme 78

A small scale click reaction was performed with the deprotected TMSA product and an azide acryloyl moiety previously synthesized in our group. The reaction was performed as a test reaction to verify whether the click reaction, incorporating a warhead such as the acryloyl group, would afford the desired product. The click reaction was carried out as shown in scheme 78. The product was purified (**94**) by column chromatography and obtained in a low yield of 26%. The same reaction was performed using the benzyl-protected indolylmaleimide starting material, but purification of the product by means of column chromatography proved to be extremely difficult.

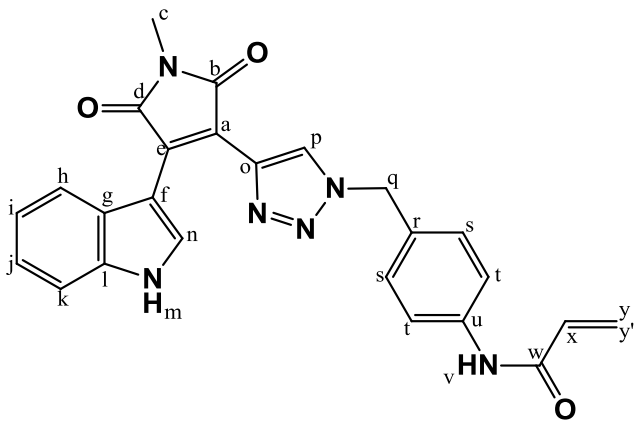

The ^{1}H NMR spectrum (figure 77) of the product (**94**) clearly showed the presence of two broad –NH signals at 11.92 ppm and 9.92 ppm. The indicative triazole H_p was located at 8.18 ppm as a singlet, and was a verification that the click reaction did work. Furthermore, the distinctive vinyl protons H_x/$H_{x'}$and H_w were located at 6.27 ppm ($H_{y'}$), 5.78 ppm (H_y), and 6.53-6.43 ppm (H_x), respectively. The methylene H_q was found at 5.68 ppm and integrated for two. The remainder of the aromatic proton signals and *N*-Me-maleimide could all be accounted for in the spectrum. The ^{13}C NMR spectrum of the product (**94**) revealed all the carbon signals corresponding to the number of carbon atoms of the product. Only a few of the signals could be assigned. The carbonyl carbon signals $C_{b/d}$ were located at 171.0 ppm and 170.8 ppm, while the acryloyl carbonyl C_w was found at 163.8 ppm. The methylene C_q was located upfield at 49.6 ppm, and the methyl C_c at 24.1 ppm.

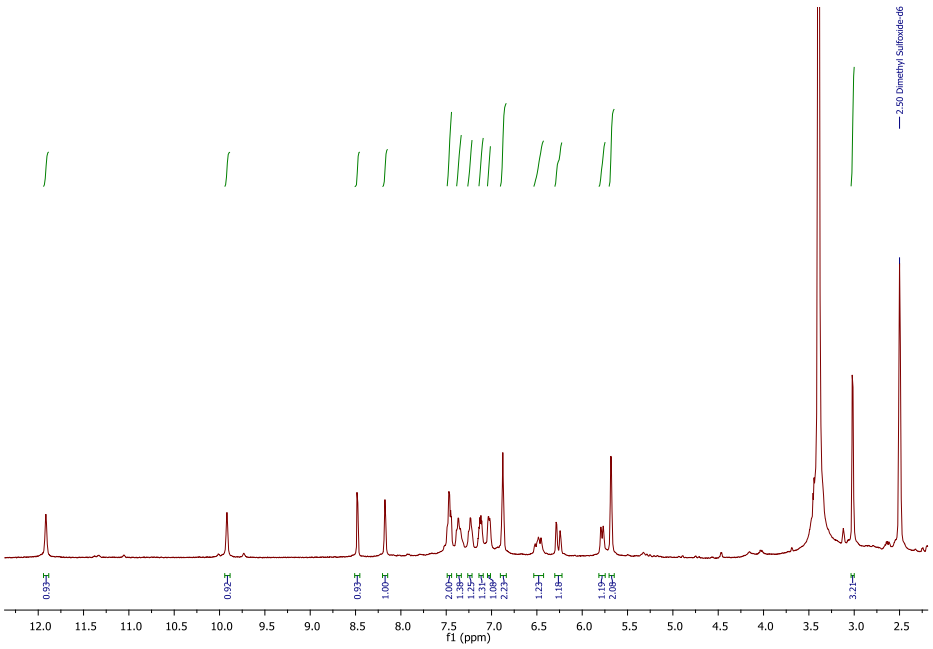

Figure 77
^{1}H NMR spectrum of compound **94**.

4.3.8 Attempted synthesis of 3-Azido-4-(1*H*-indol-3-yl)-1-methyl-1*H*-pyrrole-2,5-dione (95)

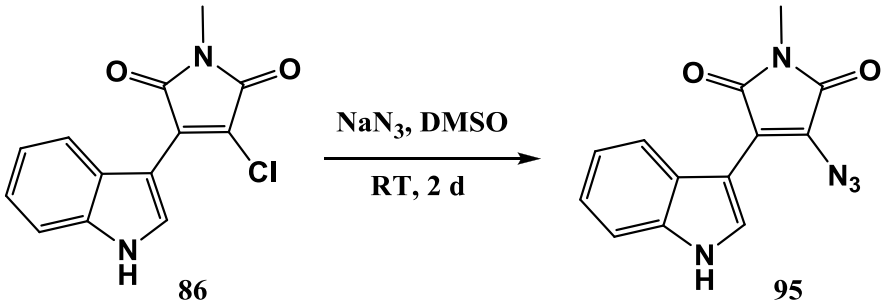

Scheme 79

In order to test whether the click reaction could be performed on the indole maleimide azide version, we attempted the synthesis of compound **95** as shown in scheme 79. The procedure utilized by Teller *et al*. was followed, with the only difference being that the researchers utilized a bromo halogen.[200] Unfortunately, the reaction was not successful. A different attempt was made in which the condensation reaction between the indole Grignard reagent and previously synthesized 3-azido-4-chloro-1-methyl-1*H*-pyrrole-2,5-dione (**76**) was carried out. To our dismay, IR revealed no azide stretch and we concluded that the desired product had not been formed. These two reactions were also attempted utilizing the benzyl-protected starting material, with no success.

4.3.9 Remarks about the indolylmaleimide click strategy

In summary, we could conclude that by employing the strategy in scheme 71, we were able to obtain the methyl indolylmaleimide click product (**94**). However, the product (**94**) shown in scheme 78, was not a viable compound to send for biochemical assay testing, since the presence of the *N*-Me group is undesirable, and prevents the formation of crucial hydrogen bonds in the kinase hinge region. Thus deprotection was required. The fact that the click products were synthesized in very low yields (19%-26%), made the imide deprotection reactions found in literature trivial. It must be noted that both the methyl and benzyl deprotection involves the generation of the anhydride, followed by treatment with ammonium acetate or urea.[176,198,201] In addition, another reason for not pursuing the imide deprotection reaction was that molecular modeling analysis revealed the structure of the compound was too large to fit into the targeted EGFR kinase domain. Furthermore, we anticipated that the reactive acryloyl moiety may not withstand the deprotection conditions.

The low yield of the click reaction was partly ascribed to the TMSA deprotection step. Although the deprotection reaction performed in section 4.3.6 was optimized, the yield remained unsatisfactory. No distinct trend could be observed between the methyl-and benzyl protecting group's effectiveness.

Improved yields were obtained for both the methyl-and benzyl indolylmaleimide, depending on the particular reaction carried out.

4.4 Towards bisamino maleimide derivatives

Awauh and Capretta recently published an article which involved the synthesis of bisaryl-maleimides, anilinoaryl-maleimides, and bisanilino-maleimides (Figure 78).[202] Their efforts focused towards the development of a procedure that allowed the necessary control to permit symmetrical or nonsymmetrical derivatives. In addition, their research investigated effective *N*-protecting groups, which would alter the electronics of the maleimide system and facilitate the second amination reaction. Another criterion for a suitable protecting group was that its deprotection had to proceed effortlessly.

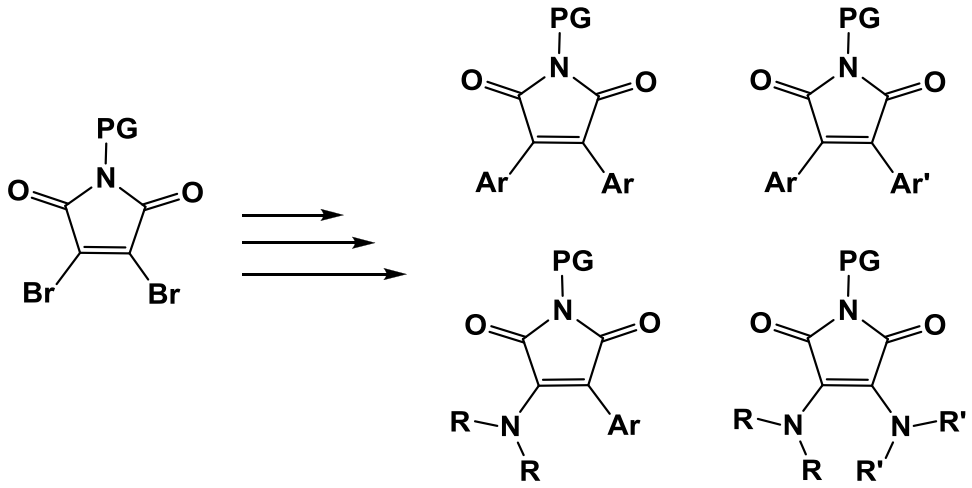

Figure 78
General representation of bisaryl-maleimides, anilinoaryl-maleimides, and bisanilino-maleimides, as proposed by Awauh and Capretta.[202]

An important observation was made in which the introduction of an amino group, by a conjugate addition/elimination reaction, altered the electronic nature on the neighboring site in such a manner that more forceful conditions (heating) were required to install the second amino group. This result was ascribed to the subtle interplay between the electron-donating ability of the first amine and the nucleophilicity of the second amine. The electrophilicity of the carbon bearing the Br is significantly reduced in the monoaminated system, since it becomes the end of an enamine system as well as an α,β-unsaturated amide.

For this reason, the second amino group introduced requires a more nucleophilic nature than the first (figure 79). These findings were very helpful in the understanding of our maleimide system and choice of protecting group.

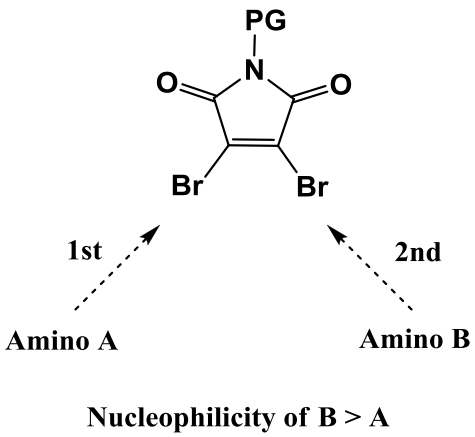

Figure 79
Crucial order of addition of the amino vectors.

Finally the synthesis towards bisamino maleimide irreversible kinase inhibitors was undertaken, by incorporating a 'warhead' (acryloyl/propargyl moiety) into the substituted maleimide system as shown in scheme 80. *p*-Nitroaniline was chosen as a suitable protecting group (PG), since its removal evolves a simple step, discussed in more detail in section 4.4.9. An important factor to note, was that the order of the amine addition was essential – the bisamination would only be successful if the less nucleophilic amine (aniline) was added first, followed by the more nucleophilic amine (*N*-Boc-piperazine). The following subsections involve the synthesis of the various compounds illustrated in scheme 80. Molecular modelling demonstrated the possibility of a potential hydrogen bond interaction forming between the dynamic target compound acryloyl carbonyl functionality and the amine of Cys797 residue within the EGFR kinase domain, which could promote the potential of a covalent bond forming between the β-carbon of the acryloyl group and the nucleophilic thiol of cysteine 797 (figure 80). All molecular modeling calculations, docking studies and image generations were carried out using Accelerys Discovery Studio software.

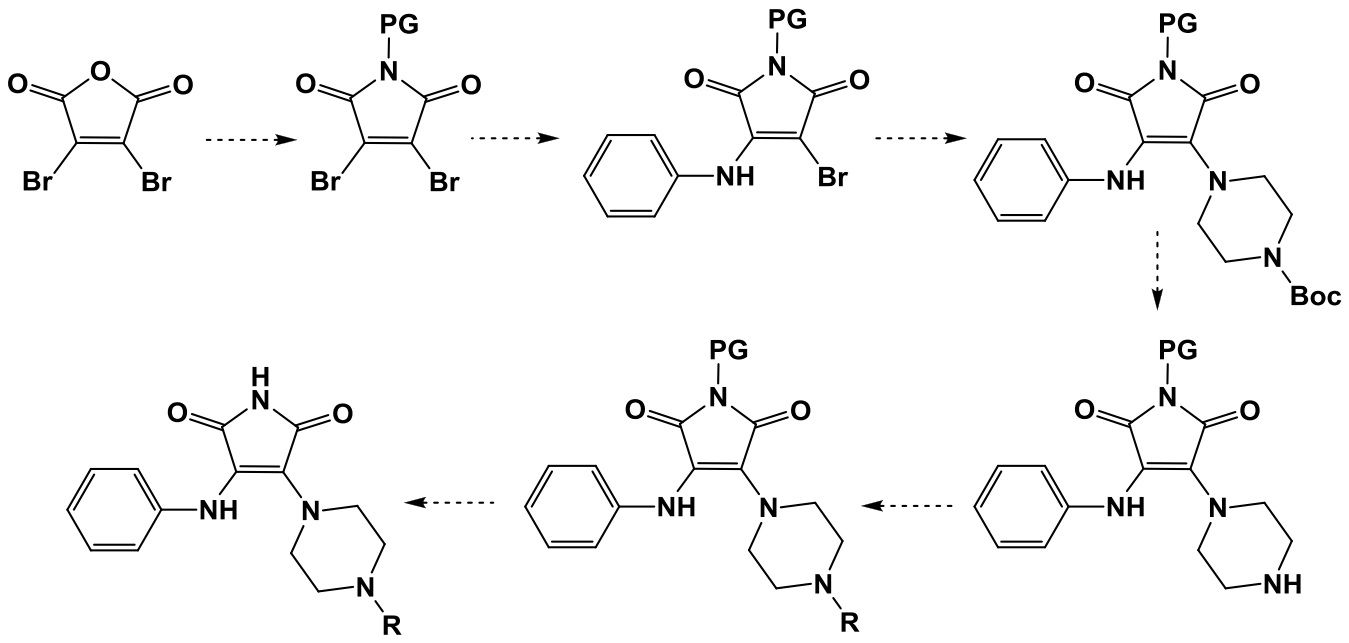

Scheme 80
Outline of strategy towards the nonsymmetrical bisamino maleimide derivatives, where R is a "warhead" (acryloyl/propargyl moiety).

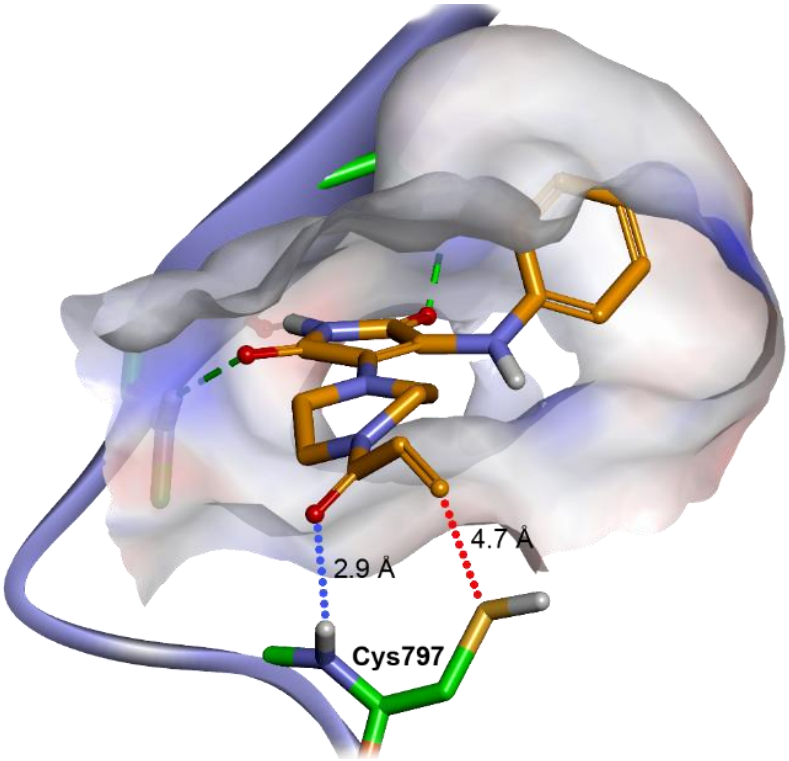

Figure 80
Molecular modelling illustrating the possible hydrogen bond formation between the acryloyl carbonyl functionality and the amine of the Cys797 residue within the EGFR domain - promoting the formation of a potential covalent bond.

4.4.2 Synthesis of 3,4-dibromo-1-(4-nitrophenyl)-1*H*-pyrrole-2,5-dione (96)

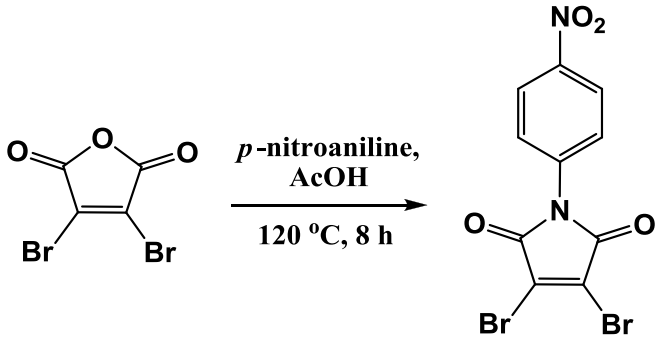

79 96

Scheme 81

The nitroaniline protected maleimide product (**96**) was successfully synthesized according to a literature procedure as shown in scheme 81.[203] The reaction was performed by heating a solution of previously synthesized dibromomaleic anhydride in AcOH, with *p*-nitroaniline at reflux. The product was purified by column chromatography, and obtained in a yield of 69%.

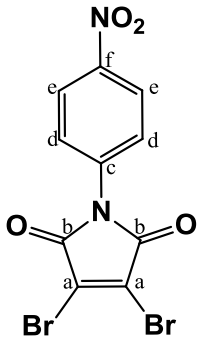

The ^{1}H NMR spectrum of the product (**96**) was compared to that in literature and corresponded well.[203] Two doublets were identified at 8.39 ppm and 7.69 ppm, and were assigned to the symmetrical H_e and H_d protons, respectively. Both of these signals integrated for two. Six carbon signals were identified in the ^{13}C NMR spectrum of the product, corresponding to the number of chemically equivalent carbon atoms in the structure.

4.4.3 Synthesis of 3-bromo-1-(4-nitrophenyl)-4-(phenylamino)-1*H*-pyrrolo-2,5-dione (97)

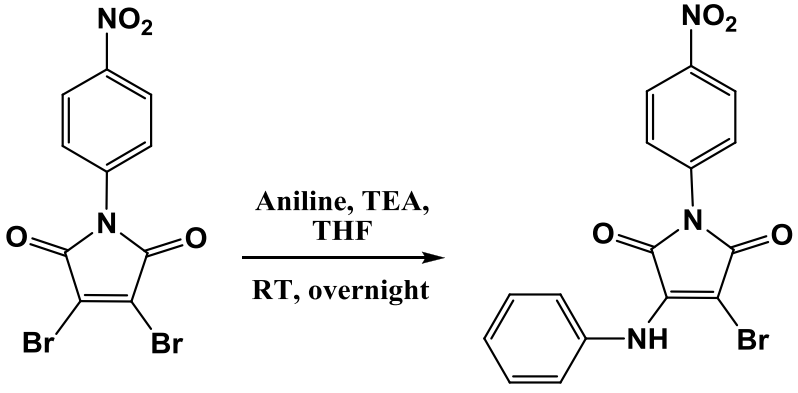

96 97

Scheme 82

The monoaminated maleimide product (**97**) was synthesized by a conjugate addition/elimination reaction as shown in scheme 82. The reaction involved the addition of a mixture of aniline and TEA in dry THF, to a solution of compound **96** in THF, at 0 °C. The reaction mixture was then left to stir at room temperature, overnight. Upon completion, a workup was carried out and the product was purified by column chromatography. The pure compound (**97**) was afforded in a very good yield of 79%.

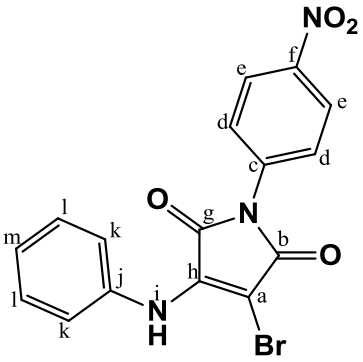

The ^{1}H NMR spectrum of the product (**97**) showed the presence of the additional proton signals of the aniline group. The broad –NH_i signal was located at 10.11 ppm, while the aniline aromatic signals (H_l, H_k, H_m) were found in the range 7.44-7.36 ppm and 7.29-7.20 ppm, altogether integrating for five.The remainder of the proton signals (H_e and H_d) were also accounted for. The number of carbon signals in the ^{13}C NMR spectrum of the product (**97**) corresponded with the number of chemically equivalent carbon atoms in the structure. The results of the mass spectral analysis of 387.9938 amu correlated with the expected mass of 387.9933 amu.

4.4.4 Synthesis of *N*-Boc-piperazine (99)

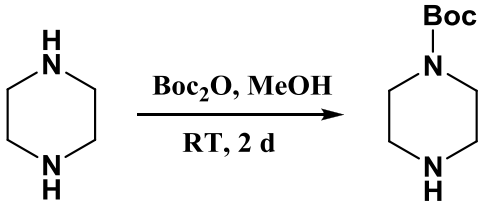

98 **99**

Scheme 83

In order to incorporate the secondary aliphatic system (**98**), onto the monoanilated maleimide product, a Boc-protection reaction was performed. The procedure utilized by Jo *et al*. was followed and the reaction proceeded smoothly by treating a concentrated solution of piperazine (**98**) in MeOH, with a diluted Boc_2O/MeOH solution.[203] The Boc_2O solution was added drop-wise to the piperizine (**98**) solution at 0 °C, and stirred at room temperature for 2 days. An acid/base workup was then carried out to separate the disubstituted product from the desired product (**99**). No further purification was required. The pure product (**99**) was afforded in a yield of 59%.

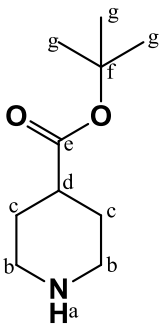

The ^{1}H NMR spectrum of the product (**99**) was compared to that reported in literature and corresponded well.[203] The broad –NH_a was located at 2.22 ppm, as a singlet. The chemically equivalent protons of H_c and H_d were identified as multiplets at 3.45-3.28 ppm and 2.86-2.72 ppm, respectively. Both signals integrated for four each. The H_g was found at 1.43 ppm as a singlet and integrated for nine.

4.4.5 Synthesis of *tert*-butyl 4-{1-(4-nitrophenyl)-2,5-dioxo-4-(phenylamino)-2,5-dihydro-1*H*-pyrrol-3-yl}piperazine-1-carboxylate (100)

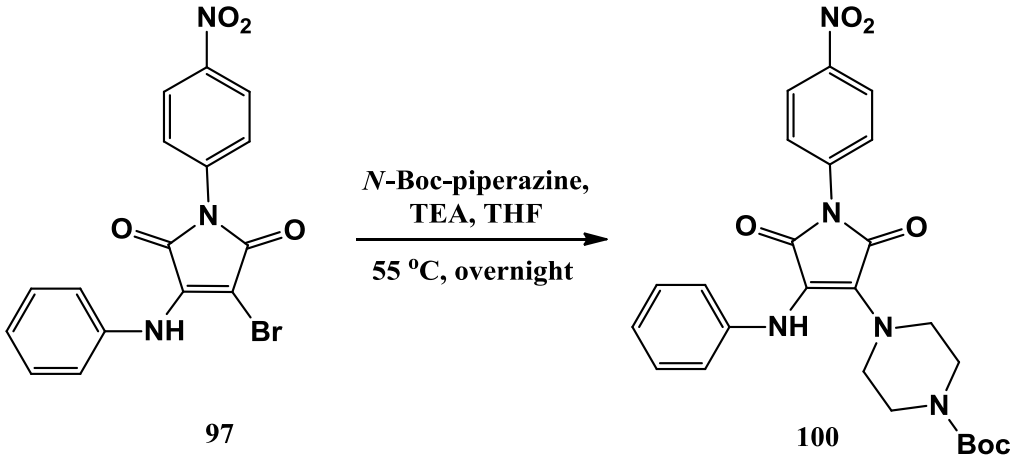

Scheme 84

The next reaction involved the introduction of the Boc-protected piperazine (**99**) to the monoaminated maleimide (**97**) as shown in scheme 84. The second amination reaction was performed in the same manner as that in subsection 4.4.3. However, the second conjugate addition/elimination reaction required an increased reaction temperature of 55 °C. The reaction did not proceed to completion, and some of the starting material (**97**) remained unreacted. Following a workup, the product was purified by column chromatography. The pure product (**100**) was obtained in a yield of 80%, when taking the recovered starting material (18%) into account.

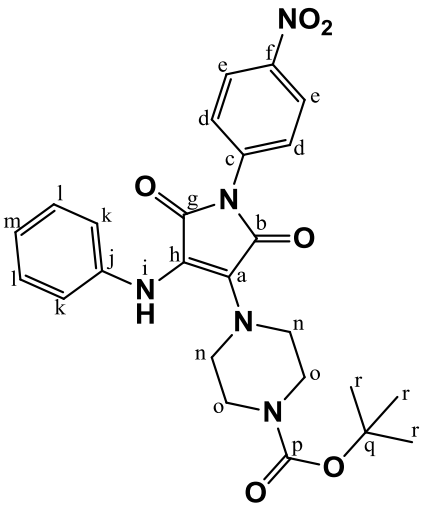

The ^{1}H NMR spectrum of the product (**100**) showed all the proton signals of the starting material. In addition, all the proton signals of the *N*-Boc piperazine group were identified, proving that the second amination reaction had worked. The two sets of chemically equivalent H_n and H_o protons were located in the range 3.30-3.25 ppm and 3.18-3.10 ppm. Both signals appeared as multiplets and integrated for four each. The Boc singlet H_r was found at 1.36 ppm and integrated for nine. The ^{13}C NMR spectrum of the product (**100**) revealed five new carbon signals. The carbonyl of the Boc group (C_p) was located at 153.7 ppm, and the C_q an C_r signals were found at 79.1 ppm and 28.0 ppm, respectively. C_n and C_o were both identified at 47.1 ppm. The results of the mass spectral analysis of 494.2043 amu correlated with the expected mass of 494.2043 amu.

4.4.6 Synthesis of 1-(4-nitrophenyl)-3-(phenylamino)-4-(piperazin-1-yl)-1*H*-pyrrole-2,5-dione (101)

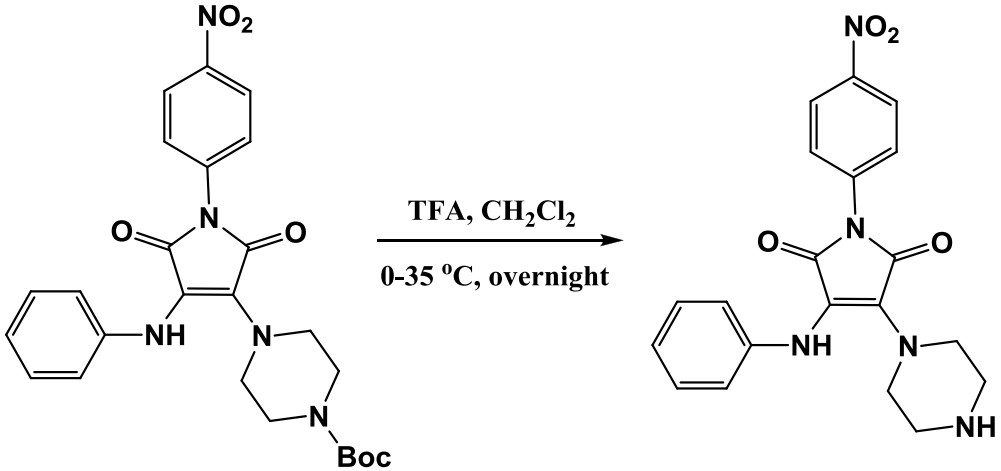

100 **101**

Scheme 85

The Boc-deprotection was carried out smoothly as shown in scheme 85. The reaction was performed by treating a solution of compound **100** in CH_2Cl_2 with diluted TFA (in CH_2Cl_2). Following the TFA addition at 0 °C, the reaction temperature was increased to 35 °C and stirred overnight. The reaction mixture was then basified and a workup was carried out. Column chromatography then afforded the pure product (**101**) in an excellent yield of 98%.

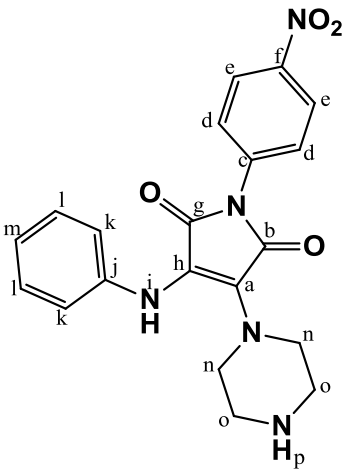

The ^{1}H NMR spectrum of the product (**101**) showed the absence of the Boc proton signal, proving that the deprotection was a success. The -NH_p signal and chemically equivalent H_n protons were identified as a multiplet in the range 3.62-3.18 ppm, integrating for five. The H_o protons were also shown as a multiplet at 2.69-2.57 ppm and integrated for four. The rest of the proton signals could all be identified. The ^{13}C NMR spectrum of the product (**101**) was similar to the starting material, but with the absence of the three carbon signals belonging to the Boc group. The results of the mass spectral analysis of 394.1510 amu correlated with the expected mass of 394.1515 amu.

4.4.7 Synthesis of 3-(4-acryloylpiperazin-1-yl)-1-(4-nitrophenyl)-4-(phenylamino)-1*H*-pyrrole-2,5-dione (102)

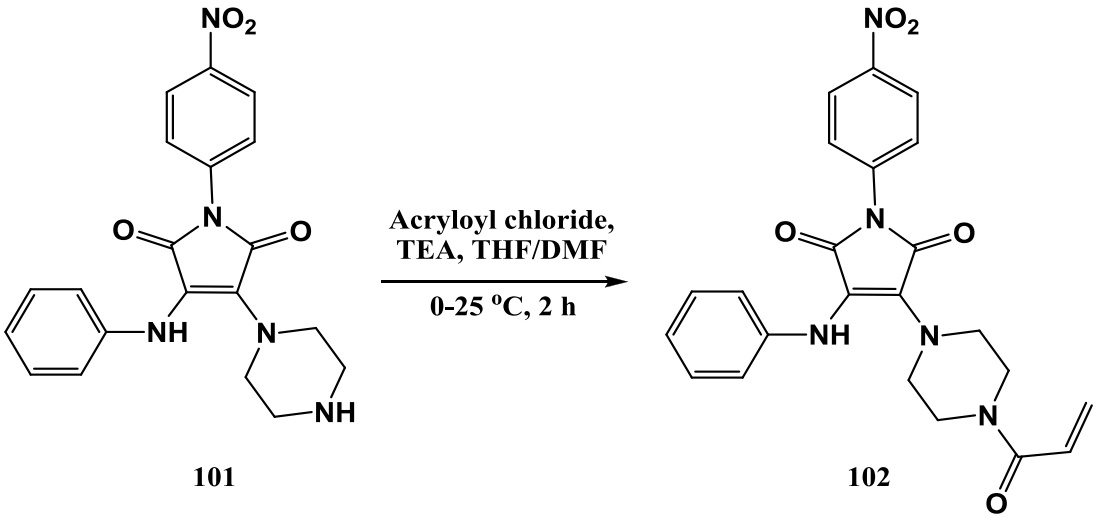

101 **102**

Scheme 86

The acryloyl 'warhead' could then be added to the bisamino maleimide scaffold as shown in scheme 86. The reaction proceeded smoothly within 2 hours at room temperature. The procedure involved the drop-wise addition of diluted acryloyl chloride (in THF), to a mixture of compound **101** and TEA dissolved in dry THF/DMF, at 0 °C. Following a workup, the crude product was purified by column chromatography to afford the pure compound (**102**) in a yield of 61%.

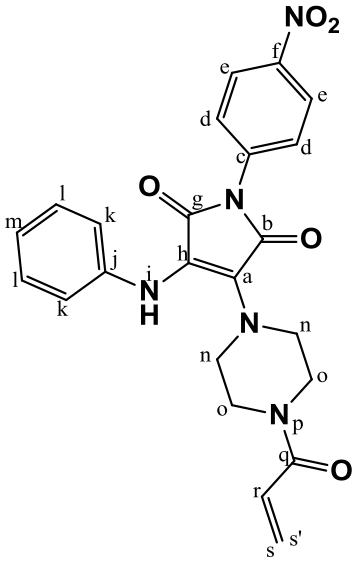

The ^{1}H NMR spectrum of the product (**102**) showed the presence of the indicative protons of the acryloyl moiety, and the absence of the –NH_p signal. The vinyl protons H_s and $H_{s'}$ were identified at 5.68 ppm and 6.26 ppm, respectively, both integrating for one. Their coupling pattern corresponded to the proton H_r, which was located at 6.47 ppm as a doublet of doublets and also integrated for one. The ^{13}C NMR spectrum of the product (**102**) revealed three additional carbon signals as expected. The carbonyl signal (C_q) was found at 165.5 ppm, while C_r and $C_{s/s'}$ were located between the aromatic carbon signals. The results of the mass spectral analysis of 448.1612 amu correlated with the expected mass of 448,1621amu

4.4.8 Synthesis of 1-(4-nitrophenyl)-3-(phenylamino)-4-(4-(prop-2-yn-1-yl)piperazin-1-yl)-1*H*-pyrrole-2,5-dione (103)

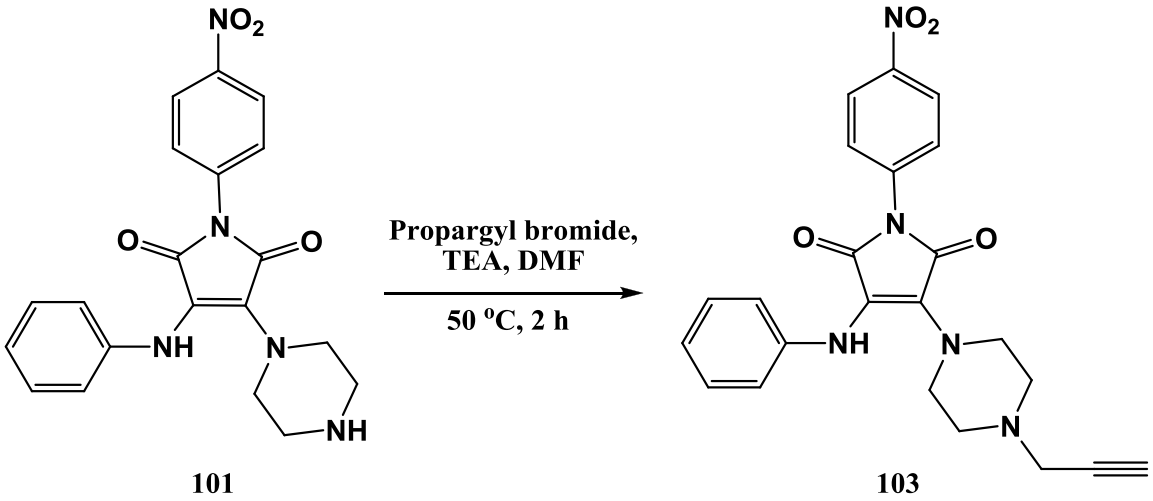

101 **103**

Scheme 87

The propargyl 'warhead' could also be incorporated into the bisamino maleimide scaffold as shown in scheme 87. The reaction was performed by treating a solution of compound **101** in DMF, with propargyl bromide. The reaction was carried out smoothly within 2 hours at 50 °C. A workup was then performed, followed by purification by column chromatography. The pure product (**103**) was obtained in a good yield of 71%.

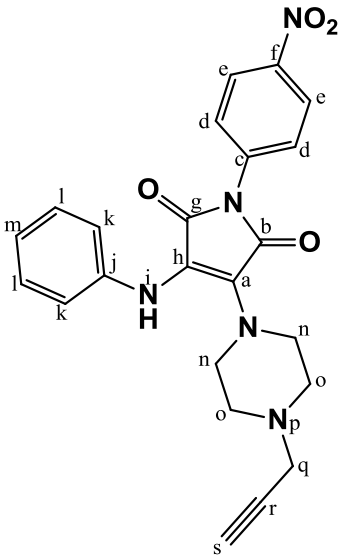

The ^{1}H NMR spectrum of the product (**103**) showed the absence of the –NH_p signal, previously present in the starting material. This signal was replaced by two additional proton signals – H_q and H_s. H_q was located as a doublet at 3.24 ppm and integrated for two, while H_s was identified at 2.25 ppm as a multiplet, integrating for one. Furthermore, the ^{13}C NMR spectrum of the product (**103**) revealed three additional carbon signals. The methylene C_q was found most upfield at 47.0 ppm. C_r and C_s were located at 78.4 ppm and 73.6 ppm, respectively. The results of the mass spectral analysis of 432.1666 amu correlated with the expected mass of 432.1667 amu.

4.4.9 Synthesis of 3-(4-acryloylpiperazin-1-yl)-4-(phenylamino)-1*H*-pyrrole-2,5-dione (104) and 3-(phenylamino)-4-(4-(prop-2-yn-1-yl)piperazin-1-yl)-1*H*-pyrrole-2,5-dione (105)

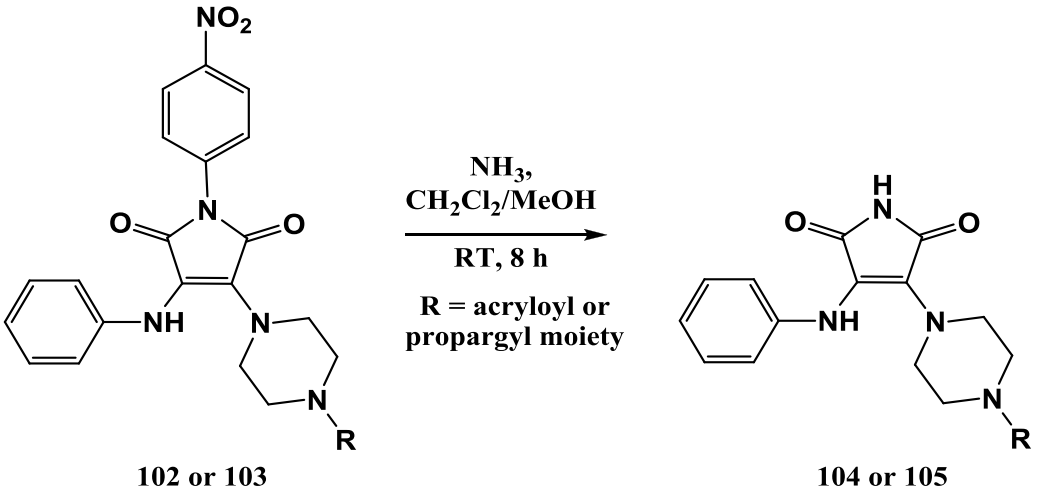

102 or 103 **104 or 105**

Scheme 88

The deprotection of the nitroaniline-protected diamino maleimide derivatives was easily carried out by an aminolysis reaction as shown in scheme 88. The procedure involved the treatment with methanolic ammonia at room temperature, as employed by Awuah and co-workers.[202] The reaction was carried out by dissolving compound **102** (or **103**) in CH_2Cl_2/MeOH, and bubbling NH_3 gas through the reaction mixture. A crucial initial step in the procedure was the evacuation under high vacuum and filling the reaction flask with Ar. Without this precaution the reaction did not proceed. Once the solution was saturated with NH_3, the reaction mixture was stirred at room temperature for 8 hours. The product was purified (**104**) by column chromatography and afforded in a very good yield of 86%.

The synthesis of (**105**) was performed in the exact same manner, and obtained the pure product (**105**) in an excellent yield of 91%.

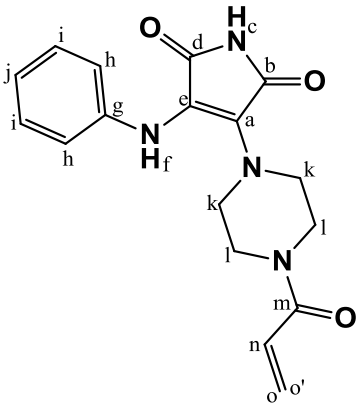

The ^{1}H NMR spectrum (figure 81) of the product (**104**) showed the presence of the new -NH_c signal at 8.16 ppm. H_k and H_l appeared as a multiplet at 3.53 – 3.21 ppm, integrating for eight. Furthermore, the aromatic signals of the nitroaniline group were lost – confirming the success of the deprotection. The ^{13}C NMR spectrum of the product (**104**) also revealed the absence of the carbon signals belonging to the protecting group. The remainder of the proton and carbon signals could all be identified. The results of the mass spectral analysis of 327.1447 amu correlated with the expected mass of 327.1457 amu. The IR spectrum showed two –NH stretches at 3317 cm^{-1} and 3141 cm^{-1}.

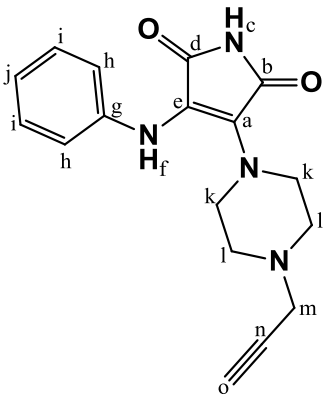

Similarly, the ^{1}H NMR (figure 82) and ^{13}C NMR spectra of the product (**105**) also revealed the absence of the nitroaniline protecting group proton and carbon signals. The new –NH_c signals was identified at 7.79 ppm in the ^{1}H NMR. The remainder of the proton and carbon signals could all be located in the spectra. The results of the mass spectral analysis of 311.1497 amu correlated with the expected mass of 311.1508 amu. The IR spectrum showed two –NH stretches at 3277 cm^{-1} and 2920 cm^{-1}.

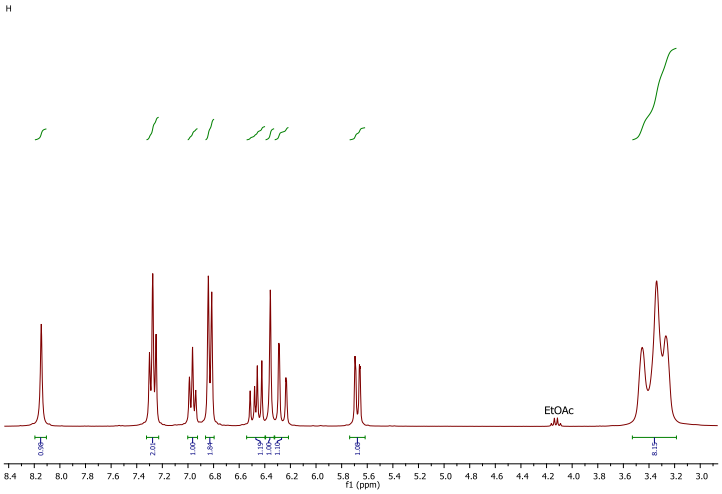

Figure 81
^{1}H NMR spectrum of compound **104**.

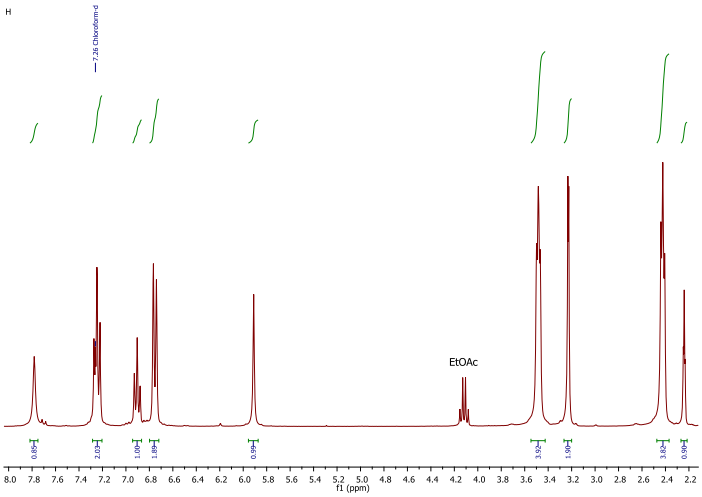

Figure 82
^{1}H NMR spectrum of compound **105**.

4.4.10 Remarks about the bisamino maleimide strategy

The strategy pertaining to the synthesis of the bisamino maleimide derivatives was carried out smoothly, generating the two final target compounds. Employing this design strategy enabled the synthesis of derivatives resembling the "open" form of the natural product staurosporine. In addition, by incorporating warhead moieties, such as acryloyl and propargyl, the compounds can potentially demonstrate irreversible kinase inhibitory activity. Overall, the structures illustrated in scheme 80, were obtained in moderate to high yields. Utilizing *p*-nitroaniline as protecting group proved to be a suitable choice, and could effectively be applied to other strategies involving maleimide scaffolds.

As part of future work, these satisfying results inspire the synthesis of a broad scope of possible bisamino maleimide kinase inhibitor derivatives.

CHAPTER 5 - BIOLOGICAL EVALUATION OF THE TARGET COMPOUNDS AND CONCLUSION

5.1 Synthesized target compounds

In total, eight target compounds were synthesized and evaluated for inhibitory activity against EGFR (figure 83). Of these compounds, six were generated in the first part of this project, and were based on the pyrrolocarbazole scaffold. The two remaining compounds, **104** and **105**, resembled the "open" form of staurosporine, and were synthesized in the second part of the project.

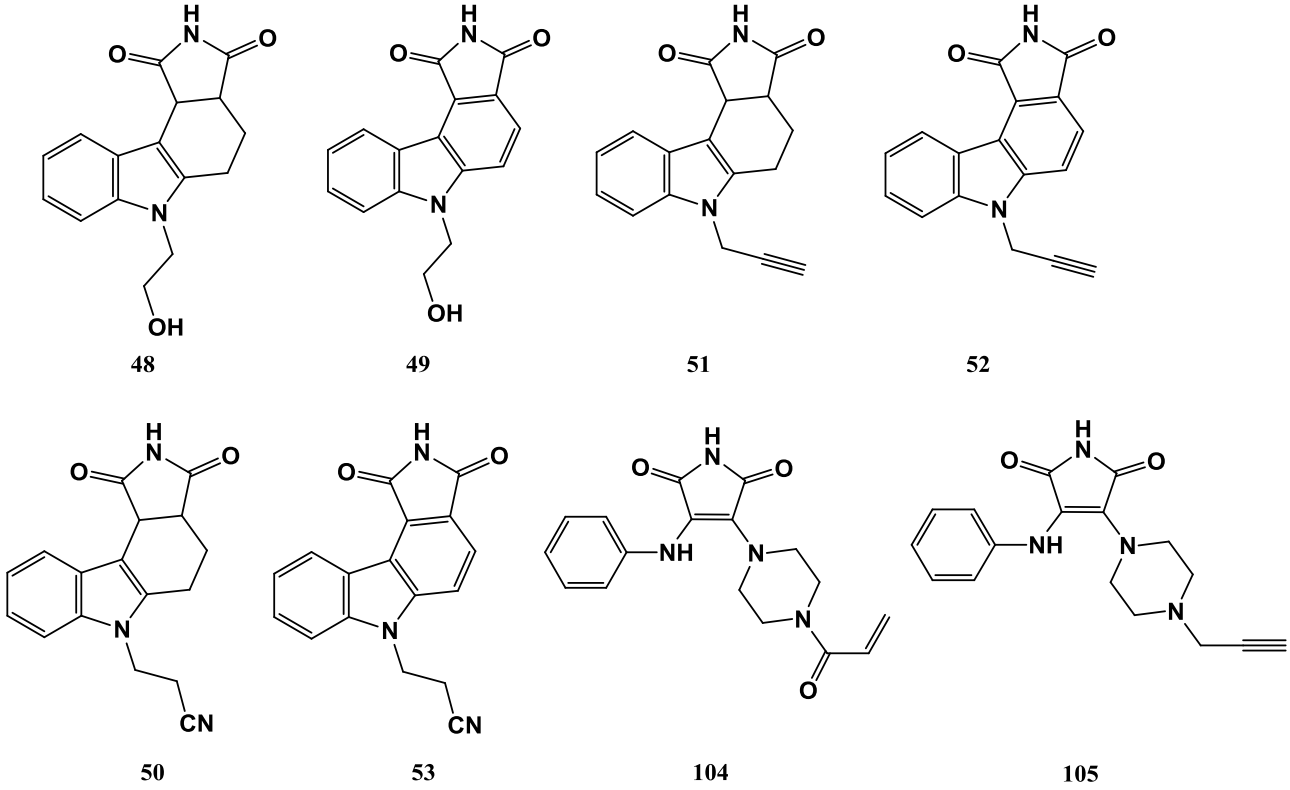

Figure 83

The eight target compounds sent for biochemical evaluation for activity against EGFR.

5.2 EGFR mutations

As previously mentioned, EGFR has a multidimensional role in the progression of cancer, and has become an attractive, well-established target for anti-cancer therapy – particularly for the treatment of NSCLC.[204] Currently, three EGFR inhibitors (Erlotinib, Gefitinib and Lapatinib) have received FDA approval. Furthermore, several second- and third-generation TKIs (afatanib, neratinib and WZ4002) are in preclinical or late stage clinical development (figure 84).[205] Despite the clear clinical benefits of these inhibitors, EGFR TKI treatment is not curative in patients.[206] The decreased efficacy of these therapeutic agents is primarily ascribed to the development of acquired resistance (AR). Several mechanisms of AR to EGFR TKIs have been identified, but in many cases the underlying mechanism remains unexplained.[207]

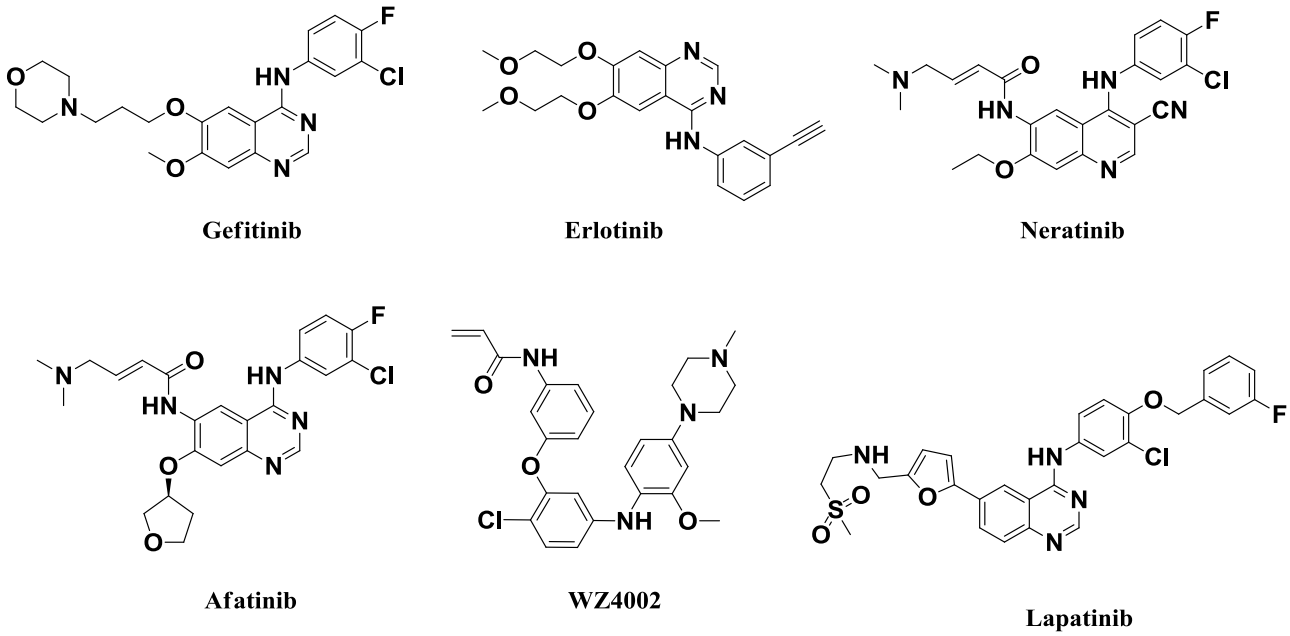

Figure 84

EGFR inhibitors that are currently in clinical development or that have received FDA approval.

One of the most important factors to cause drug resistance and sensitivity to the inhibitors is the presence of somatic mutations in the EGRF domain. The functional core of the EGFR protein (TK domain) stretches from exon 18 to exon 24, and approximately 90% of its somatic mutations are found in exon 18-21.[208] In order to develop new effective anti-cancer agents to target drug-resistant mutants, it is essential to understand the mechanism and drug response to the mutations – a pursuit of many researchers. In the work of Ai *et al*., the complete profile of several representative EGFR inhibitors in response to various EGFR mutations was investigated.[206]

In addition, several potential mutations that might cause drug resistance in EGFR were identified. During this study, it was shown that most observed mutations in the EGFR domain were far away from the ATP-binding site, and had limited effect on inhibitor binding. However, the few mutations located around the ATP-binding site (figure 85), were shown to substantially impact the inhibitor binding, by either directly preventing the reversible interaction to EGFR, or by indirectly affecting the inhibitor binding through altering the chemical environment and changing the conformation of the kinase domain.[206]

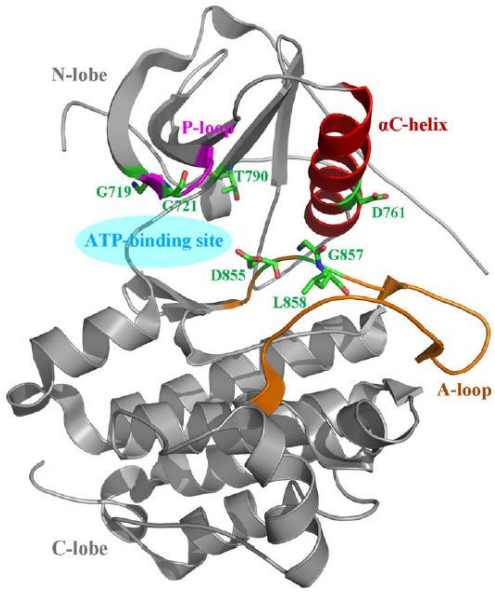

Figure 85

EGFR architecture illustrating important mutations located around ATP-binding site. Image reproduced from reference.[206]

The most common type of AR mutation – notorious for its AR to gefitinib - is known as the "gatekeeper mutation".[204] This threonine-to-methionine mutation in codon 790 (T790M) has been identified in approximately 50-60% of cases with AR to EGFR TKI treatment, as a second-site mutation in the EGFR domain that coexist with the EGFR activating mutation.[207] The drug resistance of the T790M mutation is ascribed to a co-effect of increasing ATP affinity and decreasing inhibitor affinity, rather than sterically blocking the inhibitor.[209]

Another mutation that can directly reshape the geometric and physiochemical properties of the binding site is the inhibitor-sensitizing EGFR mutation Leu858Arg (L858R). In the specific case of gefitinib, the inhibitor binds 20-fold more *tightly* to the EGFR L858R mutant than to the wild-type EGFR.[206] For the purpose of this project, our synthesized target compounds were screened against the EGFR wild-type (WT) as well as the two medicinally relevant mutant deviants – L858R and the double mutant L858R_T790M.

Interestingly, staurosporine has been shown to exhibit selective inhibitory activity on the T790M and L858R_T790M mutants.[206] The IC_{50} values of staurosporine against the EGFR WT, T790M and L858R_T790M mutants were measured to be 937, 12 and 3 nM, respectively. Staurosporine inhibitory efficacy was therefore 80-fold higher on the T790M mutant over the WT. A possible explanation for this result was obtained from investigating the complex structure model of staurosporine with the T790M mutant. It was found that the mutated M790 residue could form hydrophobic interactions and S···π interactions with the aromatic ring and amide moiety of staurosporine, as shown in figure 86. These interactions contributed stabilization energy to the complex system and eliminated some unfavourable polar interactions associated with the WT system.[206] Although staurosporine was found to have a low sensitivity to the L858R mutant, the dual L858R_T790M mutation, which is very common in AR of NSCLC, showed a significantly enhanced selectivity. Comparing the staurosporine IC_{50} value of 3 nM for the L858R_T790M double mutant, to that of gefitinib and elotinib (which is more than 5 μM), demonstrates the potency of this natural product.[210] Staurosporine could therefore be considered as a promising lead compound to develop new inhibitors that could combat AR, particularly associated with the T790M mutation.

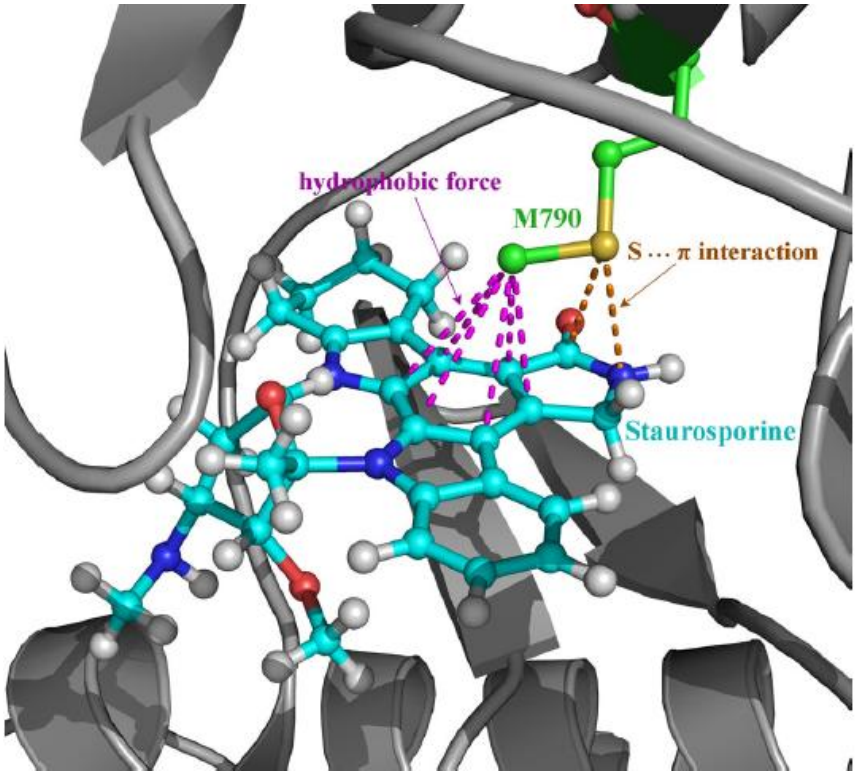

Figure 86

Hydrophobic force and S···π interactions formed between staurosporine and M790 residue in T790M mutant EGFR. Image reproduced from reference.[206]

5.3 Biochemical screening methodology

Numerous detection methodologies have been applied to evaluate and measure kinase activity.[211] Cisbio developed a simple and robust assay platform, namely HTRF, to screen compounds for their tyrosine and serine/threonine kinase inhibitory activity.[212] Homogeneous time-resolved fluorescence (HTFR) is frequently used in drug discovery, and eliminates some of the difficulties experienced by other conventional screening assay methodologies.[211,213] The technique combines standard fluorescence resonance energy transfer (FRET) technology with time-resolved measurements of fluorescence. All HTRF kinase assays follow the same general format, and are based on the method that uses FRET between two fluorophores – a donor fluorophore (Europium cryptate) and an acceptor fluorophore (XL665). In this manner, the interactions between biomolecules can be evaluated by coupling each partner with a fluorescent label and detecting the level of energy transferred.[212-213]

HTRF ® KinEASE^{TM}, is an extension of the HTRF technology (developed in partnership with Upstate), that utilizes antibody-based detection to assess kinase activity.[212] The kinase assay consists of two main steps – kinase reaction and detection of the phosphorylated product by HTRF reagents. The method involves a unique biotinylated peptide substrate containing a single phosphorylation site. Upon phosphorylation, the substrate is recognized by a monoclonal antibody labeled with the donor fluorophore (Eu^{3+}cryptate). The addition of streptavidin labeled with the acceptor fluorophore (XL665), completes the detection step. These substrate and detection reagents have been validated on many kinases, and the success of the HTRF® KinEASE^{TM} homogenous assay has been demonstrated for protein kinase selectivity studies as well as high-throughput screening campaigns.[212] A more detailed description of the exact procedure used, for the evaluation of the compounds synthesized in this project, follows.

Following the synthesis and purification of the eight target compounds, they were all sent for biochemical assay testing. IC_{50} values of our compounds were determined by utilizing the HTRF KinEASE-TK assay. The particular biochemical screening of our compounds involved the use of the EGFR wild type, and mutants (L858R and L858R_T790M). The procedure started with a control experiment in which a biotinylated poly Glu-Tyr substrate peptide was phosphorylated by EGFR. Completion of the reaction was followed by the introduction of the antiphosphotyrosine antibody labeled with Eu^{3+} cryptate and streptavidin XL665. The phosphorylation of the peptide substrate could then be quantified by measuring the FRET between the donor and acceptor fluorophores (Eu^{3+} and XL665).

Following the control experiment, the ATP concentrations were set at their respective K_m values (30 μM for the EGFR-WT, 60 μM for EGFR-L858R, and 30 μM for EGFR-L858R_T790M) and 50 nM of substrate were used for both wild type and mutant EGFR. Our synthesized inhibitors were the pre-

incubated with the specific kinase and peptide for 2 hours. After this period, the reaction was initiated by the addition of ATP. The next part of the procedure involved the detection step. This was conducted by a Tecan Safire plate reader, which measured the fluorescence of the samples at 620 nm (Eu-labeled antibody) and 665 nm (XL665 labeled streptavidin) 60 µs after excitation at 317 nm. An illustration of this HTRF® KinEASE™ assay procedure is shown in figure 86. The IC_{50} values were then determined by plotting the quotient of both readings for reactions made with eight different inhibitor concentrations, carried out in triplicate, against inhibitor concentration – fitted to a Hill-4 parameter equation. An example of a graph to determine the IC_{50} value is shown in figure 87. Furthermore, the EGFR inhibitors gefitinib and WZ4002 were used as control groups for the kinase inhibitory activity tests and IC_{50} value determination.

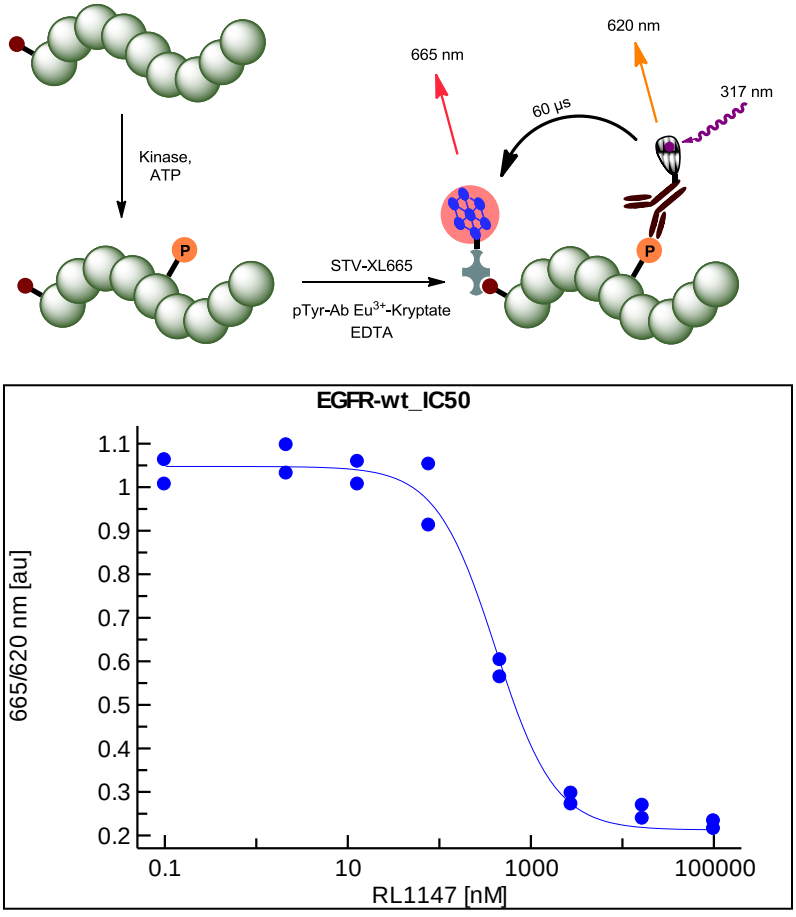

Figure 87

The HTRF® KinEASE™ assay technique, utilizing the FRET principle in order to determine the IC_{50} values. Figure used with permission.[214]

5.4 Evaluation of results and discussion

The IC_{50} values of the eight target compounds, obtained from the biochemical assays, are tabulated below (table 2). Unfortunately, the results did not show inhibitory activity for seven of these compounds at 100 µM, and no noticeable trend with regards to structure-activity relationship studies could be identified. For this reason, any conclusions drawn in relation to the inhibitor activity would be speculative. Overall, the only compound which exhibited some inhibitory activity was **49**,which demonstrated an IC_{50} value of 6.09 µM and 4.35 µM against L858R and L858R_T790M, respectively. Comparing the structure of **49** to **48**, we could deduce that the aromatized, planar pyrrolocarbazole core is necessary for inhibitor activity. Further evidence for this reasoning can be drawn from the fact that the EGFR inhibitors, illustrated in figure 83, all display a high degree of aromaticity (also see section 1.6, figure 25). In addition, when evaluating the results of **49** and compound **29**, which served as an inspiration for the design of the pyrrolocarbazole compounds, it is clear that the length of the carbon linker to the warhead significantly influences the activity of the compound. It appears as if a three carbon linker is much more beneficial than a two carbon linker (figure 88). Compounds **53**, **104**, and **105** did display some degree of inhibition against L858R, but at concentrations higher than 100 µM. As a result of the poor activity demonstrated against the EGFR WT and mutant forms, as well as time constraints, we decided against pursuing follow-up studies and optimization of these compounds.

Table 2
IC_{50} values (µM) of the eight target compounds.

	IC_{50} EGFR [µM] (HTRF)		
	WT	**L858R**	**L858R_T790M**
Gefitinib	<0.001	<0.001	0.055 ± 0.048
WZ4002	0.015 ± 0.007	0.001	0.001
48	n.i.	n.i	n.i
49	>10	6.09 ± 2.13	4.35 ± 1.08
50	n.i.	n.i.	n.i.
51	n.i.	n.i.	n.i.
52	n.i.	n.i.	n.i.
53	n.i.	>100	n.i.
104	n.i.	>100	n.i.
105	n.i.	>100	n.i.

n.i. no inhibition at 100 µM.

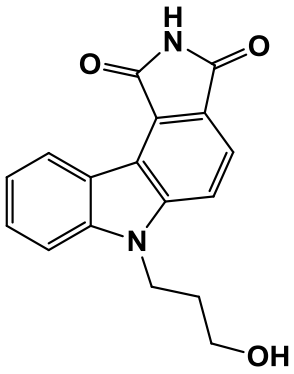

29

IC_{50} = 1.32 μM against L858R
IC_{50} = 1.19 μM against L858R-T790M

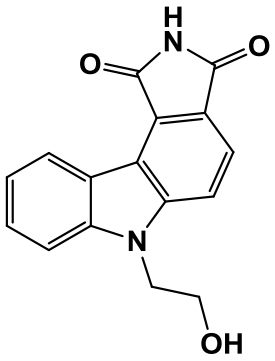

49

IC_{50} = 6.09 μM against L858R
IC_{50} = 4.35 μM against L858R-T790M

Figure 88
Comparison of the structure of our inspiration compound **29** and **49** with their respective IC_{50} values.

5.5 Conclusion

In this project, the natural product staurosporine served as a structural 'muse' to synthesize compounds as potential kinase inhibitors. The project comprised of two parts, based on the pyrrolocarbazole scaffold and the "open" form of the indolocarbazole core. With the initial aim in mind, six pyrrolocarbazole analogues were synthesized. Different warheads were incorporated into these compounds, having both unaromatized and planar (aromatized) driving portions. The second part of the project, primarily inspired by the selective kinase inhibitor enzastaurin, focused on the synthesis of bisaryl maleimides. One of the synthetic strategies, which proved problematic, involved a double-click approach. Another approach which yielded unsatisfactory results made use of click reactions on an indolyl maleimide system. Although some challenges were experienced in obtaining the bisaryl maleimides, a successful synthetic strategy based on bisamino maleimide derivatives, afforded the two final target compounds in high yields.

Upon generating the eight target compounds, their IC_{50} values were measured by collaborators at the Technische Universität Dortmund in Germany. The biochemical assays were screened against the EGFR wild-type and the two mutant forms (L858R and L858R_T790M). Of these results, only one (**49**) of the eight compounds exhibited some inhibitory activity. **49** showed IC_{50} values of 6.09 μM and 4.35 μM against L858R and L858R_T790M, respectively. We suspect that the planar pyrrolocarbazole scaffold is necessary for activity. Furthermore, it was deduced that the carbon linker length plays a vital role in the inhibitor potency.

Although the majority of the compounds did not exhibit inhibitor activity, the natural product staurosporine continues to be an inspiration and viable lead structure to design kinase inhibitors with improved selectivity and potency.

CHAPTER 6 – FUTURE WORK

6.1 Design of the pyrrolocarbazole compounds

Upon inspection of the biochemical assay results of the eight target compounds, compound **49** proved to be the only structure exhibiting inhibitory activity against EGFR and its mutant forms. Comparing **49** to the inspiration compound **29**, it was deduced that the 3-carbon linker of **29** contributed to the increased potency of the inhibitor. Furthermore, the aromatized form of the pyrrolocarbazole structures proved to be the more suitable scaffold in comparison to the unaromatized structure. For this reason, the future synthetic work pertaining to these compounds will focus on the design of aromatized pyrrolocarbazoles containing a functionalized ('warhead') tether composed of a longer (3/4) carbon linker (figure 89).

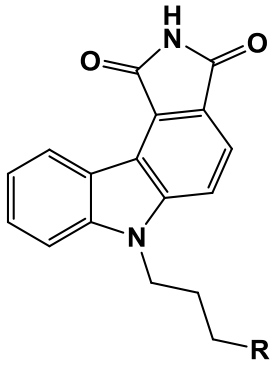

Pyrrolocarbazole Derivatives

R = Warhead for reversible or irrevesible inhibition

Figure 89
Aromatized pyrrolocarbazole derivatives containing a 3-carbon linker with warhead (R).

6.1.1 Proposed divergent synthetic route

Although the majority of the compounds afforded during the synthesis of the final target products were obtained in moderate to high yields, the route undertaken in section 3.7.4 is of particular importance. This interest arises from the fact that the design strategy involving the protected-*N*-pyrrolocarbazole is a more divergent route, when compared to the method followed in which *N*-alkylation was performed prior to the generation of the backbone scaffold (before DA reaction). Using this divergent route, and following the procedure outlined in 3.7.4.2, to afford the benzyl-protected pyrrolocarbazole derivative, various moieties, other than the nitrile group (3-carbon linkers with warhead), could potentially be introduced onto the scaffold.

The final step would involve the deprotection of the benzyl group to expose the essential –NH functionality (scheme 89). However, this *N*-benzyl deprotection directly from maleimide has not been shown to be possible.[215]

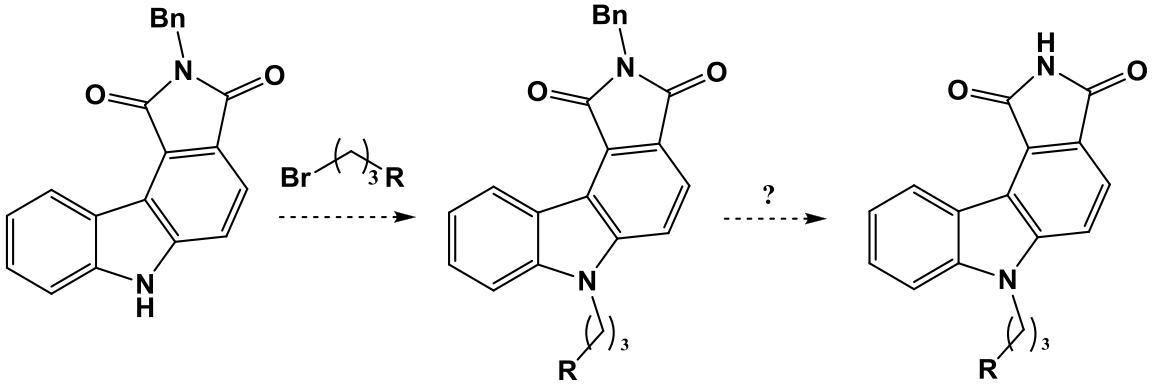

Scheme 89
Divergent strategy to incorporate various 3-carbon tether warheads (R).

The unsuccessful *N*-benzyl deprotection reaction was attempted in section 3.7.4.4 by catalytic hydrogenation, using a palladium carbon catalyst in the presence of H_2 gas (H_2, Pd/C) under pressure. However, *N*-benzyl carboxamides are known to be notoriously difficult to hydrogenolyze even when one of the most robust deprotection catalysts (for example, Pearlman's catalyst) are utilized.[215] In addition, only R groups prone to hydrogenation under these conditions would then not be tolerated. For this reason, an alternative *N*-benzyl deprotection route will be required. An indirect method which involves an alkaline hydrolysis to afford maleic anhydride, followed by heating with ammonium acetate (NH_4OAc) or urea has shown to be successful in literature.[201, 216-217] Similarly, this approach could be used to attempt the deprotection of the benzyl group from the pyrrolocarbazole compound as shown in scheme 90. Again, it should be noted that R groups sensitive to base-mediated hydrolysis would not be installable using this procedure.

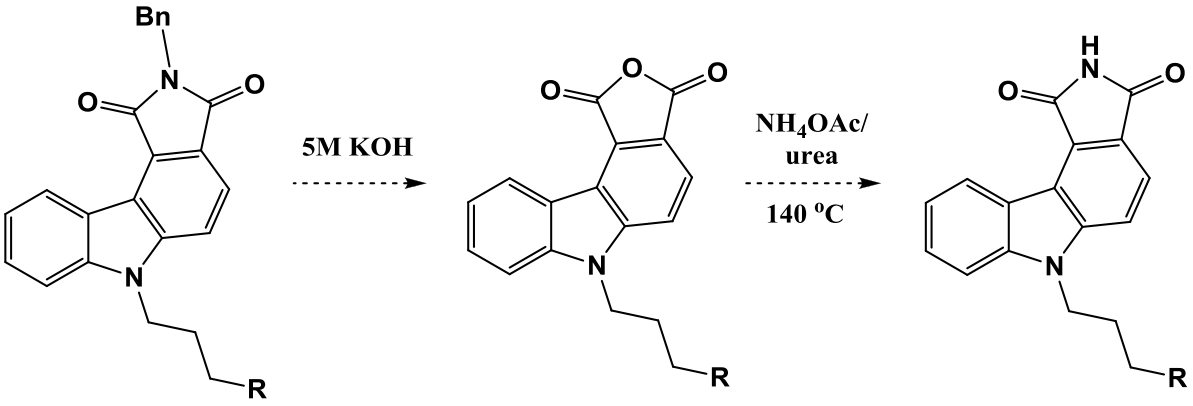

Scheme 90

Proposed strategy for *N*-benzyl deprotection involving alkaline hydrolysis and treatment with NH_4OAc or urea.

In addition, this synthetic route furnishes an approach in which maleic anhydride could be used, instead of maleimide, thereby avoiding the alkaline hydrolysis step as shown in scheme 91. However, the use of NH_4OAc or urea under the harsh reaction conditions depicted in scheme 90 and 91, could possibly alter the warhead functionality. This calls for the investigation of an alternative protecting group.

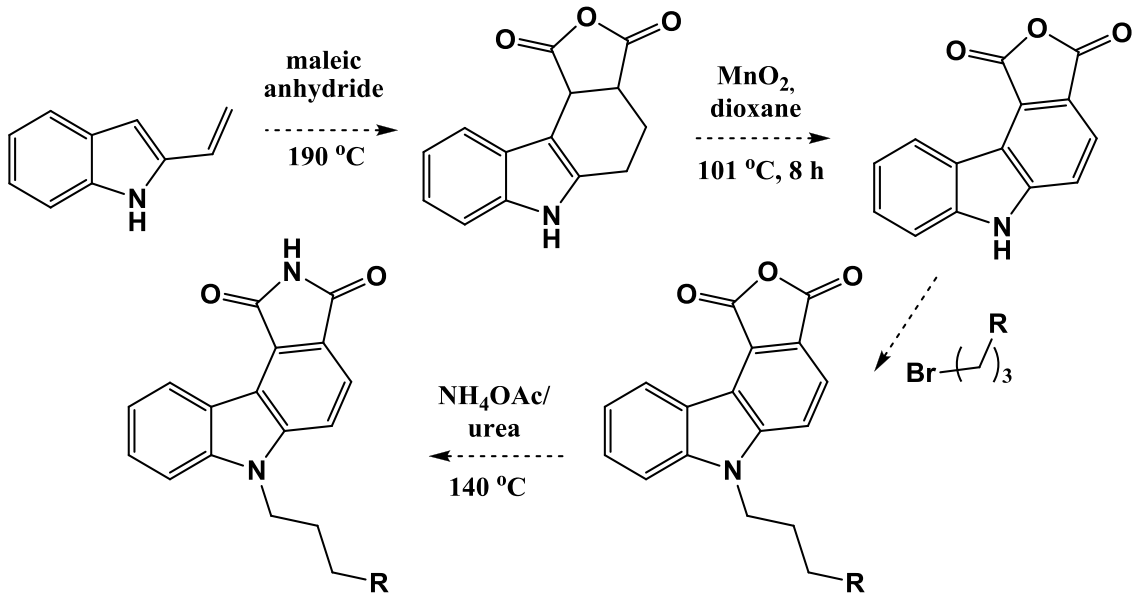

Scheme 91

Strategy incorporating maleic anhydride to build the scaffold in order to avoid the alkaline hydrolysis step.

p-Nitrophenyl in the synthesis of the bisamino maleimide target compounds (see section 4.4), proved to be a promising protecting group for the maleimide moiety. One particular advantage of this protecting group was its simple cleavage by methanolic ammonia at room temperature. Hence, the strategy to incorporate *p*-nitrophenyl as a protecting group for the pyrrolocarbazole compounds could be employed as a potential route to avoid the difficulties experienced with *N*-benzyl deprotection.

The *p*-nitrophenyl protected maleimide could be easily synthesized, following a procedure in literature.[218] This method involves treating maleic anhydride with *p*-nitroaniline, in AcOH at 140 ºC, for 5 h. The outline of this proposed strategy is shown in scheme 92.The stability of this protecting group under previously utilized thermal Diels-Alder conditions would however still have to be determined.

With the identification of an optimal protecting group, the introduction of side chains at the pyrrolocarbazole amine, as well as deprotection could then be carried out effortlessly. In this manner, a number of pyrrolocarbazole derivatives, with various warheads, could be synthesized as potential kinase inhibitors.

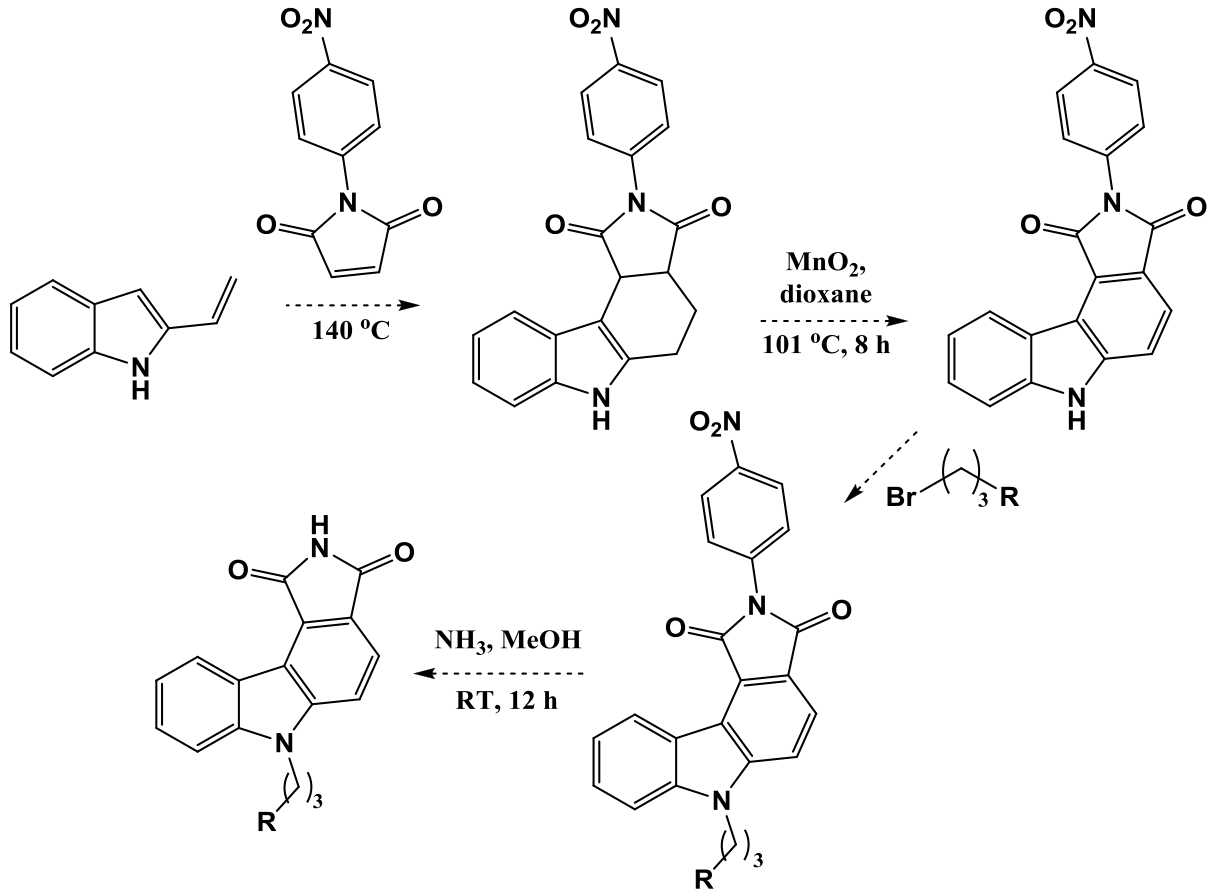

Scheme 92
Outline of strategy utilizing p-nitrophenyl as maleimide protecting group.

6.2 Design of the 'open' structure maleimide compounds

6.2.1 Derivatization of the aniline group

Although target compounds **104** and **105** did not exhibit inhibitory activity against EGFR and its mutant strains, the synthetic route undertaken for their generation proved to be successful. This efficient approach, displays potential scope as it allows for the derivatization of the preliminary structures of compound **104** and **105** to possibly improve inhibitory activity. One such strategy that could optimize these structures is the incorporation of various functional groups at the *ortho*, *meta* or *para* position of the aniline ring. Specifically, the presence of a functional group (halogen or hydroxyl) at the *ortho* position could potentially distort the planarity of the aniline phenyl ring and maleimide due to steric interactions (scheme 93). This change in orientation could affect the interactions of the inhibitor in the active site, from which further information could be deduced. In addition, the possibility of incorporating various warheads (R) also creates the opportunity to synthesize compounds with enhanced activity.

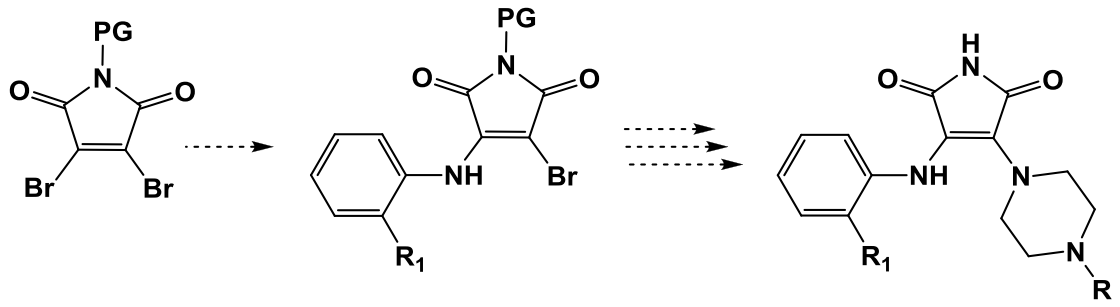

R = warhead, R_1 = X, PG = *p*-nitrophenyl

Scheme 93
Incorporating the derivatized aniline group onto the bisamino maleimides.

6.2.2 SB-415286 inspired 3-anilino-4-arylmalimides

Another feature that could possibly be altered to improve the inhibitory activity of these 'open' maleimide compounds is to replace the piperazine ring with a more rigid aromatic ring. This design is inspired by the kinase inhibitor **SB-415286**, illustrated in figure 90. **SB-415286** is a potent, selective inhibitor of GSK-3, which behaves in an ATP competitive manner.[219]

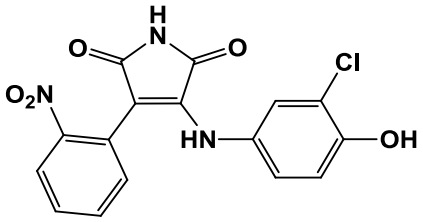

SB-415286

Figure 90
Structure of the kinase inhibitor **SB-415286**.

An outline of a proposed synthetic strategy is shown in scheme 94, and resembles the route followed by Smith and co-workers.[220] The design of the 3-anilino-4-arylmaleimides derivatives will start with a base-induced condensation of an appropriate arylacetamide with dimethyl oxalate. Once the condensation reaction affords the desired 3-hydroxy-4-aryl maleimide, chlorination of the hydroxyl, utilizing either phosphorus oxychloride in *N*,*N*-dimethylaniline or oxalyl chloride in CH_2Cl_2, will be undertaken. Finally, a number of aniline derivatives could then be introduced onto the structure, where R_1 is an *o*, *m*, *p*–halogen or -hydroxyl group. The problematic reactivity of the warhead group R could potentially be overcome by initially making use of a robust group (such as a nitro group). Following certain transformations (reduction to amine followed by acylation), an electrophilic warhead moiety could then be incorporated.

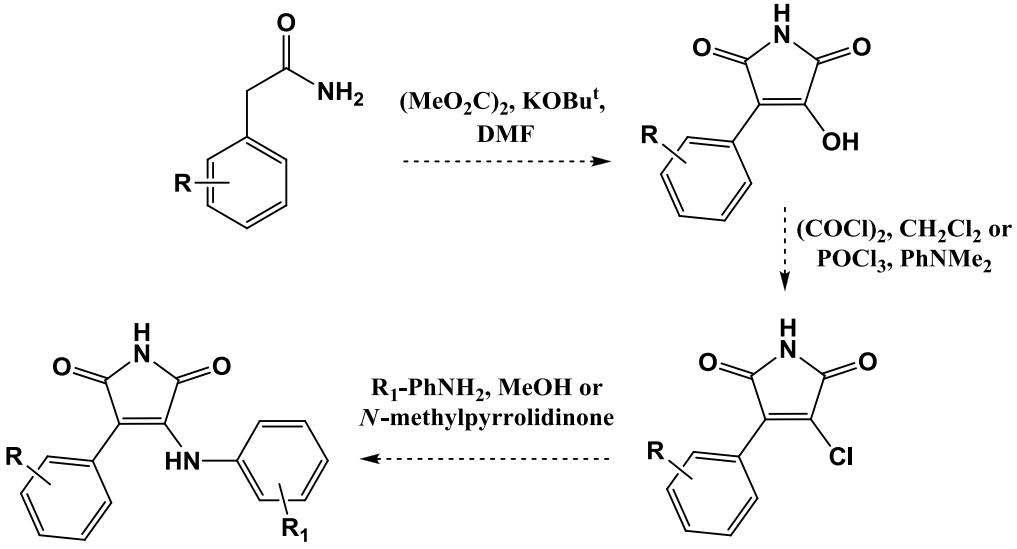

R_1 = X, OH R = warhead

Scheme 94
Design strategy of 3-anilino-4-arylmaleimide derivatives.

6.2.3 Design of bisaryl maleimides utilizing click chemistry

Once the chloro derivative of the 4-arylmaleimide is successfully synthesized, another approach would be to generate a class of triazole-based 4-arylmaleimides, as illustrated in scheme 95. This route would involve a substitution reaction using NaN_3, followed by the click reaction (CuAAC). Having several alkynes with pre-installed warheads in hand, this would allow for the synthesis of a small library of triazole based, potentially irreversible 'open' maleimide kinase inhibitors.

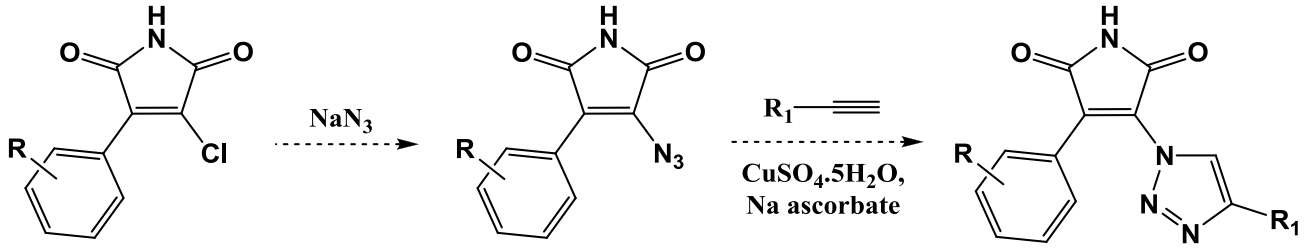

R = X, OH R_1 = warhead

Scheme 95

Design strategy towards the triazole-based 4-aryl maleimides utilizing CuAAC.

6.3 Concluding remarks pertaining to the future work

From the biochemical assay results, the synthesis of aromatized pyrrolocarbazoles having a 3-carbon tether warhead, seem to be the most promising compounds towards improving inhibitory activity. Unfortunately, no further deductions could be made from the results as to how to improve these compounds in future research. However, a more divergent synthesis is recommended, provided an optimal protecting group is identified.

The route utilized for the synthesis of the bisamino maleimides provides a promising approach to generate target compounds exhibiting improved activity. It is expected that the absence of a maleimide-protecting group for this approach, would simplify the process as deprotection would not be necessary. In addition, the kinase inhibitor **SB-415286** serves as a structural 'muse' to design various derivatives of the 'open' form of maleimide as either 3-anilino-4-arylmaleimide-or triazole-based bisaryl maleimide derivatives. In addition, incorporation of possible warheads that can impart inhibition in a reversible or irreversible manner would allow for the synthesis of potential kinase inhibitors.

CHAPTER 7 – EXPERIMENTAL WORK

7.1 General information

7.1.1 Purification of solvents and reagents

The chemicals used were purchased from either Merck or Sigma-Aldrich, or obtained from the chemical stores (De Beers building). Solvents used for chromatographic purposes were distilled by means of conventional distillation procedures. Solvents used for reaction purposes were dried over the appropriate drying agents and then distilled under N_2 gas. Tetrahydrofuran was distilled from sodium flakes with benzophenone as indicator. Toluene was distilled from sodium as well, with the absence of the benzophenone indicator. Dichloromethane, dimethylformamide and acetonitrile were distilled from calcium hydride. Triethylamine was distilled under potassium hydroxide. Diethyl ether was bought with a ≥98% purity grade from Sigma Aldrich. Other reaction solvents were dried over the appropriate size activated molecular sieves. The ethyl acetate, hexane and dichloromethane, used for column chromatography, were distilled beforehand. Other reagents requiring purification were purified according to standard procedures.

7.1.2 Chromatography

Thin layer chromatography was performed using Merck silica gel 60 F254 coated on aluminium sheets. Compounds on the TLC plates were visualized under 254 nm UV light, or stained using solutions of $KMnO_4$, Cerium ammonium molybdate (CAM) or ninhydrin followed by heating. All column chromatography was performed on Merck silica gel 60 (particle size 0.040-0.063 mm) using a combination of ethyl acetate, hexane, dichloromethane or/ and methanol as a solvent.

7.1.3 Spectroscopic and physical data

NMR spectra (^{1}H, ^{13}C) were recorded on a 300 MHz Varian VNMRS (75 MHz for ^{13}C), or a 400 MHz Varian Unity Inova (101 MHz for ^{13}C). Chemical shifts (δ) are reported in ppm and *J*-values are given in Hz. Chemical shifts were recorded using the residual solvent peak as reference. All spectra were obtained at 25 °C. Data was processed using MestReNova. Mass spectrometry was performed on a Waters SYNAPT G2. Infrared spectra were recorded on a Thermo Nicolet Nexus 470 by means of Attenuated Total Reflectance (ATR) mode. Melting points were obtained using a Gallenkamp Melting Point Apparatus and are uncorrected.

7.1.4 Other general procedures

All reactions were carried out under a positive pressure of N_2 or Ar, unless H_2O was used as solvent. Glassware was dried in an oven at 120 ºC for a minimum of 2 h. Heating of reaction mixtures was accomplished by placing the reaction flask in a paraffin oil bath. Standard Schlenk techniques were employed when necessary. Solvents were removed *in vacuo*, using a rotary evaporator, followed by removal of trace amounts of the remaining solvent using a high vacuum pump at *ca*. 0.08 mm Hg.

7.2 Experimental work pertaining to chapter 3

7.2.1 1-*tert*-Butyl 2-ethyl 1*H*-indole-1,2-dicarboxylate (32)

A 2-neck round bottom flask was charged with ethyl indole-2-carboxylate (**31**) (2.40 g, 13.0 mmol) and dissolved in dry MeCN (45 mL). Di-*tert*-butyl dicarbonate (3.60 mg, 16.5 mmol, 1.3 equiv) and DMAP (170 mg, 1.53 mmol, 0.12 equiv) were then added successively. The reaction mixture was stirred overnight at RT. The mixture was then concentrated *in vacuo* to give an oily yellow residue. The crude product was purified by column chromatography (EtOAc/Hexane, 1:20) to afford 1-*tert*-butyl 2 ethyl 1*H*-indole-1,2-dicarboxylate (**32**) as a light yellow oil (3.1 g, 85%). The ^{1}H NMR spectrum of 1-*tert*-butyl 2 ethyl 1*H*-indole-1,2-dicarboxylate (**32**) was compared to that reported in the literature and corresponded well.[138]

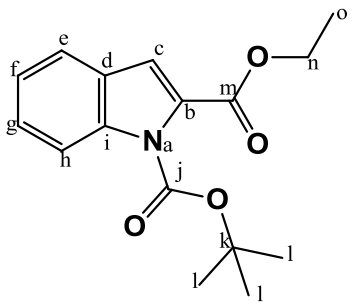

R_f = 0.65 (EtOAc/Hexane, 1:4);**^{1}H NMR (600 MHz,$CDCl_3$) δ** 8.11 (dd, *J* = 8.5, 0.6 Hz, 1H, $H_{e/h}$), 7.59 (d, *J* = 7.8 Hz, 1H, $H_{e/h}$), 7.41 (ddd, *J* = 8.5, 5.7, 1.2 Hz, 1H, $H_{f/g}$), 7.43 – 7.37 (m, 1H, $H_{f/g}$), 7.11 (s, 1H, H_c), 4.39 (q, *J* = 7.2 Hz, 2H, H_n), 1.64 (s, 9H, H_l), 1.40 (t, *J* = 7.2 Hz, 3H, H_o).

7.2.2 (1*H*-Indol-2-yl)methanol (34)

$LiAlH_4$ (0.88 g, 23 mmol, 2.2 equiv) was stirred in THF (10 mL) in a 250 mL 2-neck round bottom flask at 0 ºC under a N_2 environment. The solution appeared blue/grey in colour. A solution of commercially available ethyl indole-2-carboxylate (**31**) (2.00 g, 10.0 mmol) in THF (10 mL) was then added drop-wise to the $LiAlH_4$ solution. The ice bath was then removed and the reaction mixture was warmed to 25 ºC and stirred for 30 min.

It was cooled to 0 ºC again. H_2O (2 mL) was then added drop-wise, followed by NaOH (1 M, aq., 5 mL) and again H_2O (6 mL) successively. The solution turned white in colour. The reaction mixture was stirred for 30 min at RT. The solution was then filtered through Celite and washed with CH_2Cl_2 (100 mL). The filtrate was then washed with brine (100 mL) and the organic layer was dried over $MgSO_4$. Once the drying agent was filtered off, the product was concentrated *in vacuo*. The crude product was finally purified by column chromatography (EtOAc/Hexane, 1:4) to afford the desired product (1*H*-indol-2-yl)methanol (**34**) as an off-white solid (1.4 g, 93%). The ^{1}H NMR spectrum of (1*H*-indol-2-yl)methanol (**34**) was compared to that reported in the literature and corresponded well.[149]

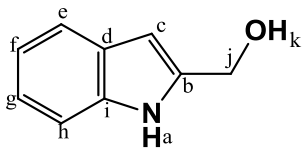

R_f = 0.39 (EtOAc/Hexane, 4:6); **^{1}H NMR (600 MHz, $CDCl_3$) δ** 8.36 (s, 1H, H_a), 7.59 (dd, *J* = 7.9, 0.8 Hz, 1H, $H_{h/e}$), 7.33 (dd, *J* = 8.1, 0.8 Hz, 1H, $H_{e/h}$), 7.19 (ddd, *J* = 8.1, 7.1, 1.2 Hz, 1H, $H_{g/f}$), 7.14 – 7.08 (m, 1H, $H_{f/g}$), 6.40 (dd, *J* = 2.0, 0.8 Hz, 1H, H_c), 4.80 (s, 2H, H_j), 1.99 (s, 1H, H_k).

7.2.3 1*H*-Indole-2-carbaldehyde (35)

The (1*H*-Indol-2-yl)methanol (**34**) (1.42 g, 9.68 mmol) was dissolved in freshly distilled MeCN (90 mL) in a 2-neck round bottom flask. MnO_2 (8.41 g, 96.8 mmol, 10 equiv) was added to the solution turning it black in colour. The mixture was then stirred at RT for 6 h. The MnO_2 was then removed by filtration through Celite after which the reaction mixture was washed with EtOAc (50 mL). The filtrate appears orange in colour. The solvent was removed *in vacuo* to afford 1*H*-indole-2-carbaldehyde (**35**) as a yellow/orange solid (1.11 g, 76%) which required no further purified. The ^{1}H NMR spectrum of 1*H*-indole-2-carbaldehyde (**35**) was compared to that reported in the literature and corresponded well.[139,149]

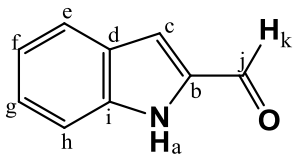

R_f = 0.77 (EtOAc/Hexane, 2:3); **^{1}H NMR (300 MHz, $CDCl_3$) δ** 9.86 (s, 1H, H_k), 9.36 (s, 1H, H_a), 7.77 (ddd, *J* = 8.1, 1.5, 0.9 Hz, 1H, $H_{e/h}$), 7.48 (dd, *J* = 8.4, 1.2 Hz, 1H, $H_{e/h}$), 7.40 (ddd, *J* = 8.4, 6.8, 1.5 Hz, 1H, $H_{g/f}$), 7.29 (dd, *J* = 2.1, 0.9 Hz, H_c), 7.19 (ddd, *J* = 8.1, 6.8, 1.2 Hz, 1H, $H_{g/f}$).

7.2.4 *tert*-Butyl 2-formyl-1*H*-indole-1-carboxylate (36)

1*H*-Indole-2-carbaldehyde (**35**) (587 mg, 3.99 mmol) was added to a 2-neck round bottom flask and dissolved in 25 mL dry CH_2Cl_2. Di-*t*-butyl dicarbonate (1.13 g, 5.19 mmol, 1.3 equiv) and DMAP (53 mg, 0.48 mmol, 0.12 equiv) were then added to the flask successively. The reaction mixture was stirred overnight at RT. The solution was then concentrated *in vacuo* to give an oily yellow residue.

The crude product was purified by column chromatography (EtOAc/Hexane, 1:20) to afford *tert*-butyl 2-formyl-1*H*-indole-1-carboxylate (**36**) as a yellow solid (0.94 g, 88%). The ^{1}H NMR spectrum of *tert*-butyl 2-formyl-1*H*-indole-1-carboxylate (**36**) was compared to that reported in the literature and corresponded well.[149]

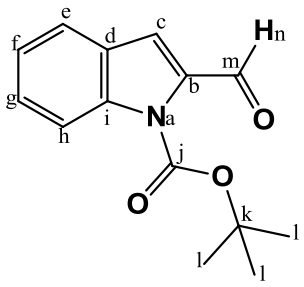

R_f= 0.75 (EtOAc/Hexane, 3:7); **^{1}H NMR (300 MHz, $CDCl_3$) δ** 10.44 (s, 1H, H_n), 8.17 (dd, *J* = 8.5, 0.8 Hz, 1H, $H_{e/h}$), 7.67 (d, J = 8.0 Hz, 1H, $H_{e/h}$), 7.48 (ddd, *J* = 8.5, 7.2, 1.3 Hz, 1H, $H_{f/g}$), 7.44 (s, 1H, H_c), 7.30 (ddd, *J* = 8.0, 7.2, 1.3 Hz, 1H, $H_{g/f}$), 1.72 (s, 9H, H_l).

7.2.5 1-(Phenylsulfonyl)-1*H*-indole (39)

Indole (**38**) (500 mg, 4.27 mmol) was added to a 2-neck round bottom flask and dissolved in dry DMF (5 mL). The flask was placed in an ice bath and NaH (60% dispersion in oil) (204 mg, 5.13 mmol, 1.2 equiv) was added slowly, forming a white slurry. To this, benzenesulfonyl chloride (0.66 mL, 5.1 mmol, 1.2 equiv) was added drop-wise and left to stir overnight. The reaction mixture was then diluted with CH_2Cl_2 (120 mL) and washed with NH_4Cl_{sat} (120 mL). The organic layer collected was concentrated *in vacuo* and diluted using Et_2O (50 mL). This was then washed with H_2O (4 × 30 mL), brine (50 mL) and dried over $MgSO_4$. The solvent was finally removed *in vacuo* affording 1-(phenylsulfonyl)-1*H*-indole (**39**) as an orange solid (612 mg, 55%). No further purification was required. The ^{1}H NMR spectrum of 1-(phenylsulfonyl)-1*H*-indole (**39**) was compared to that reported in the literature and corresponded well.[157]

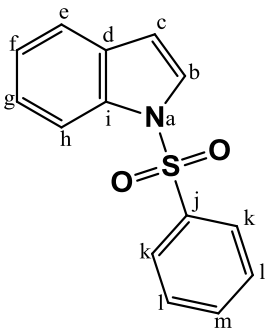

R_f= 0.31 (EtOAc/Hexane, 1:9); **^{1}H NMR (300 MHz, $CDCl_3$) δ** 7.99 (ddd, *J* = 8.3, 1.8, 0.8 Hz, 1H, H_{Ar}), 7.90 – 7.84 (m, 2H, H_{Ar}), 7.56 (d, *J* = 3.7 Hz, 1H, H_{Ar}), 7.55 – 7.48 (m, 2H, H_{Ar}), 7.46 – 7.37 (m, 2H, H_{Ar}), 7.31 (ddd, *J* = 8.3, 7.3, 1.3 Hz, 1H, H_{Ar}), 7.25 – 7.17 (m, 1H, H_{Ar}), 6.66 (dd, *J* = 3.7, 0.8 Hz, 1H, H_{Ar}).

7.2.6 1-(Phenylsulfonyl)-1*H*-indole-2-carbaldehyde (40)

Dry THF (20 mL) was added to a 2-neck round bottom flask and stirred under a N_2 atmosphere. TMP (0.20 mL, 2.3 mmol, 1.5 equiv) was added to the flask containing THF at -78 °C, followed by the drop-wise addition of *n*-BuLi (1.24 mL, 1.86 mmol, 1.2 equiv). The solution was left to stir at -78 °C for 10 min. The dry ice acetone slurry was then replaced with an ice bath and the solution was further stirred at 0 °C for 30 min. The solution was again cooled to -78 °C and 1-(phenylsulfonyl)-1*H*-indole (**39**) (400 mg, 1.55 mmol) was added and stirred for 1 h. The temperature was again increased to 0 °C for 20 min after which the dry ice slurry was again introduced. DMF (0.20 mL, 2.32 mmol, 1.5 equiv) was added to the yellow reaction mixture and stirred overnight at RT. The solution was then added to a flask containing saturated NH_4Cl (50 mL) and extracted using EtOAc (2 × 50 mL). The organic layers were combined, washed with brine (100 mL) and dried over $MgSO_4$. The drying salts were then filtered and the solvent removed *in vacuo*. The crude product was purified by column chromatography (EtOAc/Hexane, 5:95). 1-(Phenylsulfonyl)-1*H*-indole-2-carbaldehyde (**40**) was obtained as an off-white solid (160 mg, 36%). The ^{1}H NMR spectrum of 1-(phenylsulfonyl)-1*H*-indole-2-carbaldehyde (**40**) was compared to that reported in the literature and corresponded well.[158]

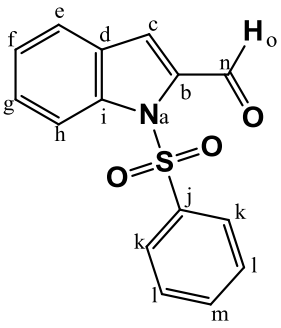

R_f= 0.35 (EtOAc/Hexane, 1:9); **^{1}H NMR (600 MHz, $CDCl_3$) δ** 10.53 (s, 1H, H_o), 8.24 (d, *J* = 8.6 Hz, 1H, $H_{e/h}$), 7.78(d, *J* = 8.3 Hz, 2H, H_k), 7.63 (d, *J* = 7.8 Hz, 1H, $H_{e/h}$), 7.57 – 7.51 (m, 2H, H_l), 7.48 (s, 1H, H_c), 7.42 (m, 2H, $H_{e/g}$), 7.32 (m, 1H_m).

7.2.7 2-Vinyl-1*H*-indole (41)

Methyltriphenylphosphonium bromide ($MePPh_3Br$) (7.39 g, 20.7 mmol, 6 equiv) and dry THF (140 mL) were added to a 2-neck round bottom flask under a N_2 atmosphere.The flask was placed in an ice bath and *n*-BuLi (13.5 mL, 19.0 mmol, 5.5 equiv) was added drop-wise, using a syringe, to the solution at 0 °C. During this time the colour of the solution changed from white to a deep yellow. The ice bath was then removed and the temperature increased to 30 ºC. The solution was stirred for 30 min at this temperature and then placed on an ice bath again. The 1*H*–indole-2-carbaldehyde (**35**) (500 mg, 3.45 mmol) was dissolved in THF (20 mL). This solution was then transferred drop-wise, using a syringe, to the methylenetriphenylphosphorane solution at 0 ºC.

The ice bath was removed and the mixture was stirred overnight at RT under N_2 atmosphere. Et_2O (80 mL) was added to the reaction mixture and it was washed with H_2O (2 × 80 mL). The aqueous layer was collected and was further extracted with Et_2O (2 × 50 mL). The organic layers were combined, washed with brine (200 mL) and dried over $MgSO_4$. The drying salts were removed by filtration and the solvent was removed *in vacuo*. Purification was done by column chromatography (EtOAc/Hexane, 5:95) and the product 2-vinyl-1*H*-indole (**41**) was isolated as an off-white solid (361 mg, 74%). The ^{1}H NMR spectrum of 2-vinyl-1*H*-indole (**41**) was compared to that reported in the literature and corresponded well.[139]

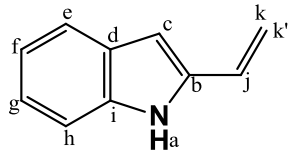

R_f= 0.47 (EtOAc/Hexane, 1:9); **^{1}H NMR (300 MHz, $CDCl_3$) δ** 8.15 (s, 1H, H_a), 7.58 (ddd, *J* = 8.2, 1.1, 0.9 Hz, 1H, $H_{e/h}$), 7.33 (ddd, *J* = 8.1, 1.5, 0.9 Hz, 1H, $H_{e/h}$), 7.19 (ddd, *J* = 8.2, 7.1, 1.5 Hz, 1H, $H_{f/g}$), 7.09 (ddd, *J* = 8.1, 7.1, 1.1 Hz, 1H, $H_{f/g}$), 6.75 (dd, *J* = 17.8, 11.2 Hz, 1H, H_j), 6.53 (d, *J* = 2.1Hz, 1H, H_c), 5.55 (d, *J* = 17.8 Hz, 1H, H_k), 5.27 (d, *J* = 11.2 Hz, 1H, $H_{k'}$).

7.2.8 4,5,6,10*c*-Tetrahydropyrrolo[3,4-*c*]carbazole-1,3(2*H*,3a*H*)-dione (42)

2-Vinyl-1*H*-indole **(4)** (500 mg, 3.50 mmol) and maleimide (407 mg, 4.19 mmol, 1.2 equiv) were added neat to a small round bottom flask. The flask was placed in an oil bath which was preheated to 190 °C. As the temperature increased, the compounds melted at 40 °C and then solidified. The temperature was kept at 190 °C for 1 h. The crude product was obtained as a dark brown highly insoluble solid (840 mg) which was used in the following step without further purification.

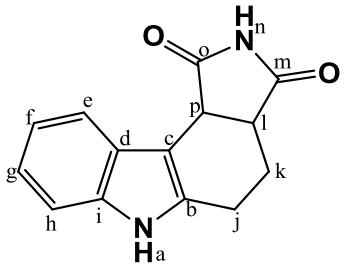

Mp = 160-162 ºC; **R_f** = 0.22 (MeOH/EtOAc/Hexane, 1:1:3); **IR (ATR, cm^{-1}):** 3382, 3222 (2° amine/amide, N-H str), 2961, 2943 (alkanes C-H str), 1703 (carbonyl, C=O str), 756,745 (aromatics C-H); **(^{1}H NMR 300 MHz, DMSO) δ** 10.95 (s, 1H, H_a), 7.70 (d, *J* = 7.2 Hz, 1H, $H_{e/h}$), 7.26 (d, *J* = 7.4 Hz, 1H, $H_{h/e}$), 7.07 – 6.93 (m, 2H, $H_{f\&g}$), 4.17 (d, *J* = 8.1 Hz, 1H, H_p), 3.50 – 3.42 (m, 1H, $H_{k/j}$), 3.17 (d, *J* = 5.1 Hz, 1H, H_l), 2.77 – 2.66 (m, 1H, $H_{k/j}$), 2.33 – 2.22 (m, 1H, $H_{k/j}$), 1.88 – 1.73 (m, 1H, $H_{k/j}$). **HRMS:** calcd for $C_{14}H_{13}N_2O_2^+$ $[M+H]^+$, 241.0977, found 241.0966.

7.2.9 Pyrrolo[3,4-*c*]carbazole-1,3(2*H*,6*H*)-dione (43)

4,5,6,10*c*-Tetrahydropyrrolo[3,4-*c*]carbazole-1,3(2*H*,3*aH*)-dione **(7) (**150 mg, 0.630 mmol) was added to a small round bottom flask.

The compound was dissolved in DMSO (7 mL) and stirred at 30 ° C under a N_2 atmosphere. DDQ (286 mg, 1.26 mmol, 2 equiv) was then added and the temperature was increased to 50 °C and stirred for 2 h. H_2O (10 mL) was then added drop-wise and a precipitate formed. The precipitate was filtered off and washed with Et_2O, and further dried under high vacuum to afford the desired product pyrrolo[3,4-*c*]carbazole-1,3(2*H*,6*H*)-dioneas a brown solid (74 mg, 40%).

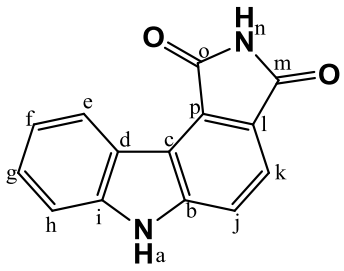

Mp = 250-252 ºC; **R_f** = 0.84 (EtOAc); **IR (ATR, cm^{-1}):** 3186, 3057 (2° amine/amide, N-H str), 1697 (carbonyl, C=O str), 1451 (aromatic C-C str), 740 (aromatics C-H);**^{1}H NMR (300 MHz, DMSO) δ**12.08 (s, 1H, H_{NH}), 11.12 (s, 1H, H_{NH}), 8.82 (d, *J* = 8.0 Hz, 1H, $H_{e/h}$), 7.85 (d, *J* = 8.2 Hz, 1H, $H_{k/j}$), 7.79 (d, *J* = 8.2 Hz, 1H, $H_{k/j}$)7.65 – 7.52 (m, 2H, $H_{e/h/f/g}$), 7.32 (ddd, *J* = 8.2, 6.8, 1.3 Hz, 1H, $H_{f/g}$); **^{13}C NMR (300 MHz, DMSO) δ** 170.4($C_{m/o}$), 170.3 ($C_{m/o}$),144.1 (C_{Car}), 141.5 (C_{Car}), 128.1 (C_{Car}), 126.7 (C_{Car}), 124.7 (C_{Car}), 123.8 (C_{Car}), 120.1 (C_{Car}), 120.0 (C_{Car}), 119.42 (C_{Car}), 118.3 (C_{Car}), 115.6 (C_{Car}), 111.6 (C_{Car}); **HRMS:** calcd for $C_{14}H_9N_2O_2^+$ $[M+H]^+$, 237.0664, found 234.2000.

7.2.10 *tert*-Butyl 2,5-dioxo-2,5-dihydro-1*H*-pyrrole-1-carboxylate (45)

To a 2-neck round bottom flask, under an Ar atmosphere, was added maleimide (50 mg, 0.52 mmol) and di-*tertiary* butyl-dicarbonate (123 mg, 0.567 mmol, 1.1 equiv). The mixture was dissolved in chloroform (5 mL) and stirred for 5 min. A spatula tip of DMAP was then added and the solution changed colour from clear to brown. The reaction mixture was stirred for a further 6 h at RT. The mixture was then washed with $NaHCO_{3(sat)}$ (10 mL) followed by H_2O (2 × 5 mL). The aqueous layers were combined and extracted with CH_2Cl_2 (15 mL). The organic layer was then washed with brine (30 mL) and dried over $MgSO_4$. The drying salts were filtered off and the solvent was finally removed *in vacuo*. The crude product was purified by column chromatography (EtOAc/Hexane, 3:7), affording the product *tert*-butyl 2,5-dioxo-2,5-dihydro-1*H*-pyrrole-1-carboxylate (**45**) as an opaque solid (68 mg, 67%). The ^{1}H NMR spectrum of *tert*-butyl 2,5-dioxo-2,5-dihydro-1*H*-pyrrole-1-carboxylate (**45**) was compared to that reported in the literature and corresponded well.[166]

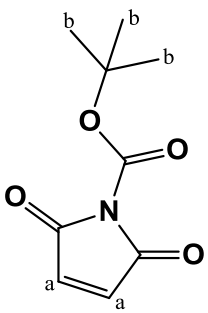

R_f= 0.64 (EtOAc/Hexane, 4:6), **^{1}H NMR (300 MHz, $CDCl_3$) δ** 6.78 (s, 2H, H_a), 1.57 (s, 9H, H_b).

7.2.11 *tert*-Butyl 1,3-dioxo-1,3,3a,4,5,10c-hexahydropyrrolo[3,4-*c*]carbazole-2(6*H*)-carboxylate (46)

The 2-vinyl-1*H*-indole (100 mg, 0.699 mmol) and Boc-maleimide (138 mg, 0.700 mmol, 1 equiv) were added neat to a small round bottom flask. The flask was placed in an oil bath preheated to 70 °C, and stirred under a N_2 atmosphere for 30 min. TLC indicated some 2-vinyl-1*H*-indole remained unreacted. The crude product was purified by column chromatography (EtOAc/Hexane, 3:7) affording *tert*-butyl1,3-dioxo-1,3,3a,4,5,10c-hexahydropyrrolo[3,4-*c*]carbazole-2(6*H*)-carboxylate (140 mg) as an off-white solid and recovering 23 mg of the starting reagent 2-vinyl-1*H*-indole. Yield: 59% (77% brsm).

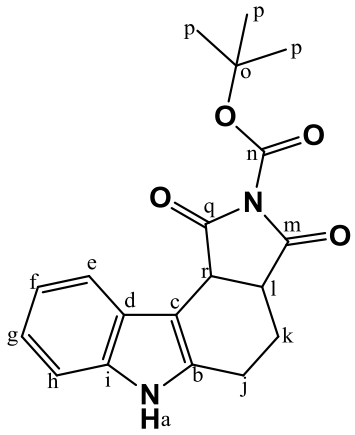

Mp = 266-268 ºC; **R_f**= 0.51 (EtOAc/Hexane, 4:6); **IR (ATR, cm^{-1}):** 3379 (2° amine, N-H str), 2982 (alkanes C-H str), 1755 (ester C=O str), 1709 (carbonyl, C=O str), 738 (aromatics C-H);**^{1}H NMR (300 MHz, DMSO) δ** 11.07 (s, 1H, H_a), 7.69 (d, *J* = 7.5 Hz, 1H, $H_{e/h}$), 7.29 (d, *J* = 7.7 Hz, 1H, $H_{e/h}$), 7.11 – 6.96 (m, 2H, $H_{f\&g}$), 4.33 (d, *J* = 8.0 Hz, 1H, H_r), 3.74 – 3.64 (m, 1H, H_l), 2.80 – 2.67 (m, 1H, H_j), 2.64 – 2.54 (m, 1H, $H_{j/k}$), 2.38 – 2.27 (m, 1H, $H_{j/k}$), 1.86 (ddd, *J* = 16.3, 10.6, 5.2 Hz, 1H, H_k), 1.45 (s, 9H, H_p); **^{13}C NMR (300 MHz, DMSO) δ** 175.7 ($C_{q/m}$), 173.4 ($C_{m/q}$), 147.1 (C_n), 136.1 (C_{indole}), 135.8 (C_{In}), 126.8 (C_{In}), 121.4 (C_{In}), 119.5 (C_{In}), 119.3 (C_{In}), 111.4 (C_{In}), 101.8 (C_{In}), 85.6 (C_o), 40.4 (2C, $C_{r/l}$), 27.7 (3C, C_p), 21.0 ($C_{k/j}$), 19.6 ($C_{j/k}$); **HRMS:** calcd for $C_{19}H_{20}N_2O_4Na^+$ $[M+Na]^+$, 363.1321 , found 363.1321.

7.2.12 (2-Bromoethoxy)(*tert*-butyl)dimethylsilane (55)

Imidazole (1.3 g, 19 mmol, 1.2 equiv) was added to a 2-neck round bottom flask and dissolved in dry MeCN (20 mL) under a N_2 atmosphere. The flask was placed in an ice bath and 2-bromoethanol (**54**) (2.0 g, 16 mmol) was added to the solution, followed by *tert*-butyldimethylsilane (2.4 g, 18 mmol, 1.1 equiv). The reaction mixture was stirred at RT overnight. The white precipitate formed was filtered off and the solvent was removed *in vacuo.* The crude product was re-dissolved in EtOAc, forming more precipitate, which was removed by filtration. The solvent was removed *in vacuo*, affording the product (2-bromoethoxy)(*tert*-butyl)dimethylsilane (**55**) as a clear oil (3.0 g, 74 %). The ^{1}H NMR spectrum of (2-bromoethoxy)(*tert*-butyl)dimethylsilane (**55**) was compared to that reported in the literature and corresponded well.[167]

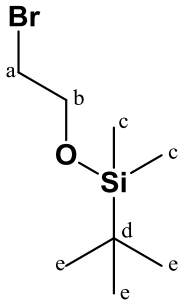

^{1}H NMR (300 MHz, CDCl3) δ 3.89 (t, J = 6.5 Hz, 2H, H_b), 3.39 (t, J = 6.5 Hz, 2H, H_a), 0.90 (s, 9H, H_9), 0.09 (s, 6H, H_c).

7.2.13 Ethyl 1-{2-(*tert*-butyldimethylsilyloxy)ethyl}-1*H*-indole-2-carboxylate (56)

A dry, 2-neck round bottom flask charged with commercially available ethyl indole-2-carboxylate (1.50 g, 7.90 mmol) was evacuated under high vacuum and filled with Ar. Dry DMF (10 mL) was added to the flask which was placed in an ice bath. NaH (0.37 g, 9.5 mmol, 1.2 equiv) was added in portions at 0 ° C and stirred for 10 min. (2-bromoethoxy)(*tert*-butyl)dimethylsilane (2.10 g, 8.7 mmol, 1.1 equiv) in DMF (5 mL) was then added drop-wiseto the reaction mixture and stirred at 40 ° C, under N_2, overnight. Upon completion, the mixture was cooled to RT, poured onto cold H_2O (50 mL) and extracted with EtOAc (50 mL). The organic layer was then washed with brine (80 mL), dried over $MgSO_4$ and filtered. The solvent was finally removed *in vacuo* and the crude product was purified by column chromatography (EtOAc/Hexane, 5:95) affording the product ethyl 1-{2-(*tert*-butyldimethylsilyloxy)ethyl}-1*H*-indole-2 carboxylate (**56**) as a clear liquid (0.27 g, 73%).

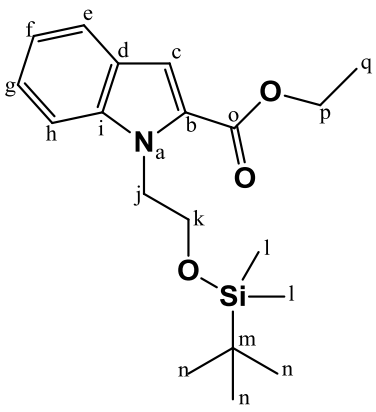

R_f = 0.88 (EtOAc/Hexane, 2:8); **IR (ATR, cm^{-1}):** 2957, 2929, 2857 (alkane C-H str), 1708 (ester C=O str), 1358 (alkane C-H rock), 1252 (-Si$(CH_3)_2$-O- str), 1220, 1196, 1080 (C-O str), 835, 777, 749 (-Si$(CH_3)_2$-O- str); **^{1}H NMR (300 MHz, $CDCl_3$) δ** 7.60 (d, *J* = 7.9 Hz, 1H, $H_{h/e}$), 7.44 (d, *J* = 8.3 Hz, 1H, $H_{e/h}$), 7.22 (m, 2H, $H_{g/f\,\&\,c}$), 7.08 (dd, *J* = 10.9, 3.9 Hz, 1H, $H_{f/g}$), 4.64 (t, *J* = 5.4 Hz, 2H, $H_{j/k}$), 4.32 (q, *J* = 7.2 Hz, 2H, H_p), 3.89 (t, *J* = 5.4 Hz, 2H, $H_{k/j}$), 1.36 (t, *J* = 7.2 Hz, 3H, H_q), 0.70 (s, 9H, H_n), -0.26 (s, 6H, H_l); **^{13}C NMR (300 MHz, $CDCl_3$) δ** 162.3 (C_o), 140.2 (C_{In}), 127.7 (C_{In}) 126.0 (C_{In}), 124.9 (C_{In}), 122.5 (C_{In}), 120.6 (C_{In}), 111.5 (C_{In}), 110.8 (C_{In}), 63.2 ($C_{k/j}$), 60.6 ($C_{p/j/k}$), 47.0 ($C_{j/p}$), 25.9 (C_n), 18.3 (C_m), 14.5 (C_q), -5.6 (C_l); **HRMS:** calcd for $C_{19}H_{30}NO_3Si^+$ $[M+H]^+$, 348.1995, found 348.2007.

7.7.14 [1-{2-(*tert*-Butyldimethylsilyloxy)ethyl}-1*H*-indol-2-yl]methanol (57)

$LiAlH_4$ (0.22 g, 5.8 mmol, 2 equiv) was added to a 2-neck round bottom flask under an Ar atmosphere and stirred in dry THF (10 mL).A solution of ethyl 1-{2-(*tert*-butyldimethylsilyloxy)ethyl}-1H-indole-2-carboxylate(**56**)(1.0 g, 2.9 mmol) dissolved in dry THF (10 mL) was added drop wise to the $LiAlH_4$ solution at 0 ºC. The reaction mixture was stirred for 15 min at 0 ºC. Upon complete consumption of starting reagent, H_2O (2 mL), NaOH (1 M, aq., 5 mL) and more H_2O (6 mL) were successively added drop-wise. The solution became white in colour when stirred at RT for 30 min. Upon completion of the reaction, the solution was filtered through Celite and washed with CH_2Cl_2 (50 mL). The filtrate was then washed with brine (50 mL) and the organic layer was dried over $MgSO_4$. Once the drying agent was filtered off, the product was concentrated *in vacuo*. The crude product was purified by column chromatography (EtOAc/Hexane, 2:8) affording [1-{2-(*tert*-butyldimethylsilyloxy)ethyl}-1*H*-indol-2-yl]methanol (**57**) as a white solid (0.85 g, 97%).

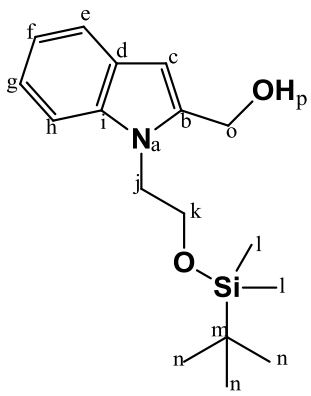

Mp = 66-68 ºC; **R_f**= 0.84 (EtOAc/Hexane, 4:6); **IR (ATR, cm^{-1}):** 3258 (O-H str), 2926, 2854 (alkane C-H str), 1251(-Si$(CH_3)_2$-O- str), 1111 (C-O str), 780, 832 (-Si$(CH_3)_2$-O- str); **^{1}H NMR (400 MHz, $CDCl_3$) δ** 7.61 (d, *J* = 7.8 Hz, 1H, $H_{h/e}$), 7.40 (d, *J* = 8 Hz, 1H, $H_{e/f}$), 7.30 – 7.27 (m, 1H , $H_{g/f}$), 7.24 – 7.18 (m, 1H, $H_{f/g}$), 6.48 (s, 1H, H_c), 4.78 (s, 2H, H_o), 4.37 (t, *J* = 5.2 Hz, 2H, $H_{j/k}$), 4.00 (t, *J* = 5.2 Hz, 2H, $H_{k/j}$), 3.23 (s, 1H, H_p), 0.78 (s, 9H, H_n), -0.13 (d, *J* = 3.0 Hz, 6H, H_l); **^{13}C NMR (400 MHz, $CDCl_3$) δ** 139.7 (C_{indole}), 137.0 (C_{indole}), 127.9 (C_{indole}), 121.9 (C_{indole}), 121.2 (C_{indole}), 119.8 (C_{indole}), 109.5 (C_{indole}), 101.8 (C_{indole}), 62.2 ($C_{k/j}$), 57.0 ($C_{o/j/k}$), 45.7 ($C_{j/o/k}$), 25.9 (C_n), 18.5 (C_m), -5.7 (C_l); **HRMS:** calcd for $C_{17}H_{28}NO_2Si^+$ $[M+H]^+$, 306.1889, found 306.1889.

7.2.15 1-{2-(*tert*-Butyldimethylsilyloy)ethyl}-1*H*-indole-2-carbaldehyde (58)

1-{2-(*Tert*-butyldimethylsilyloy)ethyl}-1H-indol-2-yl)methanol (2.9 g, 9.9 mmol) was dissolved in dry MeCN (100 mL) in a 2-neck round bottom flask. MnO_2 (8.4 g, 96 mmol, 10 equiv) was added to the solution and the reaction was left to proceed at RT under N_2 for 8 h. The reaction mixture was then filtered through Celite and was washed with EtOAc (80 mL). The filtrate appears orange in colour. The solvent was removed *in vacuo* affording the product 1-{2-(*tert*-Butyldimethylsilyloy)ethyl}-1*H*-indole-2-carbaldehyde as a light yellow oily solid (2.4 g, 83%). No further purification was required.

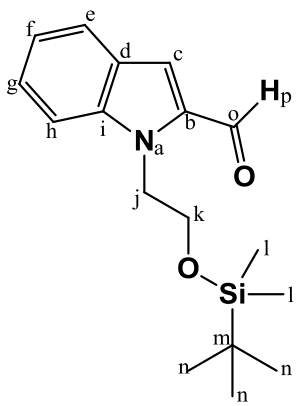

R_f = 0.79 (EtOAc/Hexane, 2:8); **IR (ATR, cm^{-1}):** 2953, 2925,2854 (alkane C-H str), 2804, 2726 (aldehyde H-C=O: C-H str), 1668 (aldehyde C=O str), 1249 (-Si(CH_3)$_2$-O- str), 775, 835 (-Si(CH_3)$_2$-O- str); **^{1}H NMR (300 MHz, $CDCl_3$) δ** 9.88 (s, 1H, H_p), 7.71 (d, *J* = 8.1 Hz, 1H, $H_{h/e}$), 7.52 (d, *J* = 8.5 Hz, 1H, $H_{e/h}$), 7.39 (m, 1H, $H_{g/f}$), 7.28 (s, H_c), 7.20 – 7.11 (m, 1H, $H_{f/g}$), 4.66 (t, *J* = 5.2 Hz, 2H, $H_{j/k}$), 3.95 (t, *J* = 5.2 Hz, 2H, $H_{k/j}$), 0.73 (s, 9H, H_n), -0.23 (s, 6H, H_l); **^{13}C NMR (300 MHz, $CDCl_3$) δ** 182.7 (C_o), 141.5 (C_{In}), 135.4 (C_{In}), 126.9 (C_{In}), 126.4 (C_{In}), 123.22 (C_{In}), 121.03 (C_{In}), 118.26 (C_{In}), 111.88 (C_{In}), 63.16 ($C_{k/j}$), 47.14 ($C_{j/k}$), 25.9 (C_n), 18.2 (C_m), -5.7 (C_l);**HRMS:** calcd for $C_{17}H_{26}NO_2Si^+$ $[M+H]^+$, 304.1733, found 304.1730

7.2.16 1-{2-(*tert*-Butyldimethylsilyloxy)ethyl}-2-vinyl-1*H*-indole (59)

A dry, 2-neck round bottom flask charged with $MePPh_3Br$ (5.58 g, 15.6 mmol, 6 equiv) was flushed with N_2 and placed in an ice bath. Dry THF (80 mL) was added to the flask and allowed to stir for 10 min. *n*-BuLi (9.87 mL, 14.3 mmol, 5.5 equiv) was then slowly added drop-wise using a syringe at 0 °C. During this time the colour of the solution changed from white to yellow. The ice bath was then removed and the reaction mixture was stirred for 30 min at 30 ºC. 1-{2-(tert-Butyldimethylsilyloy)ethyl}-1*H*-indole-2-carbaldehyde (**58**) (0.79 g, 2.6 mmol) was then dissolved in THF (15 mL) and transferred drop-wise using a syringe to the methylenetriphenylphosphorane solution at 0 ºC.The reaction mixture was then stirred at RT for 8 h. Upon completion, the reaction mixture was diluted with Et_2O (100 mL) and washed with H_2O (2 × 100 mL). The combined aqueous layers were further extracted with Et_2O (2 × 80 mL). The organic layers were then combined, washed with brine (150 mL), and dried over $MgSO_4$. After filtration the solvent was finally removed *in vacuo*. Purification of the crude product was done by column chromatography (EtOAc/Hexane, 3:97) affording the product 1-{2-(*tert*-butyldimethylsilyloxy)ethyl}-2-vinyl-1*H*-indole (**59**) as an opaque oil (0.62 g, 79%).

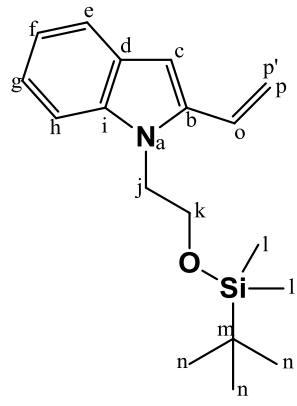

R_f = 0.75 (EtOAc/Hexane, 1:9); **IR (ATR, cm^{-1}):** 3052 (alkene =C-H str), 2926, 2854 (alkane C-H str), 1251 (-Si(CH_3)$_2$-O- str), 831, 774 (-Si(CH_3)$_2$-O- str), 731, 662 (alkene =C-H bend); **^{1}H NMR (400 MHz, $CDCl_3$) δ** 7.49 (d, *J* = 7.8 Hz, 1H, $H_{h/e}$),7.23 (d, *J* = 8.2 Hz, 1H, $H_{e/h}$), 7.09 (dd, *J* = 8.2, 7.0 Hz, 1H, $H_{g/f}$), 7.03 – 6.98 (m, 1H, $H_{f/g}$), 6.77 (dd, *J* = 17.4, 11.2 Hz, 1H, H_o), 6.62 (s, 1H, H_c), 5.76 (dd, *J* = 17.4, 1.3 Hz, 1H, $H_{q'}$), 5.26 (dd, *J* = 11.2, 1.3 Hz, 1H, H_q), 4.20 (t, *J* = 6.1 Hz, 2H, $H_{j/k}$), 3.81 (t, *J* = 6.1 Hz, 2H, $H_{k/j}$), 0.75 (s, 9H, H_n), -0.21 (s, 6H, H_l); **^{13}C NMR (400 MHz, $CDCl_3$) δ** 138.6 (C), 137.5 (C),

128.0 (C), 126.4 (C), 121.7 (C), 120.6 (C), 119.9 (C), 116.4 (C), 109.6 (C), 99.0 (C), 62.3 ($C_{k/j}$), 45.6 ($C_{j/k}$), 26.0 (C_n), 18.4 (C_m), -5.6 (C_l); **HRMS:** calcd for $C_{18}H_{28}NOSi^+$ $[M+H]^+$, 302.1940, found 301.1941.

7.2.17 6-{2-(*tert*-Butyldimethylsilyloxy)ethyl}-4,5,6,10c-tetrahydropyrrolo[3,4-*c*]carbazole-1,3(2*H*,3a*H*)-dione (60)

1-{2-(*tert*-butyldimethylsilyloxy)ethyl}-2-vinyl-1*H*-indole (190 mg, 0.630 mmol) and maleimide (73 mg0.76 mmol, 1.2 equiv) were addedneat to a small round bottom flask. The flask was placed in an oil bath preheated to 190 °C and stirred for 30 min. TLC indicates some 1-{2-(*tert*-butyldimethylsilyloxy)ethyl}-2-vinyl-1*H*-indoleremained unreacted. The crude product appears as a red/orange oily solid together with highly insoluble red solid. Purification by column chromatography (EtOAc/Hexane, 3:7) afforded 6-{2-(*tert*-butyldimethylsilyloxy)ethyl}-4,5,6,10*c*-tetrahydropyrrolo[3,4-*c*]carbazole-1,3(2*H*,3a*H*)-dione (**60**) as a light orange solid (155 mg) and recovered 40 mg of 1-{2-(*tert*-butyldimethylsilyloxy)ethyl}-2-vinyl-1*H*-indole (**59**). Yield: 62% (78% brsm).

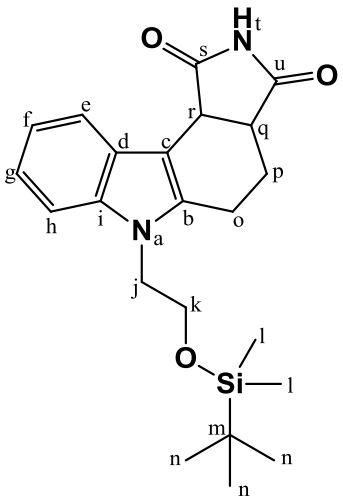

Mp = 140-142 ° C; $\mathbf{R_f}$ = 0.21 (EtOAc/Hexane, 2:8); **IR (ATR, cm^{-1}):** 3181 (amide N-H str), 2951, 2928, 2854 (alkane C-H str), 1700 (carbonyl C=O str), 1250, 837, 778 (-Si(CH_3)$_2$-O- str); **^{1}H NMR (300 MHz, DMSO) δ** 10.95 (s, 1H, H_t), 7.73 (d, *J* = 7.6 Hz, 1H, $H_{e/h}$), 7.37 (d, *J* = 7.9 Hz, 1H, $H_{h/e}$), 7.11 – 6.97 (m, 2H, $H_{f\ \&\ g}$), 4.23 – 4.14 (m, 3H, $H_{j/k\ \&\ r/q}$), 3.84 – 3.76 (m, 2H, $H_{k/j}$), 3.52 – 3.39 (m, 1H, $H_{r/q}$), 2.92 – 2.80 (m, 1H, $H_{o/p}$), 2.55 (m, 1H, $H_{o/p}$), 2.37 – 2.22 (m, 1H, $H_{o/p}$), 1.85 – 1.69 (m, 1H, $H_{o/p}$), 0.70 (s, 9H, H_n), -0.27 (s, 6H, H_l); **^{13}C NMR (300 MHz, DMSO) δ** 180.3 ($C_{u/s}$), 178.6 ($C_{s/u}$), 136.5 (C_{In}), 136.1 (C_{In}), 126.3 (C_{In}), 120.7 (C_{In}), 119.5 (C_{In}), 118.8 (C_{In}), 109.5 (C_{In}), 102.8 (C_{In}), 61.8 ($C_{k/j}$), 44.7 ($C_{j/k}$), 40.7 ($C_{q/r}$), 40.5 ($C_{r/q}$), 25.7 (C_n), 20.9 (C_m), 18.4 ($C_{o/p}$), 17.9 ($C_{o/p}$), -5.8 (C_l); **HRMS:** calcd for $C_{22}H_{31}N_2O_3Si^+$ $[M+H]^+$, 399.2104, found 399.2109.

7.2.18 6-(2-Hydroxyethyl)-4,5,6,10c-tetrahydropyrrolo[3,4-*c*]carbazole-1,3(2*H*,3a*H*)-dione (48)

To a dry 2-neck round bottom flask was added 6-{2-(*tert*-butyldimethylsilyloxy)ethyl}-4,5,6,10*c*-tetrahydropyrrolo[3,4-*c*]carbazole-1,3(2*H*,3a*H*)-dione (**60**) (256 mg, 0.642 mmol) and dissolved in THF (8 mL). The flask was placed in an ice bath and TBAF·3H_2O (1.01 g 3.21 mmol, 5 equiv) was added in one portion. The reaction mixture was stirred at RT under N_2 atmosphere for 30 min. CH_2Cl_2 (20 mL) was added to the reaction mixture and washed with $NaHCO_{3\ (sat)}$ (20 mL).

The aqueous layer was collected and extracted with CH_2Cl_2 (2 × 20 mL). The organic layers were then combined and washed with brine (50 mL) and dried over $MgSO_4$. After filtration the solvent was finally removed *in vacuo*. The crude product was purified by column chromatography (EtOAc/Hexane, 7:3) affording the product6-(2-hydroxyethyl)-4,5,6,10*c*-tetrahydropyrrolo[3,4-*c*]carbazole-1,3(2*H*,3a*H*)-dione (**48**) as a yellow solid (155 mg, 86%).

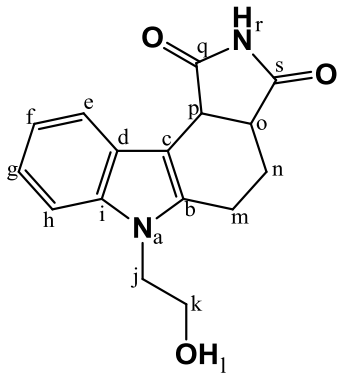

Mp = 166-169 º C; **R_f** = 0.39 (EtOAc/Hexane, 8:2); **IR (ATR, cm^{-1}):** 3421 (alcohol O-H str), 1704 (carbonyl C=O str), 740 (aromatic C-H); **^{1}H NMR (300 MHz, DMSO) δ** 10.97 (s, 1H, H_r), 7.74 (d, *J* = 7.5 Hz, 1H, $H_{h/e}$), 7.39 (d, *J* = 7.9 Hz, 1H, $H_{e/h}$), 7.12 – 6.97 (m, 2H, $H_{f\&g}$), 4.84 (s, 1H, H_l), 4.24 – 4.15 (m, 1H, $H_{p/o}$), 4.10 (m, 2H, $H_{j/k}$), 3.66 – 6.57 (m, 2H, $H_{k/j}$), 3.51 – 3.42 (m, 1H, $H_{o/p}$), 2.93 - 2.80 (d, *J* = 16.3 Hz, 1H, $H_{m/n}$), 2.60 – 2.52 (m, 1H, $H_{m/n}$), 2.35 – 2.24 (m, 1H, $H_{n/m}$), 1.90 – 1.73 (m, 1H, $H_{n/m}$);**^{13}C NMR (300 MHz, DMSO) δ** 180.4 ($C_{s/q}$), 178.7 ($C_{q/s}$), 136.6 (C_{In}) , 136.2 (C_{In}), 126.3 (C_{In}), 120.7 (C_{In}), 119.5 (C_{In}), 118.8 (C_{In}), 109.4 (C_{In}), 102.6 (C_{In}), 60.1 ($C_{k/j}$), 45.1 ($C_{j/k}$), 40.7 ($C_{o/p}$), 40.5 ($C_{p/o}$), 21.1 ($C_{n/m}$), 18.4 ($C_{m/n}$); **HRMS:** calcd for $C_{16}H_{17}N_2O_3^+$ $[M+H]^+$, 285.1239, found 285.1246.

7.2.19 6-(2-Hydroxyethyl)pyrrolo[3,4-*c*]carbazole-1,3(2*H*,6*H*)-dione (49)

A 2-neck round bottom flask charged with 6-(2-hydroxyethyl)-4,5,6,10c-tetrahydropyrrolo[3,4-*c*]carbazole-1,3(2*H*,3a*H*)-dione (**48**) (188 mg, 0.661 mmol)was evacuated under high vacuum and filled with Ar. Dry dioxane (15 mL) was then added, followed by MnO_2 (1.26 g, 14.5 mmol, 22 equiv). The reaction mixture was heated at reflux under a N_2 atmosphere overnight. Upon cooling to RT, the MnO_2 was removed by filtration through Celite. The solvent was then finally removed *in vacuo* and column chromatography (EtOAc/Hexane, 8:2) afforded the product 6-(2-hydroxyethyl)pyrrolo[3,4-*c*]carbozole-1,3(2*H*,6*H*)-dione (**49**) as a yellow solid (98 mg, 53%).

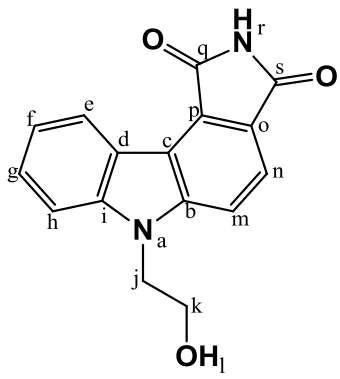

Mp = 322-324 º C; **R_f** = 0.57 (EtOAc/Hexane, 8:2); **IR (ATR, cm^{-1}):** 3372 (alcohol O-H str), 1710 (carbonyl C=O str), 747 (aromatic C-H); **^{1}H NMR (300 MHz, DMSO) δ** 11.15 (s, 1H, H_r), 8.87 (d, *J* = 7.8 Hz, 1H, H_{Car}), 8.01 (d, *J* = 8.3 Hz, 1H, H_{Car}), 7.84 (d, *J* = 8.3 Hz, 1H, H_{Car}), 7.75 (d, *J* = 8.2 Hz, 1H, H_{Car}), 7.62 (t, *J* = 7.6 Hz, 1H, $H_{g/f}$), 7.36 (t, *J* = 7.4 Hz, 1H, $H_{f/g}$), 4.90 (t, *J* = 4.9 Hz, 1H, H_l), 4.55 (d, *J* = 4.4 Hz, 2H, $H_{j/k}$), 3.82 (d, *J* = 4.8 Hz, 2H, $H_{k/j}$); **^{13}C NMR (300 MHz, DMSO) δ** 171.0 ($C_{q/s}$), 170.9 ($C_{s/q}$), 145.3 (C_{Car}), 142.9 (C_{Car}), 128.7 (C_{Car}), 127.3 (C_{Car}), 125.4 (C_{Car}),

124.5 (C_{Car}), 120.9 (C), 120.4 (C_{Car}), 119.9 (C_{Car}), 118.7 (C_{Car}), 115.2 (C_{Car}), 111.1 (C_{Car}), 60.2 ($C_{k/j}$), 46.4 ($C_{j/k}$); **HRMS:** calcd for $C_{16}H_{13}N_2O_3^+$ $[M+H]^+$, 281.0926, found 281.0937

7.2.20 1-(2-Propynyl)-2-vinyl-1*H*-indole (61)

A 2-neck round bottom flask charged with 2-vinyl-1*H*-indole (**41**) (505 mg, 3.53 mmol) was evacuated under high vacuum and filled with Ar. Dry DMF (80 mL) was then added followed by Cs_2CO_3 (3.45 g, 10.6 mmol, 3 equiv) and propargyl bromide (1.51 g, 10.6 mmol, 3 equiv). The reaction mixture was stirred at 60 °C for 2 d under N_2. Upon completion, the solution was diluted with EtOAc (50 mL) and washed with H_2O (3 × 50 mL). The organic layers were combined, washed with brine (150 mL) and dried over $MgSO_4$. Filtration was followed by removal of the solvent *in vacuo*. The crude product was purified by column chromatography (EtOAc/Hexane, 5:95) to obtain 1-(2-propynyl)-2-vinyl-1*H*-indole (**61**) as a yellow solid (0.29 g, 45%). The ^{1}H NMR spectrum of 1-(2-propynyl)-2-vinyl-1*H*-indole **(61**) was compared to that reported in the literature and corresponded well.[168]

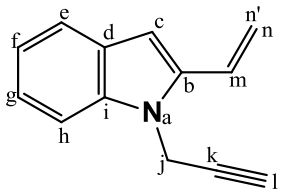

R_f= 0.68 (EtOAc/Hexane, 1:9);**^{1}H NMR (300 MHz, $CDCl_3$) δ** 7.59 (d, *J* = 7.8 Hz, 1H, $H_{e/h}$), 7.38 (d, *J* = 8.2 Hz, 1H, $H_{h/e}$), 7.26 (m, 1H, $H_{f/g}$), 7.13 (m, 1H, $H_{g/f}$), 6.90 (dd, *J* = 17.4, 11.2,Hz, 1H, H_m), 6.73 (s, 1H, H_c), 5.86 (dd, *J* = 17.4, 0.7 Hz, 1H, $H_{n'}$), 5.43 (dd, *J* = 11.2, 0.7 Hz, 1H, H_n), 4.90 (d, *J* = 2.4 Hz, 2H), 2.31 (t, J = 2.4 Hz, 1H, H_l).

7.2.21 6-(2-Propynyl)-4,5,6,10c-tetrahydropyrrolo[3,4-*c*]carbazole-1,3(2*H*,3a*H*)-dione (51)

1-(2-Propynyl)-2-vinyl-1*H*-indole (**61**) (114 mg, 0.629 mmol) and maleimide (92 mg 0.94 mmol, 1.5 equiv) were added neat to a small round bottom flask. The flask was placed in an oil bath preheated to 160 °C and the mixture solidified within a few seconds. The reaction was kept at this temperature for 30 min. TLC indicated some1-(2-propynyl)-2-vinyl-1*H*-indole remained unreacted. The crude product appeared as a brown solid (soluble in CH_2Cl_2) which was purified by column chromatography (EtOAc/Hexane, 3:7) affording 48 mg of the product 6-(2-propynyl)-4,5,6,10c-tetrahydropyrrolo[3,4-*c*]carbozole-1,3(2*H*,3a*H*)-dione (**51**) as a light yellow solid and recovering 40 mg of the starting reagent 1-(2-propynyl)-2-vinyl-1*H*-indole (**61**). The crude product also consists of 35 mg 6-(2-propynyl)-4,5,6,10c-tetrahydropyrrolo[3,4-*c*]carbazole-1,3(2*H*,3a*H*)-dione (**51**) of the product as a dark brown solid (insoluble in CH_2Cl_2) which requires no further purification (75 mg). Yield range from 35 – 58%.

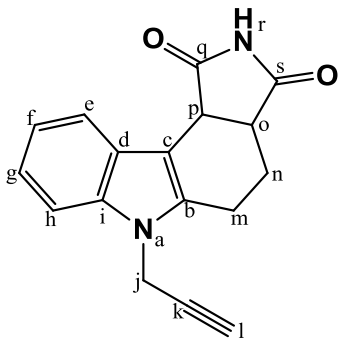

Mp = 252-254 ° C; **R_f**= 0.45 (EtOAc/Hexane, 4:8); **IR (ATR, cm^{-1}):** 3293 (amide N-H str), 1700 (carbonyl C=O str), 751 (aromatic C-H), 671 (alkyne -C≡C-H); **^{1}H NMR (300 MHz, DMSO) δ** 11.03 (s, 1H, H_r), 7.77 (d, *J* = 7.6 Hz, 1H, $H_{e/h}$), 7.49 (d, *J* = 7.9 Hz, 1H, $H_{h/e}$), 7.20 – 7.02 (m, 2H, $H_{g\&f}$), 5.00 (s, 2H, H_j), 4.21 (d, *J* = 7.7 Hz, 1H, $H_{p/o}$), 3.54 – 3.42 (m, 1H, $H_{o/p}$), 3.28 (s, 1H, H_l), 2.93 – 2.81 (m, 1H, H_m), 2.64 – 2.54 (m, 1H, $H_{m/n}$), 2.39 – 2.24 (m, 1H, $H_{n/m}$), 1.85 (dd, *J* = 14.1, 9.1 Hz, 1H, $H_{n/m}$); **^{13}C NMR (300 MHz, DMSO) δ** 180.7 ($C_{s/q}$), 179.0 ($C_{q/s}$), 136.3 (C_{In}), 136.1 (C_{In}), 126.8 (C_{In}), 121.7 (C_{In}), 120.2 (C_{In}), 119.8 (C_{In}), 109.9 (C_{In}), 104.4 (C_{In}), 79.9 (C_k), 75.2 (C_l), 41.1 ($C_{o/p/j}$), 40.9 ($C_{p/o/j}$), 32.2 ($C_{j/o/p}$), 21.4 ($C_{n/m}$), 18.5 ($C_{m/n}$); **HRMS:** calcd for $C_{17}H_{15}N_2O_2^+$ $[M+H]^+$, 279.1134, found 279.1126.

7.2.22 6-(2-Propynyl)pyrrolo[3,4-*c*]carbozole-1,3(2*H*,6*H*)-dione (52)

To a 2-neck round bottom flask was added 6-(2-propynyl)-4,5,6,10c-tetrahydropyrrolo[3,4-*c*]carbozole-1,3(2*H*,3a*H*)-dione (**51**) (120 mg, 0.43 mmol). Dry dioxane (15 mL) was then added followed by MnO_2 (0.825, 9.49 mmol, 22 equiv). The reaction mixture was then heated to reflux for 8 h. Upon completion and cooling to RT, the dioxane was removed *in vacuo*. The crude product was triturated with CH_2Cl_2 and acetone affording 6-(2-propynyl)pyrrolo[3,4-*c*]carbozole-1,3(2*H*,6*H*)-dione (**52**) as a yellow solid (92 mg, 72%). No further purification was required.

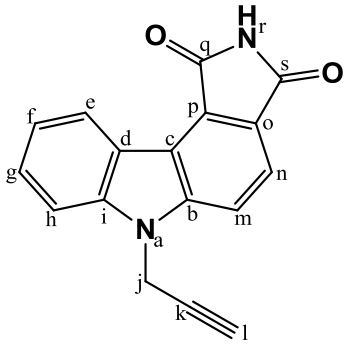

Mp = 278-280 ºC; **R_f**= 0.84 (EtOAc/Hexane, 7:3); **IR (ATR, cm^{-1}):** 3271 (amide N-H str), 1720, 1701 (carbonyl C=O str), 745 (aromatic C-H), 657 (alkyne -C≡C-H); **^{1}H NMR (300 MHz, DMSO) δ** 11.22 (s, 1H, H_r), 8.87 (d, *J* = 7.9 Hz, 1H, $H_{e/h}$), 8.08 (d, *J* = 8.3 Hz, 1H, $H_{n/m}$), 7.90 (d, *J* = 8.3 Hz, 1H, $H_{n/m}$), 7.83 (d, *J* = 8.2 Hz, 1H, $H_{e/h}$), 7.67 (m, 1H, $H_{f/g}$), 7.40 (m, 1H, $H_{g/f}$), 5.46 (s, 2H, H_j), 3.56 (s, 1H, H_l); **^{13}C NMR (300 MHz, DMSO) δ** 170.1 ($C_{q/s}$), 170.1 ($C_{s/q}$), 143.6 (C_{Car}), 141.3 (C_{Car}), 128.4 (C_{Car}), 126.9 (C_{Car}), 125.0 (C_{Car}), 124.7 (C_{Car}), 121.0 (C_{Car}), 120.1(C_{Car}), 119.8 (C_{Car}), 118.5 (C_{Car}), 114.3 (C_{Car}), 110.3 (C_{Car}), 78.44 (C_k), 75.1 (C_l), 32.4 (C_j); **HRMS:** calcd for $C_{17}H_{11}N_2O_2^+$ $[M+H]^+$, 275.0821 , found 275.0316.

7.2.23 3-(2-Vinyl-1*H*-indol-1-yl)propanenitrile (62)

A 2-neck round bottom flask charged with 2-vinyl-1*H*-indole (**41**) (750 mg, 5.24 mmol) was evacuated under high vacuum and filled with Ar. Dry MeCN (20 mL) was added and the solution was treated with acrylonitrile (2.40 mL, 36.7 mmol, 7 equiv), followed by 1.8-diazabicyclo[5.4.0]under-7-ene (20 drops). The reaction mixture was stirred at RT under a N_2 atmosphere for 8 h. The solution was then diluted with H_2O (30 mL) and extracted with EtOAc (30 mL). The organic layer was washed with brine (50 mL) and dried over $MgSO_4$. The drying salts were then filtered off and the solvent was finally removed *in vacuo.* The crude product was purified by column chromatography (EtOAc/Hexane, 1:9) affording 3-(2-vinyl-1*H*-indol-1-yl)propanenitrile (**62**) as an opaque solid (750 mg) and recovering 98 mg of 2-vinyl-1*H*-indole (**41**). Yield: 73% (84% brsm).

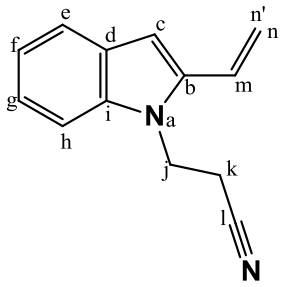

Mp = 83-85 ºC; $\mathbf{R_f}$= 0.22 (EtOAc/Hexane, 1:9);**IR (ATR, cm^{-1}):** 2247 (nitrile C≡N str), 786, 748 (alkene =C-H), 735(aromatic C-H); **^{1}H NMR (400 MHz, $CDCl_3$) δ** 7.59 (d, *J* = 7.8 Hz, 1H, $H_{e/h}$), 7.29 – 7.20 (m, 2H, $H_{f/g\&e/h}$), 7.16 – 7.11 (m, 1H, $H_{f/g}$), 6.76 (dd, J = 17.3, 11.2, 1H, H_m), 6.72 (s, 1H, H_c), 5.86 (d, *J* = 17.3 Hz, 1H, $H_{n'}$), 5.44 (d, *J* = 11.2 Hz, 1H, H_n), 4.47 (t, *J* = 7.2 Hz, 2H, H_j), 2.73 (t, *J* = 7.2 Hz, 2H, H_k); **^{13}C NMR (400 MHz, $CDCl_3$) δ** 137.6 (C), 136.7 (C), 128.4 (C), 125.0 (C), 122.6 (C), 121.2 (C), 120.8 (C), 118.1 (C), 117.1 (C), 108.8 (C), 100.8 (C), 39.0 ($C_{j/k}$), 18.6 ($C_{k/j}$); **HRMS:** calcd for $C_{13}H_{13}N_2^+$ $[M+H]^+$, 197.1079, found 197.1072.

7.2.24 3-{1,3-Dioxo-1,2,3,3a,4,5-hexahydropyrrolo[3,4-*c*]carbazol-6(10c*H*)-yl}-propanenitrile (50)

To a solution of 3-(2-vinyl-1*H*-indol-1-yl)propanenitrile (**62**) (280 mg, 1.43 mmol) in toluene (15 mL) was added maleimide (208 mg, 2.14 mmol, 1.5 equiv) and $SnCl_2$ (5.41 mg, 0.03 mmol, 0.02 equiv). The reaction mixture was then heated to reflux under N_2 for 16 h. Upon completion, the reaction mixture was allowed to reach RT. $NaHCO_{3\,(sat)}$ (30 mL) was added to the mixture and it was extracted with CH_2Cl_2 (2 × 30 mL). The combined organic layers were then washed with brine (80 mL) and dried over $MgSO_4$. After filtration of the drying salts the solvent was finally removed *in vacuo*. The crude product was purified by column chromatography (EtOAc/Hexane, 1:1). 50 mg of 3-(2-vinyl-1*H*-indol-1-yl)propanenitrile(**62**)was recovered and the product 3-{1,3-Dioxo-1,2,3,3a,4,5-hexahydropyrrolo[3,4-*c*]carbazol-6(10c*H*)-yl}propanenitrile (**50**) was obtained as a yellow solid (243 mg). Yield: 58% (71% brsm).

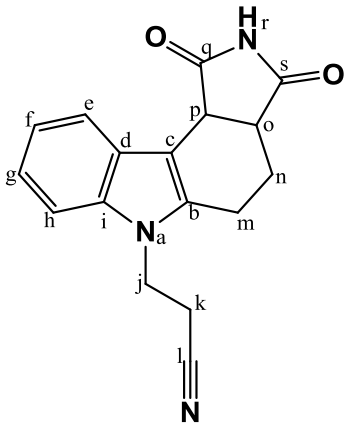

Mp = 160-162 ºC; **R_f**= 0.21 (EtOAc/Hexane, 6:4); **IR (ATR, cm^{-1}):** 2246 (nitrile C≡N str), 1703 (carbonyl C=O), 734 (aromatic C-H); **^{1}H NMR (300 MHz, DMSO) δ** 11.02 (s, 1H, H_r), 7.76 (d, *J* = 7.5 Hz, 1H, $H_{e/h}$), 7.51 (d, *J* = 8.0 Hz, 1H, $H_{h/e}$), 7.17 – 7.02 (m, 2H, $H_{f\&g}$), 4.43 (t, *J* = 6.3 Hz, 2H, $H_{j/k}$), 4.21 (d, *J* = 8.0 Hz, 1H, $H_{p/o}$), 3.54 – 3.43 (m, 1H, $H_{o/p}$), 2.92 (t, *J* = 6.3 Hz, 2H, $H_{k/j}$), 2.88 – 2.82 (m, 1H, H_m), 2.67 – 2.55 (m, 1H, $H_{m/n}$), 2.38 – 2.25 (m, 1H, $H_{n/m}$), 1.90 – 1.75 (m, 1H, $H_{n/m}$); **^{13}C NMR (300 MHz, DMSO) δ** 180.3 ($C_{q/s}$), 178.5 ($C_{q/s}$), 135.9 ($C_{In/l}$), 135.7 ($C_{In/l}$), 126.5 ($C_{In/l}$), 121.1 ($C_{In/l}$), 119.7 ($C_{In/l}$), 119.4 ($C_{In/l}$), 118.9 ($C_{In/l}$), 109.5 ($C_{In/l}$), 103.7 ($C_{In/l}$), 40.6 ($C_{o/p/j}$), 38.7 ($C_{j/o/p}$), 38.0 ($C_{p/o/j}$), 21.1 ($C_{m/n/k}$), 18.2 ($C_{m/n/k}$), 18.0 ($C_{m/n/k}$); **HRMS:** calcd for $C_{17}H_{16}N_3O_2^+$ $[M+H]^+$, 294.1243, found 294.1253.

7.2.25 3-{1,3-Dioxo-2,3-dihydropyrrolo[3,4-*c*]carbazol-6(1*H*)-yl}propanenitrile (53)

To a 2-neck round bottom flask, under an Ar atmosphere, was added 3-{1,3-Dioxo-1,2,3,3a,4,5-hexahydropyrrolo[3,4-*c*]carbazol-6(10c*H*)-yl}propanenitrile (490 mg, 1.67 mmol). Dry dioxane (20 mL) was added followed by MnO_2 (3.20 g, 36.8 mmol, 22 equiv). The reaction mixture was then heated to reflux for 8 h under N_2. Upon completion and cooling to RT, the dioxane was removed *in vacuo*. The crude product was recrystallized from DMF. The yellow solid was collected, washed with hexane, and dried under high vacuum (145 mg, 30 %).

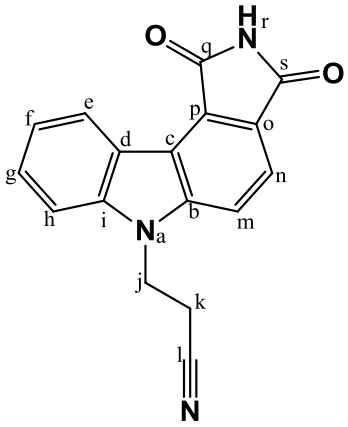

Mp = 298-300 ºC; **R_f** = 0.32 (EtOAc/Hexane, 6:4); **IR (ATR, cm^{-1}):** 2251 (nitrile C≡N str), 1716, 1697 (carbonyl C=O), 747 (aromatic C-H); **^{1}H NMR (300 MHz, DMSO) δ** 11.21 (s, 1H, H_r), 8.88 (d, *J* = 7.8 Hz, 1H, $H_{e/h}$), 8.16 (d, *J* = 8.3 Hz, 1H, $H_{e/h/m/n}$), 7.88 (d, *J* = 8.5 Hz, 2H, $H_{e/h/m/n}$), 7.69 – 7.60 (m, 1H, $H_{f/g}$), 7.44 – 7.35 (m, 1H, $H_{f/g}$), 4.89 (t, *J* = 6.3 Hz, 2H, $H_{j/k}$), 3.10 (t, *J* = 6.2 Hz, 2H, $H_{k/j}$); **^{13}C NMR (300 MHz, DMSO) δ** 170.1 ($C_{q/s}$) , 170.1 ($C_{s/q}$), 143.8 (C_{Car}), 141.4 C_{Car}), 128.3 (C_{Car}), 126.8 (C_{Car}), 124.9 (C_{Car}), 124.5 (C_{Car}), 120.9 (C_{Car}), 120.0 (C_{Car}), 119.6 (C_{Car}), 118.7 (C_{Car}), 118.3 (C_{Car}), 114.4 (C_{Car}), 110.3 (C_{Car}), 38.6 ($C_{j/k}$), 17.0 ($C_{k/j}$); **HRMS:** calcd for $C_{17}H_{12}N_3O_2^+$ $[M+H]^+$, 290.0930 , found 290.0928.

7.2.26 1-Benzyl-1*H*-pyrrole-2,5-dione (64)

To a 2-neck round bottom flask was added maleic anhydride (280 mg, 2.86 mmol) and dissolved in AcOH (10 mL). Benzylamine (0.25 mL, 2.3 mmol, 0.8 equiv) was then added and the reaction mixture was heated to reflux for 2 h.

The solvent was removed under reduced pressure and the crude product was purified by column chromatography (EtOAc/Hexane, 3:7) affording the product 1-benzyl-1*H*-pyrrole-2,5-dione as a white solid (330 mg, 62%). The ^{1}H NMR spectrum of 1-benzyl-1*H*-pyrrole-2,5-dionewas compared to that reported in the literature and corresponded well.[173]

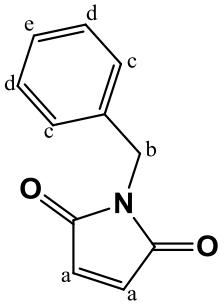

Rf= 0.85 (EtOAc/Hexane, 4:6), **^{1}H NMR (300 MHz, $CDCl_3$) δ** 7.24 (m, 5H, H_{Ar}), 6.64 (s, 2H, H_a), 4.61 (s, 2H, H_b).

7.2.27 2-Benzylpyrrolo[3,4-*c*]carbazole-1,3(2*H*,6*H*)-dione (65)

2-Vinyl-1*H*-indole (**41**) (96 mg, 0.67 mmol) and 1-benzyl-1*H*-pyrrole-2,5-dione(125 mg, 0.668 mmol, 1 equiv) were added neat to a small round bottom flask. The flask was placed in an oil bath preheated to 140 °C and stirred for 40 min. The crude product was dissolved in dry dioxane (10 mL) and transferred to a 2-neck round bottom flask. MnO_2 (695 mg, 7.99 mmol, 22 equiv) was then added to the solution and heated to reflux for 5 h. The Mn_2O was then filtered off through Celite and the solvent was finally removed *in vacuo*. The crude product was purified by column chromatography (EtOAc/Hexane, 3:7) affording the product 2-benzylpyrrolo[3,4-*c*]carbazole-1,3(2*H*,6*H*)-dione (**65**) as a yellow solid (120 mg, 84%).

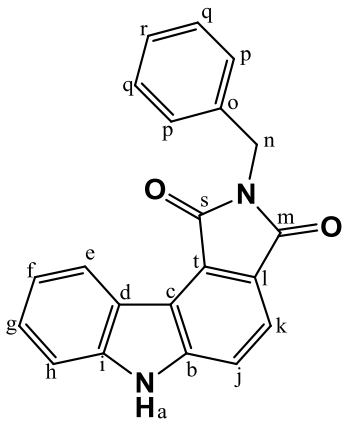

Mp = 257-258 ºC; **R_f** = 0.73 (EtOAc/Hexane, 1:1); **IR (ATR, cm^{-1}):** 3287 (2° amine, N-H str), 2927 (alkanes C-H str), 1683 (carbonyl, C=O str), 749, 715, 692 (aromatics C-H); (**^{1}H NMR (400 MHz, DMSO) δ** 12.10 (s, 1H, H_a), 8.79 (d, *J* = 7.3 Hz, 1H, $H_{e/h}$), 7.83 (d, *J* = 6.5 Hz, 2H, H_{Car}), 7.63 – 7.52 (m, 2H, $H_{f\&g}$), 7.39 – 7.21 (m, 6H, $H_{Ar\&Car}$), 4.82 (s, 2H, H_n); **^{13}C NMR (400 MHz, DMSO) δ** 169.4 ($C_{s/m}$), 169.4 ($C_{m/s}$), 144.9 ($C_{Ar/Car}$), 142.3 ($C_{Ar/Car}$), 137.8 ($C_{Ar/Car}$), 129.3 (2C,$C_{q/p}$), 129.0 ($C_{Ar/Car}$), 128.1 (2C, $C_{p/q}$), 128.0 ($C_{Ar/Car}$), 126.2 ($C_{Ar/Car}$), 125.3 ($C_{Ar/Car}$), 123.1 ($C_{Ar/Car}$), 120.9 ($C_{Ar/Car}$), 120.5 ($C_{Ar/Car}$), 120.4 ($C_{Ar/Car}$), 119.1 ($C_{Ar/Car}$), 116.3 ($C_{Ar/Car}$), 112.4 ($C_{Ar/Car}$), 41.4 (C_n); **HRMS:** calcd for $C_{21}H_{15}N_2O_2^+$ [M+H], 327.1134, found 327.1131.

7.2.28 3-{2-Benzyl-1,3-dioxo-2,3-dihydropyrrolo[3,4-*c*]carbazol-6(1*H*)-yl}propanenitrile (66)

A 2-neck round bottom flask charged with 2-benzylpyrrolo[3,4-*c*]carbazole-1,3(2*H*,6*H*)-dione (**65**) (60 mg, 0.18 mmol) was evacuated under high vacuum and filled with Ar. Dry benzene (2 mL) was added and the solution was treated with NaOH (50%, 1 mL), followed by tetra-*N*-butyl ammonium hydrogen sulfate (31 mg, 0.092 mmol, 0.5 equiv). The colour of the solution changed from yellow to dark red. 3-bromopropionitrile (0.02 mL, 0.2 mmol, 1.1 equiv) was then added and the reaction mixture was stirred for 14 h at RT. On addition of the bromopropionitrile, the colour of the solution changed to yellow, then red and finally to orange. Once completed, the reaction mixture was diluted in CH_2Cl_2 (5 mL), washed with brine (10 mL) and dried over $MgSO_4$. The drying salts were filtered off and the solvent was finally removed *in vacuo*. The crude product was purified by column chromatography (EtOAc/Hexane, 3:7) affording the product 3-{2-benzyl-1,3-dioxo-2,3-dihydropyrrolo[3,4-*c*]carbazol-6(1*H*)-yl}propanenitrile (**66**)as a yellow solid (42 mg, 60 %).

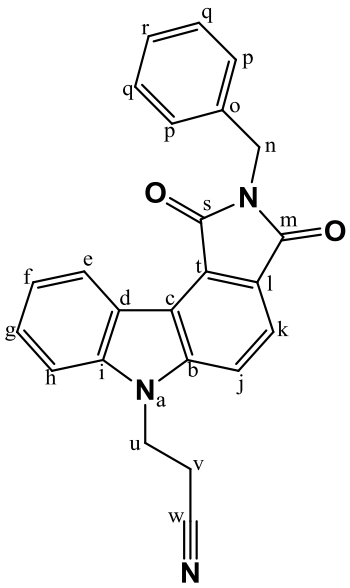

Mp = 200-202 ºC; **R_f**= 0.69 (EtOAc/Hexane, 4:6); **IR (ATR, cm^{-1}):** 2949 (alkanes C-H str), 2251 (nitrile C≡N str), 1696 (carbonyl, C=O str), 744, 702 (aromatics C-H); **^{1}H NMR (400 MHz, DMSO) δ** 8.81 (dd, *J* = 7.8, 4.0 Hz, 1H, $H_{e/h}$), 8.10 (dd, *J* = 8.3, 4.5 Hz, 1H, $H_{e/h}$), 7.89 (dd, *J* = 8.3, 4.5 Hz, 1H, $H_{g/h}$), 7.83 (dd, *J* = 7.8, 4.5 Hz, 1H, $H_{g/h}$), 7.63 (dd, *J* = 11.7, 7.4 Hz, 1H, $H_{k/j}$), 7.42 – 7.30 (m, 5H, H_{Ar}), 7.29 –7.23 (m, 1H, $H_{k/j}$), 4.91 – 4.76 (m, 4H, $H_{u\&n}$), 3.13 – 3.04 (m, 2H, H_v); **^{13}C NMR (400 MHz, DMSO) δ** 169.1 ($C_{s/m}$), 169.1 ($C_{m/s}$), 144.6 ($C_{Ar/Car}$), 142.1 ($C_{Ar/Car}$), 137.7 ($C_{Ar/Car}$), 129.3 (2C, $C_{q/p}$), 129.2 (2C, $C_{p/q}$), 128.1 ($C_{Ar/Car}$), 128.1 ($C_{Ar/Car}$), 126.2 ($C_{Ar/Car}$), 125.5 ($C_{Ar/Car}$), 123.8 ($C_{Ar/Car}$), 121.6 ($C_{Ar/Car}$), 120.5 ($C_{Ar/Car}$), 120.5 ($C_{Ar/Car}$), 119.4 ($C_{Ar/Car}$), 119.2 ($C_{Ar/Car}$), 115.0 ($C_{Ar/Car}$), 111.0 ($C_{Ar/Car}$), 65.7 ($C_{Ar/Car}$), 41.5 ($C_{u/n}$), 39.2 ($C_{n/u}$), 18.6 ($C_{Ar/Car}$), 17.7 (C_v); **HRMS:** calcd for $C_{24}H_{18}N_3O_2^+$ [M+H], 380.1399, found 380.1401.

7.3 Experimental work pertaining to chapter 4

7.3.1 Synthesis of the 'double click' products using NH-maleimides

7.3.1.1 3,4-Dichlorofuran-2,5-dione (69)

A 2-neck round bottom flask charged with maleic anhydride (**68**) (2.00 g, 20.4 mmol) was evacuated under high vacuum and filled with Ar (× 3). $SOCl_2$ (20 mL) was added to the flask and it was placed in an ice bath. The reaction mixture was stirred under a N_2 atmosphere while adding pyridine (3.31 g, 41.8 mmol, 2.05 equiv) drop-wise to the solution at 0 °C. During this time the colour of the solution changed from orange to dark brown as more pyridine was added. The ice bath was then removed and the temperature increased to 75 °C. The reaction mixture was stirred at this temperature for 20 min. Upon removal of the $SOCl_2$*in vacuo*, a solid residue formed. The solid was then triturated with benzene (× 4) and filtered. The benzene filtrate was collected and the solvent removed under reduced pressure. The product 3,4-dichlorofuran-2,5-dione (**69**) was obtained as a yellow solid (2.39 g, 70%) which required no further purification. The ^{13}C NMR spectrum of 3,4-dichlorofuran-2,5-dione (**69**) was compared to that reported in literature and corresponded well.[177]

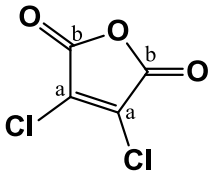

^{13}C NMR (400 MHz, DMSO) δ 162.0 (2C, C_b), 130.4 (2C, C_a).

7.3.1.2 3,4-Dichloro-1*H*-pyrrole-2,5-dione (70)

3,4-Dichlorofuran-2,5-dione (**69**) (1.50 g, 8.98 mmol), urea (567 mg, 9.43 mmol, 1.05 equiv) and NaCl (1.84 g, 31. 4 mmol, 3.5 equiv) were added to a mortar and mixed by grinding the solids together with a pestle.The mixture was added to a round bottom flask and reacted under N_2 atmosphere. The flask was placed in an oil bath and the temperature increased to 120 °C. As the temperature increased, the solids fused together. The reaction mixture was left at this temperature for 20 min followed by a methanol-water (2:1 v/v) recrystallization. The precipitate was collected and washed with hexane, affording the product 3,4-dichloro-1*H*-pyrrole-2,5-dione as a brown solid (855 mg, 57%). No further purification was required. The ^{1}H NMR spectrum of 3,4-dichloro-1*H*-pyrrole-2,5-dione (**70**) was compared to that reported in literature and corresponded well.[178]

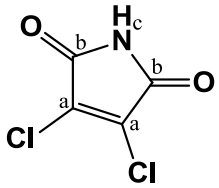

R_f= 0.22 (EtOAc/Hexane, 1:9); **^{1}H NMR (400 MHz, DMSO) δ** 11.71 (s, H_c).

7.3.1.3 3-Azido-4-chloro-1*H*-pyrrolo -2,5-dione (71)

3,4-Dichloro-1*H*-pyrrole-2,5-dione (**70**) (200 mg, 1.21 mmol) was added to a 2-neck round bottom flask and dissolved in acetone (12 mL). NaN_3 (78.3 mg, 1.21 mmol, 1 equiv) was dissolved in H_2O (3 mL) and added to the flask. The reaction mixture was stirred at RT overnight under a N_2 atmosphere. Upon completion, the acetone was removed *in vacuo*. The solution was then diluted with H_2O (15 mL) and extracted with CH_2Cl_2 (2 × 15 mL). The organic layers were combined, washed with brine (30 mL) and dried over $MgSO_4$. The drying salts were then filtered off and the solvent was finally removed under reduced pressure. The crude product was purified by column chromatography (EtOAc/Hexane, 1:9) affording the product 3-azido-4-chloro-1*H*-pyrrolo -2,5-dione (**71**) as a light yellow solid (164 mg, 79%).

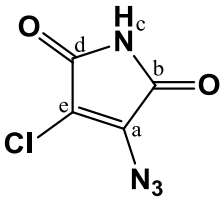

Mp = 125-127 ºC; **R_f**= 0.39 (EtOAc/Hexane, 2:8); **IR (ATR, cm^{-1}):** 3199 (N-H str), 2149 (N_3 str), 1714 (C=O str), 659 (C-Cl str); **^{1}H NMR (400 MHz, DMSO) δ** 11.46 (s, H_c); **^{13}C NMR (400 MHz, DMSO) δ** 165.1 ($C_{b/d}$), 164.9 ($C_{b/d}$), 136.7 (C_e), 111.0 (C_a); **HRMS:** calcd for C4H2ClN4O2$^+$ $[M+H]^+$, 172.9866, found 172.9700.

7.3.1.4 3,4-Diazido-1*H*-pyrrolo -2,5-dione (72)

3,4-Dichloro-1*H*-pyrrole-2,5-dione (**70**) (120 mg, 0.723 mmol) was added to a 2-neck round bottom flask and dissolved in acetone (8 mL). NaN_3 (141 mg, 2.17 mmol, 3 equiv) was dissolved in H_2O (2 mL) and added to the flask. The reaction mixture was stirred at RT overnight under a N_2 atmosphere. Upon completion, the acetone was removed *in vacuo*. The solution was then diluted with H_2O (15 mL) and extracted with CH_2Cl_2 (2 × 15 mL). The organic layers were combined, washed with brine (30 mL) and dried over $MgSO_4$. The drying salts were then filtered off and the solvent was finally removed under reduced pressure. The crude product was purified by column chromatography (EtOAc/Hexane, 1:9) affording the product 3,4-diazido-1*H*-pyrrolo -2,5-dione (**72**) as a yellow solid (86 mg, 66%).

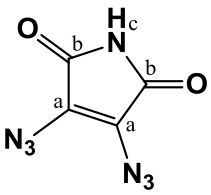

Mp = 105-106 ºC; **R_f =** 0.46 (EtOAc/Hexane, 2:8); **IR (ATR, cm^{-1}):** 3209 (N-H str), 2088 (N_3 str), 1699 (C=O str);**^{1}H NMR (400 MHz, DMSO) δ** 11.28 (s, H_c); **^{13}C NMR (400 MHz, DMSO) δ** 166.4 (C_b), 120.0 (C_a); **HRMS:** calcd for $C_4H_2N_7O_2^+$ $[M+H]^+$, 180.0270. The MS technique utilized did not result in detection of the molecular ion of compound **72**.

7.3.1.5 3,4-bis(4-Phenyl-1*H*-1,2,3-triazol-1-yl)-1*H*-pyrrole-2,5-dione (73)

3,4-Diazido-1*H*-pyrrolo-2,5-dione (**72**) (56 mg, 0.31 mmol) and phenyl acetylene (0.14 mL, 1.3 mmol, 4 equiv) were added to a 2-neck round bottom flask and dissolved in MeOH (2 mL). $CuSO_4$•$5H_2O$ (6.2 mg, 0.025 mmol, 0.08 equiv) and Na ascorbate (50 mg, 0.25 mmol, 0.8 equiv) were then dissolved in H_2O (1 mL) and added to the reaction mixture. The solution became cloudy in colour and was stirred for 2 d at 40 °C under a N_2 atmosphere. During this time, TLC monitoring indicated unreacted starting reagents and no further reaction of the materials could be observed at longer reaction time. The MeOH was then removed *in vacuo* and the reaction mixture was diluted with CH_2Cl_2 (10 mL). The solution was then washed with H_2O (5 mL), $NH_4Cl_{(sat)}$ (5 mL), brine (20 mL) and dried over $MgSO_4$. Filtration of the drying salts was followed by removal of the solvent under reduced pressure. Column chromatography (EtOAc/Hexane, 2:8) afforded trace amounts of the product 3,4-bis(4-Phenyl-1*H*-1,2,3-triazol-1-yl)-1*H*-pyrrole-2,5-dione (**73**) as a yellow solid.

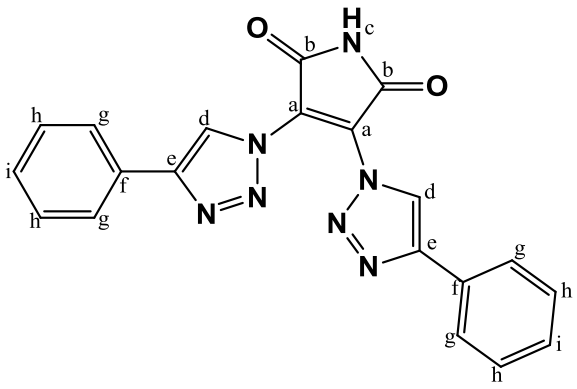

R_f = 0.29 (EtOAc/Hexane, 2:8); **^{1}H NMR (300 MHz, DMSO) δ** 11.28 (s, 1H, H_c), 8.75 (s, 2H, H_d), 7.93 (d, *J* = 7.5 Hz, 4H, H_g), 7.84 – 7.28 (m, 6H, $H_{h\&i}$); **^{13}C NMR (300 MHz, DMSO) δ** 167.3 (2C, C_b), 140.6 (2C, C_d), 130.3 (2C), 128.9 (4C, $C_{g/h}$), 128.1 (2C), 125.4 (4C, $C_{g/h}$), 121.1 (2C).

7.3.2 Synthesis of the 'double click' product using NMe-maleimides

7.3.2.1 3,4-Dichloro-1-methyl-1*H*-pyrrole-2,5-dione (75)

To a 2-neck round bottom flask was added 3,4-dichlorofuran-2,5-dione(**69**) (300 mg, 1.80 mmol) and glacial acetic acid (15 mL). The solution was stirred under a N_2 atmosphere and the flask was placed in an ice bath. Methylamine hydrochloride (133 mg, 1.98 mmol, 1.1 equiv) followed by NaOMe (107 mg, 1.98 mmol, 1.1 equiv) were then added to the solution. The reaction mixture was heated to reflux and stirred for 4 h. Once the reaction mixture cooled to RT the solution appeared orange in colour with some precipitate formation. The acetic acid was then removed *in vacuo* and EtOAc (15 mL) was added to the reaction mixture.

The solution was then washed with H_2O (15 mL) and the aqueous layer extracted with EtOAc (2 × 15 mL). The organic layers were combined, washed with brine (30 mL) and dried over $MgSO_4$. The drying salts were then filtered off and the solvent was finally removed under reduced pressure. The crude product was purified by column chromatography (EtOAc/Hexane, 1:9) affording the product 3,4-dichloro-1-methyl-1*H*-pyrrole-2,5-dione (**75**) as an off-white solid (201 mg, 62%). The ^{1}H NMR spectrum of 3,4-dichloro-1-methyl-1*H*-pyrrole-2,5-dione (**75**) was compared to that reported in literature and corresponded well.[180]

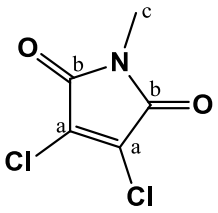

R_f = 0.51 (EtOAc/Hexane, 1:9);**^{1}H NMR (400 MHz, DMSO) δ** 2.95 (s, 3H, H_c).

7.3.2.2 3-Azido-4-chloro-1-methyl-1*H*-pyrrole-2,5-dione (76)

3,4-dichloro-1-methyl-1*H*-pyrrole-2,5-dione (**75**) (200 mg, 1.11 mmol) was added to a 2-neck round bottom flask and dissolved in acetone (4 ml). NaN_3 (72.2 mg, 1.11 mmol, 1 equiv) was dissolved in H_2O (1 mL) and added to the flask. The reaction mixture was stirred at RT overnight under a N_2 atmosphere. Upon completion, the acetone was removed *in vacuo*. The solution was then diluted with H_2O (10 mL) and extracted with CH_2Cl_2 (2 × 15 mL). The organic layers were combined, washed with brine (30 mL) and dried over $MgSO_4$. The drying salts were then filtered off and the solvent was finally removed under reduced pressure. The crude product was purified by column chromatography (EtOAc/Hexane, 1:9) affording the product 3-azido-4-chloro-1-methyl-1*H*-pyrrole-2,5-dione (**76**) as an off-white solid (189 mg, 98%).

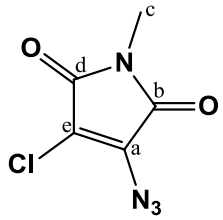

Mp = 110-112 ºC; **R_f =** 0.58 (EtOAc/Hexane, 2:8); **IR (ATR, cm^{-1}):** 2149, 2115 (N_3 str), 1705 (C=O str), 1642 (alkene C=C str), 733 (C-Cl str); **^{1}H NMR (400 MHz, $CDCl_3$) δ** 3.07 (s, 3H, $H_{\text{-NMe}}$).**^{13}C NMR (400 MHz, $CDCl_3$) δ** 164.2 ($C_{b/d}$), 164.1 ($C_{d/b}$), 135.79 (C_e), 113.1 (C_a), 24.7 (C_c); **HRMS:** calcd for $C_5H_4N_4ClO_2i^+$ $[M+H]^+$, 187.0023. The MS technique utilized did not result in detection of the molecular ion of compound **76**.

7.3.2.3 3,4-Diazido-1-methyl-1*H*-pyrrole-2,5-dione (77)

3,4-Dichloro-1-methyl-1*H*-pyrrole-2,5-dione (**75**) (200 mg, 1.15 mmol) was added to a 2-neck round bottom flask and dissolved in acetone (4 mL). NaN_3 (225 mg, 3.46 mmol, 3 equiv) was dissolved in H_2O (1 mL) and added to the flask.

The reaction mixture was stirred at RT overnight under a N_2 atmosphere. Upon completion, the acetone was removed *in vacuo*. The solution was then diluted with H_2O (10 mL) and extracted with CH_2Cl_2 (2 × 15 mL). The organic layers were combined, washed with brine (30 mL) and dried over $MgSO_4$. The drying salts were then filtered off and the solvent was finally removed under reduced pressure. The crude product was purified by column chromatography (EtOAc/Hexane, 1:9) affording the product 3,4-diazido-1-methyl-1*H*-pyrrole-2,5-dione (**77**) as a yellow solid (146 mg, 68 %).

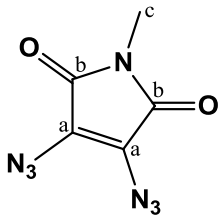

Mp = 55-58 ºC; **R_f** = 0.58 (EtOAc/Hexane, 2:8); **IR (ATR, cm^{-1}):** 2096, 2049(N_3 str);**^{1}H NMR (300 MHz, $CDCl_3$) δ** 3.02 (s, 3H, H_c);**^{13}C NMR (300 MHz, $CDCl_3$) δ** 164.8 (C_b), 119.8(C_a), 24.2 (C_c); **HRMS:** calcd for (compound -2N_2) $C_5H_4N_3O_2^+$ $[M+H]^+$, 138.0304, found 138.0315.

7.3.2.4 1-Methyl-3,4-bis(4-phenyl-1*H*-1,2,3-triazol-1-yl)-1*H*-pyrrole-2,5-dione (78)

3,4-Diazido-1-methyl-1*H*-pyrrole-2,5-dione (**77**)(50 mg, 0.26 mmol) and phenyl acetylene (0.06 mL, 1.3 mmol, 2.2 equiv) were added to a 2-neck round bottom flask and dissolved in MeOH (2 mL). $CuSO_4.5H_2O$ (2.6 mg, 0.010 mmol, 0.04 equiv) and Na ascorbate (21 mg, 0.10 mmol, 0.4 equiv) were then dissolved in H_2O (1 mL) and added to the reaction mixture. The solution became cloudy in colour and was stirred for 2 d at 40 °C under a N_2 atmosphere. During this time, TLC monitoring indicated unreacted starting reagents and no further reaction of the materials could be observed at longer reaction times. The MeOH was removed *in vacuo* and the reaction mixture was diluted with CH_2Cl_2 (10 mL). The solution was then washed with H_2O (5 mL), NH_4Cl $_{(sat)}$ (5 mL), brine (10 mL) and dried over $MgSO_4$. Filtration of the drying salts was followed by removal of the solvent under reduced pressure. Column chromatography (EtOAc/Hexane, 4:6) afforded trace amounts of the product 1-methyl-3,4-bis(4-phenyl-1*H*-1,2,3-triazol-1-yl)-1*H*-pyrrole-2,5-dione (**78**) as a yellow solid.

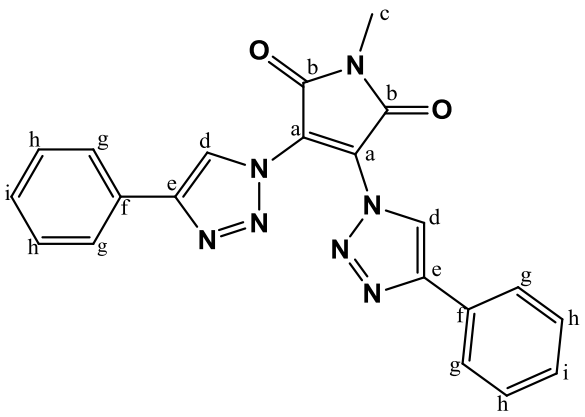

R_f = 0.33 (EtOAc/Hexane, 1:1);**^{1}H NMR (400 MHz, $CDCl_3$) δ** 8.75 (s, 2H, H_d), 7.94 (d, *J* = 7.0 Hz, 4H, H_g), 7.47 (m, 4H, H_h), 7.37 (m, 2H, H_i), 2.94 (s, 3H, H_c).

7.3.3 Synthesis of the 'double click' product using dialkynylated maleimides

7.3.3.1 3,4-Dibromomaleic anhydride (79)

A solution of maleic anhydride (**68**) (750 mg, 7.65 mmol), $AlCl_3$ (14 mg, 0.11 mmol, 0.014 equiv), and Br_2 (0.750 mL, 15.3 mmol, 2 equiv) was added to a Schlenk tube under an Ar atmosphere and sealed. The flask was placed in an oil bath preheated to 120 ° C and stirred for 16 h. The reaction mixture was left to reach RT and diluted with EtOAc (30 mL). It was then filtered and the filtrate was concentrated *in vacuo*. $CHCl_2$ (20 mL) was then added and the product (**79**) precipitated as a white solid (1.402 g, 72%). The ^{1}H NMR spectrum of 3,4-dibromomaleic anhydride (**79**) was compared to that reported in literature and corresponded well.

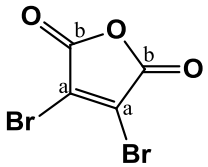

^{13}C NMR (300 MHz, DMSO) δ 167.6 (2C, C_b), 163.2 (2C, C_a).

7.3.3.2 1-Benzyl-3,4-dibromo-1*H*-pyrrole-2,5-dione (80)

3,4-Dibromomaleic anhydride (**79**) (1.35 g, 5.28 mmol) was added to a 2-neck round bottom flask and dissolved in AcOH (10 mL). Benzylamine (0.63 mL, 5.8 mmol, 1.1 equiv) was slowly added to the solution while stirring at RT. The reaction mixture was then heated to reflux for 3 h under a N_2 atmosphere. The solvent was finally removed *in vacuo* and the crude product was purified by column chromatography (EtOAc/Hexane, 5:95) affording the product 1-benzyl-3,4-dibromo-1*H*-pyrrole-2,5-dione (**80**) as a white solid (993 mg, 55%). The ^{1}H NMR spectrum of 1-benzyl-3,4-dibromo-1*H*-pyrrole-2,5-dione (**80**) was compared to that reported in literature and corresponded well.[187]

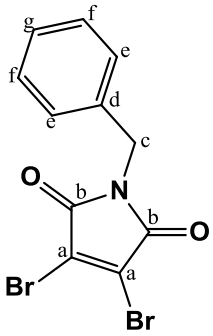

R_f = 0.69 (EtOAc/Hexane, 2:8); **^{1}H NMR (400 MHz, DMSO) δ** 7.44 - 7.3 (m, 5H, H_{Ar}), 4.8 (s, 2H, H_c). **IR (ATR, cm^{-1}):** 1707 (C=O str), 697 (C-Br str).

7.3.3.3 1-Benzyl-3,4-bis{(trimethylsilyl)ethynyl}-1*H*-pyrrole-2,5-dione (81)

To a dry Schlenk tube was added dry THF (8 mL) and DIPEA (0.5 mL). Standard freeze-pump-thaw techniques were employed, followed by degassing with N_2 to ensure an inert, O_2 free environment. 1-Benzyl-3,4-dibromo-1H-pyrrole-2,5-dione (**80**) (400 mg, 1.60 mmol), $PdCl_2(PPh_3)_2$ (41 mg, 0.058 mmol, 0.05 equiv) and CuI (22 mg, 0.12 mmol, 0.1 equiv) were then added successively to the Schlenk tube and stirred for 5 min. TMSA (0.41 mL, 2.9 mmol, 2.5 equiv) was then added to the solution and the reaction mixture was stirred at RT overnight under a N_2 atmosphere. The solution was then washed with H_2O (20 mL), followed by $NH_4Cl_{(sat)}$ (20 mL). The aqueous layers were combined and extracted with EtOAc (2 × 30 mL). The combined organic layers were then washed with brine (80 mL) and dried over $MgSO_4$. The drying slats were removed by filtration and the solvent was finally removed *in vacuo*. The crude product was purified by column chromatography (EtOAc/Hexane, 1:9) to obtain the desired product 1-benzyl-3,4-bis{(trimethylsilyl)ethynyl}-1*H*-pyrrole-2,5-dione (**81**)as a light yellow solid (304 mg, 68%). The ^{1}H NMR spectrum of 1-benzyl-3,4-bis{(trimethylsilyl)ethynyl}-1*H*-pyrrole-2,5-dione (**81**) was compared to that reported in literature and corresponded well.[176]

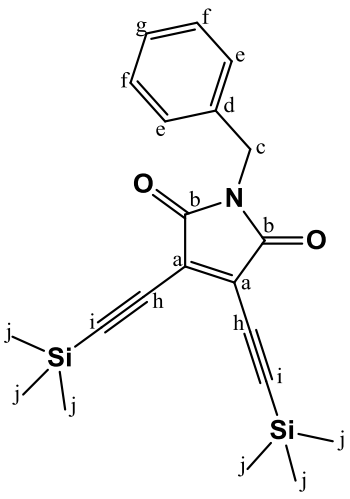

R_f = 0.75 (EtOAc/Hexane, 2:8); **^{1}H NMR (300 MHz, DMSO) δ** 7.07 – 6.98 (m, 5H, H_{Ar}), 4.40 (s, 2H, H_c), 0.3 (s, 18H, H_j).

7.3.3.4 1-Methyl-3,4-bis{(trimethylsilyl)ethynyl}-1*H*-pyrrole-2,5-dione (83)

To a dry Schlenk tube was added dry THF (5 mL) and dry TEA (20 mL). Standard freeze-pump-thaw techniques were employed, followed by degassing with N_2 to ensure an inert, O_2 free environment. 3,4-Dichloro-1-methyl-1*H*-pyrrole-2,5-dione (**75**) (150 mg, 0.833 mmol), $PdCl_2(PPh_3)_2$ (37 mg, 0.042 mmol, 0.05 equiv) and CuI (16 mg, 0.083 mmol, 0.1 equiv) were then added successively to the Schlenk tube and stirred for 5 min. TMSA (327 mg, 3.33 mmol, 4 equiv) was then added to the solution and the reaction mixture was stirred at RT overnight under a N_2 environment.

The solution was then washed with H_2O (50 mL), followed by $NH_4Cl_{(sat)}$ (50 mL). The aqueous layers were combined and extracted with EtOAc (2 × 50 mL). The combined organic layers were washed with brine (100 mL) and dried over $MgSO_4$. After filtration the solvent was finally removed *in vacuo*. The crude product was purified by column chromatography (EtOAc/Hexane, 5:95) affording the product 1-methyl-3,4-bis{(trimethylsilyl)ethynyl}-1*H*-pyrrole-2,5-dione (**83**) as a brown oily solid (108 mg, 43%).

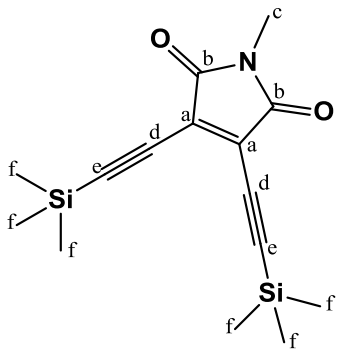

R_f = 0.63 (EtOAc/Hexane, 1:9); **^{1}H NMR (300 MHz, DMSO) δ** 2.87 (s, 1H, H_c), 0.26 (s, 18H, H_f); **^{13}C NMR (300 MHz, DMSO) δ** 166.3 (C_b), 129.5 (C_a), 117.1 ($C_{d/e}$), 94.4 ($C_{e/d}$), 24.6 (C_c), -0.6 (6C,C_f).

7.3.3.5 3,4-bis(1-Benzyl-1*H*-1,2,3-triazol-4-yl)-1-methyl-1*H*-pyrrole-2,5-dione (84)

To a 2-neck round bottom flask was added 1-methyl-3,4-bis{(trimethylsilyl)ethynyl}-1*H*-pyrrole-2,5-dione (**83**) (100 mg, 0.330 mmol) and dissolved in THF/MeOH (1:1, 6 mL). TBAF (1 M in THF) (174 mg, 0.666 mmol, 2.02 equiv) was then added to the solution and stirred under N_2 for 1 h. The reaction mixture was then treated with benzyl azide (87.8 mg, 0.659 mmol, 2 equiv), $CuSO_4.5H_2O$ (3.3 mg, 0.013 mmol, 0.04 equiv) and Na ascorbate (26 mg, 0.13 mmol, 0.4 equiv) and stirred overnight at RT under a N_2 atmosphere. Upon completion of the reaction, the solvent was removed under reduced pressure. The reaction mixture was then diluted with EtOAc (10 mL) and washed with $NH_4Cl_{(sat)}$ (2 × 10 mL), brine (20 mL) and dried over $MgSO_4$. Filtration of the drying salts was followed by removal of the solvent *in vacuo*. Column chromatography (EtOAc/Hexane, 2:8) afforded the product 3,4-bis(1-benzyl-1*H*-1,2,3-triazol-4-yl)-1-methyl-1*H*-pyrrole-2,5-dione (**84**) as a brown solid (7 mg, 5%).

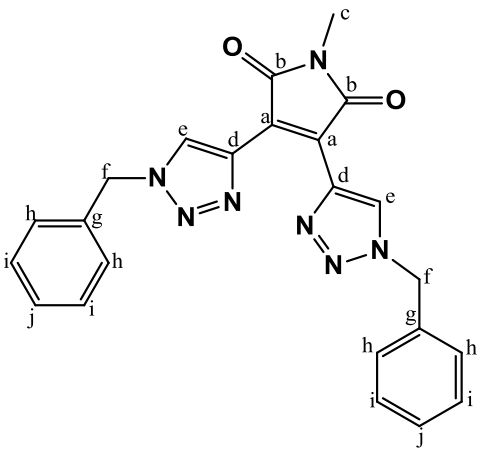

R_f = 0.52 (EtOAc/Hexane, 2:8);**^{1}H NMR (300 MHz, DMSO) δ** 8.62 (s, 2H, H_e), 7.84 (d, *J* = 7.8 Hz, 4H, H_h), 7.46 – 7.29 (m, 6H, $H_{h,i\&j}$), 5.64 (s, 4H, H_f) H_c not found (masked by H_2O peak); **^{13}C NMR (300 MHz, DMSO) δ**146.7 (2C, $C_{Ar/b}$), 136.0 (2C, C_{Ar}), 130.7 (2C), 128.9 (4C, $C_{h/i}$), 128.8 (4C, $C_{h/i}$), 128.2 (2C, $C_{Ar/e/d/a}$), 127.9 (4C, $C_{Ar/e/d/a}$), 125.2 (4C, $C_{Ar//e/d/a}$), 121.5 (2C, $C_{Ar/e/d/a}$), 53.0 (2C, C_f).

7.3.4 Synthesis of the click products using indolylmaleimides

7.3.4.1 1-Benzyl-3,4-dichloro-1*H*-pyrrole-2,5-dione (85)

A 2-neck round-bottomed flask was charged with 3,4-dichlorofuran-2,5-dione (**69**) (1.14 g, 6.83 mmol) and dissolved in AcOH (20 mL). The solution was then treated with benzylamine (804.90 mg, 7.51, 1.1 equiv) and heated to reflux for 2 h. Upon completion the AcOH was removed under reduced pressure. The crude product was then purified by column chromatography (EtOAc/Hexane, 5:95) to afford the product 1-benzyl-3,4-dichloro-1*H*-pyrrole-2,5-dione (**85**) as an off-white solid. The ^{1}H NMR spectrum of the product 1-benzyl-3,4-dichloro-1*H*-pyrrole-2,5-dione (**85**) was compared to that reported in literature and corresponded well.[202]

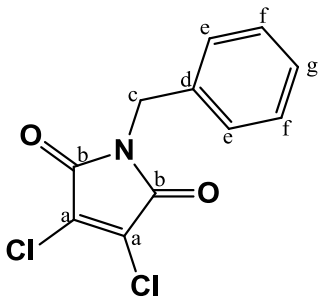

R_f = 0.41 (EtOAc/Hexane, 1:9);**^{1}H NMR (300 MHz, $CDCl_3$) δ** 4.73 (s, 2H, H_c), 7.40-7.23 (m, 5H, H_{Ar}).

7.3.4.2 3-Chloro-4-(1*H*-indol-3-yl)-1-methyl-1*H*-pyrrole-2,5-dione (86)

Indole (600 mg, 4.89 mmol, 1.1 equiv) and dry THF (20 mL) were added to a Schlenk tube. 3,4-Dichloro-1-methyl-1*H*-pyrrole-2,5-dione (**75**) (800 mg, 4.45 mmol) was dissolved in another Schlenk tube in dry THF (15 mL). Standard freeze-pump-thaw techniques were employed to both THF solutions, followed by degassing with N_2 to ensure an inert, O_2 free environment. EtMgBr (1.66 mL, 4.98 mmol, 1.12 equiv) was then added drop-wise to the indole solution at 0 °C. The colour of the solution changed from clear to yellow on addition of the EtMgBr. After stirring for 1 h at 60 °C, the solution of 3,4-dichloro-1-methyl-1*H*-pyrrole-2,5-dione (**75**) was added to the reaction mixture and the colour became dark red. The temperature was further increased to 65 °C and the mixture was stirred for 2 h. H_2O (30 mL) was then added to the reaction mixture and it was extracted with EtOAc (2 × 30 mL). The organic layers were combined, washed with $NH_4Cl_{(sat)}$, brine and dried over $MgSO_4$. Filtration of the drying salts was followed by removal of the solvent *in vacuo*. The crude product was purified by column chromatography (EtOAc/Hexane, 1:9) to obtain the desired product 3-chloro-4-(1*H*-indol-3-yl)-1-methyl-1*H*-pyrrole-2,5-dione (**86**) as an orange solid (679 mg, 57%). The ^{1}H NMR spectrum of 3-chloro-4-(1*H*-indol-3-yl)-1-methyl-1*H*-pyrrole-2,5-dione (**86**) was compared to that reported in literature and corresponded well.[86]

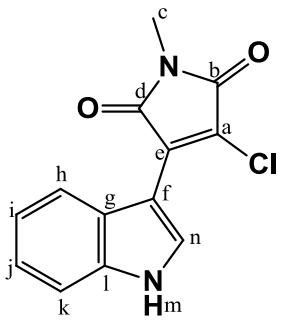

R_f = 0.22 (EtOAc/Hexane, 2:8); **^{1}H NMR (400 MHz, DMSO) δ** 12.14 (s, 1H, H_m), 8.08 (d, *J* = 2.9 Hz, 1H, H_n), 7.93 (d, *J* = 8.0 Hz, 1H, $H_{k/h}$), 7.52 (d, *J* = 8.0 Hz, 1H, $H_{h/k}$), 7.23 (m, 1H, $H_{i/j}$), 7.16 (m, 1H, $H_{i/j}$), 3.00 (s, 3H, H_c).

7.3.4.3 1-Benzyl-3-chloro-4-(1*H*-indol-3-yl)-1*H*-pyrrole-2,5-dione (87)

Indole (383 mg, 3.12 mmol, 1.1 equiv) and dry THF (12 mL) were added to a Schlenk tube. 1-Benzyl-3,4-dichloro-1*H*-pyrrole-2,5-dione (**85**) (730 mg, 2.84 mmol) was dissolved in another Schlenk tube in dry THF (12 mL).Standard freeze-pump-thaw techniques were employed to both THF solutions, followed by degassing with N_2 to ensure an inert, O_2 free environment. EtMgBr (1.06 mL, 3.18 mmol, 1.12 equiv) was then added drop-wise to the indole solution at 0 °C. The colour of the solution changed from clear to yellow on addition of the EtMgBr. After stirring for 1 h at 60 °C, the solution of 1-benzyl-3,4-dichloro-1H-pyrrole-2,5-dione (**85**) was added to the reaction mixture and the colour became dark red. The temperature was further increased to 65 °C and the mixture was stirred for 2 h. H_2O (30 mL) was then added to the reaction mixture and it was extracted with EtOAc (2 × 30 mL). The organic layers were combined, washed with $NH_4Cl_{(sat)}$, brine and dried over $MgSO_4$. Filtration of the drying salts was followed by removal of the solvent *in vacuo.* The crude product was purified by column chromatography (EtOAc/Hexane, 1:9) to obtain the desired product 1-benzyl-3-chloro-4-(1*H*-indol-3-yl)-1*H*-pyrrole-2,5-dione (**87**) as a red solid (410 mg, 43%).

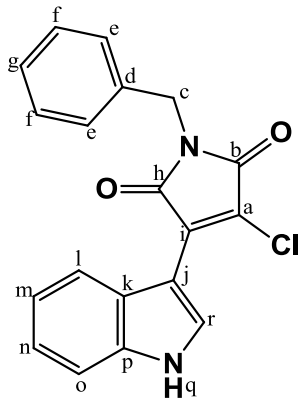

Mp = 198-200 ° C; **R_f =** 0.24 (EtOAc/Hexane, 2:8); **IR (ATR, cm^{-1}):** 3279 (N-H str), 2917 (alkane C-H str)**,** 1696 (C=O str), 1594 (Ar C-C str), 736 (Ar C-H), 696 (C-Cl str). **^{1}H NMR (400 MHz, DMSO) δ** 12.18 (s, 1H, H_q), 8.12 (d, *J* = 4.5 Hz, 1H, H_r), 7.95 (dd, *J* = 7.8, 4.5 Hz, 1H, $H_{l/o}$), 7.52 (dd, *J* = 7.8, 4.6 Hz, 1H, $H_{o/l}$), 7.38 – 7.27 (m, 5H, H_{Ar}), 7.25 – 7.21 (m, 1H, $H_{m/n}$), 7.20 – 7.13 (m, 1H, $H_{m/n}$), 4.73 (s, 2H, H_c).**^{13}C NMR (400 MHz, DMSO) δ** 168.4 ($C_{h/b}$), 165.9 ($C_{b/h}$), 136.6 (C), 133.5 (C), 131.7 (C), 128.6 (2C, $C_{f/e}$), 127.5 (C), 127.4 (2C, $C_{e/f}$), 124.7 (C), 122.7 (C), 122.1 (C), 121.5 (C), 120.7 (C), 112.5 (C), 103.3 (C), 41.6 (C_c). **HRMS:** calcd for $C_{19}H_{14}ClN_2O_2^+$ $[M+H]^+$, 337.0744, found 337.0736.

7.3.4.4 3-(1*H*-Indol-3-yl)-1-methyl-4-{(trimethylsilyl)ethynyl}-1*H*-pyrrole-2,5-dione (88)

To a dry Schlenk tube was added dry THF (3 mL) and TEA (9 mL). Standard freeze-pump-thaw techniques were employed, followed by degassing with N_2 to ensure an inert, O_2 free environment. 3-Chloro-4-(1*H*-indol-3-yl)-1-methyl-1*H*-pyrrole-2,5-dione (**86**) (100 mg, 0.376 mmol), $PdCl_2(PPh_3)_2$ (26 mg, 0.038 mmol, 0.1 equiv) and CuI (7.1 mg, 0.038 mmol, 0.1 equiv) were then added successively to the Schlenk tube and stirred for 5 min. TMSA (0.11 mL, 0.77 mmol, 2.05 equiv) was then added to the solution and the reaction mixture was stirred at RT overnight. $NH_4Cl_{(sat)}$ (20 mL) was added to the reaction mixture and it was extracted with ether (3 × 20 mL). The combined organic layers were then washed with brine and dried over $MgSO_4$. The drying slats were removed by filtration and the solvent removed *in vacuo*. The crude product was purified by column chromatography (EtOAc/Hexane, 3:7) to obtain the desired product 3-(1*H*-indol-3-yl)-1-methyl-4-{(trimethylsilyl)ethynyl}-1*H*-pyrrole-2,5-dione (**88**) as a red solid (105 mg, 87%). The ^{1}H NMR spectrum of 3-(1*H*-indol-3-yl)-1-methyl-4-{(trimethylsilyl)ethynyl}-1*H*-pyrrole-2,5-dione (**88**) was compared to that reported in literature and corresponded well.[86]

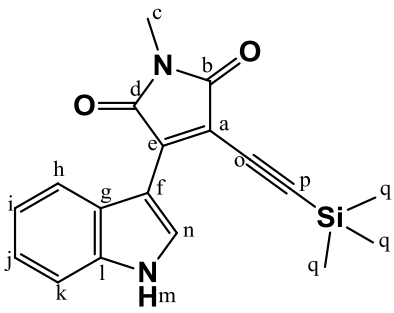

R_f = 0.44 (EtOAc/Hexane, 4:6); **^{1}H NMR (300 MHz, DMSO) δ** 12.29 (s, 1H, H_m), 8.34 – 8.29 (m, 2H, $H_{n/h/k}$), 7.52 (d, *J* = 8.0 Hz, 1H, $H_{h/k}$), 7.26 (m, 1H, $H_{i/j}$), 7.16 (m, 1H, $H_{i/j}$), 2.96 (s, 3H, H_c), 0.23 (s, 9H, H_q).

7.3.4.5 1-Benzyl-3-(1*H*-indol-3-yl)-4-{(trimethylsilyl)ethynyl}-1*H*-pyrrole-2,5-dione (89)

To a dry Schlenk tube was added dry THF (12 mL) and TEA (50 mL). Standard freeze-pump-thaw techniques were employed, followed by degassing with N_2 to ensure an inert, O_2 free environment. 1-Benzyl-3-chloro-4-(1*H*-indol-3-yl)-1*H*-pyrrole-2,5-dione (**87**) (738 mg, 2.19 mmol), $PdCl_2(PPh_3)_2$ (154 mg, 0.219 mmol, 0.1 equiv) and CuI (42 mg, 0.22 mmol, 0.1 equiv) were then added successively to the Schlenk tube and stirred for 5 min. TMSA (0.64 mL, 4.5 mmol, 2.05 equiv) was then added to the solution and the reaction mixture was stirred at RT overnight. $NH_4Cl_{(sat)}$ (50 mL) was added to the reaction mixture and it was extracted with ether (3 × 50 mL). The combined organic layers were then washed with brine and dried over $MgSO_4$. The drying salts were removed by filtration and the solvent removed *in vacuo*.

The crude product was purified by column chromatography (EtOAc/Hexane, 3:7) to obtain the desired product 1-benzyl-3-(1*H*-indol-3-yl)-4-{(trimethylsilyl)ethynyl}-1*H*-pyrrole-2,5-dione (**89**) as a red solid (712 mg, 83%).

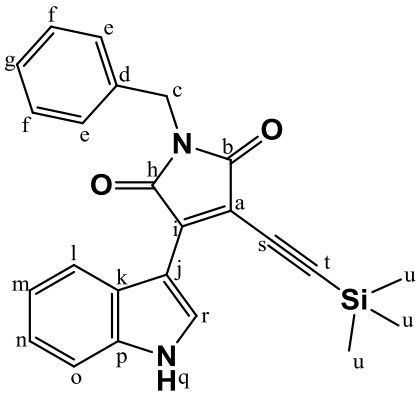

Mp = 182-184 °C; **R_f =** 0.35 (EtOAc/Hexane, 3:7); **IR (ATR, cm^{-1}):** 3335 (N-H str), 2955 (alkane C-H str), 2138 (C≡C str), 1697 (C=O str), 1585 (Ar C-C str), 840 (N-H wag), 741 (Ar C-H). (**^{1}H NMR (400 MHz, $CDCl_3$) δ** 8.88 (s, 1H, H_q), 8.31 (d, *J* = 7.9 Hz, 1H, $H_{l/o}$), 8.12 – 8.09 (m, 1H, H_r), 7.29 – 7.23 (m, 2H, H_{In}), 7.20 – 7.05 (m, 6H, $H_{Ar/m/n}$), 4.63 (d, *J* = 2.1 Hz, 2H, H_c), 0.09 (s, 9H, H_u).**^{13}C NMR (400 MHz, $CDCl_3$) δ** 170.9 ($C_{b/h}$), 169.1 ($C_{h/b}$), 138.7, 136.5, 136.4, 131.5, 128.8 (2C, $C_{e/f}$), 128.6 (2C, $C_{f/e}$), 128.0 (C), 125.5 (C), 124.3 (C), 123.8 (C), 121.3 (C), 113.4 (C), 112.3 (C), 111.8 (C), 108.0 (C_t), 97.2 (C_s), 42.3 (C_c), -0.2 (C_u). **HRMS:** calcd for $C_{25}H_{24}N_2O_2Si^+$ $[M+H]^+$, 399.1529 , found 399.1528.

7.3.4.6 3-(1-Benzyl-1*H*-1,2,3-triazol-4-yl)-4-(1*H*-indol-3-yl)-1-methyl-1*H*-pyrrole-2,5-dione (90)

To a 2-neck round bottom flask was added 3-(1*H*-indol-3-yl)-1-methyl-4-{(trimethylsilyl)ethynyl}-1*H*-pyrrole-2,5-dione (**88**) (100 mg, 0.304 mmol) and dissolved in THF/MeOH (1:1, 8 mL). TBAF (96 mg, 0.304 mmol, 1 equiv) was then added to the solution and stirred under N_2 for 30 min. The reaction mixture was then treated with benzyl azide (40.5 mg, 0.304 mmol, 1 equiv), $CuSO_4$•$5H_2O$ (1.6 mg, 0.0061 mmol, 0.02 equiv) and Na ascorbate (12 mg, 0.061 mmol, 0.2 equiv) and stirred overnight at RT. The solvent was removed under reduced pressure. The reaction mixture was then diluted with EtOAc (20 mL) and washed with $NH_4Cl_{(sat)}$ (2 × 10 mL), brine and dried over $MgSO_4$. Filtration of the drying salts was followed by removal of the solvent *in vacuo*. Column chromatography (EtOAc/Hexane, 3:7) afforded the product 3-(1-benzyl-1*H*-1,2,3-triazol-4-yl)-4-(1*H*-indol-3-yl)-1-methyl-1*H*-pyrrole-2,5-dione (**90**) as a yellow solid (22 mg, 19%).

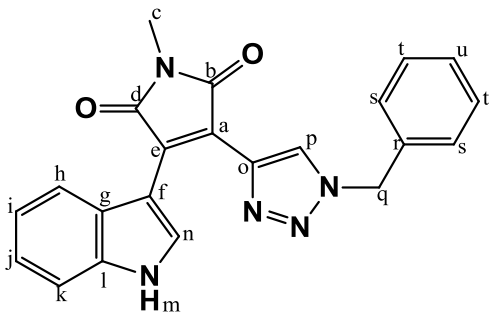

R_f = 0.36 (EtOAc/Hexane, 1:1); **^{1}H NMR (400 MHz, DMSO) δ** 11.92 (s, 1H, H_m), 8.56 (d, *J* = 3.3 Hz, 1H, H_n), 8.20 (m, 1H, $H_{p/h/k}$), 7.75 – 7.66 (m, 1H, $H_{In/Ar}$), 7.48 – 7.28 (m, 5H, $H_{Ar/In}$), 7.15-7.09 (m, 1H, $H_{In/Ar}$), 6.83 (m, 1H, $H_{In/Ar}$), 5.70 (d, *J* = 2.7 Hz, 2H, H_q), 3.02 (s, 3H, H_c). **^{13}C NMR (400 MHz, DMSO) δ** 170.9 ($C_{b/d}$), 170.8 ($C_{d/b}$), 136.5 (C), 136.0

(C), 132.3 (C), 131.8 (C), 128.8 (2C, $C_{s/t}$), 128.1 (C), 127.7 (2C, $C_{t/s}$), 126.0 (C), 125.0 (C), 122.0 (C), 121.6 (C), 119.9 (C), 119.8 (C), 112.1, 104.7 (C), 52.8 (C_q), 24.1 (C_c).

7.3.4.7 1-Benzyl-3-(1-benzyl-1*H*-1,2,3-triazol-4-yl)-4-(1*H*-indol-3-yl)-1*H*-pyrrole-2,5-dione (91)

To a 2-neck round bottom flask was added 1-benzyl-3-(1*H*-indol-3-yl)-4-{(trimethylsilyl)ethynyl}-1*H*-pyrrole-2,5-dione (**89**) (50 mg, 0.304 mmol) and dissolved in THF/MeOH (1:1, 6 mL). TBAF·$3H_2O$ (40 mg, 0.13 mmol, 1 equiv) was added to the solution and stirred under N_2 for 30 min. The reaction mixture was treated with benzyl azide (17 mg, 0.13 mmol, 1 equiv), $CuSO_4.5H_2O$ (0.64 mg, 0.0026 mmol, 0.02 equiv) and Na ascorbate (5 mg, 0.03 mmol, 0.2 equiv) and stirred overnight atRT. The solvent was removed under reduced pressure. The reaction mixture was then diluted with CH_2Cl_2 (20 mL) and washed with $NH_4Cl_{(sat)}$ (2 × 10 mL), brine and dried over $MgSO_4$. Filtration of the drying salts was followed by removal of the solvent *in vacuo*. Column chromatography (EtOAc/Hexane, 4:6) afforded the product 1-benzyl-3-(1-benzyl-1*H*-1,2,3-triazol-4-yl)-4-(1*H*-indol-3-yl)-1*H*-pyrrole-2,5-dione (**91**) as an orange solid (12 mg, 20%).

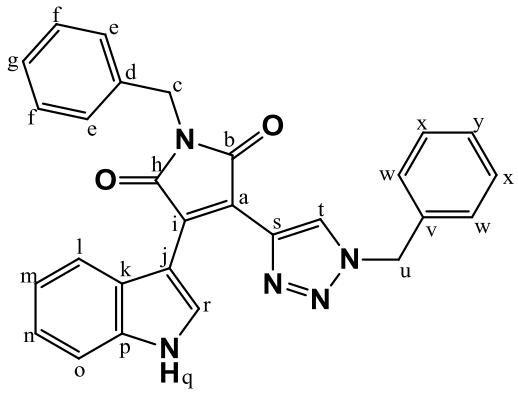

R_f = 0.38 (EtOAc/Hexane, 4:6); **^{1}H NMR (400 MHz, DMSO) δ** 12.0 (s, 1H, H_q), 8.6 (d, *J* = 6.0 Hz, 1H, $H_{r/t}$), 8.2 (s, 1H, $H_{r/t}$), 7.5 – 7.4 (m, 1H, H_{In}), 7.4 – 7.3 (m, 11H, $H_{In/Ar}$), 7.1 (s, 1H, H_{In}), 6.9 – 6.8 (m, 1H, H_{In}), 5.7 (d, *J* = 5.6 Hz, 2H, $H_{c/u}$), 4.8 (d, *J* = 5.4 Hz, 2H, $H_{c/u}$).

7.3.4.8 3-Ethynyl-4-(1*H*-indol-3-yl)-1-methyl-1*H*-pyrrole-2,5-dione (92)

To a 2-neck round bottom flask was added 3-(1*H*-indol-3-yl)-1-methyl-4-{(trimethylsilyl)ethynyl}-1*H*-pyrrole-2,5-dione (**88**) (380 mg, 1.16 mmol). The solid was dissolved in THF/$NH_4Cl_{(sat)}$ (1:1, 15 mL) and stirred for 5 min. TBAF·$3H_2O$ (547 mg, 1.73 mmol, 1.5 equiv) was then added to the solution and stirred in the dark under N_2, overnight. H_2O (10 mL) was added to the reaction mixture and extracted with CH_2Cl_2 (2 × 30 mL). The combined organic layers were then washed with brine and dried over $MgSO_4$. Filtration of the drying salts was followed by removal of the solvent *in vacuo*. The crude product was purified by column chromatography (EtOAc/Hexane, 3:7) to afford the desired product 3-ethynyl-4-(1*H*-indol-3-yl)-1-methyl-1*H*-pyrrole-2,5-dione (**92**) as a red solid (131 mg, 44%).

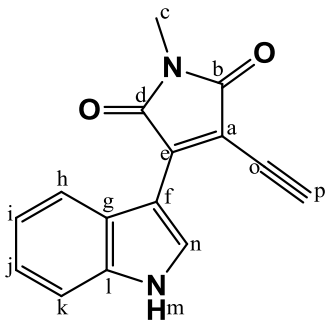

R_f = 0.49 (EtOAc/Hexane, 4:6); **^{1}H NMR (400 MHz, DMSO) δ** 12.25 (s, 1H, H_m), 8.30 (d, *J* = 2.4 Hz, 1H, H_n), 8.24 (d, *J* = 7.7 Hz, 1H, $H_{h/k}$), 7.53 (d, *J* = 8.0 Hz, 1H, $H_{k/h}$), 7.25 (m, 1H, $H_{i/j}$), 7.17 (m, 1H, $H_{i/j}$), 5.10 (s, 1H, H_p), 2.97 (s, 3H, H_c). **^{13}C NMR (400 MHz, DMSO) δ** 170.3 ($C_{b/d}$), 168.8 ($C_{d/b}$), 139.7 (C), 136.8 (C), 132.6 (C), 124.9 (C), 122.9 (C), 122.8 (C), 120.7 (C), 112.5 (C), 109.6 (C), 106.0 (C), 96.1 (C), 76.7 ($C_{o/p}$) 24.3 (C_c).

7.3.4.9 1-Benzyl-3-ethynyl-4-(1*H*-indol-3-yl)-1*H*-pyrrole-2,5-dione (93)

To a 2-neck round bottom flask was added 1-benzyl-3-(1*H*-indol-3-yl)-4-{(trimethylsilyl)ethynyl}-1*H*-pyrrole-2,5-dione (**89**) (552 mg, 1.42 mmol). The solid was dissolved in THF/$NH_4Cl_{(sat)}$ (1:1, 30 mL) and stirred for 5 min. TBAF·$3H_2O$ (670 mg, 2.12 mmol, 1.5 equiv) was then added to the solution and stirred in the dark at RT, under N_2, overnight. H_2O (50 mL) was added to the reaction mixture and extracted with CH_2Cl_2 (2 × 50 mL). The combined organic layers were then washed with brine and dried over $MgSO_4$. Filtration of the drying salts was followed by removal of the solvent *in vacuo*. The crude product was purified by column chromatography (EtOAc/Hexane, 3:7) to afford the desired product 1-benzyl-3-ethynyl-4-(1*H*-indol-3-yl)-1*H*-pyrrole-2,5-dione (**93**) as a red solid (274 mg, 59%).

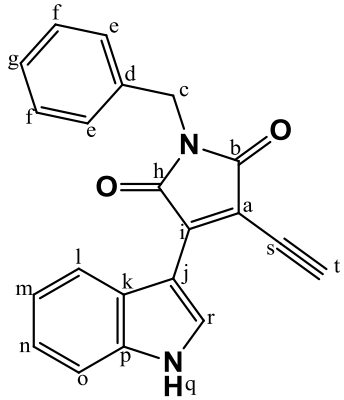

R_f = 0.59 (EtOAc/Hexane, 4:6);**^{1}H NMR (400 MHz, DMSO) δ** 12.2 (s, 1H, H_q), 8.1 (s, 1H, H_r), 7.9 (d, *J* = 7.9 Hz, 1H, $H_{l/o}$), 7.5 (d, *J* = 7.9 Hz, 1H, $H_{o/l}$), 7.4 – 7.2 (m, 5H, H_{Ar}), 7.3 – 7.2 (m, 1H, $H_{m/n}$), 7.2 (m, 1H, $H_{n/m}$), 4.7 (s, 2H, H_c), 1.2 (s, 1H, H_t).

7.3.4.10 *N*-(4-[4-{4-(1*H*-indol-3-yl)-1-methyl-2,5-dioxo-2,5-dihydro-1*H*-pyrrol-3-yl}-1*H*-1,2,3-triazol-1-yl]phenyl)acrylamide (94)

To a 2-neck round bottom flask was added 3-ethynyl-4-(1*H*-indol-3-yl)-1-methyl-1*H*-pyrrole-2,5-dione (**92**) (40 mg, 0.16 mmol) and dissolved in THF/MeOH (1:1, 4 mL). To the solution was then added *N*-(4-azidophenyl)acrylamide (37 mg, 0.19 mmol, 1.2 equiv), $CuSO_4.5H_2O$ (1.6 mg, 0.0062 mmol, 0.04 equiv) and Na ascorbate (12 mg, 0.062 mmol, 0.4 equiv) and stirred overnight at RT.

The solvent was removed under reduced pressure. The reaction mixture was then diluted with CH_2Cl_2 (15 mL) and washed with $NH_4Cl_{(sat)}$ (2 × 15 mL), brine and dried over $MgSO_4$. Filtration of the drying salts was followed by removal of the solvent *in vacuo*. Column chromatography (EtOAc/Hexane, 7:3) afforded the product *N*-(4-[4-{4-(1*H*-indol-3-yl)-1-methyl-2,5-dioxo-2,5-dihydro-1*H*-pyrrol-3-yl}-1*H*-1,2,3-triazol-1-yl]phenyl)- acrylamide (**94**) as an orange solid (18 mg, 26%).

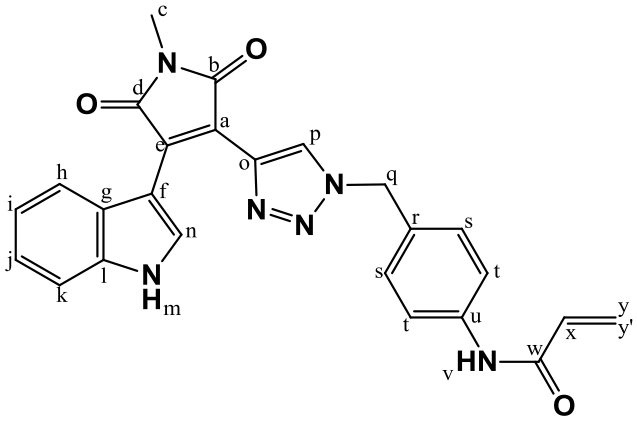

R_f = 0.72 (EtOAc/Hexane, 8:2); **^{1}H NMR (400 MHz, DMSO) δ** 11.92 (s, 1H, $H_{m/u}$), 9.92 (s, 1H, $H_{m/u}$), 8.48 (d, *J* = 3.7 Hz, 1H, H_n), 8.18 (s, 1H, H_p), 7.50 – 7.44 (m, 2H, $H_{r/s}$), 7.40 – 7.32 (m, 1H, H_{indole}), 7.26– 7.20 (m, 1H, H_{indole}), 7.15 – 7.09 (m, 1H, H_{indole}), 7.05 – 7.01 (m, 1H, H_{indole}), 6.89 – 6.86 (m, 2H, $H_{r/s}$), 6.53 – 6.43 (m, 1H, H_w), 6.27 (m, 1H, $H_{x/x'}$), 5.78 (m, 1H, $H_{x/x'}$), 3.02 (s, 3H, H_c). **^{13}C NMR (400 MHz, DMSO) δ** 171.0 ($C_{b/d}$), 170.8 ($C_{b/d}$), 163.8 (C_v), 137.0 (C), 136.5 (C), 135.4 (C), 132.1 (C), 131.8 (C), 131.4 (C), 130.3 (C), 128.7 (C), 128.4 (C), 127.2 (C), 126.2 (C), 126.1 (C), 125.8 (C), 125.1 (C), 122.0 (C), 121.7 (C), 119.9 (C), 119.8 (C), 112.1 (C), 104.8 (C), 24.1 (C_c).

7.3.5 Synthesis of the bisamino maleimide target compounds 104 and 105

7.3.5.1 3,4-Dibromo-1-(4-nitrophenyl)-1*H*-pyrrole-2,5-dione (96)

A 2-neck round bottom flask charged with 3,4-dibromomaleic anhydride (**79**) (2.15 g, 8.40 mmol), was evacuated under high vacuum and filled with Ar. It was then dissolved in AcOH (30 mL), followed by the addition of *p*-nitroaniline (1.28 g, 9.24 mmol, 1.1 equiv). The reaction mixture was then heated to reflux for 8 hours under a N_2 atmosphere. Upon completion, the solvent was removed *in vacuo* and the crude product was purified by column chromatography (EtOAc/Hexane, 3:7) to afford the product 3,4-dibromo-1-(4-nitrophenyl)-1*H*-pyrrole-2,5-dione (**96**) as a light yellow solid (2.16 g, 69%). The ^{1}H NMR spectrum of 3,4-dibromo-1-(4-nitrophenyl)-1*H*-pyrrole-2,5-dione (**96**) was compared to that reported in literature and corresponded well.[202]

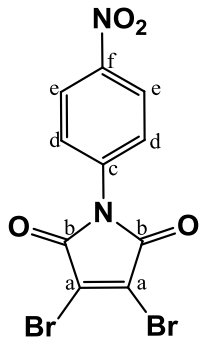

R_f = 0.77 (EtOAc/Hexane, 4:6); **^{1}H NMR (300 MHz, DMSO) δ** 8.39 (d, *J* = 8.9 Hz, 2H, H_e), 7.69 (d, *J* = 8.9 Hz, 2H, H_d); **^{13}C NMR (75 MHz, DMSO) δ** 163.3 (2C, C_b), 146.8 (C_f), 137.5 (C_c), 130.5 (2C, C_a), 127.7 (2C, C_d), 124.9 (2C, C_e).

7.3.5.2 3-Bromo-1-(4-nitrophenyl)-4-(phenylamino)-1*H*-pyrrolo-2,5-dione (97)

A Schlenk tube charged with 3,4-dibromo-1-(4-nitrophenyl)-1*H*-pyrrole-2,5-dione (**96**) (474 mg, 1.27 mmol) was evacuated under high vacuum and filled with Ar. Dry THF (3.5 mL) was added to the Schlenk and it was stirred in an ice bath for 5 min. A solution of aniline (0.12 mL, 1.3 mmol, 1.05 equiv), THF (11 mL) and TEA (0.44 mL, 3.2 mmol, 2.5 equiv) was then prepared, stirred and added drop-wise to the Schlenk solution at 0 °C. The reaction mixture was stirred overnight at RT under a N_2 atmosphere. Upon completion, the mixture was diluted with CH_2Cl_2 (20 mL), washed with H_2O (20 mL) and brine. It was then dried over $MgSO_4$ salts, filtered and the solvent was removed *in vacuo*. The mixture was purified by column chromatography (EtOAc/Hexane, 2:8) to afford the product 3-bromo-1-(4-nitrophenyl)-4-(phenylamino)-1*H*-pyrrolo-2,5-dione **(97)** as a yellow solid (386 mg, 79%).

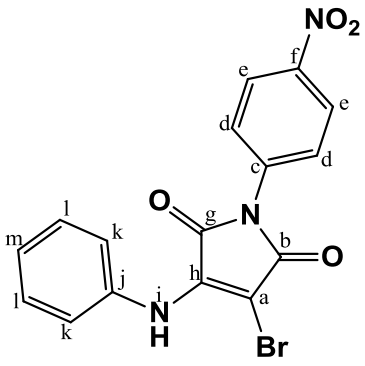

Mp = 210-212 ° C; **R_f** = 0.70 (EtOAc/Hexane, 4:6); **IR (ATR, cm^{-1}):**3326 (amine N-H str), 1708 (carbonyl C=O str), 666 (C-Br str), 1519, 1314 (nitro N-O str); **^{1}H NMR (400 MHz, DMSO) δ** 10.11 (s, 1H, H_i), 8.37 (d, *J* = 8.1 Hz, 2H, H_e), 7.75 (d, *J* = 8.1 Hz, 2H, H_d), 7.44 – 7.36 (m, 2H, H_l), 7.29 – 7.20 (m, 3H, $H_{k\&m}$); **^{13}C NMR (400 MHz, DMSO) δ** 165.8 ($C_{b/g}$), 164.3 ($C_{b/g}$), 145.5 ($C_{f/c/h/j}$), 141.9 ($C_{f/c/h/j}$), 137.7 ($C_{f/c/h/j}$), 136.3 ($C_{f/c/h/j}$), 128.2 (2C, $C_{e/d/k/l}$), 126.3 (2C, $C_{e/d/k/l}$), 125.6 (C_m), 124.8 (2C, $C_{e/d/k/l}$), 124.2 (2C, $C_{e/d/k/l}$), 80.8 (C_a); **HRMS:** calcd for $C_{16}H_{11}N_3O_4^+$ $[M+H]^+$, 387.9933, found 387.9938.

7.3.5.3 *N*-Boc-piperazine

Piperazine (**98**) (1.54 g, 17.9 mmol, 1.8 equiv) was added to a 2-neck round bottom flask and dissolved in MeOH (40 mL). The flask was placed in an ice bath and the solution was stirred for 5 min. A solution of di-*tert*-butyl dicarbonate (2.17 g, 9.95 mmol) in MeOH (20 mL) was then added drop-wise at 0 ° C to the flask containing the piperazine solution. The reaction mixture was stirred at RT for 2 days. The MeOH was then removed *in vacuo* and the mixture was diluted with Et_2O (60 mL). The aqueous solution was then obtained by extracting the organic solution with 1M citric acid (3 × 30 mL) and washing it with EtOAc (3 × 30 mL), removing the disubstituted byproduct.1 M NaOH was then added to the aqueous solution until the pH was adjusted to 11. The solution was then extracted with EtOAc (3 × 50 mL). The organic layers were combined, washed with brine and dried over $MgSO_4$. After filtration of the drying salts and removal of the solvent under reduced pressure, the desired product *N*-Boc-piperazine (**99**) was obtained as an off-white solid (1.09 g, 59%). The ^{1}H NMR spectrum of *N*-Boc-piperazine (**99**) was compared to that in literature and corresponded well.[203]

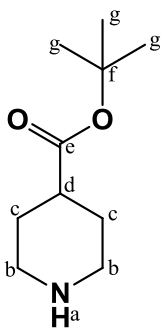

^{1}H NMR (300 MHz, $CDCl_3$) δ 3.45 – 3.28 (m, 4H, H_c), 2.86 – 2.72 (m, 4H, H_b), 2.22 (s, 1H, H_a), 1.43 (s, 9H, H_g).

7.3.5.4 *tert*-Butyl 4-{1-(4-nitrophenyl)-2,5-dioxo-4-(phenylamino)-2,5-dihydro-1*H*-pyrrol-3-yl}piperazine-1-carboxylate (100)

A Schlenk tube charged with 3-bromo-1-(4-nitrophenyl)-4-(phenylamino)-1*H*-pyrrolo-2,5-dione (**97**) (750 mg, 1.95 mmol) was evacuated under high vacuum and filled with Ar. Dry THF (15 mL) was added to the Schlenk and it was stirred in an ice bath for 5 min. A solution of *N*-Boc-piperazine(**99**)(549 mg, 2.93 mmol, 1.5 equiv), THF (30 mL) and TEA (0.68 mL, 4.9 mmol, 2.5 equiv) was prepared, stirred and added drop-wise to the Schlenk solution at 0 °C. The reaction mixture was stirred overnight at 55 °C. Upon completion, the solvent was removed *in vacuo* and diluted with CH_2Cl_2 (50 mL). The solution was washed with H_2O (2 × 30 mL). The organic layers were combined, washed with brine and dried over $MgSO_4$. Once the drying salts were removed by filtration, the solvent was removed *in vacuo*.

Purification by column chromatography (EtOAc/Hexane; 2:8) afforded 174 mg of the starting reagent (**97**) and 590 mg of the desired product *tert*-butyl 4-{1-(4-nitrophenyl)-2,5-dioxo-4-(phenylamino)-2,5-dihydro-1*H*-pyrrol-3-yl}piperazine-1-carboxylateas (**100**) an orange solid. Yield: 62% (80% brsm).

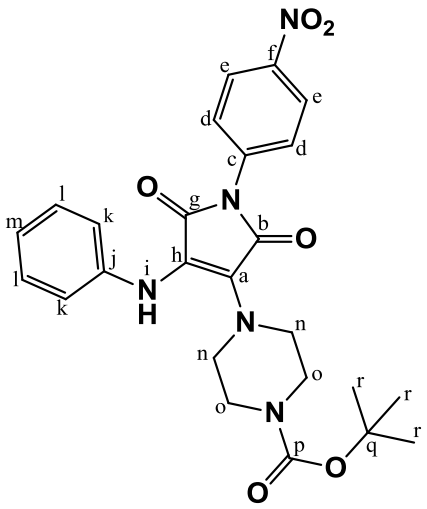

Mp = 115-117 ºC; $\mathbf{R_f}$ = 0.64 (EtOAc/Hexane, 4:6), **IR (ATR, cm^{-1}):** 3332 (amine N-H str),1689 (carbonyl C=O str), 1517, 1334 (nitro N-O str);**^{1}H NMR (300 MHz, DMSO) δ** 8.34 (d, *J* = 8.7 Hz, 2H, $H_{e/d}$), 8.25 (s, 1H, H_i), 7.70 (d, *J* = 8.7 Hz, 2H, $H_{e/d}$), 7.29 – 7.20(m, 2H, H_l), 6.88 (d, *J* = 8.3 Hz, 2H, H_k), 6.86 – 8.80(m, 1H, H_m), 3.30 – 3.25 (m, 4H, $H_{n/o}$), 3.18 – 3.10 (m, 4H, $H_{n/o}$), 1.36 (s, 9H, H_r).**^{13}C NMR (75 MHz, DMSO) δ** 166.8 ($C_{h/g}$), 165.9 ($C_{g/h}$), 153.7 (C_p), 144.9 (C), 141.9 (C), 137.9 (C), 128.7 (C), 128.6 (2C, $C_{e/d/k/l}$), 125.9 (2C, $C_{e/d/k/l}$), 124.1 (2C, $C_{e/d/k/l}$), 119.9 (C), 117.1 (2C, $C_{e/d/k/l}$), 114.8 (C), 79.1 (C_q), 47.1 (4C, $C_{n\&o}$), 28.0 (C_r); **HRMS:** calcd for $C_{25}H_{28}N_5O_6^+$ $[M+H]^+$, 494.2040, found 494.2043.

7.3.5.5 1-(4-Nitrophenyl)-3-(phenylamino)-4-(piperazin-1-yl)-1*H*-pyrrole-2,5-dione (101)

tert-Butyl 4-{1-(4-nitrophenyl)-2,5-dioxo-4-(phenylamino)-2,5-dihydro-1*H*-pyrrol-3-yl}piperazine-1-carboxylate (**100**) (220 mg, 0.449 mmol) was added to a 2-neck round bottom flask and dissolved in CH_2Cl_2 (20 mL). The flask was placed in an ice bath and the solution was stirred for 5 min under a N_2 atmosphere.TFA (0.71 mL, 9.0 mmol, 20 equiv), diluted in CH_2Cl_2 (4 mL), was then added drop-wise at 0 °C. The reaction mixture became dark red in colour. The ice bath was then removed and the reaction mixture was stirred overnight at 35 °C. The solution was then transferred to a flask containing $NaHCO_{3\,(sat)}$ (40 mL) and stirred at 0 °C. The addition of K_2CO_3 adjusted the pH to 10. The product was then obtained by extracting with CH_2Cl_2 (3 × 20 mL). The organic layers were combined, washed with brine and dried over $MgSO_4$. The drying salts were removed by filtration and the solvent was removed under reduced pressure. Column chromatography (MeOH/CH_2Cl_2; 1:9) afforded the desired product 1-(4-nitrophenyl)-3-(phenylamino)-4-(piperazin-1-yl)-1*H*-pyrrole-2,5-dione (**101**) as a red solid (170 mg, 98%).

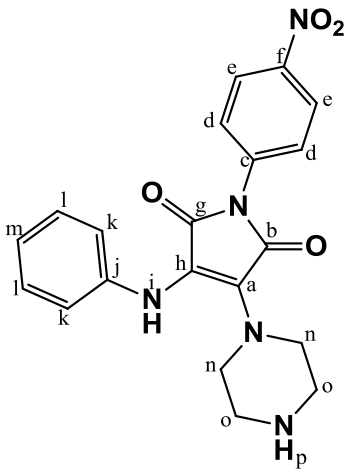

Mp = 200-202 ºC; **R_f** = 0.47 (MeOH:CH_2Cl_2, 1:9), **IR (ATR, cm^{-1}):** 3329 (amine N-H str), 1689 (carbonyl C=O str), 1494, 1335 (nitro N-O str);**^{1}H NMR (300 MHz, DMSO) δ** 8.33 (d, *J* = 8.8 Hz, 2H, H_e), 8.10 (s, 1H, H_i), 7.70 (d, *J* = 8.8 Hz, 2H, H_d), 7.27 – 7.17 (m, 2H, H_l), 6.90 – 6.78 (m, 3H, $H_{k/m}$), 3.95 –3.71 (s, 5H, H_p), 3.39 (s, 4H, H_n), 2.64 (s, 4H, H_o).**^{13}C NMR (300 MHz, DMSO) δ** 166.9 ($C_{g/b}$), 165.8 ($C_{g/b}$), 144.9 ($C_{f/c/h/j}$), 142.7 ($C_{f/c/h/j}$), 138.0 ($C_{f/c/h/j}$), 130.3 ($C_{f/c/h/j}$), 128.6 (2C, $C_{e/d/k/l}$), 125.8 (2C, $C_{e/d/k/l}$), 124.1 (2C, $C_{e/d/k/l}$), 119.4 ($C_{f/c/h/j}$), 116.5 (2C, $C_{e/d/k/l}$), 112.8 ($C_{f/c/h/j}$), 47.5 (2C,C_n), 44.8 (2C,C_o); **HRMS:** calcd for $C_{20}H_{20}N_5O_4^+$ $[M+H]^+$, 394.1515, found 394.1510.

7.3.5.6 3-(4-Acryloylpiperazin-1-yl)-1-(4-nitrophenyl)-4-(phenylamino)-1*H*-pyrrole-2,5-dione (102)

To a 2-neck round bottom flask was added 1-(4-nitrophenyl)-3-(phenylamino)-4-(piperazin-1-yl)-1*H*-pyrrole-2,5-dione (101) (85 mg, 0.22 mmol) and dissolved in a mixture of THF and DMF (10 mL: 10 mL). The flask was placed in an ice bath and TEA (0.09 mL, 0.65 mmol, 3 equiv) was added to the solution. The reaction mixture was stirred for 10 min at 0 °C, followed by the drop-wise addition of acryloyl chloride (0.05 mL, 0.65 mmol, 3 equiv) diluted in THF (2 mL). The reaction mixture was stirred at RT for 2 h. The THF was then removed *in vacuo* and the mixture was diluted in Et_2O (30 mL). The organic layer was then washed with H_2O (5 × 20 mL), brine and dried over $MgSO_4$. The drying salts were then removed by filtration and the solvent was removed *in vacuo*. Purification by column chromatography (EtOAc/Hexane, 1:1) afforded the desired product 3-(4-acryloylpiperazin-1-yl)-1-(4-nitrophenyl)-4-(phenylamino)-1*H*-pyrrole-2,5-dione (**102**) as an orange solid (59 mg, 61%).

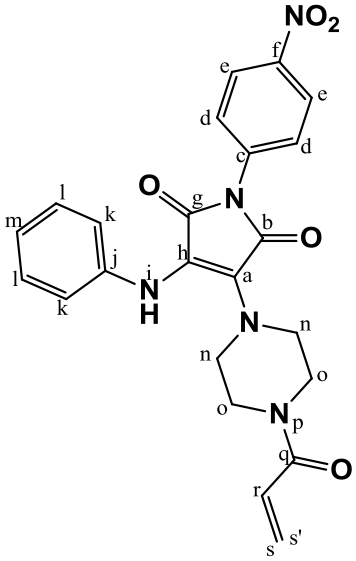

Mp = 195-197 ºC; **R_f** = 0.47 (EtOAc/Hexane, 1:1), **IR (ATR, cm^{-1}):** 3391, 3295 (amine N-H str), 3073 (alkene C=C-H), 1694 (carbonyl C=O str), 1503, 1343 (nitro N-O str); **^{1}H NMR (300 MHz, cdcl$_3$) δ** 8.30 (d, *J* = 8.8 Hz, 2H, H_e), 7.70 (d, J = 8.8, 2H, H_d), 7.38 – 7.29 (m, 2H, H_l), 7.10 – 7.02 (m, 1H, H_m), 6.91 (d, *J* = 7.8 Hz, 2H, H_k), 6.47 (dd, *J* = 16.8, 10.4 Hz, 1H, H_r), 6.37 (s, 1H, H_i), 6.26 (d, *J* = 16.8 Hz, 1H, $H_{s'}$), 5.68 (d, *J* = 10.4 Hz, 1H, H_s), 3.36 (m, 8H, $H_{n/o}$). **^{13}C NMR (300 MHz, CDCl$_3$) δ** 167.0 ($C_{b/g}$), 166.7 ($C_{g/b}$), 165.5 (C_q), 145.6 (C), 139.1 (C), 137.7 (C), 129.2 (2C, $C_{e/d/k/l}$), 128.6 (C), 127.1 (C), 124.9 (2C, $C_{e/d/k/l}$), 124.5 (2C, $C_{e/d/k/l}$), 123.10 (C), 122.5 (C), 119.2 (2C, $C_{e/d/k/l}$), 118.1 (C), 48.4 ($C_{n/o}$),

48.2 ($C_{n/o}$), 45.9 ($C_{n/o}$), 41.8 ($C_{n/o}$); **HRMS:** calcd for $C_{24}H_{22}N_5O_5^+$ $[M+H]^+$, 448.1621, found 448.16.1612

7.3.5.7 1-(4-Nitrophenyl)-3-(phenylamino)-4-(4-(prop-2-yn-1-yl)piperazin-1-yl)-1*H*-pyrrole-2,5-dione (103)

To a 2-neck round bottom flask was added 1-(4-nitrophenyl)-3-(phenylamino)-4-(piperazin-1-yl)-1*H*-pyrrole-2,5-dione (101) (205 mg, 0.521 mmol) and dissolved in DMF (15 mL). TEA (0.11 mL, 0.78 mmol, 1.5 equiv) was then added to the solution, followed by the drop-wise addition of propargyl bromide (80% in toluene) (112 mg, 0.782 mmol, 1.5 equiv). The reaction mixture was stirred for 2 h at 50 °C. Upon completion, the reaction mixture was taken up in Et_2O (50 mL) and washed with H_2O (6 × 25 mL). The organic layer was then washed with brine and dried over $MgSO_4$ salts. The drying salts were removed by filtration and the solvent was removed *in vacuo*.Purification by column chromatography (EtOAc/Hexane, 4:6) afforded the desired product 1-(4-nitrophenyl)-3-(phenylamino)-4-(4-(prop-2-yn-1-yl)piperazin-1-yl)-1*H*-pyrrole-2,5-dione (**103**) as an orange solid (160 mg, 71%).

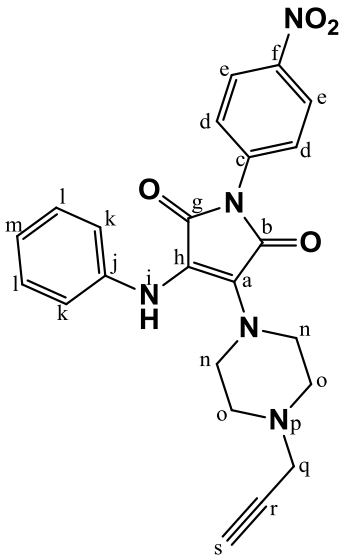

Mp = 192-194 ºC; $\mathbf{R_f}$ =0.29 (EtOAc/Hexane, 4:6), **IR (ATR, cm^{-1}):** 3253 (amine N-H str), 1698 (carbonyl C=O str), 1495, 1334 (nitro N-O), 684 (alkyne C≡C-H);**^{1}H NMR (300 MHz, $CDCl_3$) δ** 8.29 (d, *J* = 9.1 Hz, 2H, H_e), 7.70 (d, *J* = 9.1 Hz, 2H, H_d), 7.36 – 7.25 (m, 2H, H_l), 7.03 - 6.95 (m, 1H, H_m), 6.84 (d, *J* = 7.7 Hz, 2H, H_k), 6.09 (s, 1H, H_i), 3.54 – 3.43 (m, 2H, $H_{n/o}$), 3.24 (d, *J* = 2.3 Hz, 2H, H_q), 2.47 – 2.38 (m, 2H, $H_{n/o}$), 2.25 (m, 1H, H_s). **^{13}C NMR (300 MHz, $CDCl_3$) δ** 167.4 ($C_{b/g}$), 166.4 ($C_{b/g}$), 145.5 (C), 140.7 (C), 137.9 (C), 129.3 (2C, $C_{e/d/k/l}$), 126.1 (C), 124.9 (2C, $C_{e/d/k/l}$), 124.4 (2C, $C_{e/d/k/l}$), 122.1 (C), 118.0 (2C, $C_{e/d/k/l}$), 115.0 (C), 78.4 (C_r), 73.6 (C_s), 51.7 (2C, $C_{n/o}$), 47.7 (2C, $C_{n/o}$), 47.0 (C_q). **HRMS:** calcd for $C_{23}H_{22}N_5O_4^+$ $[M+H]^+$, 432.1672, found 432.16.1666.

7.3.5.8 3-(4-Acryloylpiperazin-1-yl)-4-(phenylamino)-1*H*-pyrrole-2,5-dione (104)

A Schlenk tube charged with 3-(4-acryloylpiperazin-1-yl)-1-(4-nitrophenyl)-4-(phenylamino)-1*H*-pyrrole-2,5-dione (**102**) (60 mg, 0.13 mmol) was evacuated under high vacuum and filled with Ar. A mixture of CH_2Cl_2 and MeOH (3 mL: 3 mL) was added to the Schlenk and the solution was then saturated with NH_3 by bubbling NH_3 gas through the liquid for 5 min. The reaction mixture was stirred for 8 h at RT under a N_2 atmosphere. The solvent was removed *in vacuo* and purification by column chromatography (EtOAc/Hexane, 1:1) afforded the desired product 3-(4-acryloylpiperazin-1-yl)-4-(phenylamino)-1*H*-pyrrole-2,5-dione (**104**) as an orange solid (38 mg, 86%).

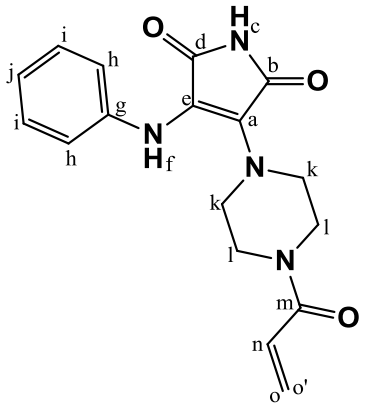

Mp = 161-163 ºC; **R_f** = 0.24 (EtOAc/Hexane, 1:1), **IR (ATR, cm^{-1}):** 3317, 3141 (amine N-H str), 3036 (alkene C=CH_2 str), 1698 (carbonyl C=O str);**^{1}H NMR (300 MHz, $CDCl_3$) δ** 8.16 (s, 1H, H_c), 7.34 – 7.24 (m, 2H, H_i), 7.02 - 6.94 (m, 1H, H_j), 6.84 (d, *J* = 8.0 Hz, 2H, H_h), 6.48 (dd, *J* = 16.8, 10.4 Hz, 1H, H_n), 6.37 (s, 1H, H_f), 6.27 (dd, *J* = 16.8, 1.5 Hz, 1H, $H_{o/o'}$), 5.69 (dd, *J* = 10.4, 1.5 Hz, 1H, $H_{o/o'}$), 3.53 – 3.21 (m, 8H, $H_{k/l}$).**^{13}C NMR (300 MHz, $CDCl_3$) δ** 169.3 ($C_{b/d}$), 169.0 ($C_{b/d}$), 165.5 (C_m), 140.1 (C_g), 129.0 (2C, $C_{h/i}$), 128.5 (C), 127.1 (C), 124.4 (C), 122.0 (C), 118.2 (2C, $C_{i/h}$), 117.1 (C), 48.0 ($C_{k/l}$), 47.7 ($C_{k/l}$), 45.9 ($C_{k/l}$), 41.9 ($C_{k/l}$). **HRMS:** calcd for $C_{17}H_{18}N_4O_3^+$ $[M+H]^+$, 327.1457, found 327.1447.

3.7.5.9 3-(Phenylamino)-4-(4-(prop-2-yn-1-yl)piperazin-1-yl)-1*H*-pyrrole-2,5-dione (105)

A Schlenk tube charged with 1-(4-nitrophenyl)-3-(phenylamino)-4-(4-(prop-2-yn-1-yl)piperazin-1-yl)-1*H*-pyrrole-2,5-dione (**103**) (90 mg, 0.21 mmol) was evacuated under high vacuum and filled with Ar. A mixture of CH_2Cl_2 and MeOH (4 mL: 4 mL) was added to the Schlenk tube and the solution was saturated with NH_3 by bubbling NH_3 gas through the liquid for 5 min. The reaction mixture was stirred for 10 h at RT under a N_2 atmosphere. The solvent was removed *in vacuo* and purification by column chromatography (EtOAc/Hexane, 4:6) afforded the desired product 3-(phenylamino)-4-(4-(prop-2-yn-1-yl)piperazin-1-yl)-1*H*-pyrrole-2,5-dione (**105**) as an orange solid (59 mg, 91%).

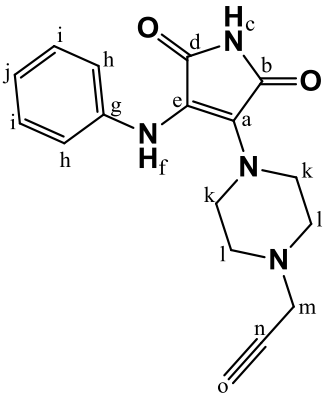

Mp = 82-84 ºC; **R_f** = 0.35 (EtOAc/Hexane, 1:1); **IR (ATR, cm^{-1}):** 3277, 2920 (amine N-H str) 1694 (carbonyl C=O str), 691 (alkyne C≡C-H str);**^{1}H NMR (300 MHz, $CDCl_3$) δ** 7.79 (s, 1H, H_c), 7.30 – 7.22 (m, 2H, H_h), 6.95 – 6.89 (m, 1H, H_j), 6.74 (d, *J* = 7.8 Hz, 2H, H_i), 5.90 (s, 1H, H_f), 3.55 – 3.40 (m, 4H, $H_{k/l}$), 3.22 (d, *J* = 2.3 Hz, 2H, H_m), 2.48 – 2.35 (m, 4H, $H_{k/l}$), 2.28 – 2.24 (m, 1H, H_o).**^{13}C NMR (300 MHz, $CDCl_3$) δ** 169.6 ($C_{b/d}$), 168.5 ($C_{d/b}$), 141.9 (C), 129.2 (2C, $C_{h/i}$), 128.5 (C), 121.1 (C), 117.1 (2C, $C_{h/i}$), 113.4 (C), 78.3 (C_n), 73.7 (C_o), 51.7 (2C, $C_{k/l}$), 47.2 (2C, $C_{k/l}$), 46.9 (C_m). **HRMS:** calcd for $C_{17}H_{18}N_4O_2^+$ $[M+H]^+$, 311.1508, found 311.1497.

CHAPTER 8 – REFERENCES

[1] Olson, J. S., *Making Cancer History: Disease and Discovery at the University of Texas M. D. Anderson Cancer Center*, Houston, Texas, Johns Hopkins University Press, **2009**.

[2] Galgut, C., Murray, J., Coulter, C., *The Psychological Impact of Breast Cancer: A Psychologist's Insights as a Patient*, Oxfordshire, Radcliffe Publishing, **2010**.

[3] Anand, P., Kunnumakara, A., Sundaram, C., Harikumar, K., Tharakan, S., Lai, O. S., Sung, B., Aggarwal, B. B., *Pharmaceutical Research* **2008**, *25*, 2097-2116.

[4] Roberts, M., BBC News *Health*, **2014**. http://www.bbc.com/news/health-26031748 (accessed 04/0914).

[5] Gallagher, J., BBC News *Health*, **2014**. http://www.bbc.com/news/health-26014693 (accessed 04/09/14).

[6] International Agency for Research on Cancer, *Central European Journal of Public Health*, **2014**. http://www.iarc.fr/en/media-centre/pr/2014/pdfs/pr224_E.pdf (accessed 04/09/2014).

[7] DeVita, V. T., Rosenberg, S. A., *New England Journal of Medicine* **2012**, *366*, 2207-2214.

[8] Hanahan, D., Weinberg, R. A., *Cell* **2000**, *100*, 57-70.

[9] Hanahan, D., Weinberg, R. A., *Cell* **2011**, *144*, 646-674.

[10] Cutter, M. A., Sigstedt, J., Venne, V., *Cell Biology and Cancer: NIH Curriculum Supplement Series*, **1999**. http://science.education.nih.gov/supplements/nih1/cancer/guide/understanding1.htm (accessed 08/09/2014).

[11] National Cancer Institute, **2014**. http://www.cancer.gov/cancertopics/cancerlibrary/what-is-cancer (accessed 08/09/2014).

[12] Downward, J., Jain, R., Kouzarides, T., Sawyers, C., Sebolt-Leopold, J., Norvatic Oncology, **2005**. http://www.nature.com/nrc/posters/pathways/index.html (accessed 08/09/2014)

[13] Frantz, S., *Nature Milestones* **2006**, *8*, 22-23.

[14] Abou-Jawde, R., Choueiri, T., Alemany, C., Mekhail, T., *Clinical Therapeutics* **2003**, *25*, 2121-2137.

[15] Strebhardt, K., Ullrich, A., *Nature Reviews Cancer* **2008**, *8*, 473-480.

[16] Chabner, B. A., Roberts, T. G., *Nature Reviews Cancer* **2005**, *5*, 65-72.

[17] Goldman, J. M., Melo, J. V., *New England Journal of Medicine* **2003**, *349*, 1451-1464.

[18] Pierotti, M. A., Negri, T., Tamborini, E., Perrone, F., Pricl, S., Pilotti, S., *Molecular Oncology* **2010**, *4*, 19-37.

[19] Zuccotto, F., Ardini, E., Casale, E., Angiolini, M., *Journal of Medicinal Chemistry* **2009**, *53*, 2681-2694.

[20] Stout, T. J., Foster, P. G., Matthews, D. J., *Current Pharmaceutical Design* **2004**, *10*, 1069-1082.

[21] Kalyn, R., *Journal of Oncology Pharmacy Practice* **2007**, *13*, 199-205.

[22] Gerber, D. E., *American Family Physician* **2008**, *77*, 311-319.

[23] Cohen, P., *Nature Cell Biology* **2002**, *4*, E127-E130.

[24] Ubersax, J. A., Ferrell Jr, J. E., *Nature Reviews Molecular Cell Biology* **2007**, *8*, 530-541.

[25] Manning, G., Whyte, D. B., Martinez, R., Hunter, T., Sudarsanam, S., *Science* **2002**, *298*, 1912-1934.

[26] Blume-Jensen, P., Hunter, T., *Nature* **2001**, *411*, 355-365.

[27] Hanks, S. K., *Genome Biology* **2003**, *4*, 1-7.

[28] Hanks, S. K., Quinn, A. M., Hunter, T., *Science* **1988**, *241*, 42-52.

[29] Hanks, S. K., Hunter, T., *The FASEB Journal* **1995**, *9*, 576-596.

[30] Sciences's signal transduction knowledge environment, American Association for the Advancement of Science, **2002**. http://www.sciencemag.org/content/suppl/2002/12/13/298.5600.1912.DC2/KinomePoster.pdf (accessed 11/09/2014).

[31] Hunter, T., *Cold Spring Harbor Perspectives in Biology* **2014**, *6*, 1-4.

[32] Gschwind, A., Fischer, O. M., Ullrich, A., *Nature Reviews Cancer* **2004**, *4*, 361-370.

[33] Goodsell, D., RCSB Protein Data Bank, **2010**. http://www.rcsb.org/pdb/101/motm.do?momID=126 (accessed 15/09/2014).

[34] Lemmon, M. A., *Experimental Cell Research* **2009**, *315*, 638-648.

[35] Robinson, K., Sandler, A., *Current Oncology Reports* **2013**, *15*, 396-404.

[36] Taylor, S. S., Kornev, A. P., *Trends in Biochemical Sciences*, *36*, 65-77.

[37] Taylor, S. S., Keshwani, M. M., Steichen, J. M., Kornev, A. P., *Philosophical Transactions of the Royal Society B: Biological Sciences* **2012**, *367*, 2517-2528.

[38] Ghose, A. K., Herbertz, T., Pippin, D. A., Salvino, J. M., Mallamo, J. P., *Journal of Medicinal Chemistry* **2008**, *51*, 5149-5171.

[39] Irie, T., Fujii, I., Sawa, M., *Bioorganic & Medicinal Chemistry Letters* **2012**, *22*, 591-596.

[40] Garuti, L., Roberti, M., Bottegoni, G., *Current Medicinal Chemistry* **2011**, *18*, 2981-2994.

[41] Noble, M. E. M., Endicott, J. A., Johnson, L. N., *Science* **2004**, *303*, 1800-1805.

[42] Simard, J. R., Getlik, M., Grütter, C., Pawar, V., Wulfert, S., Rabiller, M., Rauh, D., *Journal of the American Chemical Society* **2009**, *131*, 13286-13296.

[43] Johnson, L. N., Noble, M. E. M., Owen, D. J., *Cell* **1996**, *85*, 149-158.

[44] Hubbard, S. R., *Nature Structural Biology* **1999**, *6*, 711.

[45] Fedorov, O., Müller, S., Knapp, S., *Nature Chemical Biology* **2010**, *6*, 166-169.

[46] Cohen, P., *Nature Reviews Drug Discovery* **2002**, *1*, 309-315.

[47] Zhao, Z., Wu, H., Wang, L., Liu, Y., Knapp, S., Liu, Q., Gray, N. S., AC*S Chemical Biology* **2014**, *9*, 1230-1241.

[48] Fang, Z., Grütter, C., Rauh, D., *ACS Chemical Biology* **2012**, *8*, 58-70.

[49] Liu, Y., Gray, N. S., *Nature Chemical Biology* **2006**, *2*, 358-364.

[50] Zhang, J., Yang, P. L., Gray, N. S., *Nature Reviews Cancer* **2009**, *9*, 28-39.

[51] Bogoyevitch, M. A., Fairlie, D. P., *Drug Discovery Today* **2007**, *12*, 622-633.

[52] Carmi, C., Mor, M., Petronini, P. G., Alfieri, R. R., *Biochemical Pharmacology* **2012**, *84*, 1388-1399.

[53] Liu, Q., Sabnis, Y., Zhao, Z., Zhang, T., Buhrlage, S. J., Jones, L. H., Gray, N. S., *Chemistry & Biology* **2013**, *20*, 146-159.

[54] Singh, J., Petter, R. C., Baillie, T. A., Whitty, A., *Nature Reviews Drug Discovery* **2011**, *10*, 307-317.

[55] Klüter , S., Simard , J. R., Rode, H. B., Grütter, C., Pawar, V., Raaijmakers, H. C., Barf, T. A., Rabiller, M., van Otterlo W. A. L., Rauh, D., *ChemBioChem* **2010**, *11*, 2557-2566.

[56] Leproult, E., Barluenga, S., Moras, D., Wurtz, J.-M., Winssinger, N., *Journal of Medicinal Chemistry* **2011**, *54*, 1347-1355.

[57] Michalczyk, A., Klüter, S., Rode, H. B., Simard, J. R., Grütter, C., Rabiller, M., Rauh, D., *Bioorganic & Medicinal Chemistry* **2008**, *16*, 3482-3488.

[58] Walter, A. O., Sjin, R. T. T., Haringsma, H. J., Ohashi, K., Sun, J., Lee, K., Dubrovskiy, A., Labenski, M., Zhu, Z., Wang, Z., Sheets, M., St Martin, T., Karp, R., van Kalken, D., Chaturvedi, P., Niu, P., Nacht, M., Petter, R. C., Westlin, W., Lin, K., Jaw-Tsai, S., Raponi, M., van Dyke, T., Etter, J., Weaver, Z., Pao, W., Singh, J., Simmons, A. D., Harding, T. C., Allen, A., *Cancer Discovery* **2013**, *3*, 1404-1415.

[59] Doebele, R. C., Oton, A. B., Peled, N., Camidge, D. R., Bunn, P. A., Jr., *Lung Cancer*, *69*, 1-12.

[60] Schwartz, P. A., Kuzmic, P., Solowiej, J., Bergqvist, S., Bolanos, B., Almaden, C., Nagata, A., Ryan, K., Feng, J., Dalvie, D., Kath, J. C., Xu, M., Wani, R., Murray, B. W., *Proceedings of the National Academy of Sciences* **2014**, *111*, 173-178.

[61] Ward, R. A., Anderton, M. J., Ashton, S., Bethel, P. A., Box, M., Butterworth, S., Colclough, N., Chorley, C. G., Chuaqui, C., Cross, D. A. E., Dakin, L. A., Debreczeni, J. E., Eberlein, C., Finlay, M. R. V., Hill, G. B., Grist, M., Klinowska, T. C. M., Lane, C., Martin, S., Orme, J. P., Smith, P., Wang, F., Waring, M. J., *Journal of Medicinal Chemistry* **2013**, *56*, 7025-7048.

[62] Antonello, A., Tarozzi, A., Morroni, F., Cavalli, A., Rosini, M., Tarrozi, A., Tumiatti, V., Melchiorre, C., *Journal of Medicinal Chemistry* **2006**, *49*, 6642-6645.

[63] Darling, D., *The Worlds of David Darling - Encyclopedia of science*, **1999**. http://www.daviddarling.info/encyclopedia/A/Aristotle.html (accessed 16/09/2014).

[64] Poupon, E., Nay, B., *Biomimetic Organic Synthesis, Vol. 2*, Wiley-VCH, **2011**.

[65] Cragg, G. M., Newman, D. J., *Biochimica et Biophysica Acta 1830* **2013**, 3670-3695.

[66] Butler, M. S., *Natural Product Reports* **2008**, *25*, 475-516.

[67] Mishra, B. B., Tiwari, V. K., *European Journal of Medicinal Chemistry* **2011**, *46*, 4769-4807.

[68] Liu, J., Hu, Y., Waller, D. L., Wang, J., Liu, Q., *Natural Product Reports* **2012**, *29*, 392-403.

[69] Lachance, H., Wetzel, S., Kumar, K., Waldmann, H., *Journal of Medicinal Chemistry* **2012**, *55*, 5989-6001.

[70] Wetzel, S., Bon, R. S., Kumar, K., Waldmann, H., *Angewandte Chemie International Edition* **2011**, *50*, 10800-10826.

[71] Newman, D. J., *Journal of Medicinal Chemistry* **2008**, *51*, 2589-2599.

[72] Pfisterer, P. H., Wolber, G., Efferth, T., Rollinger, J. M., Stuppner, H., *Current Pharmaceutical Design* **2010**, *16*, 1718-1741.

[73] Bon, R. S., Waldmann, H., *Accounts of Chemical Research* **2010**, *43*, 1103-1114.

[74] Augen, J., *Drug Discovery Today* **2002**, *7*, 315-323.

[75] Kaiser, M., Wetzel, S., Kumar, K., Waldmann, H., *Cellular and Molecular Life Sciences* **2008**, *65*, 1186-1201.

[76] Hübel, K., Leßmann, T., Waldmann, H., *Chemical Society Reviews* **2008**, *37*, 1361-1374.

[77] Mann, J., *Nature Reviews Cancer* **2002**, *2*, 143-148.

[78] Bharate, S. B., Sawant, S. D., Singh, P. P., Vishwakarma, R. A., *Chemical Reviews* **2013**, *113*, 6761-6815.

[79] Giddings, L.-A., Newman, D., *Journal of Industrial Microbiology & Biotechnology* **2013**, *40*, 1181-1210.

[80] Omura, S., Iwai, Y., Hirano, A., Nakagawa, A., Awaya, J., Tsuchya, H., Takahashi, Y., Masuma, R., *The Journal of Antibiotics* **1977**, *30*, 275-282.

[81] Nakano, H., Omura, S., *The Journal of Antibiotics* **2009**, *62*, 17-26.

[82] Tamaoki, T., Nomoto, H., Takahashi, I., Kato, Y., Morimoto, M., Tomita, F., *Biochemical and Biophysical Research Communications* **1986**, *135*, 397-402.

[83] Gescher, A., *Critical Reviews in Oncology/Hematology* **2000**, *34*, 127-135.

[84] Tanramluk, D., Schreyer, A., Pitt, W. R., Blundell, T. L., *Chemical Biology & Drug Design* **2009**, *74*, 16-24.

[85] Acero, N., Braña, M. F., Añorbe, L., Domínguez, G., Muñoz-Mingarro, D., Mitjans, F., Piulats, J., *European Journal of Medicinal Chemistry* **2012**, *48*, 108-113.

[86] Gu, G., Wang, H., Liu, P., Fu, C., Li, Z., Cao, X., Li, Y., Fang, Q., Xu, F., Shen, J., Wang, P. G., *Chemical Communications* **2012**, *48*, 2788-2790.

[87] Kolb, H. C., Finn, M. G., Sharpless, K. B., *Angewandte Chemie International Edition* **2001**, *40*, 2004-2021.

[88] Kolb, H. C., Sharpless, K. B., *Drug Discovery Today* **2003**, *8*, 1128-1137.

[89] Moses, J. E., Moorhouse, A. D., *Chemical Society Reviews* **2007**, *36*, 1249-1262.

[90] Bock, V. D., Hiemstra, H., van Maarseveen, J. H., *European Journal of Organic Chemistry* **2006**, *2006*, 51-68.

[91] Tornøe, C. W., Christensen, C., Meldal, M., *The Journal of Organic Chemistry* **2002**, *67*, 3057-3064.

[92] Meldal, M., Tornøe, C. W., *Chemical Reviews* **2008**, *108*, 2952-3015.

[93] Rostovtsev, V. V., Green, L. G., Fokin, V. V., Sharpless, K. B., *Angewandte Chemie International Edition* **2002**, *114*, 2708-2711.

[94] Zhang, L., Chen, X., Xue, P., Sun, H. H. Y., Williams, I. D., Sharpless, K. B., Fokin, V. V., Jia, G., *Journal of the American Chemical Society* **2005**, *127*, 15998-15999.

[95] Worrell, B. T., Malik, J. A., Fokin, V. V., *Science* **2013**, *340*, 457-460.

[96] Himo, F., Lovell, T., Hilgraf, R., Rostovtsev, V. V., Noodleman, L., Sharpless, K. B., Fokin, V. V., *Journal of the American Chemical Society* **2004**, *127*, 210-216.

[97] Agalave, S. G., Maujan, S. R., Pore, V. S., *Chemistry – An Asian Journal* **2011**, *6*, 2696-2718.

[98] Li, F., Park, Y., Hah, J.-M., Ryu, J.-S., *Bioorganic & Medicinal Chemistry Letters* **2013**, *23*, 1083-1086.

[99] Kalesh, K. A., Liu, K., Yao, S. Q., *Organic & Biomolecular Chemistry* **2009**, *7*, 5129-5136.

[100] Poot, A. J., van Ameijde, J., Slijper, M., van den Berg, A., Hilhorst, R., Ruijtenbeek, R., Rijkers, D. T. S., Liskamp, R. M. J., *ChemBioChem* **2009**, *10*, 2042-2051.

[101] Arioli, F., Borrelli, S., Colombo, F., Falchi, F., Filippi, I., Crespan, E., Naldini, A., Scalia, G., Silvani, A., Maga, G., Carraro, F., Botta, M., Passarella, D., *ChemMedChem* **2011**, *6*, 2009-2018.

[102] Song, D., Park, Y., Yoon, J., Aman, W., Hah, J.-M., Ryu, J.-S., *Bioorganic & Medicinal Chemistry* **2014**, *22*, 4855-4866.

[103] Elsberger, B., *Critical reviews in Oncology/Hematology* **2014**, *89*, 343-351.

[104] Gargalionis, A. N., Karamouzis, M. V., Papavassiliou, A. G., *International Journal of Cancer* **2014**, *134*, 2019-2029.

[105] Kumar, A., Wang, Y., Lin, X., Sun, G., Parang, K., *ChemMedChem* **2007**, *2*, 1346-1360.

[106] Kumar, A., Ahmad, I., Chhikara, B. S., Tiwari, R., Mandal, D., Parang, K., *Bioorganic & Medicinal Chemistry Letters* **2011**, *21*, 1342-1346.

[107] Paydas, S., *Critical Reviews in Oncology/Hematology* **2014**, *89*, 242-247.

[108] Food and Drug Administration, **2012**. http://www.fda.gov/Drugs/InformationOnDrugs/ApprovedDrugs/ucm318203.htm (accessed 12/11/2014).

[109] Kumar, D., Reddy, V. B., Kumar, A., Mandal, D., Tiwari, R., Parang, K., *Bioorganic & Medicinal Chemistry Letters* **2011**, *21*, 449-452.

[110] Rao, V. K., Chhikara, B. S., Shirazi, A. N., Tiwari, R., Parang, K., Kumar, A., *Bioorganic & Medicinal Chemistry Letters* **2011**, *21*, 3511-3514.

[111] Parikh, R. A., Wang, P., Beumer, J. H., Chu, E., Appleman, L. J., *Oncotargets and Therapy* **2014**, *7*, 969-983.

[112] Maroun, C. R., Rowlands, T., *Pharmacology & Therapeutics* **2014**, *142*, 316-338.

[113] Furlan, A., Colombo, F., Kover, A., Issaly, N., Tintori, C., Angeli, L., Leroux, V., Letard, S., Amat, M., Asses, Y., Maigret, B., Dubreuil, P., Botta, M., Dono, R., Bosch, J., Piccolo, O., Passarella, D., Maina, F., *European Journal of Medicinal Chemistry* **2012**, *47*, 239-254.

[114] Colombo, F., Tintori, C., Furlan, A., Borrelli, S., Christodoulou, M. S., Dono, R., Maina, F., Botta, M., Amat, M., Bosch, J., Passarella, D., *Bioorganic & Medicinal Chemistry Letters* **2012**, *22*, 4693-4696.

[115] Trembley, J. H., Zhong, C., Unger, G., Slaton, J., Kren, B. T., van Waes, C., Ahmed, K., *Biofactors* **2010**, *36*, 187-195.

[116] Świder, R., Masłyk, M., Martín-Santamaría, S., Ramos, A., de Pascual-Teresa, B., *Molecular and Cellular Biochemistry* **2011**, *356*, 117-119.

[117] Goumans, M.-J., Lebrin, F., Valdimarsdottir, G., *Trends in Cardiovascular Medicine* **2003**, *13*, 301-307.

[118] Buijs, J. T., Stayrook, K. R., Guise, T. A., *Cancer Microenvironment* **2011**, *4*, 261-281.

[119] Veronique Calleja, M. L., Gloria de las Heras-Martinez, Peter J. Parker, Jose Requejo-Isidro and, Larijani, B., *Biochemical Society Transactions* **2014**, *42*, 1435-1440.

[120] Medina, J. R., *Journal of Medicinal Chemistry* **2013**, *56*, 2726-2737.

[121] Merkul, E., Klukas, F., Dorsch, D., Grädler, U., Greiner, H. E., Müller, T. J. J., *Organic & Biomolecular Chemistry* **2011**, *9*, 5129-5136.

[122] Suchaud, V., Gavara, L., Giraud, F., Nauton, L., Théry, V., Anizon, F., Moreau, P., *Bioorganic & Medicinal Chemistry* **2014**, *22*, 4704-4710.

[123] Letribot, B., Akué-Gédu, R., Santio, N. M., El-Ghozzi, M., Avignant, D., Cisnetti, F., Koskinen, P. J., Gautier, A., Anizon, F., Moreau, P., *European Journal of Medicinal Chemistry* **2012**, *50*, 304-310.

[124] Akué-Gédu, R., Rossignol, E., Azzaro, S., Knapp, S., Filippakopoulos, P., Bullock, A. N., Bain, J., Cohen, P., Prudhomme, M., Anizon, F., Moreau, P., *Journal of Medicinal Chemistry* **2009**, *52*, 6369-6381.

[125] Parker, B. C., Engels, M., Annala, M., Zhang, W., *The Journal of Pathology* **2014**, *232*, 4-15.

[126] Le Corre, L., Girard, A.-L., Aubertin, J., Radvanyi, F., Benoist-Lasselin, C., Jonquoy, A., Mugniery, E., Legeai-Mallet, L., Busca, P., Le Merre, Y., *Organic & Biomolecular Chemistry* **2010**, *8*, 2164-2173.

[127] Rees, D. C., Congreve, M., Murray, C. W., Carr, R., *Nature Reviews Drug Discovery* **2004**, *3*, 660-672.

[128] Merckx, A., Echalier, A., Langford, K., Sicard, A., Langsley, G., Joore, J., Doerig, C., Noble, M., Endicott, J., *Structure* **2008**, *16*, 228-238.

[129] Leroy, D., Doerig, C., *Trends in Pharmacological Sciences* **2008**, *29*, 241-249.

[130] Dar, A. C., Lopez, M. S., Shokat, K. M., *Chemistry & Biology* **2008**, *15*, 1015-1022.

[131] Pan, Z., Scheerens, H., Li, S.-J., Schultz, B. E., Sprengeler, P. A., Burril, C., Mendonca, R. V., Sweeney, M. D., Scott, K. C. K., Grothaus, P. G., Jeffrey, D. A., Spoerke, J. M., Honigberg, L. A., Young, P. R., Dalrymple, S. A., Palmer, J. T., *ChemMedChem* **2007**, *2*, 58-61.

[132] Klein, M., Dinér, P., Dorin-Semblat, D., Doerig, C., Grøtli, M., *Organic & Biomolecular Chemistry* **2009**, *7*, 3421–3429.

[133] Roffey, J., Rosse, C., Linch, M., Hibbert, A., McDonald, N. Q., Parker, P. J., *Current Opinion in Cell Biology* **2009**, *21*, 268-279.

[134] Jain, K., Ajay, D., Sobhia, M. E., *Molecular Informatics* **2011**, *30*, 329-344.

[135] Carmi, C., Galvani, E., Vacondio, F., Rivara, S., Lodola, A., Russo, S., Aiello, S., Bordi, F., Costantino, G., Cavazzoni, A., Alfieri, R. R., Ardizzoni, A., Petronini, P. G., Mor, M., *Journal of Medicinal Chemistry* **2012**, *55*, 2251-2264.

[136] Cha, M. Y., Lee, K.-O., Kim, J. W., Lee, C. G., Song, J. Y., Kim, Y. H., Lee, G. S., Park, S. B., Kim, M. S., *Journal of Medicinal Chemistry* **2009**, *52*, 6880-6888.

[137] Singh, J., Petter, R. C., Kluge, A. F., *Current Opinion in Chemical Biology* **2010**, *14*, 475-480.

[138] Stock, N. S., Bain, G., Zunic, J., Li, Y., Ziff, J., Roppe, J., Santini, A., Darlington, J., Prodanovich, P., King, C. D., Baccei, C., Lee, C., Rong, H., Chapman, C., Broadhead, A., Lorrain, D., Correa, L., Hutchinson, J. H., Evans, J. F., Prasit, P., *Journal of Medicinal Chemistry* **2011**, *54*, 8013-8029.

[139] Waser, J., Gaspar, B., Nambu, H., Carreira, E. M., *Journal of the American Chemical Society* **2006**, *128*, 11693-11712.

[140] An, J., Chang, N.-J., Song, L.-D., Jin, Y.-Q., Ma, Y., Chen, J.-R., Xiao, W.-J., *Chemical Communications* **2011**, *47*, 1869-1871.

[141] Takuya, K., Shin-ichiro, N., Yukiko, H., Hiroaki, K., Lemin, D., Nakanishi, W., Ishikawa, T., *Heterocycles* **2008**, *76*, 1155-1170.

[142] Neosome Life Sciences, LLC., Patent: *US2012/302578 A1*, **2012**.

[143] Schering Corporation, Patent:*US 20040010013 A1*, **2004**.

[144] Tsotinis, A., Afroudakis, P. A., Davidson, K., Prashar, A., Sugden, D., *Journal of Medicinal Chemistry* **2007**, *50*, 6436-6440.

[145] Zheng, C., Lu, Y., Zhang, J., Chen, X., Chai, Z., Ma, W., Zhao, G., *Chemistry – A European Journal* **2010**, *16*, 5853-5857.

[146] Nystrom, R. F., Brown, W. G., *Journal of the American Chemical Society* **1947**, *69*, 1197-1199.

[147] Burke, S. D., Danheiser, R. L., *Handbook of Reagents for Organic Synthesis*, Chichester, John Wiley & Sons, **1999**.

[148] Clayden, J., Greeves, N., Warren, S., Wothers, P., *Organic Chemistry*, Oxford, Oxford University Press, **2001**.

[149] Mo, F., Li, F., Qiu, D., Zhang, Y., Wang, J., *Chinese Journal of Chemistry* **2012**, *30*, 2297-2302.

[150] Nunes Silva da Júnior, E., *Synlett* **2008**, 149-150.

[151] Tojo, G., Fernández, M., *Oxidation of Alcohols to Aldehydes and Ketones: A Guide to Current Common Practice*, New York, Springer, **2006**.

[152] Gritter, R. J., Dupre, G. D., Wallace, T. J., *Nature* **1964**, *202*, 179-181.

[153] Johnson, A. W., *Ylides and Imines of Phosphorus*, New York, John Wiley & Sons, **1993**.

[154] Kolodiazhnyi, O. I., *Phosphorus Ylides*, Weinheim, Wiley-VCH, **1999**.

[155] Johnson, A. W., *Ylid Chemistry*, New York-London, Academic Press Inc., **1966**.

[156] Kocienski, P. J., *Protecting Groups*, 3rd ed., New York, Thieme, **2005**.

[157] Abid, M., Teixeira, L., Török, B., *Tetrahedron Letters* **2007**, *48*, 4047-4050.

[158] Saulnier, M. G., Gribble, G. W., *The Journal of Organic Chemistry* **1982**, *47*, 757-761.

[159] Bregman, H., William, D. S., Meggers, E., *Synthesis* **2005**, 1521 -1527.

[160] Tao, M., Park, C. H., Bihovsky, R., Wells, G. J., Husten, J., Ator, M. A., Hudkins, R. L., *Bioorganic & Medicinal Chemistry Letters* **2006**, *16*, 938-942.

[161] Nicolaou, K. C., Snyder, S. A., Montagnon, T., Vassilikogiannakis, G., *Angewandte Chemie International Edition* **2002**, *41*, 1668-1698.

[162] Corey, E.J., *Angewandte Chemie International Edition* **2002**, *41*, 1650-1667.

[163] Sauer, J., *Angewandte Chemie International Edition in English* **1966**, *5*, 211-230.

[164] Fernández, I., Bickelhaupt, F. M., *Journal of Computational Chemistry* **2014**, *35*, 371-376.

[165] Stoos, F., Roček, J., *Journal of the American Chemical Society* **1972**, *94*, 2719-2723.

[166] Siemens Aktiengesellschaft, Patent: *US5194629 A1*, **1993**.

[167] Wu, R., Lodwig, S. N., Schmidt, J. G., Williams, R. F., Silks, L. A. P., *Journal of Labelled Compounds and Radiopharmaceuticals* **2012**, *55*, 211-222.

[168] Perez-Serrano, L., Casarrubios, L., Dominguez, G., Gonzalez-Perez, P., Perez-Castells, J., *Synthesis* **2002**, *13*, 1810-1812.

[169] Smaill, J. B., Baker, E. N., Booth, R. J., Bridges, A. J., Dickson, J. M., Dobrusin, E. M., Ivanovic, I., Kraker, A. J., Lee, H. H., Lunney, E. A., Ortwine, D. F., Palmer, B. D., Quin, J., Squire, C. J., Thompson, A. M., Denny, W. A., *European Journal of Medicinal Chemistry* **2008**, *43*, 1276-1296.

[170] Bruson, H. A., *Organic Reactions*, John Wiley & Sons, Inc., **2004**.

[171] Muthusamy, S., Arulananda Babu, S., Gunanathan, C., *Synthetic Communications* **2002**, *32*, 3247-3254.

[172] Caballero, E., Adeva, M., Calderón, S., Sahagún, H., Tomé, F., Medarde, M., Fernández, J. L., López-Lázaro, M., Jesús Ayuso, M., *Bioorganic & Medicinal Chemistry* **2003**, *11*, 3413-3421.

[173] Robertson, A., Philp, D., Spencer, N., *Tetrahedron* **1999**, *55*, 11365-11384.

[174] Liu, Q., Luedtke, N. W., Tor, Y., *Tetrahedron Letters* **2001**, *42*, 1445-1447.

[175] Wuts, P. G. M., Greene, T. W., *Greene's Protective Groups in Organic Synthesis*, New Jersey, John Wiley & Sons, **2012**.

[176] Souffrin, A., Croix, C., Viaud-Massuard, M.-C., *European Journal of Organic Chemistry* **2012**, *2012*, 2499-2502.

[177] Relles, H. M., *The Journal of Organic Chemistry* **1972**, *37*, 3630-3637.

[178] Chow, Y. L., Naguib, Y. M. A., *Journal of the Chemical Society Perkin Transactions 1* **1984**, 1165 -1171.

[179] Edge, S., Charlton, A., Hansen, T. K., Varma, K. S., Underhill, A. E., Becher, J., Kathirgamanathan, P., Khosravi, E., *Journal of Polymer Science Part A: Polymer Chemistry* **1992**, 30, 2773-2780.

[180] Nirogi, R., Dwarampudi, A., Kambhampati, R., Bhatta, V., Kota, L., Shinde, A., Badange, R., Jayarajan, P., Bhyrapuneni, G., Dubey, P. K., *Bioorganic & Medicinal Chemistry Letters* **2011**, *21*, 4577-4580.

[181] Chinchilla, R., Nájera, C., *Chemical Reviews* **2007**, *107*, 874-922.

[182] Deore, P. S., Argade, N. P., *Synthesis* **2014**, *46*, 281-289.

[183] Chinchilla, R., Nájera, C., *Chemical Society Reviews* **2011**, *40*, 5084-5121.

[184] Sonogashira, K., Tohda, Y., Hagihara, N., *Tetrahedron Letters* **1975**, *16*, 4467-4470.

[185] Sonogashira, K., *Journal of Organometallic Chemistry* **2002**, *653*, 46-49.

[186] Castañeda, L., Maruani, A., Schumacher, F. F., Miranda, E., Chudasama, V., Chester, K. A., Baker, J. R., Smith, M. E. B., Caddick, S., *Chemical Communications* **2013**, *49*, 8187-8189.

[187] Cheng, C.-F., Lai, Z.-C., Lee, Y.-J., *Tetrahedron* **2008**, *64*, 4347-4353.

[188] Sun, S., Zhu, C., Song, D., Li, F., Hu, A., *Polymer Chemistry* **2014**, *5*, 1241-1247.

[189] Pajak, B., Orzechowska, S., Gajkowska, B., Orzechowski, A., *Advances in Medical Sciences* **2008**, *53*, 21.

[190] Peifer, C., Alessi, D. R., *ChemMedChem* **2008**, *3*, 1810-1838.

[191] Seyferth, D., *Organometallics* **2009**, *28*, 1598-1605.

[192] Gary S. Silverman, P. E. R., *Handbook of Grignard Reagents*, New York, Marcel Dekker Inc., **1996**.

[193] Powers, J. C., Meyer, W. P., Parsons, T. G., *Journal of the American Chemical Society* **1967**, *89*, 5812-5820.

[194] Heacock, R. A., Kašpárek, S., *Advances in Heterocyclic Chemistry, Vol. 10*, Academic Press, **1969**, pp. 43-112.

[195] Marminon, C., Pierré, A., Pfeiffer, B., Pérez, V., Léonce, S., Pierré, A., Pfeiffer, B., Renard, P., Prudhomme, M., *Journal of Medicinal Chemistry* **2003**, *46*, 609-622.

[196] Ye, Q., Xu, G., Lv, D., Cheng, Z., Li, J., Hu, Y., *Bioorganic & Medicinal Chemistry* **2009**, *17*, 4302-4312.

[197] Delarue-Cochin, S., McCort-Tranchepain, I., *Organic & Biomolecular Chemistry* **2009**, *7*, 706-716.

[198] Brenner, M., Rexhausen, H., Steffan, B., Steglich, W., *Tetrahedron* **1988**, *44*, 2887-2892.

[199] Holz, J., Zayas, O., Jiao, H., Baumann, W., Spannenberg, A., Monsees, A., Riermeier, T. H., Almena, J., Kadyrov, R., Börner, A., *Chemistry – A European Journal* **2006**, *12*, 5001-5013.

[200] Teller, S., Eluwa, S., Koller, M., Uecker, A., Beckers, T., Baasner, S., Böhmer, F. D., Mahboobi, S., *European Journal of Medicinal Chemistry* **2000**, *35*, 413-427.

[201] Stewart, S. G., Polomska, M. E., Lim, R. W., *Tetrahedron Letters* **2007**, *48*, 2241-2244.

[202] Awuah, E., Capretta, A., *The Journal of Organic Chemistry* **2011**, *76*, 3122-3130.

[203] Jo, Y. S., van der Vlies, A. J., Gantz, J., Thacher, T. N., Antonijevic, S., Cavadini, S., Demurtas, D., Stergiopulos, N., Hubbel, J. A., *Journal of the American Chemical Society* **2009**, *131*, 14413-14418.

[204] Yin, K.-H., Hsieh, Y.-H., Sulake, R. S., Wang, S.-P., Chao, J.-I., Chen, C., *Bioorganic & Medicinal Chemistry Letters* **2014**, *24*, 5247-5250.

[205] Ohashi, K., Maruvka, Y. E., Michor, F., Pao, W., *Journal of Clinical Oncology* **2013**, *31*, 1070-1080.

[206] Ai, X., Sun, Y., Wang, H., Lu, S., *Amino Acids* **2014**, *46*, 1635-1648.

[207] Remon, J., Morán, T., Majem, M., Reguart, N., Dalmau, E., Márquez-Medina, D., Lianes, P., *Cancer Treatment Reviews* **2014**, *40*, 93-101.

[208] Vallath, S., Hynds, R. E., Succony, L., Janes, S. M., Giangreco, A., *European Respiratory Journal* **2014**, erj01464-02013.

[209] Yun, C.-H., Mengwasser, K. E., Toms, A. V., Woo, M. S., Greulich, H., Wong, K.-K., Meyerson, M., Eck, M. J., *Proceedings of the National Academy of Sciences* **2008**, *105*, 2070-2075.

[210] Costa, D. B., Schumer, S. T., Tenen, D. G., Kobayashi, S., *Journal of Clinical Oncology* **2008**, *26*, 1182-1184.

[211] Kolb, A. J., Kaplita, P. V., Hayes, D. J., Park, Y.-W., Pernell, C., Major, J. S., Mathis, G., *Drug Discovery Today* **1998**, *3*, 333-342.

[212] Harbert, C., Marshall, J., Soh, S., Steger, K., *Current Chemical Genomics* **2008**, *1*, 20.

[213] Degorce, F., Card, A., Soh, S., Trinquet, E., Knapik, G.P., Xie, B., *Current Chemical Genomics* **2009**, *3*, 22-32.

[214] Engel, J., Technische Universität Dortmund, Germany, **2014**.

[215] Johnson, D. C., Widlanski, T. S., *Tetrahedron Letters* **2004**, *45*, 8483-8487.

[216] Sasaki, S., Hashimoto, T., Obana, N., Yasuda, H., Uehara, Y., Maeda, M., *Bioorganic & Medicinal Chemistry Letters* **1998**, *8*, 1019-1022.

[217] Xie, G., Gupta, R., Atchison, K., Lown, J. W., *Journal of Medicinal Chemistry* **1996**, *39*, 1049-1055.

[218] Nascimento-Júnior, N. M., Mendes, T. C. F., Leal, D. M., Corrêa, C. M. N., Sudo, R. T., Zapata-Sudo, G., Barreiro, E. J., Fraga, C. A. M., *Bioorganic & Medicinal Chemistry Letters* **2010**, *20*, 74-77.

[219] Coghlan, M. P., Culbert, A. A., Cross, D. A. E., Corcoran, S. L., Yates, J. W., Pearce, N. J., Rausch, O. L., Murphy, G. J., Carter, P. S., Cox, L. R., Mills D., Brown, M. J., Haigh, D., Ward, R. W., Smith, D. G., Murray, K. J., Reith A. D., and J. C., Holder, *Chemistry & Biology* **2000**, *7*, 793-803.

[220] Smith, D. G., Buffet, M., Fenwick, A. E., Haigh, D., Ife, R. J., Saunders, M., Slingsby, B. P., Stacey, R., Ward, R. W., *Bioorganic & Medicinal Chemistry Letters* **2001**, *11*, 635-639.